Coordination Behavior of Penicillaminato Digold(I) Metalloligands with Sterically Constrained Diphosphines

(立体制約をもつジホスフィンで架橋された ペニシラミナト金(I)二核錯体配位子の配位挙動)

Takuma Itai

Department of Chemistry

Graduate School of Science

Osaka University

2017

Contents

Chapter I. General Introduction

Supramolecular chemistry is focusing on the aggregated structures supported by non-covalent intermolecular interactions, such as hydrogen bonding, metallophilic, and π···π interactions. Such aggregates have attracted much attention because of their unique structures and properties.[1,2] To create such interesting compounds, it is important to use well-designed components showing suitable interactions. The use of coordination compounds as a molecular building block has been studied greatly,[3] because the tuning of molecular and supramolecular structures and their physical properties is easier than those of organic compounds by the change of the subcomponents consisting of metal ions and ligands.

One of the most popular methods for the creation of such metallosupramolecules is the one-pot reaction of well-designed organic ligands and metal ions, which leads to the formation of complexes composed of a single kind of metal ions and a single kind of organic ligands. However, there is a problem for this method. That is, difficult organic reactions are needed for the creation of organic ligands that have several functional groups with different properties, such as hydrophobicity vs. hydrophilicity, because of their different solubilities in solvents. The difficulty in the selection of a reaction solvent also arises when ligands that have different functional groups are reacted with metal ions in one step synthesis. The use of metalloligand with more than one kind of ligands is an effective way for solving this problem. The metalloligand is generally prepared by the stepwise addition of several ligands to metal ions. Therefore, this synthetic methodology allows us to prepare heteroleptic metal complexes having a few kinds of organic ligands with different functional groups. [4]

The metal complexes composed of bridging and terminal ligands are supposed to be best metalloligands, in which a bridging ligand works as a linker and a terminal ligand works as coordination donor sites for secondary metal ions (Chart 1-1). Even though a number of metalloligands have been used for the creation of heteroleptic multinuclear coordination compounds, examples of metalloligands composed of bridging and terminal ligands have been less reported.[5]

Recently, our laboratory found that the Au^{I}_2 metalloligand, $[Au^{I}_2(dppe)(D\text{-pen})_2]^{2-}$, composed of one diphosphine bridging ligand and two amino acid terminal ligands, leads to the creation of a unique supramolecular structure by the reaction with Co^{II} in air (dppe = 1,2-bis(diphenylphosphino)ethane, D-pen = D-penicillaminate. Scheme 1-1).[6,7] This reaction gave the divalent $Au^{I}_4Co^{III}_2$ complex cation, $[Au^{I}_4Co^{III}_2(dppe)_2(D\text{-pen})_4]^{2+}$, in which two metalloligands bridge two Co^{III} ions via the bis(tridentate-*N*,*O*,*S*) bridging mode, and each Co^{III} ions is situated in a *cis*(*N*)*trans*(*O*)*cis*(*S*)-$N_2O_2S_2$ geometry formed

by two terminal D-pen ligands from two metalloligands (Figure 1-1a). It was found that this cationic complex is crystallized with a variety of inorganic anions, such as nitrate, perchlorate, chloride, bromide, azide, tetrafluoroborate, sulfate, and hexafluorosilicate. As a representative among this class of complexes, the crystal structure of the nitrate salt, $[Au^{I}_4Co^{III}_2(dppe)_2(D\text{-pen})_4](NO_3)_2$, is explained as follows.

In crystal, six complex cations are aggregated in an octahedral manner through intermolecular 24 CH···π and 12 NH_2···OCO hydrogen bonding interactions, accommodating an NO_3^- ion in the center (Figure 1-1b). These cationic supramolecular octahedrons are packed in a face centered cubic (fcc) arrangement by CH···π interactions. The fcc structure contains a single kind of octahedral interstice, in which one NO_3^- ion is accommodated. In addition, there are two kinds of larger tetrahedral interstices, one of which is surrounded by amine groups and another is surrounded by phenyl and methyl groups (Figure 1-1d). The former hydrophilic tetrahedral interstice accommodates ten nitrate ions, forming an adamantane-like nitrate cluster (Figure 1-1c). Another hydrophobic tetrahedral interstice accommodates water molecules. This is a very rare metallosupramolecule that shows the separate aggregation of anionic and cationic species in crystal (Scheme 1-1, Figure 1-1).

To investigate the importance of homochirality to the formation of such an anomalous crystal structure, the effects of the chirality of metalloligand, the kind of metal ions, and the molecular shapes have also been studied. The meso $Au^{I}_4Co^{III}_2$ complex having DDLL-penicillaminate ligands, $[Au^{I}_4Co^{III}_2(dppe)_2(D\text{-pen})_2(L\text{-pen})_2]^{2+}$, showed the normal alternate arrangement of cations and anions in the crystal structure of nitrate salt, which is in sharp contrast to the unique crystal structure found in the homochiral salt, $[Au^{I}_4Co^{III}_2(dppe)_2(D\text{-pen})_2](NO_3)_2$, indicating the importance of homochirality.[6,8] The $Au^{I}_4Ni^{II}_2$ complex, $[Au^{I}_4Ni^{II}_2(dppe)_2(D\text{-pen})_4]$, which is a neutral complex, showed the almost same molecular structure as that of $[Au^{I}_4Co^{III}_2(dppe)_2(D\text{-pen})_4]^{2+}$, but has a straight chain structure formed by the hydrogen bonds between amine and carboxylate groups of D-pen, suggesting the importance of the molecular charge (Scheme 1-1, Figures 1-2a, b).[6,9] The $Au^{I}_4Ni^{II}_2$ complex showed an interesting reactivity: the single-crystal-to-single-crystal (SCSC) transformation from the straight chain structure to the helical structure by soaking the crystals in water (Figure 1-2c). The effect of the molecular shape on the metallosupramolecular structure has been studied by the change of a phosphine linker. An analogous gold(I) metalloligand having a triphosphine ligand, $[Au^{I}_3(tdme)(D\text{-Hpen})_3]$ (tdme = 1,1,1-tris(diphenylphosphinomethyl)ethane), led to the discrete multinuclear complexes, $[Au^{I}_6Co^{II}_3(tdme)_2(D\text{-pen})_6]$, $[Au^{I}_6Co^{III}_3(tdme)_2(D\text{-pen})_6]^{3+}$, and $[Au^{I}_3Co^{III}(tdme)(D\text{-pen})_3]$

by the reactions with Co^{II} (Chart 1-2), while in the packing structures did not show the non-alternate arrangement of cationic and anionic species as found in the crystal structure of $[Au^{I}_4Co^{III}_2(dppe)_2(D\text{-}pen)_2](NO_3)_2$.[6,11] Thus, it was clarified that the molecular structures containing tri- or mono-phosphines are very different from those containing dppe ligand. In that circumstance, the study of different metalloligands having a different diphosphine ligand with 2 carbon atoms (C2 linker) is highly desirable to establish the effect of the diphosphine linker on the construction of supramolecular structures and on the finely tuning of their physical properties.

In this thesis, to investigate the effect of a bridging diphosphine ligand on the molecular and metallosupramolecular structures, two kinds of conformationally constrained diphosphines with a C2 linker were used instead of dppe (Scheme 1-2). The constrains originate from two distinct regions of a diphosphine ligand. One is the bridging C2 linker unit (Chapter II and III), and another is the functional group on phosphorus atoms (Chapter IV).

In the Chapter II and III, *trans*-dppee (*trans*-1,2-bis(diphenylphosphino)ethylene) having a vinylene carbon chain (-CH=CH-) was used as the bridging diphosphine ligand instead of dppe. The change from the single bond to the double bond in the C2 linker of diphosphine ligand makes the molecular structure more rigid, which affects the molecular and supramolecular structures of the resulting hexanuclear complexes, $[Au^{I}_4M_2(trans\text{-}dppee)_2(D\text{-}pen)_4]^{n+}$ (M = Co^{III} or Ni^{II}). The synthesis and the coordination behavior of the analogue Au^{I} metalloligand having the *trans*-dppee linker, $[Au^{I}_2(trans\text{-}dppee)(Hpen)_2]$ (H_2[**2**]), toward Co^{II} and Ni^{II} ions were investigated and the effect of chirality was also examined in these Chapters.

The reaction of the homochiral metalloligand (D_2- or L_2-$[\mathbf{2}]^{2-}$) having *trans*-dppee with Co^{II} gave the analogue cationic $Au^{I}_4Co^{III}_2$ complex, $[Au^{I}_4Co^{III}_2(trans\text{-}dppee)_2(D\text{-}pen)_4]^{2+}$. Upon the crystallization with nitrate ions, this complex formed a similar charge-separate aggregation structure like the dppe system. However, small differences were found in the molecular and supramolecular structures. The slight difference in molecular structure made the hydrophilic interstices slightly smaller, which forced the distance between the inorganic anions in the anionic cluster to be shorter with a different orientation of anions.

Treatment of a racemic mixture of the metalloligands (D_2- and L_2-$[\mathbf{2}]^{2-}$) with Co^{II} in the absence of oxidant gave the meso (DDLL) $Au^{I}_4Co^{II}_2$ complex. On the other hand, a similar treatment in the presence of PbO_2 gave not only the meso (DDLL) $Au^{I}_4Co^{III}_2$ complex, but also a homochiral pair (DDDD/LLLL) of $Au^{I}_4Co^{III}_2$ complexes. This chirality-dependent isolation of different oxidation states are discussed, together with

the resulting metallosupramolecular structures.

Reactions of a racemic mixture of the metalloligands (D_2- and L_2-[**2**]$^{2-}$) with Ni^{II} gave three kinds of crystals; homochiral (DDDD) $Au^{I}_4Ni^{II}_2$ hexanuclear, homochiral (DD) $Au^{I}_2Ni^{II}$ trinuclear, and heterochiral (DDLL) $Au^{I}_4Ni^{II}_2$ hexanuclear complexes. The homochiral hexanuclear complex crystallized under acidic conditions, and they were found to incorporate inorganic acids. Of note is that the acid-incorporated crystals can absorb ammonia from both gaseous and aqueous media to neutralize crystals via a single-crystal-to-single-crystal (SCSC) transformation. The removal of basic molecules from the neutralized crystals also occurred with the retention of their single-crystallinity to give the acid-incorporated crystal. The differences in molecular and supramolecular structures and the reaction behavior with the basic molecule were discussed in terms of the diphosphine linker unit (*trans*-dppee or dppe) and the coordinated metal ions (Au^{I}-Co^{III} or Au^{I}-Ni^{II}).

In the Chapter IV, the aliphatic diphosphine, dcpe (1,2-bis(dicyclohexylphosphino)ethane), was used as a bridging ligand instead of dppe (Scheme 1-3). The dcpe ligand has the same alkyl chain as dppe (-CH_2CH_2-), but it has cyclohexyl rings on the phosphorus atoms, instead of the phenyl rings in the dppe ligand. The cyclohexyl rings are larger than phenyl rings, which causes steric hindrance on the conformation of a bridging unit. Moreover, in terms of the interactions, the dcpe ligand lacks the ability to form π···π or CH···π intermolecular interactions as found in the dppe system because there is no π electrons on the cyclohexyl ring. Such differences in the interaction ability may influence on the aggregation behavior. Thus, the metalloligands with dcpe linker unit, D_2, and DL-[Au^{I}_2(dcpe)(Hpen)$_2$] (D_2- and DL-H_2[**12**]), were newly synthesized, and their reactions with Co^{II} or Ni^{II} were investigated. In homochiral system, the reaction with Co^{II} led to the formation of the cationic hexanuclear $Au^{I}_4Co^{III}_2$ complex, $[Au^{I}_4Co^{III}_2(dcpe)_2(D\text{-pen})_4]^{2+}$. The molecular structure of the dcpe complex was topologically the same as that of $[Au^{I}_4Co^{III}_2(dppe)_2(D\text{-pen})_4]^{2+}$, but the hexanuclear $Au^{I}_4Co^{III}_2$ structure with dcpe possessed a metalloring with a bent structure, which is different from that with dppe that has a twisted structure (Chart 1-3). By the reaction with Co^{II} or Ni^{II} in the heterochiral system, the trinuclear complexes ($Au^{I}_2Ni^{II}$, $Au^{I}_2Co^{III}$) with a similar molecular structure were obtained. It was found that the trinuclear structures are composed of meso-metalloligands, but they possess chirality on the metal centers due to the coordination of the metalloligands. Despite their similarity of the molecular structures, the aggregation behaviors were largely different from each other. While the cationic $Au^{I}_2Co^{III}$ complexes crystallized as a racemate, the neutral $Au^{I}_2Ni^{II}$ complexes crystallized in a non-centrosymmetric space group because of the

spontaneous resolution. This is a rare example of spontaneous resolution of discrete complexes with a meso-species. The differences in molecular and supramolecular structures were discussed in terms of diphosphine linker units (dcpe or dppe) and the reacting metal ions (AuCo or AuNi).

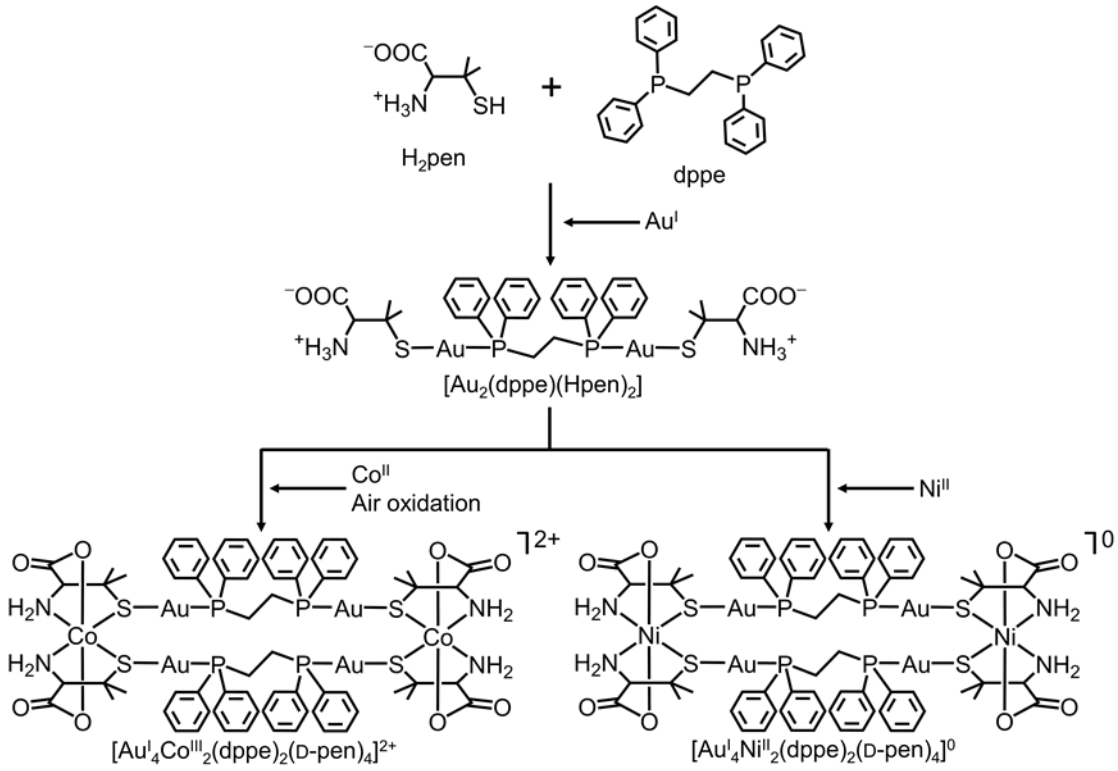

Scheme 1-1. Structures of metalloligand, $[Au_2(dppe)(Hpen)_2]$, penicillamine (H_2pen), and 1,2-bis(diphenylphosphino)ethane (dppe), and the preparation of $[Au_4Co_2(dppe)_2(D\text{-}pen)_4]^{2+}$ and $[Au_4Ni_2(dppe)_2(D\text{-}pen)_4]$ from the metalloligand.

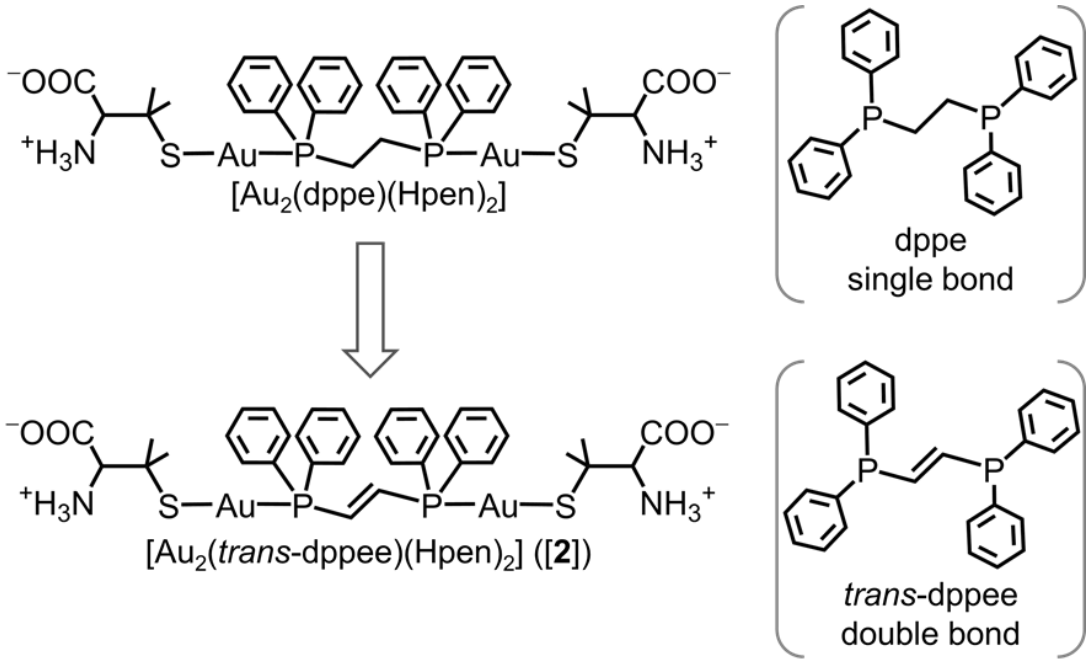

Scheme 1-2. Change of diphosphine linker from dppe to *trans*-dppee.

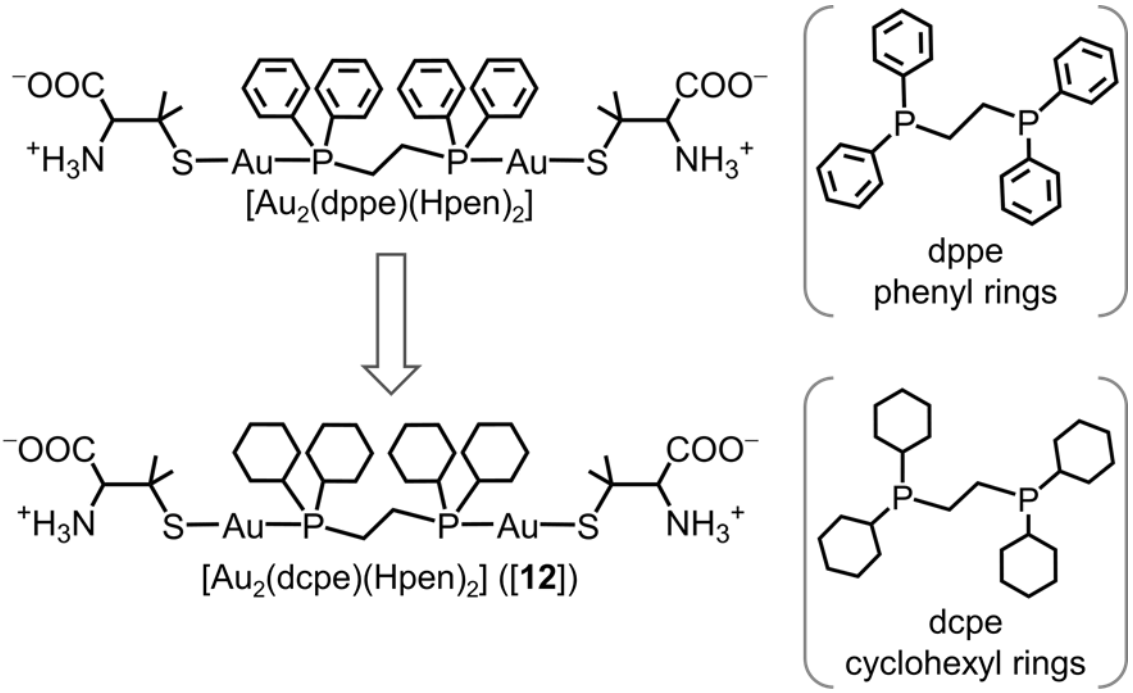

Scheme 1-3. Change of diphosphine linker from dppe to dcpe.

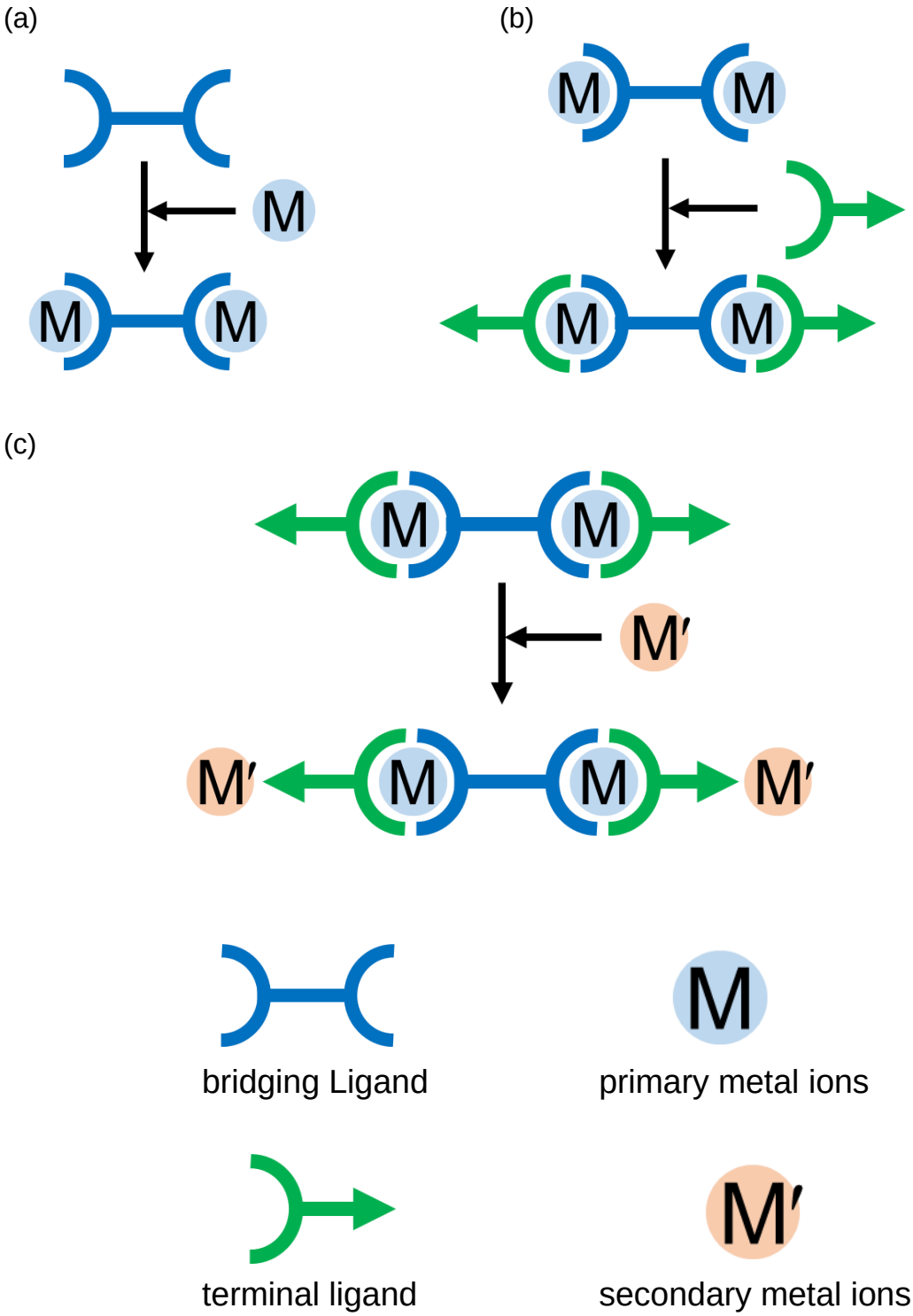

Chart 1-1. Schematic representation of the synthesis of metalloligand composed of bridging ligand and terminal ligands at the step of (a) linking of the metal centers by bridging ligand, (b) the reaction with terminal ligand to give the coordination ability to the molecule to work as metalloligand, and (c) the coordination to secondary metal ions and the construction of the desired multimetallic complex with two kinds of ligands.

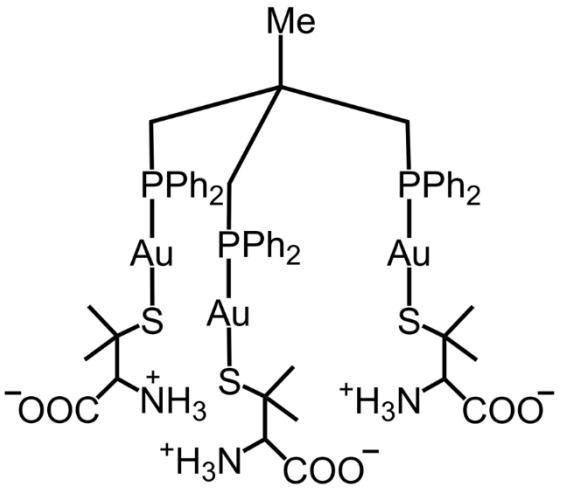

Chart 1-2. Molecular structure of the Au^{I}_{3} triphosphine metalloligand with tdme.

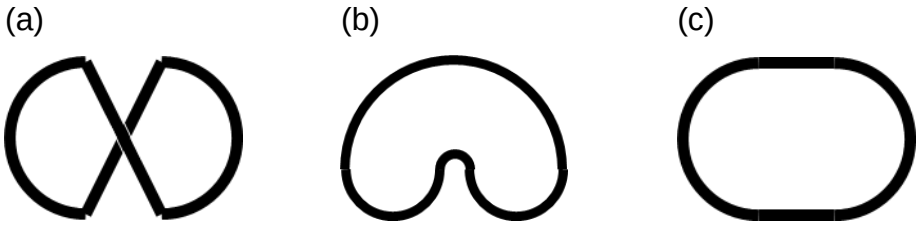

Chart 1-3. Schematic representation of (a) twisted, (b) bent, and (c) normal ring structures.

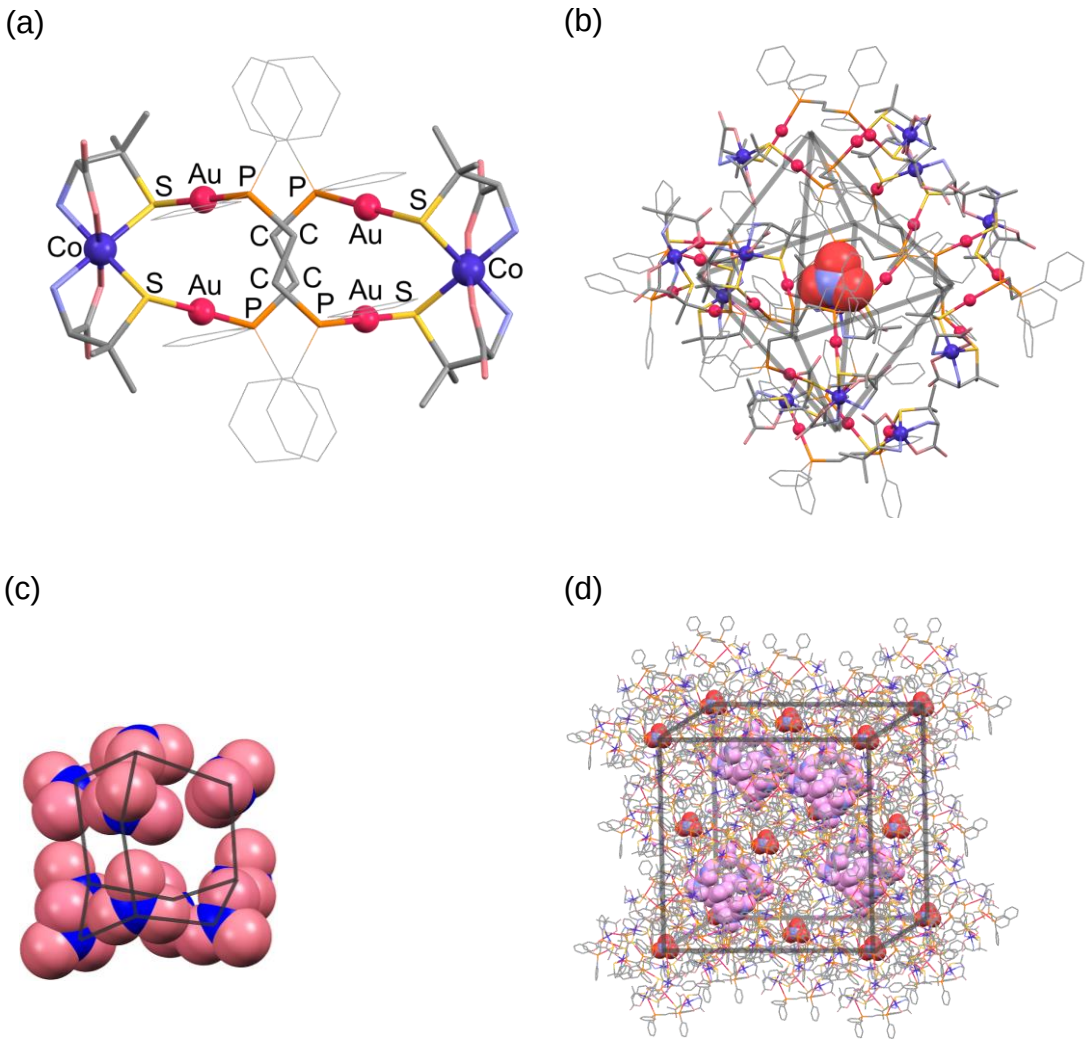

Figure 1-1. Separate aggregation of cations and anions in $[Au^{I}_4Co^{III}_2(dppe)_2(D\text{-pen})_4](NO_3)_2$. (a) Molecular structure of a divalent complex cation $[Au^{I}_4Co^{III}_2(dppe)_2(D\text{-pen})_4]^{2+}$ with a twisted 18-membered metalloring, (b) 6 complex cations are aggregated in an octahedral manner $([Au^{I}_4Co^{III}_2(dppe)_2(D\text{-pen})_4]^{2+})_6$, through intermolecular interactions, accommodating an NO_3^- ion in the center, (c) structure of adamantane-like $(NO_3^-)_{10}$ aggregate in $[Au^{I}_4Co^{III}_2(dppe)_2(D\text{-pen})_4](NO_3)_2$, and (d) face centered cubic (fcc) packing structure of $[Au^{I}_4Co^{III}_2(dppe)_2(D\text{-pen})_4](NO_3)_2$.

(a)

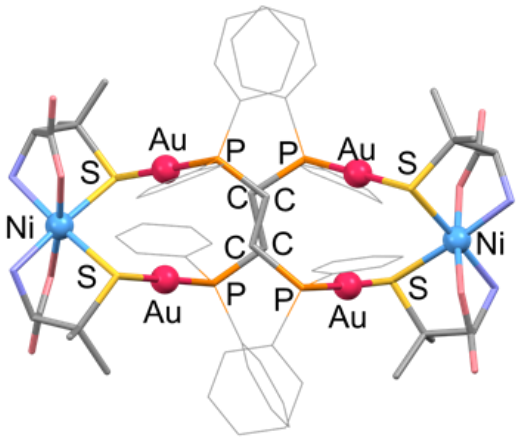

(b)

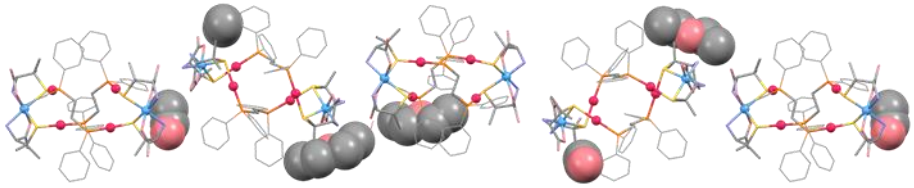

(c)

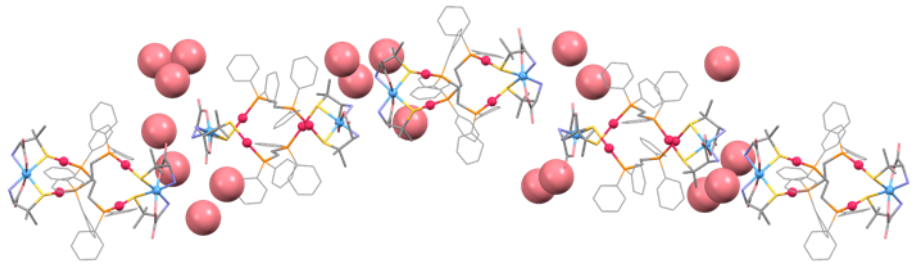

Figure 1-2. Perspective views of $[Au^{I}_{4}Ni^{II}_{2}(dppe)_{2}(D\text{-pen})_{4}]$. (a) Molecular structure of $[Au^{I}_{4}Ni^{II}_{2}(dppe)_{2}(D\text{-pen})_{4}]$, (b) straight linear supramolecular structure of $[Au^{I}_{4}Ni^{II}_{2}(dppe)_{2}(D\text{-pen})_{4}]\cdot 0.5EtOH\cdot 0.5Et_{2}O\cdot 7.25H_{2}O$, and (c) helical supramolecular structure of $[Au^{I}_{4}Ni^{II}_{2}(dppe)_{2}(D\text{-pen})_{4}]\cdot 16H_{2}O$. The molecules shown in space-filling models are the solvent molecules found in the crystal structure (ethanol and diethyl ether molecules for Figure 1-2b and water for Figure 1-2c, respectively).

Chapter II. Coordination Behavior of Digold(I) Metalloligand with *trans*-dppee toward Co^{II}

II-1. Introduction

trans-dppee (*trans*-1,2-bis(diphenylphosphino)ethylene) is a well-known diphosphine ligand that acts as a bridging ligand.[12,13,14,15] This ligand is more rigid than dppe owing to the sp^2 nature of the carbon chain linking two phosphorus atoms, and its rigidity affects the crystal structures strongly.[13] Although *trans*-dppee has been used as a subcomponent of the metalloligands in some cases,[5d,5e,14] no examples of the crystal structures of the supramolecular complexes containing *trans*-dppee have been reported.

Recently, our group reported that the reaction of the metalloligand, $[Au_2(dppe)(D\text{-}Hpen)_2]$, with cobalt(II) in air led to the air oxidization of Co^{II} to Co^{III} to form the divalent complex cation, $[Au^{I}_4Co^{III}_2(dppe)_2(D\text{-}pen)_4]^{2+}$. When the complex was crystallized with a variety of inorganic anions, six complex cations were aggregated in an octahedral manner and 10 monovalent anions were extraordinary aggregated in an adamantane-like structure, constructing a unique separate aggregation of cationic and anionic species.[6,7] Furthermore, the crystallization of Co^{III} complexes with DL-terminal ligands, *i.e.* in heterochiral conditions, caused two kinds of chiral aggregations dependent on the counteranion. By the addition of hexafluorophosphate anion as a counteranions, only heterochiral trinuclear complex cation was crystalized, while the nitrate anion promoted the simultaneous crystallization of two homochiral and one heterochiral crystals.[7c,8]

In this chapter, to investigate the effect of the bridging ligand in the metalloligand not only on the molecular structures but also on the supramolecular structures, *trans*-dppee was used as a bridging ligand instead of dppe. In comparison with dppe, *trans*-dppee has the same C2 linker but the vinylene carbon chain, which is sterically restrained and more rigid. This difference led us to expect a huge effect on the molecular structure and the aggregation behavior of the resulting Au^{I}-Co^{III} complexes. For instance, the fixed *trans* geometry on the linker carbon chain cannot have the chelate coordination mode, which is found in the heterochiral dppe system, $[Au^{I}_2Co^{III}(dppe)(D\text{-}pen)(L\text{-}pen)]^{+}$. Also, the lower solubility of the complex with *trans*-dppee may lead to the precipitation of the novel product which is different from the dppe system.

The reactions of the novel metalloligand, $[Au^{I}_2(trans\text{-}dppee)(D\text{-}Hpen)_2]$ (D_2-H_2[**2**]), with Co^{II} in air gave single-crystals of a divalent hexanuclear $Au^{I}_4Co^{III}_2$ complex cation with several inorganic anions ($[Au^{I}_4Co^{III}_2(trans\text{-}dppee)_2(D\text{-}pen)_4]X_2$ ([**3**]X_2), X_2 = $(NO_3^-)_2$, $(ClO_4^-)_2$, $(BF_4^-)_2$ or SO_4^{2-}). In the crystal, the aggregation behavior was almost the same as those in the $Au^{I}_4Co^{III}_2$ crystals in the dppe system. However, the slight

difference of molecular structures between the *trans*-dppee and dppe system resulted in the different anion arrangement.

The aggregation behavior in the heterochiral system was also studied by mixing D-/L-penicillaminate metalloligands, D_2-H_2[**2**] and L_2-H_2[**2**] or DL-H_2[**2**] in the reaction with Co^{II}. Unexpectedly, the heterochiral $Au^{I}_4Co^{II}_2$ complex, [$Au^{I}_4Co^{II}_2$(*trans*-dppee)$_2$(D-pen)$_2$(L-pen)$_2$] ([**5**]), was isolated by the fast crystallization before air oxidation. Such Co^{II} intermediate species have never been isolated in the dppe system. By adding PbO_2 as an oxidizing agent, the corresponding Co^{III} species, [$Au^{I}_4Co^{III}_2$(*trans*-dppee)$_2$(D-pen)$_2$(L-pen)$_2$]$^{2+}$ ([**6**]$^{2+}$), was obtained but the trinuclear complex, ([$Au^{I}_2Co^{III}$(*trans*-dppee)(D-pen)(L-pen)]$^{+}$), was not formed due to the fixed *trans* geometry.

Experimental Section.

II-2-1. Materials.

All starting materials were commercially available and used without further purification. All experiments were performed in the air.

II-2-2. Preparation of the Metalloligand and AuCo Complexes.

II-2-2-1. [Au_2Cl_2(*trans*-dppee)] ([1]).[15]

A colorless solution containing 0.40 g (1.0 mmol) of *trans*-dppee in $CHCl_3$ (6 mL) and MeOH (1.4 mL) was added to a colorless solution containing 0.84 g (2.1 mmol) of $Na[AuCl_4]\cdot 2H_2O$ and 0.80 g (6.6 mmol) of $S(CH_2CH_2OH)_2$ in MeOH (11 mL) and water (6.7 mL). The solution was stirred at room temperature for 1 h in the dark. The resulting white precipitate of [**1]** was collected by filtration and washed with water and EtOH. Yield: 0.76 g (88%). IR spectrum (cm^{-1}, KBr disk): 1436 ($\nu_{P\text{-}Ph}$), 1103, and 743-691 (ν_{Ph}). ^1H NMR spectrum in $CDCl_3$ (δ, ppm from TMS): 7.72-7.46 (m, 20H), 7.21-7.11 (t, 2H).

II-2-2-2a. [Au_2(*trans*-dppee)(D-Hpen)$_2$] (D$_2$-H$_2$[2]).

To a white suspension containing 1.20 g (1.4 mmol) of [**1**] in EtOH (600 mL) was added 0.48 g (3.2 mmol) of D-H_2pen and 0.1 M aqueous NaOH solution (32 mL). The mixture was stirred at room temperature for 1.5 h in the dark to give a colorless solution, the resulting solution of D$_2$-H$_2$[**2**] was evaporated to dryness and washed with water and EtOH. Yield: 1.4 g (86%). Anal. Calcd for $[Au_2$(*trans*-dppee)(D-Hpen)$_2]\cdot 4.5H_2O$ = $Au_2C_{36}H_{51}N_2O_{8.5}P_2S_2$: C, 37.03; H, 4.40; N, 2.40%. Found: C, 36.99; H, 4.22; N, 2.38%. IR spectrum (cm^{-1}, KBr disk): 1625 (ν_{CO}), 1102, and 748-692 (ν_{Ph}). ^1H NMR spectrum in CD_3OD (δ, ppm from TMS): 7.68-7.64 (m, 8H), 7.58-7.53 (m, 12H), 7.33-7.25 (t, 2H), 3.51 (s, 2H), 1.75 (s, 6H), 1.39 (s, 6H). ^{31}P NMR spectrum in CD_3OD (δ, ppm from 85% H_3PO_4) 32.9 (s). Colorless crystals of D$_2$-H$_2$[**2**] were obtained by standing the reaction solution for a week in draft.

II-2-2-2b. [Au_2(*trans*-dppee)(L-Hpen)$_2$] (L$_2$-H$_2$[2]).

To a white suspension containing 0.40 g (0.46 mmol) of [**1**] in EtOH (200 mL) was added 0.16 g (1.1 mmol) of L-H_2pen and 0.1 M aqueous NaOH solution (10.6 mL). The mixture was stirred at room temperature for 2 h in the dark to give a colorless solution. The resulting solution of L$_2$-H$_2$[**2]** was evaporated to dryness and washed with water and EtOH. Yield: 0.27 g (50%). Anal. Calcd for $[Au_2$(*trans*-dppee)(L-Hpen)$_2]\cdot 4.5H_2O$ = $Au_2C_{36}H_{51}N_2O_{8.5}P_2S_2$: C, 37.03; H, 4.40; N, 2.40%. Found: C, 37.05; H, 4.13; N, 2.43%. IR spectrum (cm^{-1}, KBr disk): 1623 (ν_{CO}), 1102, and 742-693 (ν_{Ph}). ^1H NMR spectrum

in CD_3OD (δ, ppm from TMS): 7.69-7.65 (m, 8H), 7.59-7.55 (m, 12H), 7.36-7.28 (t, 2H), 3.52 (s, 2H), 1.75 (s, 6H), 1.40(s, 6H).

II-2-2-3a. [Au_4Co_2(*trans*-dppee)$_2$(D-pen)$_4$]$(NO_3)_2$ ([3]$(NO_3)_2$).

Method A. To a white suspension containing 0.10 g (0.085 mmol) of D_2-H_2[**2**] in MeOH (10 mL) was added 0.025 g (0.10 mmol) of $Co(OAc)_2{\cdot}4H_2O$, which was stirred at room temperature for 1 h. A $NaNO_3$ aqueous solution (1 M, 0.1 mL) was added to the resulting orange solution. Purple crystals of [**3**]$(NO_3)_2$ appeared by slow evaporation at room temperature for 3 weeks, which were collected by filtration and washed with water and MeOH. Yield: 0.090 g (80%). Anal. Calcd for [Au_4Co_2(*trans*-dppee)$_2$(D-pen)$_4$]$(NO_3)_2{\cdot}9H_2O$ = $C_{72}H_{104}Au_4Co_2N_6O_{26}P_4S_4$: C, 33.60; H, 3.84; N, 3.27%. Found: C, 33.42; H, 3.79; N, 3.26%. IR spectrum (cm^{-1}, KBr disk): 1654 (ν_{CO}), 1384 (ν_{NO3^-}), and 748-692 (ν_{Ph}). ^1H NMR spectrum in CD_3OD/D_2O (1:2) (δ, ppm from TMS): 7.66-7.44 (m, 22), 3.94 (s, 2H), 1.80 (s, 6H), 1.40 (s, 6H).

Method B. To a white suspension containing 0.10 g (0.085 mmol) of D_2-H_2[**2**] in EtOH (10 mL) was added 0.029 g (0.10 mmol) of $Co(NO_3)_2{\cdot}6H_2O$. The mixture was stirred at room temperature for 2 h in the dark to give an orange solution. The solution was stood at room temperature in the dark for 4 days. The resulting purple crystals of [**3**]$(NO_3)_2$ were collected by filtration and washed with water and EtOH. Yield: 0.042 g (37%). IR spectrum (cm^{-1}, KBr disk): 1655 (ν_{CO}), 1385 (ν_{NO3^-}), and 748-691 (ν_{Ph}).

II-2-2-3b. [Au_4Co_2(*trans*-dppee)$_2$(D-pen)$_4$]$(ClO_4)_2$ ([3]$(ClO_4)_2$).

To a white suspension containing 0.050 g (0.042 mmol) of D_2-H_2[**2**] in MeOH (7.5 mL) was added 0.012 g (0.049 mmol) of $Co(OAc)_2{\cdot}4H_2O$, which was stirred at room temperature for 30 min. A $NaClO_4$ aqueous solution (0.5 M, 0.1 mL) was added to the resulting orange solution. Purple crystals of [**3**]$(ClO_4)_2$ appeared by slow evaporation at room temperature for 8 weeks, which were collected by filtration and washed with water and EtOH. Yield: 0.023 g (43%). Anal. Calcd for [Au_4Co_2(*trans*-dppee)$_2$(D-pen)$_4$]$(ClO_4)_2{\cdot}7H_2O$ = $C_{72}H_{94}Au_4Cl_2Co_2N_4O_{23}P_4S_4$: C, 33.10; H, 3.63; N, 2.14%. Found: C, 33.07; H, 3.68; N, 2.27%. IR spectrum (cm^{-1}, KBr disk): 1656 (ν_{CO}), 1103 (ν_{ClO4^-}), and 748-692 (ν_{Ph}).

II-2-2-3c. [Au_4Co_2(*trans*-dppee)$_2$(D-pen)$_4$]$(BF_4)_2$ ([3]$(BF_4)_2$).

To a white suspension containing 0.050 g (0.042 mmol) of D_2-H_2[**2**] in MeOH (7.5 mL) was added 0.013 g (0.050 mmol) of $Co(OAc)_2{\cdot}4H_2O$, which was stirred at room temperature for 1 h. A KPF_6 aqueous solution (0.5 M, 0.1 mL) was added to the resulting

orange solution. Purple crystals of [**3**]$(BF_4)_2$ appeared by slow evaporation at room temperature for 2 weeks, which were collected by filtration and washed with water and MeOH. Yield: 0.015 g (71%). Anal. Calcd for [Au_4Co_2(*trans*-dppee)$_2$(D-pen)$_4$]$(BF_4)_2\cdot 9H_2O$ = $C_{72}H_{98}Au_4B_2Co_2F_8N_4O_{17}P_4S_4$: C, 32.97; H, 3.77; N, 2.14%. Found: C, 32.99; H, 3.74; N, 2.33%. IR spectrum (cm^{-1}, KBr disk):1653 (ν_{CO}), 1103 (ν_{BF4^-}), and 747-692 (ν_{Ph}).

II-2-2-4. [Au_4Co_2(*trans*-dppee)$_2$(D-pen)$_4$]SO_4 ([3]SO_4).

An orange solution containing 0.050 g (0.044 mmol) of D$_2$-H_2[**2**] and 0.014 g (0.055 mmol) of $Co(OAc)_2\cdot 4H_2O$ in MeOH (5 mL) was stirred at room temperature for 1 h, to which was added a $KHSO_4$ aqueous solution (0.1 M, 0.45 mL). Purple precipitate of [**3**]SO_4 were obtained from the resulting white suspension by slow evaporation at room temperature for 1 month. They were collected by filtration and washed with water. Yield 0.024 g (34 %). The crystals suitable for X-ray analysis were obtained by similar method in a different batch, but the yield was very low. Anal. Calcd for [Au_4Co_2(*trans*-dppee)$_2$(D-pen)$_4$]$SO_4\cdot 8H_2O$ = $C_{72}H_{96}Au_4Co_2N_4O_{20}P_4S_5$: C, 33.21; H, 3.83; N, 2.22%. Found: C, 34.08; H, 3.73; N, 2.11%. IR spectrum (cm^{-1}, KBr disk): 1656 (ν_{CO}), 1103 ($\nu_{SO4^{2-}}$), and 748-692 (ν_{Ph}).

II-2-2-5. [Au_4Co_2(*trans*-dppee)$_2$(L-pen)$_4$]$(NO_3)_2$ ([4]$(NO_3)_2$).

To a white suspension containing 0.050 g (0.044 mmol) of L$_2$-H_2[**2**] in MeOH (4 mL) was added 0.012 g (0.047 mmol) of $Co(OAc)_2\cdot 4H_2O$ and 25 mg (0.11 mmol) of PbO_2, which was stirred at room temperature for 80 min. A $NaNO_3$ aqueous solution (1 M, 0.06 mL) was added to the resulting purple suspension, and the suspension was filtered to remove PbO_2. The purple crystals of [**4**]$(NO_3)_2$ were obtained by slow evaporation of the filtrate at room temperature for a week. They were collected by filtration and washed with water and MeOH. Yield 0.025 g (45%). IR spectrum (cm^{-1}, KBr disk): 1653 (ν_{CO}), 1385 (ν_{NO3^-}), and 747-691 (ν_{Ph}).

II-2-2-6. [Au_2(*trans*-dppee)(D-Hpen)(L-Hpen)] (DL-H_2[2])

To a white suspension containing 0.30 g (0.35 mmol) of [**1**] in EtOH (150 mL) was added 0.12 g (0.80 mmol) of DL-H_2pen and 0.5 M aqueous NaOH solution (1.6 mL). The mixture was stirred at room temperature for 1.5 h in the dark to give a white suspension. The resulting white powder of DL-H_2[**2**] was collected by filtration and washed with water. From the filtrate, white crystalline powder of DL-H_2[**2**] was obtained again by slow evaporation at room temperature for a month. Total yield: 0.10 g (23%). Anal. Calcd for

[Au_2(*trans*-dppee)(Hpen)$_2$]·6.5H_2O = $Au_2C_{36}H_{55}N_2O_{10.5}P_2S_2$: C, 35.92; H, 4.60; N, 2.33%. Found: C, 35.70; H, 4.29; N, 2.32%. IR spectrum (cm^{-1}, KBr disk): 1625 (ν_{CO}), 1101, and 745-692 (ν_{Ph}). ^1H NMR spectrum in CD_3OD (δ, ppm from TMS): 7.68-7.64(m, 8H), 7.55-7.53 (m, 12H), 7.36 (t, 2H), 1.69 (s, 6H), 1.33 (s, 6H). Colorless crystals of DL-H_2[**2**] were obtained by recrystallization from EtOH/water (1:1) with adding $Mg(OAc)_2$.

II-2-2-7. Reaction of the metalloligand with Co^{II} in heterochiral condition.

Method A. To a white suspension containing 0.030 g (0.026 mmol) of D$_2$-H_2[**2**] and 0.030 g (0.026 mmol) of L$_2$-H_2[**2**] in MeOH (2 mL) was added 0.015 g (0.060 mmol) of $Co(OAc)_2·4H_2O$, which gave an orange solution with a small amount of white precipitate. After decantation, the resulting solution was stood at room temperature overnight to afford orange platelet crystals of [**5**], which were collected by filtration and washed with water and MeOH. Yield: 0.033 g (54%). Anal. Calcd for [$Au^I_4Co^{II}_2$(*trans*-dppee)$_2$ (D-pen)$_2$(L-pen)$_2$]·7H_2O = $C_{72}H_{94}N_4Au_4Co_2O_{15}P_4S_4$: C, 35.83; H, 3.93; N, 2.32%. Found: C, 35.58; H, 3.74; N, 2.34%. IR spectrum (cm^{-1}, KBr disk): 1598 (ν_{CO}), 748-694 (ν_{Ph}).

Method B. To a white suspension containing 0.050 g (0.042 mmol) of D$_2$-H_2[**2**] and 0.050 g (0.042 mmol) of L$_2$-H_2[**2**] in EtOH (5 mL) and water (5 mL) was added 0.025 g (0.10 mmol) of $Co(OAc)_2·4H_2O$ to give an orange solution. The orange block crystals of [**5**]' were obtained by slow evaporation at room temperature for a week, which were collected by filtration and washed with water and EtOH. Yield: 0.051 g (50%). IR spectrum (cm^{-1}, KBr disk): 1598 (ν_{CO}) and 748-694 (ν_{Ph}).

II-2-2-8. Reaction of the metalloligand with Co^{II} and PbO_2 in heterochiral condition.

Method A. To a white suspension containing 0.015 g (0.013 mmol) of D$_2$-H_2[**2**] and 0.015 g (0.013 mmol) of L$_2$-H_2[**2**] in EtOH (2 mL) was added 0.007 g (0.029 mmol) of $Co(OAc)_2·4H_2O$ in water (1 mL). To the resulting orange solution was added 0.020 g (0.083 mmol) of PbO_2, and stirred at room temperature for 4 h. After filtration of unreacted PbO_2, 0.5 M $NaNO_3$ aqueous solution (0.12 mL) was added to the resulting brown solution. The solution was divided into four vials. Purple triangular crystals of [**3**]$(NO_3)_2$ and [**4**]$(NO_3)_2$ together with purple platelet crystals of [**6**]$(NO_3)_2$ were grown by slow evaporation at room temperature for a week in three vials, whereas only the platelet crystals of [**6**]$(NO_3)_2$ were obtained in another vial.

Method B. To a white suspension containing 0.030 g (0.026 mmol) of D$_2$-H_2[**2**] and 0.030 g (0.026 mmol) of L$_2$-H_2[**2**] in *t*-BuOH (2.4 mL) was added 0.020 g (0.080 mmol) of $Co(OAc)_2·4H_2O$ in water (0.6 mL). To the resulting orange solution was added 0.020 g

(0.083 mmol) of PbO_2, which was stirred for 30 min. After filtration of unreacted PbO_2, a $NaNO_3$ aqueous solution (0.5 M, 0.3 mL) was added to the resulting brown solution. Only the purple platelet crystals of [**6**]$(NO_3)_2$ were obtained by slow evaporation at room temperature for 2 days. The crystals were collected by filtration and washed with water. Yield: 0.011 g (15%). Anal. Calcd for $[Au^{I}_4Co^{III}_2$(*trans*-dppee)$_2$(D-pen)$_2$ (L-pen)$_2$]$(NO_3)_2\cdot 14H_2O = C_{72}H_{108}N_6Au_4Co_2O_{28}P_4S_4$: C, 32.47; H, 4.09; N, 3.16%. Found: C, 32.31; H, 3.93; N, 2.99%. IR spectrum (cm^{-1}, KBr disk): 1650 (ν_{CO}), 1385 (ν_{NO3^-}), and 747-693 (ν_{Ph}). ^{1}H NMR spectrum in CD_3OD/D_2O (1:2) (δ, ppm from TMS): 7.67-7.22 (m, 22), 3.99 (s, 1H), 3.95 (s, 1H), 1.98 (s, 3H), 1.87 (s, 3H), 1.51 (s, 3H), 1.41 (s, 3H).

Method C. To a white suspension containing 0.050 g (0.042 mmol) of DL-H_2[**2**] and in 1:1 mixture of EtOH and water (10 mL) was added 0.012 g (0.049 mmol) of $Co(OAc)_2\cdot 4H_2O$. To the resulting orange solution was added 0.015 g (0.063 mmol) of PbO_2, which was stirred for 1 h. After filtration of unreacted PbO_2, a NH_4PF_6 aqueous solution (0.1 M, 0.75 mL) was added to the resulting purple solution. The purple platelet crystals of [**6**]$(PF_6)_2$ were obtained by slow evaporation at room temperature for 4 days. The crystals were obtained by separating white cloudy precipitate, and collected by filtration and washed with water. Yield: 0.022 g (37%). Anal. Calcd for $[Au^{I}_4Co^{III}_2$(*trans*-dppee)$_2$(D-pen)$_2$(L-pen)$_2$]$(PF_6)_2\cdot 11H_2O$ = $C_{72}H_{102}N_4Au_4Co_2O_{19}F_{12}P_6S_4$: C, 31.16; H, 3.72; N, 2.06%. Found: C, 31.16; H, 3.70; N, 2.02%. IR spectrum (cm^{-1}, KBr disk): 1647 (ν_{CO}), 842 (ν_{PF6^-}), and 747-693 (ν_{Ph}).

II-2-3 Physical measurements.

The elemental analyses (C/H/N) were performed at Osaka University using a YANACO CHN Coda MT-5 and MT-6 analyzers. The IR spectra were recorded on a JASCO FT/IR-4100 infrared spectrometer using a KBr disk at room temperature. The electric absorption spectra were recorded on a JASCO V-660 spectrometer, and the CD spectra were recorded on a JASCO J-840 spectropolarimeter using a 1 cm quartz cell at room temperature. Diffuse reflection spectra were recorded on a JASCO V-570 spectrometer, and the solid CD spectra were recorded on a JASCO J-840 or a JASCO J-820 spectropolarimeter at room temperature. The ^{1}H and ^{31}P NMR spectra were recorded with a JEOL GSX400 (400 MHz), JEOL ECS400 (400 MHz), or JEOL ECA500 (500 MHz) spectrometer at room temperature, using tetramethylsilane (TMS) as the internal standard for ^{1}H and 85% H_3PO_4 as the external standard for ^{31}P. The X-ray fluorescence spectrometries were performed on HORIBA MESA-500 spectrometer or SHIMADZU EDX-720. The emission and excitation spectra were recorded on a JASCO FP-8500 spectrofluorometer at 77K. The ESR spectrum was recorded on JEOL JES-FA200 at 4K.

High-quality powder X-ray diffraction patterns were recorded at room temperature in transmission mode [synchrotron radiation, λ = 0.999698(2) Å; 2θ range = 0–78°; step width = 0.01°; data collection time = 1 min] with a diffractometer equipped with a white imaging plate detector at the SPring-8 BL02B2 beamline; these experiments were conducted with the approval of the Japan Synchrotron Radiation Research Institute (JASRI). The crystals were placed into 0.3 mm glass capillary tubes, which were rotated during the measurements. The diffraction patterns were collected with a large Debye-Scherrer camera. The powder simulation patterns were generated from the single-crystal X-ray structures using the Mercury 3.5.1 program.

II-2-4 X-ray Structural Determination.

The single-crystal X-ray diffraction measurements for D-H_2[**2**], [**3**]$(NO_3)_2$, [**3**]$(ClO_4)_2$, [**3**]$(BF_4)_2$, [**3**]SO_4, [**4**]$(NO_3)_2$, DL-H_2[**2**], [**5**], and [**5**]' were performed on a Rigaku RAXIS VII imaging plate and Vari-Max with graphite monochromated Mo-Kα radiation (λ = 0.71075 Å) at 200 K. The intensity data were collected by the ω-scan technique and empirically corrected for absorption. The single-crystal X-ray diffraction measurements for [**6**]$(NO_3)_2$ and [**6**]$(PF_6)_2$ were performed at 100 K with a Rigaku Mercury 2 CCD detector with synchrotron radiation (λ =0.7000 Å) at the BL02B1 beamline in "SPring-8," with the approval of the Japan Synchrotron Radiation Research Institute (JASRI).

The collected diffraction data were processed with the Rapid Auto software program. The structures of the complexes were solved via direct methods using the SHELXS2014 program.[16a,d] The structure refinements were carried out using full-matrix least-squares (SHELXL2014).[16a,d] All calculations were performed using the Yadokari-XG software package.[16b] The interstices' volumes were calculated using SQUEEZE in the PLATON package.[16c]

For D-H_2[**2**], 2 complex molecules, and 14 water molecules were crystallographically independent. All non-hydrogen atoms except the O atoms of water molecules were refined anisotropically. Hydrogen atoms were included in calculated positions except those of water molecules.

For [**3**]$(NO_3)_2$, a half of $[Au^I_4Co^{III}_2$(*trans*-dppee$)_2$(D-pen$)_4]^{2+}$ units, water, and disordered NO_3^- molecules were crystallographically independent. One of the vinylene linker and 2 phenyl rings were disordered. All non-hydrogen atoms except the C atoms of the disordered region, N atoms of nitrate molecules, and O atoms of nitrate and water molecules were refined anisotropically. Hydrogen atoms were included in calculated positions except those of water molecules. DFIX restrains were used to model nitrate anions.

For [**3**]$(ClO_4)_2$, a half of $[Au^I_4Co^{III}_2(trans\text{-dppee})_2(D\text{-pen})_4]^{2+}$ units, water, and disordered ClO_4^- molecules were crystallographically independent. One of the vinylene linker and 2 phenyl rings were disordered. All non-hydrogen atoms except the C atoms of the disordered region, Cl atoms of perchlorate molecules, and O atoms of perchlorate and water molecules were refined anisotropically. Hydrogen atoms were included in calculated positions except those of water molecules. DFIX restrains were used to model perchlorate anions.

For [**3**]$(BF_4)_2$, a half of $[Au^I_4Co^{III}_2(trans\text{-dppee})_2(D\text{-pen})_4]^{2+}$ units, water, and disordered BF_4^- molecules were crystallographically independent. All non-hydrogen atoms except the C atoms of one of the phosphine linkers, O atoms of water molecules, B atoms and F atoms of tetrafluoroborate anions were refined anisotropically. Hydrogen atoms were included in calculated positions except those of water molecules. DFIX restrains were used to model tetrafluoroborate anions.

For [**3**]SO_4, a half of $[Au^I_4Co^{III}_2(trans\text{-dppee})_2(D\text{-pen})_4]^{2+}$ units, water, and disordered SO_4^{2-} molecules were crystallographically independent. One of the vinylene linker and 2 phenyl rings were disordered. All non-hydrogen atoms except the C atoms of the disordered region, S atoms of sulfate molecule, and O atoms of sulfate and water molecules were refined anisotropically. Hydrogen atoms were included in calculated positions except those of water molecules. DFIX restrains were used to model sulfate anions.

For [**4**]$(NO_3)_2$, a half of $[Au^I_4Co^{III}_2(trans\text{-dppee})_2(L\text{-pen})_4]^{2+}$ units, water, and disordered NO_3^- molecules were crystallographically independent. One of the vinylene linker was disordered. All non-hydrogen atoms except the C atoms of the disordered region, N atoms of nitrate molecules and O atoms of nitrate and water molecules were refined anisotropically. Hydrogen atoms were included in calculated positions except those of water molecules. DFIX restrains were used to model nitrate anions.

For DL-H_2[**2**], two halves of $[Au^I_2(trans\text{-dppee})(D\text{-Hpen})(L\text{-Hpen})]$ unit, water molecules, and ethanol molecules were crystallographically independent. One of the carboxylate group and amine group were disordered. All non-hydrogen atoms except the C atoms of solvent molecules and atoms of disordered groups and solvent molecules were refined anisotropically. Hydrogen atoms were included in calculated positions except those of water molecules.

For [**5**], a half of $[Au^I_4Co^{II}_2(trans\text{-dppee})_2(D\text{-pen})_4(L\text{-pen})_4]$ units, water molecules, and methanol molecules were crystallographically independent. All non-hydrogen atoms except the C atoms and O atoms of solvent molecules were refined anisotropically. Hydrogen atoms were included in calculated positions except those of water molecules.

For [**5**]', one $[Au^{I}_4Co^{II}_2(\textit{trans}\text{-dppee})_2(\text{D-pen})_4(\text{L-pen})_4]$ units, an ethanol molecule, and water molecules were crystallographically independent. All non-hydrogen atoms except the C atoms and O atoms of solvent molecules were refined anisotropically. Hydrogen atoms were included in calculated positions except those of water molecules.

For [**6**]$(NO_3)_2$, one half of $[Au^{I}_4Co^{III}_2(\textit{trans}\text{-dppee})_2(\text{D-pen})_4(\text{L-pen})_4]^{2+}$ unit, one disordered nitrate anion, and disordered water molecules were crystallographically independent. All non-hydrogen atoms except the N atoms of the anions, and O atoms of anions and water molecules were refined anisotropically. Hydrogen atoms were included in calculated positions except those of water molecules. DFIX restrains were used to model nitrate anions and several water molecules.

For [**6**]$(PF_6)_2$, a half of $[Au^{I}_4Co^{III}_2(\textit{trans}\text{-dppee})_2(\text{D-pen})_4(\text{L-pen})_4]^{2+}$ unit, one hexafluorophosphate anion, disordered water molecules, and disordered ethanol molecules were crystallographically independent. All non-hydrogen atoms except the C and O atoms of solvent molecules were refined anisotropically. Hydrogen atoms were included in calculated positions except those of water molecules. DFIX restrains were used to model several water and ethanol molecules.

II-3. Results and Discussion.

II-3-1. Synthesis and Characterization of [Au$_2$(*trans*-dppee)(D-Hpen)$_2$] and [Au$_2$(*trans*-dppee)(L-Hpen)$_2$] (D$_2$-H$_2$[2], L$_2$-H$_2$[2]).

Reaction of [Au$_2$Cl$_2$(*trans*-dppee)][15] with D-H$_2$pen and NaOH in a 1:2:2 ratio in EtOH/water at room temperature gave a colorless solution, from which white powder (D$_2$-H$_2$[**2**]) was isolated by evaporation to dryness (Scheme 2-1). The crystals of D$_2$-H$_2$[**2**] were obtained by standing the reaction solution for a week. Because the ^{1}H NMR and IR spectra of the powder were similar to those of the crystals of D$_2$-H$_2$[**2**], the powder was used for the subsequent reaction. X-ray fluorescence spectroscopy indicated that D$_2$-H$_2$[**2**] contains Au atom and its elemental analytical data was in agreement with the formula for a 1:2 adduct of [Au$_2$(*trans*-dppee)]$^{2+}$ and D-Hpen. In the IR spectrum, a C=O stretching band for deprotonated carboxylate groups of D-pen at 1618 cm^{-1}, P-Ph stretching band at 1100 cm^{-1} and Ph bands at 742-693 cm^{-1} were observed (Figure 2-1).[17] The ^{1}H NMR spectrum in CD$_3$OD showed one set of proton signals at δ 1.45 and 1.80 ppm assigned to methyl groups of D-pen, δ 3.56 ppm assigned to the methine group of D-pen, δ 7.31-7.38 ppm assigned to the vinylene group of *trans*-dppee, and δ 7.59-7.63, 7.69-7.73 ppm assigned to phenyl groups of *trans*-dppee. The integration ratio suggested that D-pen and *trans*-dppee exist in a 1:2 ratio in D$_2$-H$_2$[**2**] (Figure 2-2). The ^{31}P NMR spectrum in CD$_3$OD showed a singlet signal at δ 32.9 ppm (Figure 2-3). The absorption spectrum of D$_2$-H$_2$[**2**] in MeOH showed no significant bands in the visible region (Figure 2-4). Its CD spectrum showed a positive band at 301 nm and negative bands at 276 and 227 nm (Figure 2-4). This complex exhibited a weak orange luminescence under UV light irradiation at room temperature. Solid-state emission spectrum of D$_2$-H$_2$[**2**] at 77 K gave emission bands at 435 nm with a vibrational substructure (Figure 2-5). Single-crystal X-ray analysis revealed that the complex molecule was comprised of two D-Hpen ligands bridged by one [Au$_2$(*trans*-dppee)]$^{2+}$ moiety through S atoms, giving a linear structure of [Au$_2$(*trans*-dppee)(D-Hpen–*S*)$_2$] (*vide infra*).

The metalloligand L$_2$-H$_2$[**2**], which was an enantiomeric isomer of D$_2$-H$_2$[**2**] was obtained by the similar reaction using L-H$_2$pen instead of D-H$_2$pen. X-ray fluorescence spectroscopic data, IR spectrum (Figure 2-1), and ^{1}H NMR spectrum in CD$_3$OD (Figure 2-2) were coincident with those of similar to D$_2$-H$_2$[**2**]. Its CD spectrum showed an opposite pattern to D$_2$-H$_2$[**2**], showing a negative band at 305 nm and a positive band at 277 nm (Figure 2-6). These results support that L$_2$-H$_2$[**2**] was the enantiomer of D$_2$-H$_2$[**2**].

II-3-2. Crystal Structure of the Homochiral Metalloligand, D$_2$-H$_2$[2].

Crystal structure of D$_2$-H$_2$[**2**] was determined by single-crystal X-ray crystallography.

Molecular and packing structures are shown in Figures 2-7, 2-8, and 2-9. The crystallographic data are summarized in Table 2-1, and the selected bond distances and angles are listed in Table 2-2. Crystal D$_2$-H$_2$[**2**] contained two [Au$_2$(*trans*-dppee) (D-Hpen)$_2$] units and 14 solvated water molecules in the asymmetric unit. The complex molecule was comprised of two D-Hpen and one [Au$_2$(*trans*-dppee)]$^{2+}$ moieties. Similar to the dppe analog, [Au$_2$(dppe)(D-Hpen)$_2$], two D-Hpen ligands were bridged by one [Au$_2$(*trans*-dppee)]$^{2+}$ moiety through S atoms, giving a linear structure of [Au$_2$(*trans*-dppee)(D-Hpen–*S*)$_2$]. Each Au atom was in a PS linear coordination geometry bound by one D-pen and one *trans*-dppee (Av. Au–S = 2.30 Å, Au–P = 2.26 Å, and P–Au–S = 177.9°). The C–C distances of the vinylene linker (Av. C–C = 1.31 Å) were shorter than those of dppe analogous compound (Av. C–C =1.55 Å), and the P–C–C angles of the vinylene linkers (Av. P–C–C = 124.8°) were larger compared with those of [Au$_2$(dppe)(D-Hpen)$_2$] (Av. P–C–C = 109.5°), because of the sp^2 character of the vinylene linker. These structural differences between the diphosphine units caused the different lengths of the diphosphine metalloligands (Av. intramolecular P···P = 4.41 Å for D$_2$-H$_2$[**2**], 4.50 Å for [Au$_2$(dppe)(D-Hpen)$_2$]; Table 2-3, Scheme 2-2). In packing structure of D$_2$-H$_2$[**2**], two complex molecules were connected to each other through Au···Au interactions (Av. Au···Au = 3.09 Å) to form a discrete dimeric structure, which was different from the linear chain packing structure found in the dppe analogous compound (Figure 2-8). The dimers were further linked by hydrogen bonds between the carboxylate and amine groups (Av. N···O = 2.83 Å) to form a 1D chain packing structure (Figures 2-8, 2-9).

II-3-3. Synthesis and Characterization of [Au$_4$Co$_2$(*trans*-dppee)$_2$(D-pen)$_4$]X$_2$ ([3]X$_2$) (X = NO$_3^-$, ClO$_4^-$, BF$_4^-$).

Reaction of multidentate-functionalized D$_2$-H$_2$[**2**] with Co(OAc)$_2$·4H$_2$O in a 1:1 ratio in MeOH at room temperature gave an orange solution, which was stood for 3 weeks after the addition of aqueous NaNO$_3$. Purple crystals with a trigonal-pyramid shape ([**3**](NO$_3$)$_2$) were isolated from the resulting brown solution (Scheme 2-3). Reaction with Co(NO$_3$)$_2$·6H$_2$O in EtOH without the addition of nitrate anions also afforded the crystals of [**3**](NO$_3$)$_2$. X-ray fluorescence spectroscopy indicated the presence of Au and Co atoms in [**3**](NO$_3$)$_2$, and its elemental analytical data was in agreement with a formula consisting of [Au$_2$(*trans*-dppee)(D-pen)$_2$]$^{2-}$ (D$_2$-[**2**]$^{2-}$) , Co^{3+}, and NO$_3^-$ in a 1:1:1 ratio. In the IR spectrum, a C=O stretching band for deprotonated carboxylate groups of D-pen at 1654 cm^{-1}, an N–O stretching band for nitrate anion at 1384 cm^{-1}, and Ph bands at 748-692 cm^{-1} were observed (Figure 2-10). The crystals of [**3**](NO$_3$)$_2$ were slightly soluble in MeOH but insoluble in other common solvents. The ^{1}H NMR spectrum in CD$_3$OD/D$_2$O

(1:2) showed one set of proton signals at δ 1.40 and 1.80 ppm assignable to methyl groups of D-pen, δ 3.94 ppm assignable to the methine group of D-pen, δ 7.66-7.44 ppm assignable to vinylene and phenyl groups of *trans*-dppee. The integration ratio suggested that D-pen and *trans*-dppee exist in a 1:2 ratio in [**3**]$(NO_3)_2$ (Figure 2-11). The fact that the proton signals were observed in a diamagnetic region indicates that this complex had a diamagnetic Co^{III} center. The absorption spectrum of [**3**]$(NO_3)_2$ in MeOH showed absorption bands at around 520 and 580 nm assigned to the d-d transitions of Co^{III} center, and a shoulder at ca. 350 nm. Its CD spectrum showed positive bands at 608 and 407 nm and negative bands at 511 and 340 nm in the region of 700-300 nm (Figure 2-12). The diffuse reflection spectrum in the solid state showed a band at 563 nm and its CD spectrum showed negative bands at 640 and 511 nm and positive bands at 582 and 416 nm in the region of 700-400 nm (Figure 2-13). These diffuse reflection and CD spectra in the solid state were essentially the same as the absorption and CD spectra in MeOH solution, indicating that the structure of [**3**]$(NO_3)_2$ in the solid state is retained in solution. Single-crystal X-ray analysis revealed that $[\mathbf{3}]^{2+}$ was a hexanuclear cationic complex, $[Au^{I}_4Co^{III}_2(\textit{trans}\text{-dppee})_2(\text{D-pen})_4]^{2+}$, in which two $[Au^{I}_2(\textit{trans}\text{-dppee})(\text{D-pen})_2]^{2-}$ moieties were bridged by two Co^{III} centers (*vide infra*).

When the other monovalent inorganic salts, $NaClO_4$ or NH_4BF_4, instead of $NaNO_3$, were added to the orange reaction solution purple crystals with a trigonal-pyramid shape of [**3**]$(ClO_4)_2$ or [**3**]$(BF_4)_2$ were obtained, respectively.

For [**3**]$(ClO_4)_2$, the X-ray fluorescence spectroscopy indicated the presence of Au and Co atoms, and its elemental analytical data was in agreement with a formula consisting of $[Au_2(\textit{trans}\text{-dppee})(\text{D-pen})_2]^{2-}$ (D_2-$[\mathbf{2}]^{2-}$) , Co^{3+}, and ClO_4^- in a 1:1:1 ratio. The IR spectrum showed the presence of D-pen and *trans*-dppee ligands based on the bands at 1656 cm^{-1} for the carboxylate group and at 748-692 cm^{-1} for the P–Ph moieties, and the presence of ClO_4^- were also confirmed by the band at 1103 cm^{-1} (Figure 2-10). This complex is almost insoluble to common solvents, and the spectral measurements in solution could not be performed. Single-crystal X-ray analysis revealed that $[\mathbf{3}]^{2+}$ was a hexanuclear cationic complex, $[Au^{I}_4Co^{III}_2(\textit{trans}\text{-dppee})_2(\text{D-pen})_4]^{2+}$, in which two $[Au^{I}_2(\textit{trans}\text{-dppee})(\text{D-pen})_2]^{2-}$ moieties were bridged by two Co^{III} centers (*vide infra*).

For [**3**]$(BF_4)_2$, the X-ray fluorescence spectroscopy indicated the presence of Au and Co atoms, and its IR spectrum showed the band of the carboxylate group of D-pen at 1653 cm^{-1}, the P–Ph bands of *trans*-dppee at 747-692 cm^{-1}, and the B–F stretching band of BF_4^- at 1103 cm^{-1} (Figure 2-10). This complex was almost insoluble to common solvents, and the spectral measurements in solution could not be performed. Single-crystal X-ray analysis revealed that $[\mathbf{3}]^{2+}$ was a hexanuclear cationic complex, $[Au^{I}_4Co^{III}_2(\textit{trans}$-

dppee)$_2$(D-pen)$_4$]$^{2+}$, in which two [Au$^{I}_2$(*trans*-dppee)(D-pen)$_2$]$^{2-}$ moieties were bridged by two Co^{III} centers (*vide infra*). The powder X-ray diffraction patterns of these three salts matched well with the simulated patterns based on the SC-XRD results, indicating high crystalline purity (Figure 2-14).

II-3-4. Synthesis and Characterization of [Au$_4$Co$_2$(*trans*-dppee)$_2$(D-pen)$_4$]SO$_4$ ([3]SO$_4$).

Reaction of D$_2$-H$_2$[**2**] with Co(OAc)$_2$·4H$_2$O in a 1:1 ratio in MeOH at room temperature gave an orange solution, which was stood at room temperature for 2 weeks after the addition of an aqueous KHSO$_4$ solution. Purple crystals with a trigonal-pyramid shape ([**3**]SO$_4$) were isolated from the resulting brown solution (Scheme 2-3).

X-ray fluorescence spectroscopy of [**3**]SO$_4$ indicated the presence of Au and Co atoms, and its elemental analytical data was in agreement with the formula consisting of [Au$_2$(*trans*-dppee)(D-pen)$_2$]$^{2-}$ (D$_2$-[**2**]$^{2-}$) , Co^{3+}, and SO$_4^{2-}$ in a 2:2:1 ratio. In the IR spectrum, a C=O stretching band for deprotonated carboxylate groups of D-pen at 1656 cm^{-1}, an S–O stretching band for sulfate anion at 1103 cm^{-1}, and Ph bands at 748-692 cm^{-1} were observed (Figure 2-10). The intensity of the band for the sulfate anion was weaker than that for the perchlorate anion in [**3**](ClO$_4$)$_2$, which corresponded to the fact that only one sulfate anion per one cationic complex was needed to satisfy the charge balance. Because this complex was almost insoluble to common solvents and the isolated yield for the crystalline sample and solid crystallinity were poor, and the spectral measurements both in the solution and in the solid states could not be performed. Single-crystal X-ray analysis revealed that [**3**]$^{2+}$ was a hexanuclear cationic complex, [Au$^{I}_4$Co$^{III}_2$(*trans*-dppee)$_2$(D-pen)$_4$]$^{2+}$, in which two [Au$^{I}_2$(*trans*-dppee)(D-pen)$_2$]$^{2-}$ moieties were bridged by two Co^{III} centers (*vide infra*).

II-3-5. Synthesis and Characterization of [Au$_4$Co$_2$(*trans*-dppee)$_2$(L-pen)$_4$](NO$_3$)$_2$ ([4](NO$_3$)$_2$).

Reaction of L$_2$-H$_2$[**2**] with Co(OAc)$_2$·4H$_2$O in a 1:1 ratio in MeOH at room temperature gave an orange solution, which was stood for a week after the addition of an aqueous NaNO$_3$ solution. Purple crystals with a trigonal-pyramid shape ([**4**](NO$_3$)$_2$) were isolated from the resulting brown solution (Scheme 2-3)

X-ray fluorescence spectroscopy indicated the presence of Au and Co atoms in [**4**](NO$_3$)$_2$. In the IR spectrum, a C=O stretching band for deprotonated carboxylate groups of D-pen at 1653 cm^{-1}, an N–O stretching band for nitrate anion at 1385 cm^{-1}, and Ph bands at 747-691 cm^{-1} were observed (Figure 2-10). The diffuse reflection spectrum

in the solid state was similar to that of [**3**]$(NO_3)_2$, showing a band at 580 nm (Figure 2-15). This suggests that the coordination geometry around the Co^{III} center was *cis*(*N*)*trans*(*O*)*cis*(*S*)-$N_2O_2S_2$ octahedral. The CD spectrum in the solid state showed almost the opposite pattern compared with that of [**3**]$(NO_3)_2$, showing positive bands at 636 and 509 nm, and negative bands at 575 and 429 nm in the region of 700-400 nm (Figure 2-15). This CD spectrum suggested that the two pen ligands around Co^{III} center had opposite chirality from that of [**3**]$^{2+}$. Based on these results, [**4**]$^{2+}$ was supposed to have the formula of $[Au^{I}_4Co^{III}_2(trans\text{-dppee})_2(\text{L-pen})_4]^{2+}$, the enantiomeric isomer of [**3**]$^{2+}$. Single-crystal X-ray analysis revealed that [**4**]$^{2+}$ was a hexanuclear cationic complex, $[Au^{I}_4Co^{III}_2(trans\text{-dppee})_2(\text{L-pen})_4]^{2+}$, in which two $[Au^{I}_2(trans\text{-dppee})(\text{L-pen})_2]^{2-}$ moieties were bridged by two Co^{III} centers (*vide infra*).

II-3-6. Crystal Structures of the Homochiral $Au^{I}Co^{III}$ Complexes.

Crystal structure of [**3**]$(NO_3)_2$ was determined by single-crystal X-ray crystallography. Molecular and packing structures are shown in Figures 2-16, 17, 18, 19, and 20. The crystallographic data are summarized in Table 2-4, and the selected bond distances and angles are listed in Table 2-5. Crystal [**3**]$(NO_3)_2$ contains a half of $[Au_4Co_2(trans\text{-dppee})_2(\text{D-pen})_4]^{2+}$ unit, two NO_3^- ions with an occupancy of 1/12, one NO_3^- ion with an occupancy of 1/3, one NO_3^- ion with an occupancy of 1/2, and 2 solvated water molecules in the asymmetric unit. The cationic complex had an S-bridged $Au^{I}_4Co^{III}_2$ hexanuclear structure consisting of two $[Au_2(trans\text{-dppee})(\text{D-pen})_2]^{2-}$ metalloligands that link two Co^{III} atoms to form a twisted 18-menbered ring structure composed of Au, Co, S, P, and C atoms (Figures 2-17, 18). The coordination geometry of each Au^{I} atoms is nearly linear bound with P and S atoms (Av. Au–S = 2.32 Å, Au–P = 2.26 Å, P–Au–S = 178.1°, and Au···Au = 3.6044(5) Å). The two D$_2$-[**2**]$^{2-}$ metalloligands each bound to two Co^{III} atoms in a bis(tridentate-*N*,*O*,*S*) mode such that each Co^{III} atoms is in a *cis*(*N*)*trans*(*O*)*cis*(*S*)-$N_2O_2S_2$ octahedral environment (Av. Co–S = 2.29 Å, Co–O = 1.93 Å, Co–N = 1.97 Å, S–Co–S = 97.39(10)°, O–Co–O= 177.2(3)°, N–Co–N = 93.1(3)°) (Figures 2-18a, b). All S atoms adopt an *R* configuration.

In [**3**]$(NO_3)_2$, six cationic complexes were aggregated into an octahedral shaped hexameric structure through intermolecular 24 CH···π and 12 NH_2···OCO hydrogen bonding interactions (shortest C···Ph = 3.62 Å, N···O = 2.890(10) Å), accommodating an NO_3^- ion in the center (Figure 2-19a). A triangular CH···π linkage of three cationic complexes sits in each of the eight triangular faces of the supramolecular octahedron (Figure 2-19b), and a triangular NH_2···OCO linkage sits on each of four triangular faces of the octahedron (Figure 2-19c). In the crystal, the cationic supramolecular octahedrons

were closely packed in a face centered cubic (fcc) structure connected by CH···π interactions. This fcc structure contains a single kind of octahedral interstices, and two kinds of larger tetrahedral interstices with one being hydrophilic surrounded by amine groups and the other being hydrophobic surrounded by phenyl and methyl groups. While one NO_3^- ion was accommodated in each of the octahedral interstices, each of the hydrophilic tetrahedral interstices accommodates ten NO_3^- ions that were closely packed to form a symmetrical adamantane-like cluster (Figures 2-20a, b). The closest O···O distance between the neighbor NO_3^- anions was 3.29 Å and the N···N distance between the neighbor NO_3^- anions was 4.69 Å. In the hydrophobic interstices, 24 O atoms of the water molecules (4 water molecules for one complex cation) were accommodated, which was less in the number as expected from the elemental analysis data, indicating the disordering of further water molecules. The aggregated 10 nitrate anions could be divided into 2 type, one was for 6 nitrate anions being settled in octahedral sites, and the other was for 4 nitrate anions being settled in tetrahedral sites. The nitrate anions in the octahedral site were ordered and were hydrogen bonded with the cationic complex (N···O = 2.929(18) Å). On the other hand, the nitrate ions in the tetrahedral site showed the disordering into two parts. One part of the disordered nitrate anions forms hydrogen bonds with the cationic complex (N···O = 2.95(6) Å), while the other part forms no significant interactions.

The crystal structure of [**3**]$(ClO_4)_2$, obtained by the similar reaction using $NaClO_4$ instead of $NaNO_3$, was isomorphous with that of [**3**]$(NO_3)_2$. The crystallographic data are summarized in Table 2-4, the selected bond distances and angles are listed in Table 2-6, and the molecular and packing structure are shown in Figures 2-21. Crystal [**3**]$(ClO_4)_2$ contains a half of $[Au_4Co_2(\textit{trans}\text{-dppee})_2(\text{D-pen})_4]^{2+}$ unit, two ClO_4^- ions with an occupancy of 1/12, one ClO_4^- ion with an occupancy of 1/3, one ClO_4^- ion with an occupancy of 1/2, and 3/2 solvated water molecules in the asymmetric unit. In [**3**]$(ClO_4)_2$, the $Au^I_4Co^{III}_2$ hexanuclear structure, the hexameric octahedrally aggregated cationic structure, and the fcc packing structure were formed, and these structures were similar to those of [**3**]$(NO_3)_2$ (Figures 2-21a, b, d). In the hydrophilic tetrahedral interstice, ten ClO_4^- ions were aggregated in an adamantane-like structure with the shortest Cl···Cl and O···O distances of 4.50 Å and 3.26 Å, respectively (Figure 2-21c). The perchlorate anions in the tetrahedral interstice were ordered, and form hydrogen bonds with the cationic complex (N···O = 3.061(18) Å for octahedral site, and 3.659(7) Å for tetrahedral site).

Crystal structure of [**3**]$(BF_4)_2$, obtained by the similar reaction using NH_4BF_4 instead of $NaNO_3$, was isomorphous with those of [**3**]$(NO_3)_2$ and [**3**]$(ClO_4)_2$. The crystallographic data are summarized in Table 2-4, the selected bond distances and angles are listed in

Table 2-7, and the molecular and packing structure are shown in Figure 2-22. Crystal [**3**]$(BF_4)_2$ contains a half of $[Au_4Co_2(trans\text{-dppee})_2(D\text{-pen})_4]^{2+}$ unit, two BF_4^- ions with an occupancy of 1/12, one BF_4^- ion with an occupancy of 1/3, one BF_4^- ion with an occupancy of 1/2, and 7/3 solvated water molecules in the asymmetric unit. Similarly, the $Au^I_4Co^{III}_2$ hexanuclear structure, the hexameric octahedrally aggregated cationic structure, and the fcc packing structure were formed in [**3**]$(BF_4)_2$ (Figures 2-22a, b, d). 10 BF_4^- ions were aggregated in an adamantane-like structure with the closest F···F and B···B distances of 3.39 Å and 4.62 Å, respectively, and this anionic decamer was accommodated in the hydrophilic tetrahedral interstice of the cationic fcc structure (Figure 2-22c). The tetrafluoroborate anions at the tetrahedral site in the tetrahedral interstice were disordered.

Crystal structure of [**3**]SO_4, obtained by the similar reaction using $KHSO_4$ instead of $NaNO_3$, was isostructural to that of [**3**]$(NO_3)_2$. The crystallographic data are summarized in Table 2-4, the selected bond distances and angles are listed in Table 2-8, and the molecular and packing structure are shown in Figure 2-23. Crystal [**3**]SO_4 contains a half of $[Au_4Co_2(trans\text{-dppee})_2(D\text{-pen})_4]^{2+}$ unit, one SO_4^{2-} ions with an occupancy of 1/2, and 17/6 solvated water molecules in the asymmetric unit. Similarly, the $Au^I_4Co^{III}_2$ hexanuclear structure and the hexameric octahedrally aggregated cationic structure were formed, but in the center of the cationic hexamer, a water molecule was accommodated (Figures 2-23a, b, d). The cationic octahedron forms the fcc packing structure, as in [**3**]$(NO_3)_2$, and its hydrophilic tetrahedral interstice accommodate six SO_4^{2-} ions forming an octahedral hexameric structure with the closest S···S and O···O distances of 6.79 Å and 4.31 Å, respectively (Figure 2-23c). The sulfate anions in the tetrahedral interstice were disordered, and each anion was connected to the cationic complex through the hydrogen bonds (N···O = 2.98(3), 2.99(3), 3.07(3) Å).

Crystal structure of [**4**]$(NO_3)_2$, obtained by the similar reaction using L_2-H_2[**2**] instead of D_2-H_2[**2**], had an enantiomeric relationship to that of [**3**]$(NO_3)_2$. The crystallographic data are summarized in Table 2-4, the selected bond distances and angles are listed in Table 2-9, and the molecular and packing structure are shown in Figure 2-24. Crystal [**4**]$(NO_3)_2$ contains a half of $[Au_4Co_2(trans\text{-dppee})_2(L\text{-pen})_4]^{2+}$ unit, two NO_3^- ions with an occupancy of 1/12, one NO_3^- ions with an occupancy of 1/3, one NO_3^- ions with an occupancy of 1/2, and 2 solvated water molecules in the asymmetric unit. The structures of [**3**]$(NO_3)_2$ and [**4**]$(NO_3)_2$ were similar, and the difference between two structures was only the chirality of the pen ligands (Figure 2-24a). The coordination geometry of each Au^I atoms was nearly linear bound with P and S atoms (Av. Au–S = 2.31 Å, Au–P = 2.24 Å, and P–Au–S = 178.2°). The two L_2-[**2**]$^{2-}$ metalloligands each bound to two Co^{III} atoms in a bis(tridentate-*N*,*O*,*S*) mode such that each Co^{III} atoms was in a *cis*(*N*)*trans*(*O*)*cis*(*S*)-

$N_2O_2S_2$ octahedral environment (Av. Co–S = 2.28 Å, Co–O = 1.93 Å, Co–N = 1.94 Å, S–Co–S = 97.66(18)°, O–Co–O= 177.0(5)°, N–Co–N = 92.1(6)°). All S atoms adopt an *S* configuration. In [**4**]$(NO_3)_2$, six cationic complexes were aggregated into an octahedral shape supramolecular structure through intermolecular 24 CH···π and 12 NH_2···OCO hydrogen bonding interactions, accommodating a NO_3^- ion in the center (Figure 2-24b). A triangular CH···π linkage of three cationic complexes sits in each of eight triangular faces of the supramolecular octahedron and a triangular NH_2···OCO linkage sits on each of four triangular faces of the octahedron. In the crystal, the cationic supramolecular octahedrons were closely packed in a fcc structure connected by CH···π interactions (Figure 2-24d). This fcc structure contains a single kind of octahedral interstice, and two kinds of larger tetrahedral interstices with one being hydrophilic surrounded by amine groups and the other being hydrophobic surrounded by phenyl and methyl groups. While one NO_3^- ion was accommodated in each of the octahedral interstice, each of hydrophilic tetrahedral interstice accommodates ten NO_3^- ions that were closely packed to form a symmetrical adamantane-like cluster (Figure 2-24c). The closest O···O and N···N distances between the neighboring NO_3^- anions was 3.29 Å and 4.69 Å, respectively. In the hydrophobic interstices no atoms were found from the structural analysis, but the water molecules should be disordered inside it. The nitrate ions at the tetrahedral site of the tetrahedral interstice were disordered.

II-3-7. Comparison with the dppe system.

As described in II-3-6 and introduction for the homochiral system, both $[Au^I_4Co^{III}_2(\textit{trans}\text{-dppee})_2(\text{D-pen})_4]^{2+}$ and $[Au^I_4Co^{III}_2(\text{dppe})_2(\text{D-pen})_4]^{2+}$ had the similar $Au^I_4Co^{III}_2$ hexanuclear structure, the hexameric octahedrally aggregated cationic structure, the fcc packing structure, and the anion aggregation structures, but the small differences were found between the two structures due to the effect of the carbon linkers in the diphosphine ligands (dppe or *trans*-dppee). Firstly, *trans*-dppee in $[\mathbf{3}]^{2+}$ had a longer P···P distance than that in dppe analogous cationic complexes because of the larger P–C–C angles of the linker site (Scheme 2-2, Table 2-10). Secondly, the longer P···P distance led to the shorter distance between the phenyl rings in a diagonal position and the longer distance between the Co ions, which meant that the overall shape of $[\mathbf{3}]^{2+}$ had slightly changed to be more slender (Scheme 2-4a, Figures 2-25). This slender shape means that the $[Au^I_4Co^{III}_2(\textit{trans}\text{-dppee})_2(\text{D-pen})_4]^{2+}$ protrude in the hydrophilic interstices rather than the case of $[Au^I_4Co^{III}_2(\text{dppe})_2(\text{D-pen})_4]^{2+}$ (Table 2-11), which in turn reduced the hydrophilic interstices' size, (Scheme 2-4b) and changed the anion aggregation structures as a result.

Focused on the aggregation structures of the inorganic anions, the small difference between the *trans*-dppee in [**3**]$(NO_3)_2$ and dppe in $[Au_4Co_2(dppe)_2(D\text{-pen})_4](NO_3)_2$ complexes was found. In both , the nitrate anions in the octahedral sites were ordered, and their positions and orientations were almost the same. On the other hand, the nitrate anions in the tetrahedral sites were disordered in both crystals. The positions of these anions were almost the same, but the orientations were slightly different between two crystals, as shown in Figures 2-26 and 2-27. As a result, the minimum O···O distances between the neighboring anions were different with the distances of 3.30 Å for [**3**]$(NO_3)_2$ and 3.38 Å for $[Au_4Co_2(dppe)_2(D\text{-pen})_4](NO_3)_2$. Accordingly, the hydrogen bonding interactions between the disordered anions in the tetrahedral site and the amine groups of the cationic complexes showed a small difference ($NH_2\cdots O_{NO3}$ = 2.95(6) Å, 3.13(5) Å, 3.13(5) Å, or 3.13(5) Å for [**3**]$(NO_3)_2$ and $NH_2\cdots O_{NO3}$ = 2.96(7) Å, 2.99(11) Å, 2.99(11) Å, or 2.99(11) Å for $[Au_4Co_2(dppe)_2(D\text{-pen})_4](NO_3)_2$; Figures 2-28).

In the perchlorate salts, $[Au_4Co_2(dppe)_2(D\text{-pen})_4](ClO_4)_2$ and [**3**]$(ClO_4)_2$, the difference between two anionic aggregation structures were clearer. In [**3**]$(ClO_4)_2$, the perchlorate anions were more closely packed compared with $[Au_4Co_2(dppe)_2(D\text{-pen})_4](ClO_4)_2$ (Cl···Cl = 4.500(5) Å for [**3**]$(ClO_4)_2$, and 4.765(7) Å for the dppe analogous compound) due to the smaller hydrophilic Td interstice's size (993 $Å^3$ for [**3**]$(ClO_4)_2$, and 1184 $Å^3$ for the dppe analogous compound; Table 2-11). Such closer aggregation of anions affected the orientation of perchlorate anions in tetrahedral site to minimize the O···O repulsion. In [**3**]$(ClO_4)_2$, the triangular faces of the two closer perchlorate ions were arranged in a face-to-face fashion (O···O = 3.26(2) Å; Figures 2-29 and 2-30), whereas in the dppe analogous compound, each of three O atoms of the tetrahedrally arranged perchlorate ion directed to the center of a triangular face of the adjacent perchlorate ion (O···O = 3.13(2) Å). The anions in the octahedral sites had a similar orientation and a hydrogen bonding mode with the dppe analogous compound ($NH_2\cdots O_{ClO4}$ = 3.061(18) Å for *trans*-dppee system, and 3.00(2) Å for dppe analogous compound, Figure 2-31).

In the tetrafluoroborate salts, the volume of the hydrophilic tetrahedral interstices also decreased (990 $Å^3$ for [**3**]$(BF_4)_2$, and 1074 $Å^3$ for the dppe analogous compound; Table 2-11), but the discussion about their orientation was difficult because the tetrafluoroborate anions at the tetrahedral site in the tetrahedral interstices severely disordered (B···B = 4.62 Å for [**3**]$(BF_4)_2$, and 4.61 Å for the dppe analogous compound) and relatively poor SC-XRD result for the dppe analogous $[Au_4Co_2(dppe)_2(D\text{-pen})_4](BF_4)_2$ crystal (Figure 2-32).

Also in the sulfate complexes, the counter anions in [**3**]SO_4 were arranged in a slightly different way from that of $[Au_4Co_2(dppe)_2(D\text{-pen})_4]SO_4$. Although the direction and disordering mode of O atoms of the sulfate anions were similar, the S···S distance was

shorter than that of the dppe analogous compound (6.790(11) Å for [**3**]SO_4 and 6.914(15) Å for the dppe analogous compound). This meant that the sulfate anions in [**3**]SO_4 were more closely packed, which was consistent with the fact that $[\mathbf{3}]^{2+}$ had the smaller hydrophilic tetrahedral interstices (Figure 2-33).

II-3-8. Synthesis and Characterization of [Au_2(*trans*-dppee)(D-Hpen)(L-Hpen)] (DL-H_2[2]).

Reaction of [Au_2Cl_2(*trans*-dppee)] with DL-H_2pen in a 1:2 ratio in EtOH at room temperature gave a white suspension, from which white powder of DL-H_2[**2**] was isolated (Scheme 2-1). X-ray fluorescence spectroscopy indicated that DL-H_2[**2**] contains Au atom and its elemental analytical data was in agreement with the formula for [Au_2(*trans*-dppee)(Hpen)$_2$]·6.5H_2O. In the IR spectrum, a C=O stretching band for deprotonated carboxylate groups of pen at 1624 cm^{-1}, a P–Ph stretching band at 1101 cm^{-1} and Ph bands at 745-692 cm^{-1} were observed (Figure 2-34). This complex was less soluble in MeOH compared with D$_2$-H_2[**2**], so quantitative absorption and ^{31}P NMR spectra were not measured. The ^{1}H NMR spectrum in CD_3OD showed one set of proton signals at δ 1.33 and 1.69 ppm assigned to methyl groups of pen, δ 7.36 ppm assigned to the vinylene group of *trans*-dppee, and δ 7.68-7.64, 7.55-7.53 ppm assigned to phenyl groups of *trans*-dppee. The integration ratio suggests that pen and *trans*-dppee exist in a 1:2 ratio. The chemical shifts of the methyl signals were slightly different from those of D$_2$-H_2[**2**] (δ 1.39, 1.75 ppm), indicating that D$_2$-H_2[**2**] or L$_2$-H_2[**2**] were not dominant species in MeOH solution. The methine peak of pen could not be observed probably because of the overlapping with the MeOH signal (Figure 2-35). No signals in the ^{31}P NMR spectra in CD_3OD were detected because of the less solubility. Colorless single-crystals of DL-H_2[**2**] suitable for X-ray diffraction measurement were obtained by the recrystallization of the powder sample of DL-H_2[**2**] from EtOH/water (1:1) solution by adding Mg(OAc)$_2$. Spectroscopic data of the crystals were coincident with those of the powder sample. This complex exhibited a weak orange luminescence under UV light irradiation at room temperature. Solid-state emission spectrum of DL-H_2[**2**] at 77 K gave an emission band at 433 nm with the vibrational structure (Figure 2-36). Single crystal X-ray analysis revealed that DL-H_2[**2**] was comprised of D/L-Hpen ligands bridged by a $[Au_2(trans\text{-dppee})]^{2+}$ moiety through S atoms, giving a linear structure of [Au_2(*trans*-dppee)(D-Hpen–*S*)(L-Hpen–*S*)] (*vide infra*). The Au^I_2 metalloligands were connected to each other through aurophilic interactions[18] to form a 1D chain structure. This polymeric structure might lead to the less solubility of DL-H_2[**2**] in contrast to the soluble homochiral metalloligand, D$_2$-H_2[**2**], having a dimeric packing structure.

II-3-9. Crystal Structure of the Heterochiral Metalloligand, (DL-H_2[2]).

The crystal structure of DL-H_2[**2**] was determined by single-crystal X-ray crystallography. Molecular and packing structures are shown in Figures 2-37, 2-38, and 2-39. The crystallographic data are summarized in Table 2-12, and the selected bond distances and angles are listed in Table 2-13. Crystal of DL-H_2[**2**] contained 2 halves of [Au_2(*trans*-dppee)(D-Hpen)(L-Hpen)] units, 2 solvated EtOH molecules, and 6 solvated water molecules in the asymmetric unit. One of the carboxylate groups in the pen moiety was disordered.

The complex molecule was composed of one D-Hpen, one L-Hpen, and one [Au_2(*trans*-dppee)]$^{2+}$ moieties. As similar to the dppe analogous compound, [Au_2(dppe)(D-Hpen)(L-Hpen)], one D-Hpen ligand and one L-Hpen ligand were bridged by a [Au_2(*trans*-dppee)]$^{2+}$ moiety through S atoms, giving a linear structure in [Au_2(*trans*-dppee)(D-Hpen-*S*)(L-Hpen-*S*)]. Each Au atom was in a PS linear coordination geometry bound by one D-pen and one *trans*-dppee (Av. Au–S = 2.31 Å, Au–P = 2.27 Å, P–Au–S =175.1°). The C–C distances and P–C–C angles of the carbon linkers (Av. C–C = 1.28 Å, P–C–C =126.8°) were similar to those of chiral analogous complex D$_2$-H_2[**2**] (Table 2-2, Table 2-13). In DL-H_2[**2**], two complex molecules were aggregated through an Au···Au interaction (Au···Au = 3.0846(5) Å) to form a linear 1D chain structure that was also found in the dppe analogous compound ([Au_2(dppe)(D-Hpen)(L-Hpen)]) (Figure 2-38). The chains were linked by hydrogen bonds between the amine and carboxylate groups (Av. N···O = 2.70 Å) to form a 3D network structure (Figure 2-39).

II-3-10. Synthesis and Characterization of Heterochiral Neutral Complex [$Au^{I}_4Co^{II}_2$(*trans*-dppee)$_2$(D-pen)$_2$(L-pen)$_2$] ([**5**]).

Reaction of a racemic mixture of the metalloligands, D$_2$-H_2[**2**], and L$_2$-H_2[**2**], with $Co(OAc)_2{\cdot}4H_2O$ in a 1:1 ratio in EtOH at room temperature without the addition of oxidant gave an orange solution, from which orange crystals with a block shape ([**5**]) were isolated (Scheme 2-4). X-ray fluorescence spectroscopy indicated the presence of Au and Co atoms in [**5**], and its elemental analytical data was in agreement with a formula consisting of [Au_2(*trans*-dppee)(pen)$_2$]$^{2-}$ ([**2**]$^{2-}$) and Co^{2+} in a 1:1 ratio. The absence of anionic species such as acetate ion suggested that the Co atom was a divalent state. In the IR spectrum, a C=O stretching band for deprotonated carboxylate groups of pen at 1598 cm^{-1}, and Ph bands at 748-694 cm^{-1} were observed (Figure 2-40). The absorption spectrum of [**5**] in MeOH/water (2:1) showed broad bands in the range of 600-450 nm,

and the d-d transition band characteristic for the Co^{III} center was not observed (Figure 2-41). Its CD spectrum was silent in the region of 700-300 nm (Figure 2-41), which indicated that [**5**] contains both D-pen and L-pen. The diffuse reflection spectrum in the solid state showed only broad bands in the region of 700-400 nm (Figure 2-42).

The magnetic susceptibility data suggested the presence of the Co^{II} centers in [**5**]. The $X_M T$ value at room temperature was 6.27 cm^3 K mol^{-1}, which was slightly larger than the spin only value of 5.99 cm^3 K mol^{-1} for two high-spin Co^{II} centers (Figure 2-43). On lowering the temperature, the $X_M T$ values retained, and then decreased gradually below 100 K. These magnetic behaviors were characteristic for the Co^{II} complexes. It seemed that there was no strong ferromagnetic interaction between two Co^{II} centers. The electron spin resonance (ESR) spectrum at 4 K showed a band at g = 3.23 indicating the existence of unpaired electron like Co^{II} species (Figure 2-44). The Co^{II} complex, bearing triphosphine ligand $[Au^{I}_6Co^{II}_3(tdme)_2(D\text{-pen})_6]$,[11] showed the characteristic ESR signals for Co^{II}. But it was not similar to the present signals, probably due to the different O–Co–O and S–Co–S angles causing a different d-orbital energy splitting.

Single-crystal X-ray analysis revealed that [**5**] was a hexanuclear neutral complex, $[Au^{I}_4Co^{II}_2(trans\text{-dppee})_2(D\text{-pen})_2(L\text{-pen})_2]$, in which two $[Au^{I}_2(trans\text{-dppee})(D\text{-pen})(L\text{-pen})]^{2-}$ moieties were bridged by two Co^{II} centers (*vide infra*).

When EtOH/water (1:1) was used instead of MeOH, orange platelet crystals ([**5**]') were produced. The IR spectrum was almost the same as that of [**5**], showing a C=O stretching band for deprotonated carboxylate groups of pen at 1598 cm^{-1}, and Ph bands at 748-694 cm^{-1} (Figure 2-40). Single-crystal X-ray analysis revealed that [**5**]' had a hexanuclear neutral complex, $[Au^{I}_4Co^{II}_2(trans\text{-dppee})_2(D\text{-pen})_2(L\text{-pen})_2]$, which was the same as that in [**5**] (*vide infra*). The difference between [**5**] and [**5**]' was the solvated molecules and the supramolecular structure of the complex molecules in the crystal structure.

II-3-11. Synthesis and Characterization of Heterochiral Cationic Complex $[Au^{I}_4Co^{III}_2(trans\text{-dppee})_2(D\text{-pen})_2(L\text{-pen})_2]^{2+}$ ([**6**]$^{2+}$).

Reaction of a racemic mixture of metalloligands, D_2-H_2[**2**] and L_2-H_2[**2**], with $Co(OAc)_2{\cdot}4H_2O$ in a 1:1 ratio in EtOH/water at room temperature with adding an excess amount of PbO_2 as an oxidant gave a brown suspension. After the removal of unreacted PbO_2, An $NaNO_3$ aqueous solution was added to the resulting brown solution, and then the reaction solution was allowed to stand at room temperature overnight to give purple crystal with a platelet shape ([**6**]$(NO_3)_2$) and, in several cases, purple crystals with a trigonal-pyramid shape ([**3**]$(NO_3)_2$, [**4**]$(NO_3)_2$) (Scheme 2-5).

Importantly, by using *t*-BuOH instead of EtOH/water as solvent, only purple platelet crystals of [**6**]$(NO_3)_2$ were isolated. X-ray fluorescence spectroscopy indicated the presence of Au and Co atoms in [**6**]$(NO_3)_2$, and its elemental analytical data was in agreement with a formula consisting of $[Au_2(\textit{trans}\text{-dppee})(pen)_2]^{2-}$ ($[\mathbf{2}]^{2-}$) , Co^{III}, and NO_3^- in a 1:1:1 ratio. In the IR spectrum, a C=O stretching band for deprotonated carboxylate groups of pen at 1650 cm^{-1}, an N–O stretching band for nitrate anions at 1385 cm^{-1}, and Ph bands at 747-693 cm^{-1} were observed (Figure 2-40). The crystals of [**6**]$(NO_3)_2$ were slightly soluble in MeOH but insoluble in other common solvents. The ^{1}H NMR spectrum in CD_3OD/D_2O (1:2) showed the two sets of proton signals at δ 1.41, 1.51, 1.87, and 1.98 ppm assigned to methyl groups of D-pen, δ 3.95 and 3.99 ppm assigned to the methine group of D-pen, and δ 7.67-7.22 ppm assigned to vinylene and phenyl groups of *trans*-dppee. From the integration ratio, it was supposed that two kinds of species were present in solution in 1:1 ratio (Figure 2-45). Because one of the two species showed the same NMR signals as that of the homochiral cationic complex $[\mathbf{3}]^{2+}$ and another showed a different set of signals, the equilibrium between heterochiral and homochiral complexes in solution was suggested(Scheme 2-6). The absorption spectrum of [**6**]$(NO_3)_2$ in MeOH showed a band at around 550 nm assignable to the d-d transition (Figure 2-46). Its CD spectrum showed no significant bands in the region of 700-300 nm (Figure 2-46), which indicated that [**6**]$(NO_3)_2$ contains equal molars of D-pen and L-pen. The diffuse reflection spectrum in the solid state showed an absorption band at around 570 nm assigned to the d-d transition of Co^{III} center in the region of 700-400 nm (Figure 2-47). Single-crystal X-ray analysis revealed that $[\mathbf{6}]^{2+}$ was a hexanuclear cationic complex, $[Au^{I}_4Co^{III}_2(\textit{trans}\text{-dppee})_2(\text{D-pen})_2(\text{L-pen})_2]^{2+}$, in which two $[Au^{I}_2(\textit{trans}\text{-dppee})(\text{D-pen})(\text{L-pen})]^{2-}$ moieties were bridged by two Co^{III} centers (*vide infra*).

The hexafluorophosphate salt, [**6**]$(PF_6)_2$, was also obtained by using hexafluorophosphate as a counteranion. X-ray fluorescence spectroscopy revealed the presence of Au and Co atoms in [**6**]$(PF_6)_2$, and its elemental analytical data was in agreement with a formula consisting of $[Au_2(\textit{trans}\text{-dppee})(pen)_2]^{2-}$ ($[\mathbf{2}]^{2-}$) , Co^{III}, and PF_6^- in a 1:1:1 ratio. In the IR spectrum, a C=O stretching band for deprotonated carboxylate groups of pen at 1647 cm^{-1}, a P–F stretching band for hexafluorophosphate anion at 842 cm^{-1}, and Ph bands at 747-693 cm^{-1} were observed (Figure 2-40). Single-crystal X-ray analysis revealed that the cationic complex in [**6**]$(PF_6)_2$ had a similar molecular structure to that in [**6**]$(NO_3)_2$ (*vide infra*). Interestingly, no crystals of homochiral $[\mathbf{3}]^{2+}$ and $[\mathbf{4}]^{2+}$ appeared from this reaction solution. This was reasonably explainable as that the hexafluorophosphate anion is too big to form the adamantane-like decamer as found in the homochiral complex salts [**3**]$(NO_3)_2$, [**3**]$(ClO_4)_2$, or [**3**]$(BF_4)_2$.

The same results were obtained by using a meso metalloligand, DL-[H_2**2**], instead of the racemic metalloligand D$_2$/L$_2$-[H_2**2**] or using the racemic metalloligand instead of a meso metalloligand, indicating that the chiral scrambling occurs in solution.

II-3-12. Crystal Structures of Heterochiral Au^ICo^{II} and Au^ICo^{III} Complexes.

The crystal structure of [**5**] was determined by single-crystal X-ray crystallography. Molecular and packing structures are shown in Figures 2-48, 2-49, 2-50, and 2-51. The crystallographic data are summarized in Table 2-14, and the selected bond distances and angles are listed in Table 2-15. Crystal [**5**] contained a half of [Au_4Co_2(*trans*-dppee)$_2$(D-pen)$_2$(L-pen)$_2$] unit, three solvated MeOH molecules, and a solvated water molecule in the asymmetric unit. As shown in Figure 2-51, the complex molecule had a neutral S-bridged $Au^I_4Co^{II}_2$ hexanuclear structure consisting of two heterochiral [Au_2(*trans*-dppee)(D-pen)(L-pen)]$^{2-}$ metalloligands that linked two Co^{II} atoms to form an 18-menbered ring structure composed of Au, Co, S, P, and C atoms. Notably, the scrambling of the metalloligands occurred to form DL-H_2[**2**] from the racemic mixture of D$_2$-H_2[**2**] and L$_2$-H_2[**2**] in the reaction solution (Scheme 2-7). The coordination geometry of each Au^I atoms was nearly linear bound with P and S atoms (Av. Au–S = 2.32 Å, Au–P = 2.27 Å, and P–Au–S = 178.2°). The two DL-[**2**]$^{2-}$ metalloligands each bound to two Co^{II} atoms in a bis(tridentate-*N*,*O*,*S*) mode such that each Co^{II} atoms was in a *cis*(*N*)*trans*(*O*)*cis*(*S*)-$N_2O_2S_2$ octahedral environment (Av. Co–S = 2.52 Å, Co–O = 2.08 Å, Co–N = 2.16 Å, S–Co–S = 103.32(11)°, O–Co–O= 171.1(3)°, N–Co–N = 100.7(3)°) (Figure 2-50a, 2-50b). The aurophilic interactions were found in the complex molecule (Au···Au = 3.1214(9) Å). In [**5**], no direct hydrogen bonding interactions between the complex molecules were formed, but instead, a hydrogen bonding 1D straight chain structure mediated by MeOH molecules was formed ($H_2N\cdots O_{MeOH}$ = 2.948(14) Å, $COO^-\cdots O_{MeOH}$ = 2.728(11) Å) (Figure 2-51). It should be noted that the sulphur coordinated CoII species in [**5**], isolated in the air is a rare example.[11a]

The crystal structure of [**5**]' was determined by single-crystal X-ray crystallography. Molecular and packing structures are shown in Figures 2-52 and 2-53. The crystallographic data are summarized in Table 2-16, and the selected bond distances and angles are listed in Table 2-17. Crystal [**5**]' contained one [Au_4Co_2(*trans*-dppee)$_2$(D-pen)$_2$(L-pen)$_2$] unit, one solvated EtOH molecules, and 16 solvated water molecule in the asymmetric unit. The complex [**5**]' had a similar molecular structure to that of [**5**], but the supramolecular structure was different. In [**5**]', the complex molecules were connected to each other through hydrogen bonds between the amine and carboxylate groups (N···O = 3.222(15) Å) to form a 1D zigzag chain structure (Figure 2-53).

The crystal structure of [**6**]$(NO_3)_2$ was determined by single-crystal X-ray crystallography. Molecular and packing structures are shown in Figures 2-54, 2-55, 2-56, and 2-57. The crystallographic data are summarized in Table 2-18, and the selected bond distances and angles are listed in Table 2-19. Crystal [**6**]$(NO_3)_2$ contained a half of $[Au_4Co_2(\textit{trans}\text{-dppee})_2(\text{D-pen})_2(\text{L-pen})_2]^{2+}$ unit, one disordered NO_3^- ion, and 14 solvated water molecules in the asymmetric unit. As shown in Figure 2-55, the cationic complex had an S-bridged $Au^I_4Co^{III}_2$ hexanuclear structure consisting of two $[Au_2(\textit{trans}\text{-dppee})(\text{D-pen})(\text{L-pen})]^{2-}$ units that linked two Co^{III} atoms to form an 18-menbered ring structure composed of Au, Co, S, P, and C atoms. The coordination geometry of each Au^I atoms was nearly linear bound with P and S atoms (Av. Au–S = 2.29 Å, Au–P = 2.24 Å, and P–Au–S = 177.8°). The two DL-[**2**]$^{2-}$ metalloligands each bound to two Co^{III} atoms in a bis(tridentate-*N*,*O*,*S*) mode such that each Co^{III} atoms were in *cis*(*N*)*trans*(*O*)*cis*(*S*)-$N_2O_2S_2$ octahedral environments (Av. Co–S = 2.28 Å, Co–O = 1.92 Å, Co–N = 1.98 Å, S–Co–S = 99.7°, O–Co–O = 176.7°, N–Co–N = 94.5°) (Figure 2-56). The shorter bond distances around the Co center in [**6**]$(NO_3)_2$ than those of [**5**] suggested that the oxidation state of the Co ion was +3 (Co–S = 2.28 Å for [**6**]$(NO_3)_2$, and 2.52 Å for [**5**]). There were intramolecular aurophilic interactions in [**6**]$^{2+}$ (Au···Au = Av. 3.05 Å), which was distinct from the homochiral $Au^I_4Co^{III}_2$ structure in [**3**]$^{2+}$ that had no aurophilic interaction with the Au···Au distance of 3.6044(5) Å. In [**6**]$(NO_3)_2$, no direct hydrogen bonding interactions were formed between the complex cations, and cationic complexes and dimeric anions were arranged alternately without the formation of large anionic cluster structure as found in homochiral systems (Figure 2-57).

In the crystal structure of [**6**]$(PF_6)_2$, similar hexanuclear molecular structure to that in [**6**]$(NO_3)_2$ was found (Av. Co–S = 2.26 Å, Co–O = 1.91 Å, Co–N = 1.95 Å, S–Co–S = 98.6°, O–Co–O = 177.9°, N–Co–N = 94.6°, Au···Au = 3.07 Å), and the cationic complexes and anions were also arranged alternatively. For detailed molecular and packing structures, see Figures 2-58 and 2-59. The crystallographic data are summarized in Table 2-20, and the selected bond distances and angles are listed in Table 2-21.

II-3-13. Chiral Behavior of the Heterochiral System.

The reaction of D_2/L_2-H_2[**2**] or DL-H_2[**2**] with $Co(OAc)_2$ without additional oxidant afforded the $Au^I_4Co^{II}_2$ complex, [**5**], while the similar treatment with PbO_2 gave the $Au^I_4Co^{III}_2$ complex, [**6**]$(NO_3)_2$, together with a minor amount of homochiral [**3**]$(NO_3)_2$ and [**4**]$(NO_3)_2$ (Schemes 2-5, 2-8, and 2-9, Figure 2-60). The production of the heterochiral $Au^I_4Co^{III}_2$ cationic complex (DDLL) from the mixture of D_2-H_2[**2**] and L_2-H_2[**2**] suggested that the chiral scrambling occurred in solution. To discuss the solution

behavior in more detail, the NMR study was performed. The ^{1}H NMR spectrum of the 1:1 mixture of homochiral [**3**]$^{2+}$ and [**4**]$^{2+}$ was also almost the same as that of heterochiral [**6**]$^{2+}$, showing two sets of signals assignable to the homochiral and heterochiral $Au^{I}_{4}Co^{III}_{2}$ structures (Figure 2-61). This result indicated that the chiral scrambling between [**3**]$^{2+}$ and [**4**]$^{2+}$ to form [**6**]$^{2+}$ occurred even after the formation of hexanuclear $Au^{I}_{4}Co^{III}_{2}$ structures.

Based on the result, it was concluded that $Au^{I}_{4}Co^{III}_{2}$ cationic complex were in the chiral scrambling equilibrium state in solution. (Scheme 2-9) Focusing on the chirality around the Co^{III} centers in [**3**]$^{2+}$, [**4**]$^{2+}$, and [**6**]$^{2+}$, all of the obtained isomers had the homochiral coordination geometry, that was, two pen ligands binding to a Co^{III} center always had the same chirality (DD or LL). Thus, the chiral scrambling might occur through the cleavage and formation of the Au–S bonds. Of note was that only three isomers (DDDD, LLLL, and DDLL) were formed even though the seven isomers were possibly formed (DDDD, LLLL, DDDL, LLLD, DDLL, DLDL, and DLLD) (Scheme 2-10). Molecular modelling examination revealed that the only all-*trans* or all-*cis* coordination modes around the cobalt center were suitable for the DL-pen coordination environment due to the steric constrained molecular backbone of penicillaminate. However, the all-*trans* coordination mode seems to be unfavorable owing to the strong trans effect of thiolate-S atoms. In addition, in the case of the all-*cis* coordination mode, the steric repulsions between phenyl rings of dppee ligands appeared in DDDL-, LLLD-, DLDL-, and DLLD-[$Au^{I}_{4}Co^{III}_{2}$ (*trans*-dppee)$_2$(pen)$_4$]$^{2+}$ model structures. This is the reason for selective formation of three isomers (DDDD, LLLL, and DDLL).

For the $Au^{I}_{4}Co^{II}_{2}$ complex, only the heterochiral (DDLL) complex, [**5**], was isolated. Since [**5**] had a good crystallinity and a less solubility, probably owing to the rigid bridging diphosphine, the intermediate Co^{II} state might be isolated as [**5**]. Unfortunately, the structures in solution state were difficult to be discussed by NMR analyses due to the paramagnetic Co^{II} centers. The attempt for the isolation of homochiral $Au^{I}_{4}Co^{II}_{2}$ complex such as the reaction under inert condition was failed. By comparing with the heterochiral (DDLL) and homochiral (DDDD or LLLL) hexanuclear structures, it was assumed that the strong Au···Au intramolecular interactions found in the heterochiral hexanuclear structure would contribute to the stabilization of the hexanuclear structure and the isolation of the crystals.

Finally, the chiral behavior was compared with the dppe case. The similar chiral scrambling behavior was found in the dppe systems; the mixing of the homochiral metalloligands, D$_2$- and L$_2$-[Au$_2$(dppe)(Hpen)$_2$], resulted in the formation of D$_2$, L$_2$, and DL isomers of the Au^{I}_{2} metalloligands. The reaction of a mixture of D$_2$- and L$_2$-[Au$_2$(dppe)(Hpen)$_2$] with Co^{III} also led to the formation of both homochiral and

heterochiral $Au^{I}Co^{III}$ structures, but the crystallization behavior was more complicated than that in the case of *trans*-dppee system. After the addition of nitrate, three kinds of crystals were obtained; two of them were the homochiral DDDD- or LLLL-$[Au^{I}_4Co^{III}_2(dppe)_2(pen)_4](NO_3)_2$ (Scheme 2-8) and the other was the heterochiral DDLL-$[Au^{I}_4Co^{III}_2(dppe)_2(pen)_4](NO_3)_2$ that had the similar molecular structure to that of $[\mathbf{6}]^{2+}$. However, the addition of hexafluorophosphate anion instead of nitrate ions led to the crystallization of another species, the heterochiral trinuclear $Au^{I}_2Co^{III}$ complex, $[Au^{I}_2Co^{III}(dppe)(D\text{-pen})(L\text{-pen})]PF_6$, in which hexadentate DL-metalloligand, $[Au_2(dppe)(D\text{-pen})(L\text{-pen})]^{2-}$, coordinated to one Co^{III} center in a chelating mode, and the dppe linker adopted a *cis* conformation (Figure 2-62).[7c] The flexible dppe ligand made it possible to form such a *cis* conformational structure, while in the *trans*-dppee complex, the rigidity of *trans*-dppee prevented from the formation of such a trinuclear complex, and only the hexanuclear complex with a *trans* conformation was produced.

II-3-14. Comparison between Homochiral and Heterochiral AuCo Complexes.

As described before, both the homochiral and heterochiral $Au^{I}Co^{III}$ complexes formed an $Au^{I}_4Co^{III}_2$ hexanuclear structure consisting of two metalloligands that linked two Co^{III} atoms to form an 18-membered metalloring, but the whole structures of the cationic complexes were different because of the steric influence (Figure 2-63). In the homochiral complex cation, the metalloring had a twisted structure without an aurophilic interaction, while in the heterochiral one, the metalloring had a normal untwisted structure with aurophilic interactions (Table 2-22). Such a difference in the molecular shapes led to the different intermolecular interactions and the different supramolecular structures. In the homochiral complex, six of the homochiral cations were aggregated into the cationic hexameric structure, and the hexamers were arranged in an fcc structure so as to form large cavities. These supramolecular structures were supported by multiple CH$\cdots\pi$ and hydrogen bonding interactions. The inorganic anions were aggregated and incorporated in the cavities. On the other hand, the heterochiral cationic complexes did not form any cluster-like assemblies because of the different orientation of amine moieties, and the common alternate arrangement for complex cation and inorganic anion was formed.

Next, the conversion between the homochiral and heterochiral $Au^{I}_4Co^{III}_2$ structures was discussed. The ^{1}H NMR spectrum of the heterochiral cationic complex $[\mathbf{6}]^{2+}$ in D_2O/CD_3OD changed after dissolution, reaching to a set of signals for the homochiral complex cations ($[\mathbf{3}]^{2+}$ and $[\mathbf{4}]^{2+}$) and the heterochiral cationic complex ($[\mathbf{6}]^{2+}$) with an almost same integration ratio after 12 h (Figures 2-45, 2-61). The same spectrum was observed by dissolution of racemic mixture ($[\mathbf{3}]^{2+}$ and $[\mathbf{4}]^{2+}$ in 1:1 ratio) after 1 d. These

results indicated that heterochiral [**6**]$^{2+}$ and homochiral [**3**]$^{2+}$ and [**4**]$^{2+}$ were convertible in solution. In addition, the final ratio between heterochiral and homochiral compounds was 1:1, indicating that the stability of homochiral and heterochiral complex cations was almost same in solution.

Finally, the stability of the oxidation states of the Co ions in the homochiral and heterochiral complex cations was discussed. In the homochiral system, only the $Au^{I}_{4}Co^{III}_{2}$ structure was formed in the reactions of D_2-H_2[**2**] with Co^{II} ion both with/without oxidant. On the other hand, the heterochiral reaction solution containing D_2-H_2[**2**], L_2-H_2[**2**], and Co^{II} ion with oxidant gave the mixture of the homochiral and heterochiral $Au^{I}_{4}Co^{III}_{2}$ structures (DDDD, LLLL, and DDLL; Scheme 2-9) and the reaction without oxidant gave only the heterochiral $Au^{I}_{4}Co^{II}_{2}$ structure (DDLL). The DDDD/LLLL-$Au^{I}_{4}Co^{III}_{2}$ structures had a twisted metalloring, of which two Au^{I}_{2} diphosphine moieties were very close to each other (the closest $C_{Ph}\cdots C_{Ph}$ = 3.18 Å). This was the reason why the cobalt ion does not adopt the +II oxidation state with the same $Au^{I}_{4}Co^{III}_{2}$ structures, in which the phenyl rings in two Au^{I}_{2} diphosphine moieties might contact to each other by the elongation of Co–S bonds as illustrated in Scheme 2-11. On the other hand, in the DDLL-$Au^{I}_{4}Co^{III}_{2}$ structures, it had an untwisted metalloring, in which two Au^{I}_{2} diphosphine moieties were far enough ($C_{Ph}\cdots C_{Ph}$ = 3.37 Å) for Co^{III} and Co^{II} oxidation states.

II-4. Summary.

In this chapter, the synthesis and coordination behavior of the novel metalloligand which has *trans*-dppee as a bridging diphosphine toward Co^{II} were investigated. By the reactions of this metalloligand, $[Au^{I}_2$(*trans*-dppee)(D or L-Hpen)$_2]$ (D$_2$-H$_2$[**2**] or L$_2$-H$_2$[**2**]) with Co^{II} in air, the $Au^{I}_4Co^{III}_2$ hexanuclear complexes, $[Au^{I}_4Co^{III}_2$(*trans*-dppee)$_2$(D or L-pen)$_4$](X) ([**3**]X or [**4**]X; X = $(NO_3)_2$, $(ClO_4)_2$, $(BF_4)_2$, SO_4), were synthesized. Single crystal X-ray analysis of these complexes revealed the presence of the $Au^{I}_4Co^{III}_2$ complex cations and inorganic anions in a 1:2 ratio for the monovalent anions and in a 1:1 ratio for the divalent anions. In the crystal structure, the six complex cations were aggregated into the large octahedron-shaped supramolecular structure through multiple interactions. These hexameric supramolecular octahedrons were closely packed in a face-centered cubic (fcc) structure. In the fcc packing structure, there were four kinds of interstices, and, ten monovalent anions with the adamantane-like aggregation structure or six divalent anions with the octahedrally aggregation structure were found in one of the four interstices. Such multistep aggregation of the complex cations accompanied with the aggregation of inorganic anions was also found in the previous dppe system, but the orientation of the inorganic anions was slightly different. The use of the rigid diphosphine linker (*trans*-dppee), instead of the flexible linker (dppe), resulted in the formation of the slightly elongated structure of the cationic complex with the more slender shape, which led to the formation of the larger hexameric cation cluster. As a result, the smaller hydrophilic tetrahedral interstices were formed in the *trans*-dppee system, and the anions in the tetrahedral interstices were arranged more closely. Thus, the subtle control of the anion-aggregation structures by changing the diphosphine linkers of the complex cations was achieved.

Secondly, in this chapter, treatment of a racemic mixture of the chiral metalloligands $[Au^{I}_2$(*trans*-dppee)(D or L-Hpen)$_2]$ (D$_2$-H$_2$[**2**], L$_2$-H$_2$[**2**]) or meso heterochiral metalloligand $[Au^{I}_2$(*trans*-dppee)(DL-Hpen)$_2]$ (DL-H$_2$[**2**]) with Co^{II} or Co^{III} was executed for investigating the effect of the chirality on the aggregation behavior and the physical properties.

The reaction of a racemic mixture of the metalloligands with Co^{II} in the presence of PbO_2 as an oxidant led to the separate crystallization of heterochiral $Au^{I}_4Co^{III}_2$ complex, $[Au^{I}_4Co^{III}_2$(*trans*-dppee)$_2$(D-pen)$_2$(L-pen)$_2$](NO$_3$)$_2$ ([**6**](NO$_3$)$_2$), in addition to the homochiral $Au^{I}_4Co^{III}_2$ complexes, $[Au^{I}_4Co^{III}_2$(*trans*-dppee)$_2$(D- or L-pen)$_4$](NO$_3$)$_2$ ([**3**](NO$_3$)$_2$ and [**4**](NO$_3$)$_2$), as in the case of dppe system. The formation of the three compounds must be accompanied by the chiral scrambling of the metalloligands. In addition, the scrambling behavior was also observed after the coordination to Co^{III} centers.

The supramolecular structures of the homochiral ([**3**]$^{2+}$, [**4**]$^{2+}$) and heterochiral ([**5**]$^{2+}$) $Au^{I}_{4}Co^{III}_{2}$ complexes were quite different, although both the complexes have essentially the same chemical formula. The unique separate aggregation of the cation and anion species was found only in the homochiral complexes, indicating the importance of the chirality on the supramolecular structure. Of note is that the trinuclear complexes having a molecular structure similar to that in the dppe system ($[Au^{I}_{2}Co^{III}$(dppe)(D-pen)(L-pen)]PF_6) were not crystalized in spite of almost the same reaction conditions. This fact was reasonably concluded from the rigidity of the *trans*-dppee unit which prevented the metalloligand to take a bent molecular structure, which is needed for the coordination in a chelating mode.

The reaction of a racemic mixture of the metalloligand with Co^{II} in air in the absence of oxidant gave the $Au^{I}_{4}Co^{II}_{2}$ heterochiral complex, $[Au^{I}_{4}Co^{II}_{2}$(*trans*-dppee)$_2$(D-pen)$_2$(L-pen)$_2$] ([**5**]). This is different from the dppe system where only the Au^{I}-Co^{III} hexanuclear or trinuclear complexes were isolated. The unusual isolation of the Co^{II} species with the S-donating ligand in air was achieved by the high crystallinity of the *trans*-dppee system. Thus, it was found that the small change of bridging diphosphine unit affected not only their molecular and supramolecular structures as explained in homochiral system, but also their electrical structures.

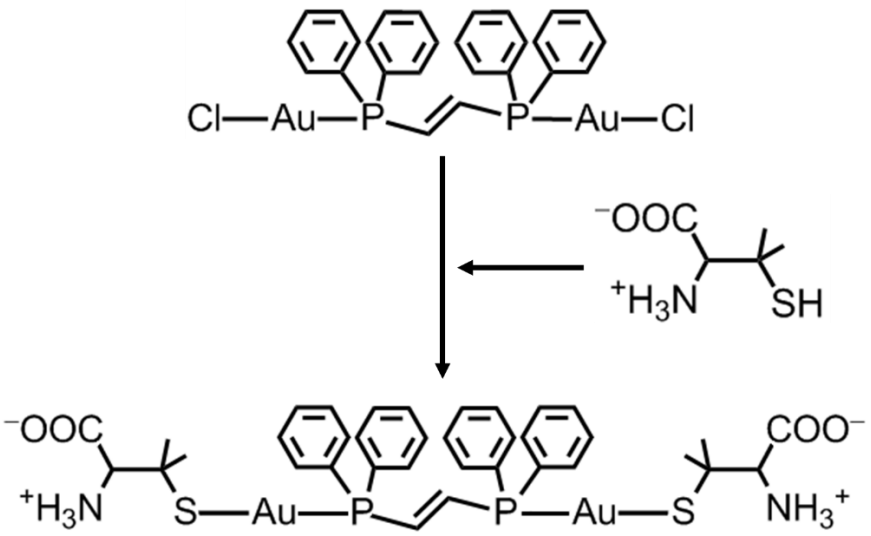

Scheme 2-1. Synthesis of metalloligand, H_2[**2**].

(a)

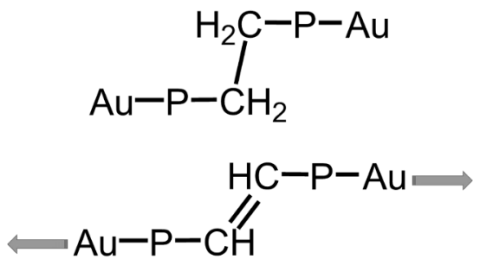

Scheme 2-2. Effect of linker carbon chain over the diphosphine moieties.

(a)

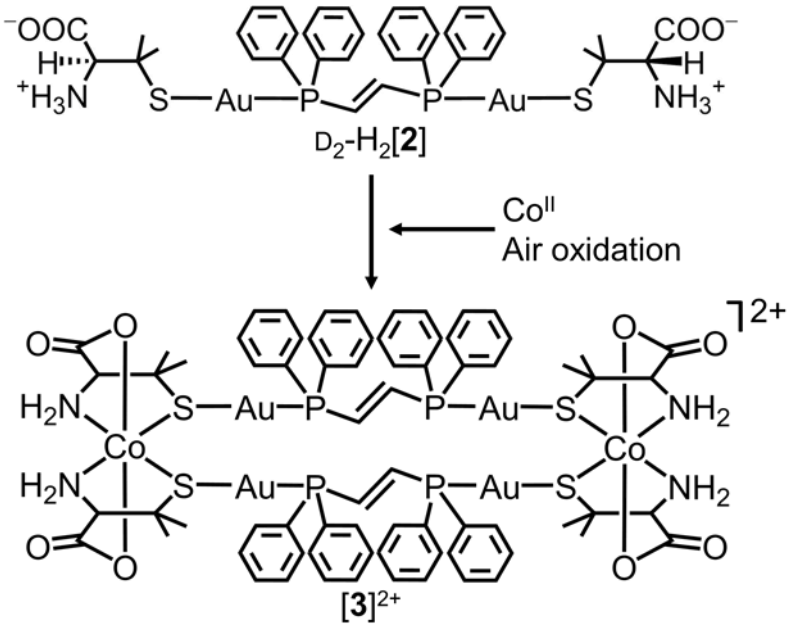

(b)

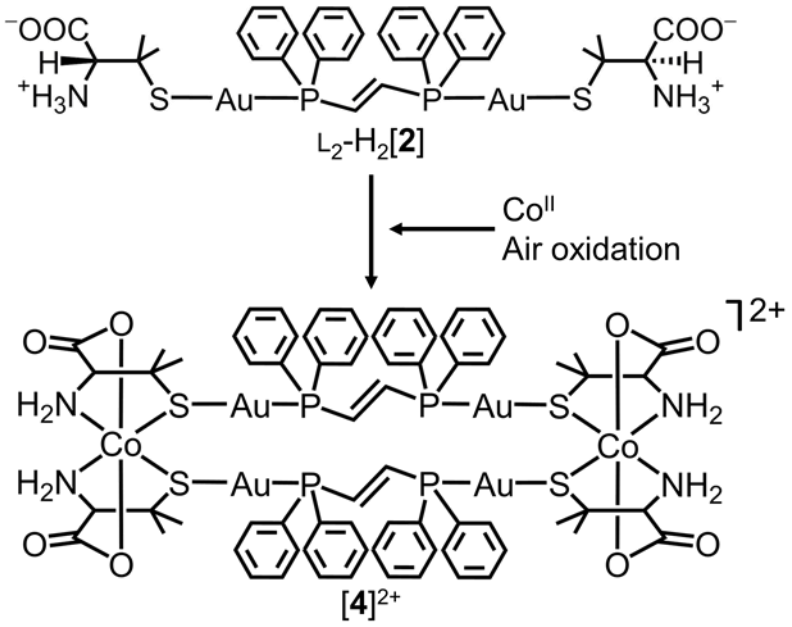

Scheme 2-3. Synthesis of $Au^{I}_{4}Co^{III}_{2}$ complex cations, (a) $[\mathbf{3}]^{2+}$ and (b) $[\mathbf{4}]^{2+}$.

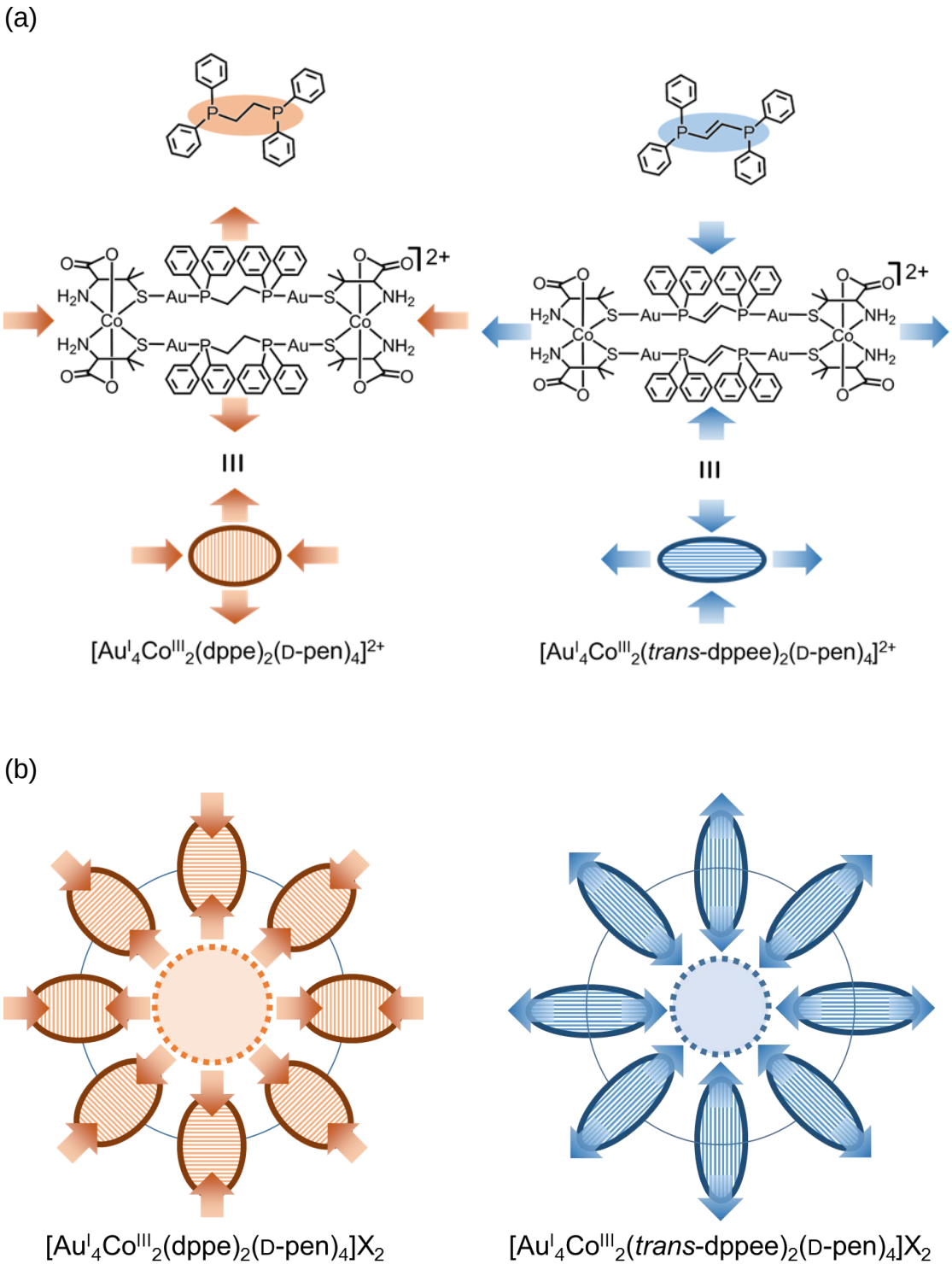

Scheme 2-4. Effect of diphosphine moieties on the (a) molecular structure of $Au^{I}_{4}Co^{III}_{2}$ complex cations and (b) supramolecular structures around the hydrophilic interstices.

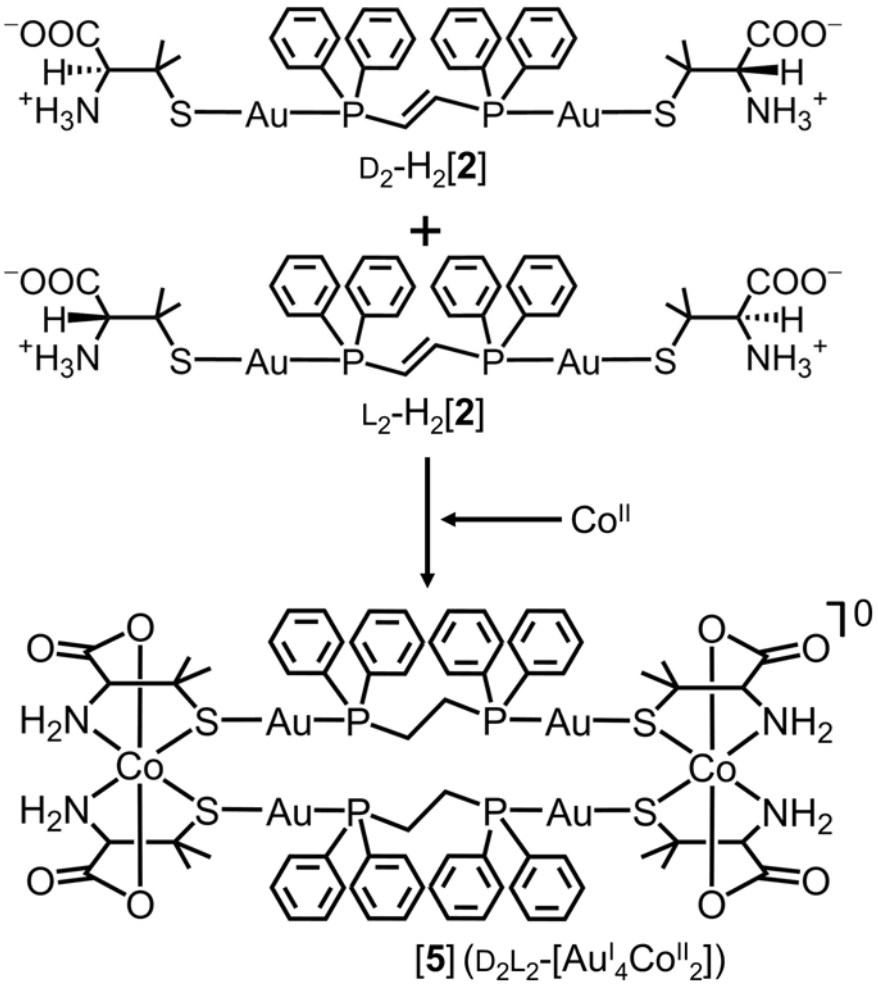

Scheme 2-5. Reaction of a mixture of D_2-H_2[**2**] and L_2-H_2[**2**] with Co^{II} ion.

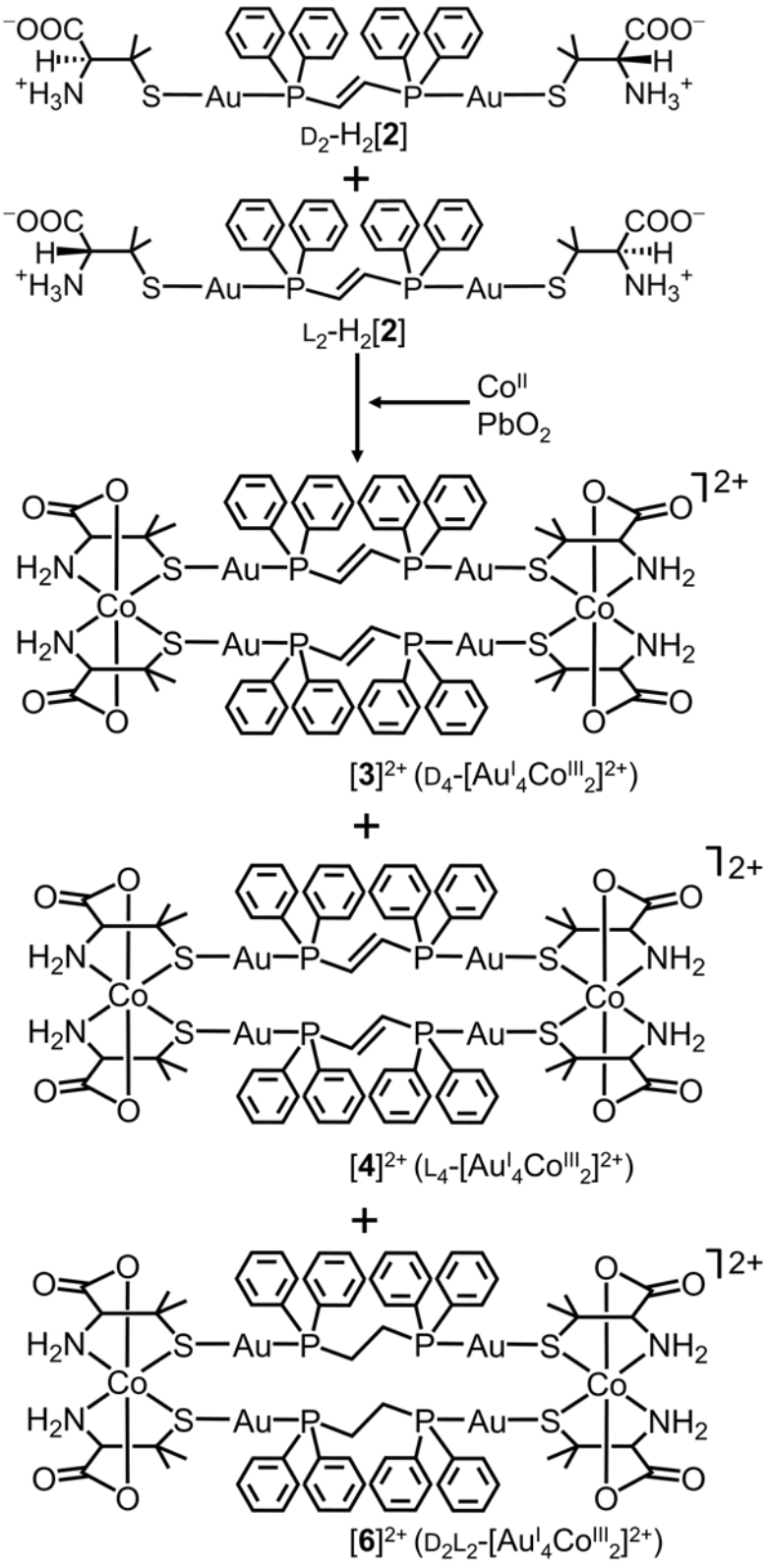

Scheme 2-6. Reaction of a mixture of D_2-H_2[**2**] and L_2-H_2[**2**] with Co^{III} ion.

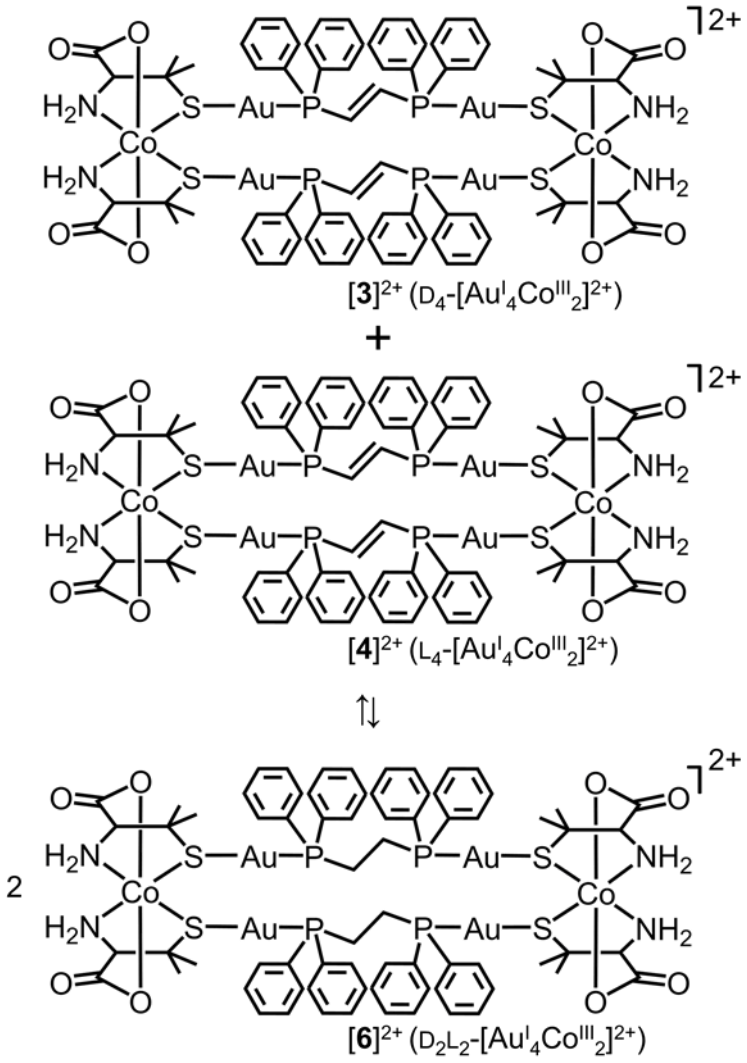

Scheme 2-7. Equilibrium between homochiral and heterochiral hexanuclear complexes.

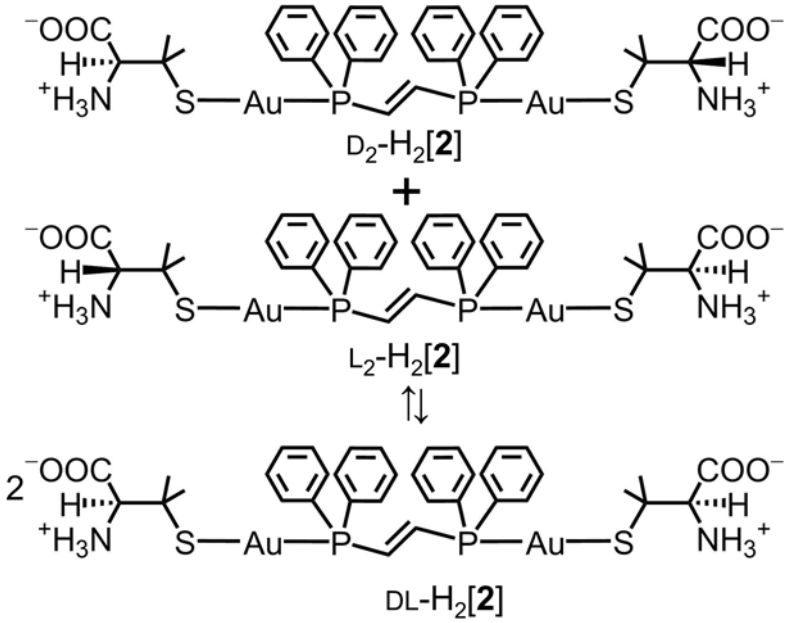

Scheme 2-8. Scrambling of the homochiral metalloligand to form heterochiral metalloligand.

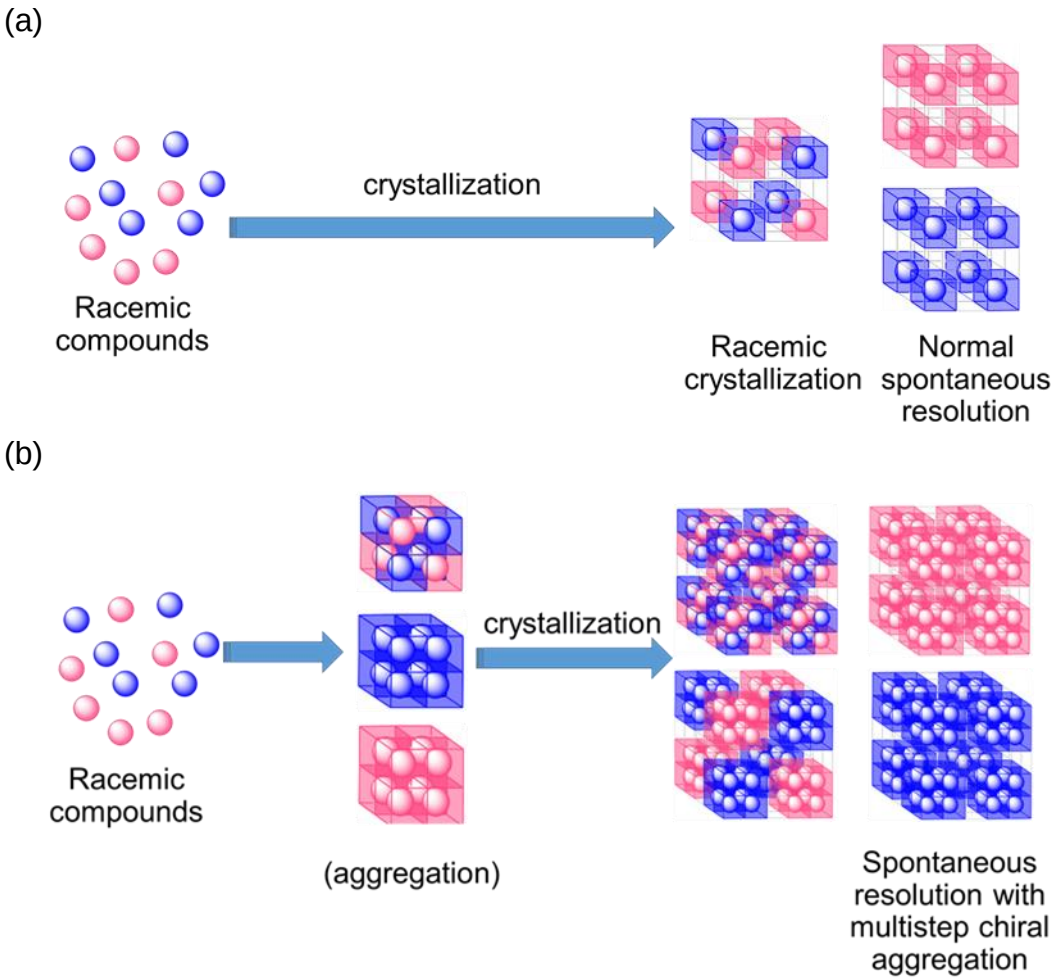

Scheme 2-9. (a) Normal crystallization behavior from racemic solution. (b) Spontaneous resolution behavior with multistep chiral aggregation.

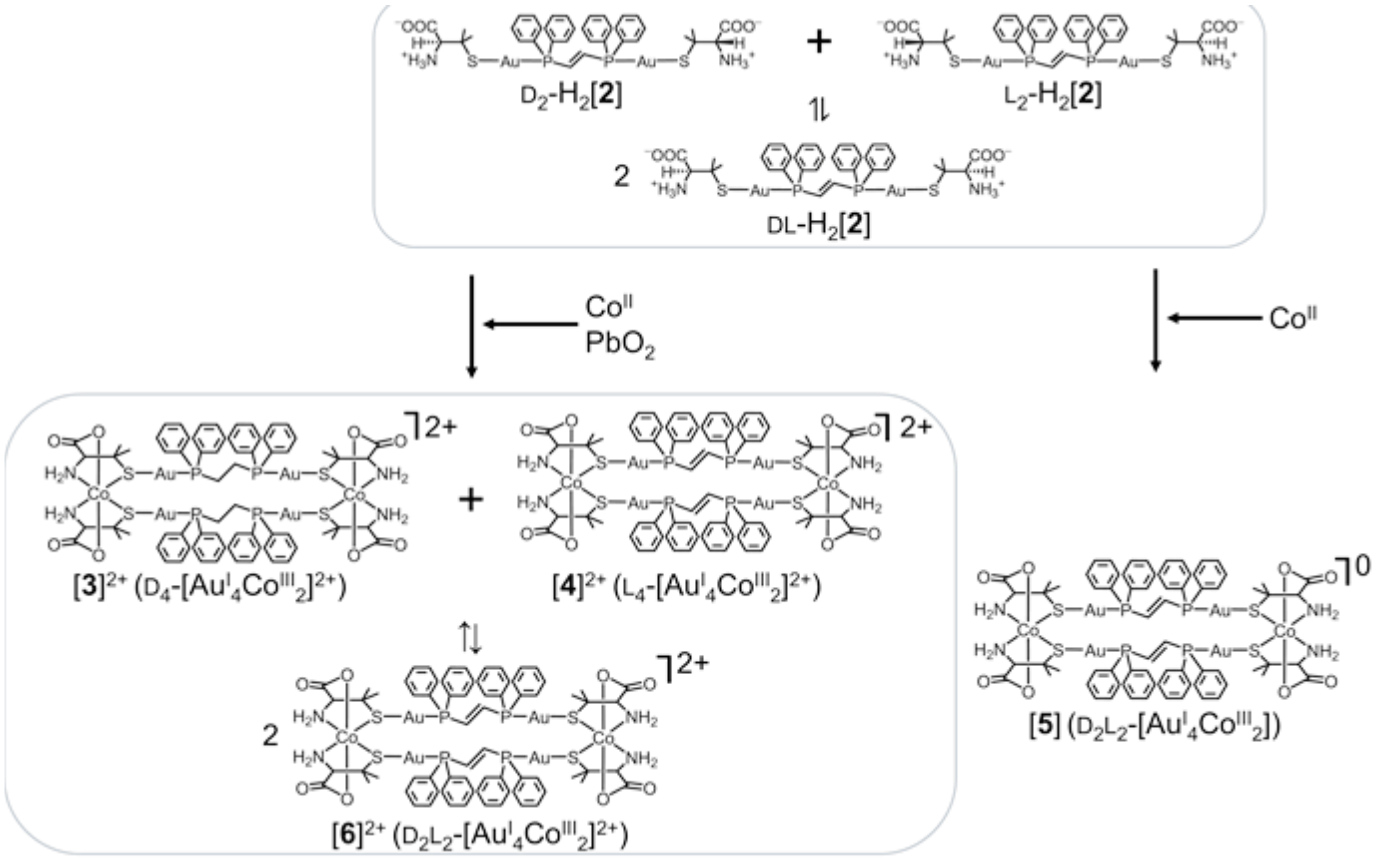

Scheme 2-10. The reaction in heterochiral condition.

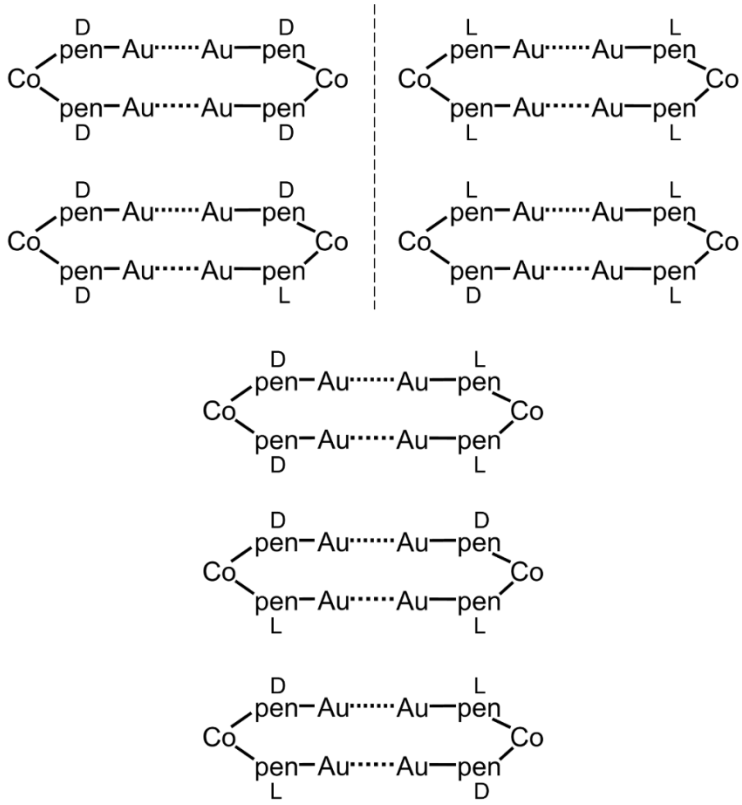

Scheme 2-11. Possible seven isomers for $[Au^{I}_{4}Co^{III}_{2}(\textit{trans}\text{-dppee})_{2}(pen)_{4}]^{2+}$.

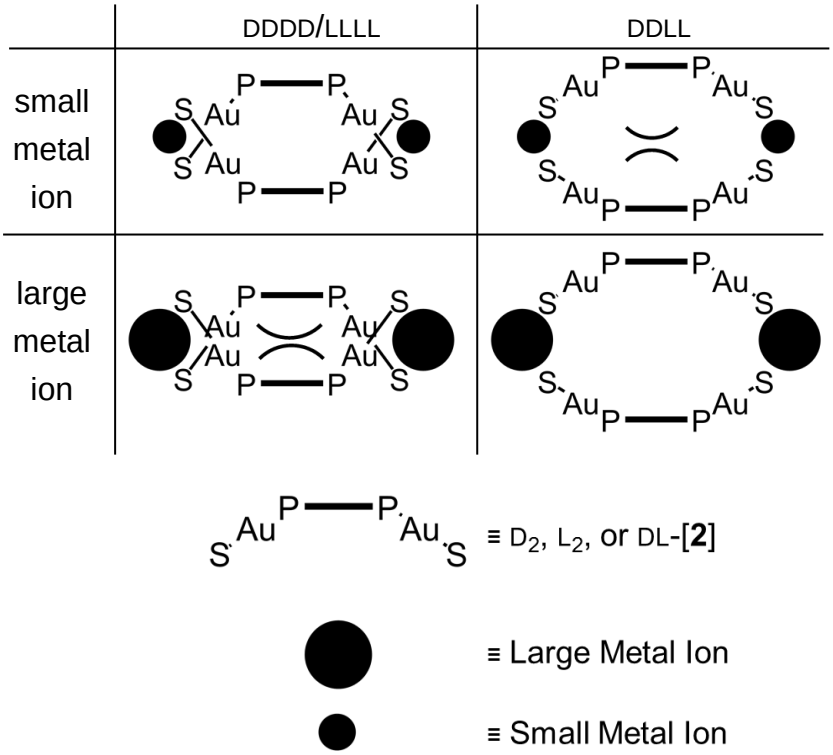

Scheme 2-12. The steric effect of metal size in the case of homochiral and heterochiral complexes.

Table 2-1. Crystallographic data for D_2-H_2[**2**].

	D_2-H_2[**2**]·7H_2O
Formula	$C_{36}H_{56}Au_2N_2O_{11}P_2S_2$
Formula weight	1212.82
Crystal color	colorless
Crystal size, mm^3	0.13 x 0.05 x 0.05
Crystal system	monoclinic
Space group	$P2_1$
a, Å	11.8903(2)
b, Å	34.5587(6)
c, Å	12.1706(2)
β, °	107.086(7)
V, $Å^3$	4780.3(2)
Z	4
ρ(calc), g/cm^3	1.685
*R*1 (*I*>2*σ*(*I*)) [a)]	0.0507
w*R*2 (*I*>2*σ*(*I*)) [b)]	0.1055
*R*1 (all data) [a)]	0.0648
w*R*2 (all data) [b)]	0.1114

a) $R1 = \Sigma||F_o|-|F_c||/\Sigma(|F_o|)$

b) $wR2 = [\Sigma_w(|F_o|^2-|F_c|^2)^2/\Sigma_w(|F_o|^2)^2]^{1/2}$

Table 2-2. Selected bond distances (Å) and angles (°) for D_2-H_2[**2**].

		bond distances	
Au(1)–S(1)	2.305(2)	Au(2)–S(2)	2.309(3)
Au(3)–S(3)	2.297(3)	Au(4)–S(4)	2.295(3)
Au(1)–P(1)	2.264(2)	Au(2)–P(2)	2.265(2)
Au(3)–P(3)	2.264(2)	Au(4)–P(4)	2.260(3)
C(21)–C(22)	1.314(13)	C(47)–C(48)	1.308(14)
Au(1)···Au(4)	3.1233(5)	Au(2)···Au(3)	3.0587(5)
		angles	
P(1)–Au(1)–S(1)	176.98(9)	P(2)–Au(2)–S(2)	178.86(10)
P(3)–Au(3)–S(3)	179.18(10)	P(4)–Au(4)–S(4)	176.59(9)
P(1)–C(21)–C(22)	125.5(8)	P(2)–C(22)–C(21)	124.1(8)
P(3)–C(47)–C(48)	125.0(8)	P(4)–C(48)–C(47)	124.4(9)

Table 2-3. Comparison of molecular structures between [Au_2(dppe)(D-Hpen)$_2$] and D_2-H_2[**2**].

	[Au_2(dppe)(D-Hpen)$_2$]	D_2-H_2[**2**]
Av. Au–P, Å	2.26	2.26
Av. Au–S, Å	2.31	2.30
Av. P–Au–S, °	172.9	177.9
Av. C–C (in linker chain), Å	1.55	1.31
Av. P–C–C (in linker chain), °	109.5	124.8
Av. P···P (in linker chain), Å	4.41	4.50

Table 2-4. Crystallographic data for [**3**]X, and [**4**]$(NO_3)_2$ (X = $(NO_3)_2$, $(ClO_4)_2$, $(BF_4)_2$, and SO_4).

	[**3**]$(NO_3)_2$·$4H_2O$	[**3**]$(ClO_4)_2$·$3H_2O$	[**3**]$(BF_4)_2$·$4.67H_2O$	[**3**]SO_4·$5.17H_2O$	[**4**]$(NO_3)_2$·$4H_2O$
Formula	$C_{72}H_{88}Au_4Co_2N_6O_{18}P_4S_4$	$C_{72}H_{86}Au_4Co_2Cl_2N_4O_{19}P_4S_4$	$C_{72}H_{80}Au_4Co_2F_8N_4O_{12.67}B_2P_4S_4$	$C_{72}H_{90.33}Au_4Co_2N_4O_{17.17}P_4S_5$	$C_{72}H_{88}Au_4Co_2N_6O_{18}P_4S_4$
Formula weight	2483.412	2540.287	2535.53	2476.39	25483.33
Crystal color	purple	purple	purple	purple	purple
Crystal size, mm^3	0.20 x 0.20 x 0.08	0.25 x 0.25 x 0.15	0.10 x 0.10 x 0.05	0.28 x 0.28 x 0.25	0.10 x 0.10 x 0.10
Crystal system	cubic	cubic	cubic	cubic	cubic
Space group	*F*23	*F*23	*F*23	*F*23	*F*23
a, Å	38.1720(7)	38.4871(7)	38.46(16)	38.2314(7)	37.866(7)
V, $Å^3$	55620.5(18)	557009.3(18)	56880(701)	55880.5(18)	54292(18)
Z	24	24	24	24	24
ρ(calc), g/cm^3	1.779	1.776	1.777	1.766	1.823
*R*1 ($I>2\sigma(I)$) [a)]	0.0492	0.0451	0.0610	0.0603	0.0763
w*R*2 ($I>2\sigma(I)$) [b)]	0.1271	0.1268	0.1164	0.1465	0.1582
*R*1 (all data) [a)]	0.0610	0.0530	0.0774	0.0856	0.1327
w*R*2 (all data) [b)]	0.1343	0.1316	0.1217	0.1592	0.1819

a) $R1 = \Sigma|(|F_o|-|F_c|)|/\Sigma(|F_o|)$

b) $wR2 = [\Sigma_w(|F_o|^2-|F_c|^2)^2/\Sigma_w(|F_o|^2)^2]^{1/2}$

Table 2-5. Selected bond distances (Å) and angles (°) for [**3**]$(NO_3)_2$.

		bond distances	
Au(1)–S(1)	2.317(2)	Au(2)–S(2)	2.331(3)
Au(1)–P(1)	2.250(3)	Au(2)–P(2)	2.271(3)
C(11)–C(12)	1.330(19)	C(13)–C(13)'	1.222(19)
Co(1)–S(1)	2.293(2)	Co(1)–S(2)	2.292(3)
Co(1)–O(1)	1.919(6)	Co(1)–O(3)	1.943(6)
Co(1)–N(1)	1.961(8)	Co(1)–N(2)	1.970(8)
Au(1)···Au(2)	3.6044(5)	Co(1)···Co(1)'	11.3463(23)
		angles	
P(1)–Au(1)–S(1)	177.88(10)	P(2)–Au(2)–S(2)	178.14(8)
P(1)–C(11)–C(12)	120.1(11)	P(1)'–C(12)–C(11)	121.1(11)
P(2)–C(13)–C(13)'	125.0(12)	S(1)–Co(1)–S(2)	97.40(10)
S(1)–Co(1)–O(1)	92.15(19)	S(1)–Co(1)–O(3)	89.4(2)
S(1)–Co(1)–N(1)	85.3(2)	S(1)–Co(1)–N(2)	172.5(3)
S(2)–Co(1)–O(1)	91.0(2)	S(2)–Co(1)–O(3)	91.0(2)
S(2)–Co(1)–N(1)	173.1(2)	S(2)–Co(1)–N(2)	85.0(3)
O(1)–Co(1)–O(3)	177.88(10)	O(1)–Co(1)–N(1)	82.6(3)
O(1)–Co(1)–N(2)	94.9(3)	O(3)–Co(1)–N(1)	95.3(3)
O(3)–Co(1)–N(2)	83.4(3)	N(1)–Co(1)–N(2)	93.1(3)

Symmetry code: (') 3/2–x, 3/2–y, z.

Table 2-6. Selected bond distances (Å) and angles (°) for [**3**]$(ClO_4)_2$.

		bond distances	
Au(1)–S(1)	2.324(2)	Au(2)–S(2)	2.337(2)
Au(1)–P(1)	2.261(3)	Au(2)–P(2)	2.269(2)
C(11)–C(12)	1.33(2)	C(13)–C(13)'	1.191(19)
Co(1)–S(1)	2.289(2)	Co(1)–S(2)	2.295(2)
Co(1)–O(1)	1.930(6)	Co(1)–O(3)	1.922(6)
Co(1)–N(1)	1.962(8)	Co(1)–N(2)	1.958(8)
Au(1)···Au(2)	3.6364(5)	Co(1)···Co(1)'	11.2617(21)
		angles	
P(1)–Au(1)–S(1)	177.45(10)	P(2)–Au(2)–S(2)	178.46(8)
P(1)–C(11)–C(12)	118.7(12)	P(1)'–C(12)–C(11)	117.4(12)
P(2)–C(13)–C(13)'	124.4(12)	S(1)–Co(1)–S(2)	96.90(9)
S(1)–Co(1)–O(1)	92.43(18)	S(1)–Co(1)–O(3)	91.09(17)
S(1)–Co(1)–N(1)	85.0(2)	S(1)–Co(1)–N(2)	172.2(2)
S(2)–Co(1)–O(1)	91.3(2)	S(2)–Co(1)–O(3)	90.83(19)
S(2)–Co(1)–N(1)	173.7(2)	S(2)–Co(1)–N(2)	85.9(3)
O(1)–Co(1)–O(3)	175.7(3)	O(1)–Co(1)–N(1)	82.7(3)
O(1)–Co(1)–N(2)	94.9(3)	O(3)–Co(1)–N(1)	95.1(3)
O(3)–Co(1)–N(2)	81.5(3)	N(1)–Co(1)–N(2)	93.1(3)

Symmetry code: (') –x, y, 1–z.

Table 2-7. Selected bond distances (Å) and angles (°) for [**3**]$(BF_4)_2$.

		bond distances	
Au(1)–S(1)	2.330(10)	Au(2)–S(2)	2.326(10)
Au(1)–P(1)	2.269(10)	Au(2)–P(2)	2.260(10)
C(11)–C(11)'	1.25(3)	C(12)–C(13)	1.30(3)
Co(1)–S(1)	2.297(10)	Co(1)–S(2)	2.294(10)
Co(1)–O(1)	1.924(12)	Co(1)–O(3)	1.934(12)
Co(1)–N(1)	1.951(14)	Co(1)–N(2)	1.985(14)
Au(1)···Au(2)	3.632	Co(1)···Co(1)'	11.295
		angles	
P(1)–Au(1)–S(1)	178.60(13)	P(2)–Au(2)–S(2)	177.42(16)
P(1)–C(11)–C(11)'	124.8(16)	P(2)–C(12)–C(13)	119.0(18)
P(2)'–C(13)–C(12)	119.4(18)	O(1)-Co(1)-O(3)	176.0(4)
O(1)-Co(1)-N(1)	81.9(4)	O(3)-Co(1)-N(1)	95.0(4)
O(1)-Co(1)-N(2)	94.9(4)	O(3)-Co(1)-N(2)	82.7(4)
N(1)-Co(1)-N(2)	92.8(5)	O(1)-Co(1)-S(2)	91.0(3)
O(3)-Co(1)-S(2)	92.0(3)	N(1)-Co(1)-S(2)	172.4(4)
N(2)-Co(1)-S(2)	85.3(3)	O(1)-Co(1)-S(1)	91.1(3)
O(3)-Co(1)-S(1)	91.3(3)	N(1)-Co(1)-S(1)	85.9(4)
N(2)-Co(1)-S(1)	173.7(4)	S(2)-Co(1)-S(1)	96.83(15)

Symmetry code: (') 1–x, 1–y, z.

Table 2-8. Selected bond distances (Å) and angles (°) for [**3**]SO_4.

		bond distances	
Au(1)–S(1)	2.325(3)	Au(2)–S(2)	2.321(4)
Au(1)–P(1)	2.251(4)	Au(2)–P(2)	2.264(4)
C(11)–C(12)	1.24(2)	C(13)–C(13)'	1.16(2)
Co(1)–S(1)	2.288(3)	Co(1)–S(2)	2.304(3)
Co(1)–O(1)	1.939(7)	Co(1)–O(3)	1.927(7)
Co(1)–N(1)	1.965(9)	Co(1)–N(2)	1.949(9)
Au(1)···Au(2)	3.6125(6)	Co(1)···Co(1)'	11.3625(29)
		angles	
P(1)–Au(1)–S(1)	177.59(12)	P(2)–Au(2)–S(2)	178.92(11)
P(1)–C(11)–C(12)	116.8(13)	P(1)'–C(12)–C(11)	121.9(14)
P(2)–C(13)–C(13)'	126.4(15)	S(1)–Co(1)–S(2)	97.29(13)
S(1)–Co(1)–O(1)	90.7(2)	S(1)–Co(1)–O(3)	90.8(2)
S(1)–Co(1)–N(1)	84.7(3)	S(1)–Co(1)–N(2)	171.7(3)
S(2)–Co(1)–O(1)	91.5(2)	S(2)–Co(1)–O(3)	91.5(3)
S(2)–Co(1)–N(1)	173.0(3)	S(2)–Co(1)–N(2)	86.4(3)
O(1)–Co(1)–O(3)	176.6(4)	O(1)–Co(1)–N(1)	81.7(4)
O(1)–Co(1)–N(2)	96.6(4)	O(3)–Co(1)–N(1)	95.4(4)
O(3)–Co(1)–N(2)	81.7(4)	N(1)–Co(1)–N(2)	92.5(4)

Symmetry code: (') 1–x, 1–y, z.

Table 2-9. Selected bond distances (Å) and angles (°) for [**4**]$(NO_3)_2$.

		bond distances	
Au(1)–S(1)	2.303(4)	Au(2)–S(2)	2.310(5)
Au(1)–P(1)	2.232(5)	Au(2)–P(2)	2.248(5)
C(11)–C(12)	1.30(3)	C(13)–C(13)'	1.22(3)
Co(1)–S(1)	2.274(5)	Co(1)–S(2)	2.285(5)
Co(1)–O(1)	1.937(10)	Co(1)–O(3)	1.923(9)
Co(1)–N(1)	1.973(13)	Co(1)–N(2)	1.908(13)
Au(1)···Au(2)	3.5774(12)	Co(1)···Co(1)'	11.2464(47)
		angles	
P(1)–Au(1)–S(1)	177.86(18)	P(2)–Au(2)–S(2)	178.63(16)
P(1)–C(11)–C(12)	119.9(19)	P(1)'–C(12)–C(11)	122(2)
P(2)–C(13)–C(13)'	123.2(19)	S(1)–Co(1)–S(2)	97.66(18)
S(1)–Co(1)–O(1)	91.5(3)	S(1)–Co(1)–O(3)	89.5(3)
S(1)–Co(1)–N(1)	85.0(4)	S(1)–Co(1)–N(2)	172.3(5)
S(2)–Co(1)–O(1)	91.7(4)	S(2)–Co(1)–O(3)	91.0(3)
S(2)–Co(1)–N(1)	172.4(4)	S(2)–Co(1)–N(2)	86.1(5)
O(1)–Co(1)–O(3)	177.0(5)	O(1)–Co(1)–N(1)	81.0(5)
O(1)–Co(1)–N(2)	95.1(6)	O(3)–Co(1)–N(1)	96.2(5)
O(3)–Co(1)–N(2)	83.7(5)	N(1)–Co(1)–N(2)	92.1(6)

Symmetry code: (') 1–x, –y, z.

Table 2-10. Comparison of $Au^{I}_4Co^{III}_2$ hexanuclear structures.

diphosphine	dppe			*trans*-dppee		
counter anion	NO_3^-	ClO_4^-	SO_4^{2-}	NO_3^-	ClO_4^-	SO_4^{2-}
Av. P–C–C (in linker chain), °	110	111	111	122	120	122
Av. P···P (in linker chain), Å	4.43	4.43	4.44	4.46	4.47	4.47
Av. Au···Au (in linker chain), Å	5.96	5.90	5.99	6.18	6.14	6.19
Co···Co (in molecule), Å	11.09	10.98	11.13	11.35	11.26	11.36

Table 2-11. Comparison of fcc supramolecular structures.

diphosphine	dppe			*trans*-dppee		
counter anion	NO_3^-	ClO_4^-	SO_4^{2-}	NO_3^-	ClO_4^-	SO_4^{2-}
cell axis, Å	38.0	38.4	38.0	38.2	38.5	38.2
cell volume /10^4, Å^3	5.51	5.67	5.49	5.56	5.70	5.59
Max. Co···Co (in the hexamer), Å	20.7	20.8	20.7	20.8	20.9	20.9
volume of hydrophobic Td interstice [a)], Å^3	1521	1860	1663	1701	1798	1679
volume of hydrophilic Td interstice [a)], Å^3	912	1184	893	826	993	860
volume of interstice inside hexamer [a)] , Å^3	64	52	50	71	73	61
volume of octahedral interstice [a)], Å^3	67	81	45	66	80	72

a) The interstice volume is calculated by PLATON program.

Table 2-12. Crystallographic data for DL-H_2[**2**].

	DL-H_2[**2**]·2EtOH·4H_2O
Formula	$C_{40}H_{62}Au_2N_2O_{10}P_2S_2$
Formula weight	1250.91
Crystal color	colorless
Crystal size, mm^3	0.20 x 0.20 x 0.06
Crystal system	triclinic
Space group	*P*-1
a, Å	12.1454(3)
b, Å	14.0439(14)
c, Å	15.753(3)
α, °	69.538(10)
β, °	80.992(6)
γ, °	88.918(6)
V, Å^3	2484.6(5)
Z	2
ρ(calc), g/cm^3	1.672
*R*1 (*I*>2*σ*(*I*)) [a)]	0.0595
w*R*2 (*I*>2*σ*(*I*)) [b)]	0.1787
*R*1 (all data) [a)]	0.0774
R_w2 (all data) [b)]	0.1891

a) $R1 = \Sigma|(|F_o|-|F_c|)|/\Sigma(|F_o|)$

b) $wR2 = [\Sigma_w(|F_o|^2-|F_c|^2)^2/\Sigma_w(|F_o|^2)^2]^{1/2}$

Table 2-13. Selected bond distances (Å) and angles (°) for DL-H_2[**2**].

		bond distances	
Au(1)–S(1)	2.317(2)	Au(2)–S(2)	2.303(2)
Au(1)–P(1)	2.286(3)	Au(2)–P(2)	2.260(2)
C(11)–C(11)'	1.252(18)	C(12)–C(12)"	1.314(16)
Au(1)···Au(2)	3.0842(5)		
		angles	
P(1)–Au(1)–S(1)	178.54(9)	P(2)–Au(2)–S(2)	171.67(8)
P(1)–C(11)–C(11)'	125.7(12)	P(2)–C(12)–C(12)"	127.9(11)

Symmetry codes: (') 2–x, –y, –z, (") 2–x, 1–y, –z.

Table 2-14. Crystallographic data for [**5**].

	[**5**]·6MeOH·2H_2O
Formula	$C_{78}H_{108}Au_4Co_2N_4O_{16}P_4S_4$
Formula weight	2525.53
Crystal color	orange
Crystal size, mm^3	0.15 x 0.10 x 0.04
Crystal system	triclinic
Space group	*P*-1
a, Å	13.084(3)
b, Å	14.161(3)
c, Å	14.442(3)
α, °	65.189(17)
β, °	80.376(7)
γ, °	74.526(14)
V, $Å^3$	2336.1(10)
Z	1
ρ(calc), g/cm^3	1.788
*R*1 (*I*>2*σ*(*I*)) [a]	0.0743
w*R*2 (*I*>2*σ*(*I*)) [b]	0.1907
*R*1 (all data) [a]	0.1141
w*R*2 (all data) [b]	0.2399

a) $R1 = \Sigma|(|F_o|-|F_c|)|/\Sigma(|F_o|)$

b) $wR2 = [\Sigma_w(|F_o|^2-|F_c|^2)^2/\Sigma_w(|F_o|^2)^2]^{1/2}$

Table 2-15. Selected bond distances (Å) and angles (°) for [**5**].

		bond distances	
Au(1)–S(1)	2.311(3)	Au(2)–S(2)	2.325(3)
Au(1)–P(1)	2.258(3)	Au(2)–P(2)	2.277(3)
C(11)–C(12)	1.298(14)	Au(1)···Au(2)	3.1214(9)
Co(1)–S(1)	2.520(4)	Co(1)–S(2)	2.520(3)
Co(1)–O(1)	2.087(8)	Co(1)–O(3)	2.064(8)
Co(1)–N(1)	2.162(8)	Co(1)–N(2)	2.154(9)
Co(1)···Co(1)'	12.6607(44)		
		angles	
P(1)–Au(1)–S(1)	176.91(11)	P(2)–Au(2)–S(2)	179.51(10)
P(1)–C(11)–C(12)	125.3(9)	P(2)'–C(12)–C(11)	123.7(10)
S(1)–Co(1)–S(2)	103.32(11)	S(1)–Co(1)–O(1)	90.5(2)
S(1)–Co(1)–O(3)	95.1(3)	S(1)–Co(1)–N(1)	79.0(3)
S(1)–Co(1)–N(2)	174.5(3)	S(2)–Co(1)–O(1)	93.3(2)
S(2)–Co(1)–O(3)	92.2(2)	S(2)–Co(1)–N(1)	170.3(2)
S(2)–Co(1)–N(2)	78.0(3)	O(1)–Co(1)–O(3)	171.1(3)
O(1)–Co(1)–N(1)	77.2(3)	O(1)–Co(1)–N(2)	94.7(3)
O(3)–Co(1)–N(1)	97.1(3)	O(3)–Co(1)–N(2)	79.4(4)
N(1)–Co(1)–N(2)	100.7(3)		

Symmetry code: (') 1–x, 1–y, 1–z.

Table 2-16. Crystallographic data for [**5**]'.

	[**5**]'·EtOH·16H_2O
Formula	$C_{74}H_{128}Au_4Co_2N_4O_{25}P_4S_4$
Formula weight	2621.57
Crystal color	orange
Crystal size, mm^3	0.20 x 0.12 x 0.07
Crystal system	monoclinic
Space group	$P2_1$
a, Å	12.944(11)
b, Å	28.71(2)
c, Å	13.042(10)
β, °	104.736(12)
V, $Å^3$	4687(7)
Z	2
ρ(calc), g/cm^3	1.857
*R*1 (*I*>2*σ*(*I*)) [a)]	0.0557
w*R*2 (*I*>2*σ*(*I*)) [b)]	0.1298
*R*1 (all data) [a)]	0.0791
w*R*2 (all data) [b)]	0.1442

a) $R1 = \Sigma|(|F_o|-|F_c|)|/\Sigma(|F_o|)$

b) $wR2 = [\Sigma_w(|F_o|^2-|F_c|^2)^2/\Sigma_w(|F_o|^2)^2]^{1/2}$

Table 2-17. Selected bond distances (Å) and angles (°) for [**5**]'.

		bond distances	
Au(1)–S(1)	2.308(4)	Au(2)–S(2)	2.304(3)
Au(3)–S(3)	2.298(4)	Au(4)–S(4)	2.299(3)
Au(1)–P(1)	2.255(4)	Au(2)–P(2)	2.245(3)
Au(3)–P(3)	2.259(3)	Au(4)–P(4)	2.243(3)
Au(1)···Au(2)	3.0600(19)	Au(3)···Au(4)	3.0200(19)
C(11)–C(12)	1.294(16)	C(23)–C(24)	1.326(18)
Co(1)–S(1)	2.512(4)	Co(1)–S(2)	2.465(4)
Co(1)–O(1)	2.058(9)	Co(1)–O(3)	2.096(9)
Co(1)–N(1)	2.119(11)	Co(1)–N(2)	2.149(10)
Co(2)–S(3)	2.507(5)	Co(2)–S(4)	2.451(4)
Co(2)–O(5)	2.121(9)	Co(2)–O(7)	2.073(9)
Co(2)–N(3)	2.106(11)	Co(2)–N(4)	2.108(12)
Co(1)···Co(2)	12.3117(80)		
		angles	
P(1)–Au(1)–S(1)	178.50(12)	P(2)–Au(2)–S(2)	178.73(12)
P(3)–Au(3)–S(3)	177.74(13)	P(4)–Au(4)–S(4)	178.19(12)
P(2)–C(11)–C(12)	124.7(9)	P(3)–C(12)–C(11)	121.2(9)
P(4)–C(23)–C(24)	126.8(11)	P(1)–C(24)–C(23)	11.5(11)
S(1)–Co(1)–S(2)	102.57(13)	S(1)–Co(1)–O(1)	91.7(3)
S(1)–Co(1)–O(3)	91.9(3)	S(1)–Co(1)–N(1)	78.5(3)
S(1)–Co(1)–N(2)	166.8(3)	S(2)–Co(1)–O(1)	91.0(3)
S(2)–Co(1)–O(3)	90.8(3)	S(2)–Co(1)–N(1)	167.6(3)
S(2)–Co(1)–N(2)	80.6(3)	O(1)–Co(1)–O(3)	175.4(4)
O(1)–Co(1)–N(1)	76.5(4)	O(1)–Co(1)–N(2)	101.1(4)
O(3)–Co(1)–N(1)	101.5(4)	O(3)–Co(1)–N(2)	75.1(4)
N(1)–Co(1)–N(2)	101.2(5)	S(3)–Co(2)–S(4)	102.57(14)
S(3)–Co(2)–O(5)	89.4(3)	S(3)–Co(2)–O(7)	93.9(3)
S(3)–Co(2)–N(3)	81.5(4)	S(3)–Co(2)–N(4)	170.9(3)
S(4)–Co(2)–O(5)	90.5(3)	S(4)–Co(2)–O(7)	92.2(3)
S(4)–Co(2)–N(3)	166.0(3)	S(4)–Co(2)–N(4)	80.2(3)
O(5)–Co(2)–O(7)	175.1(4)	O(5)–Co(2)–N(3)	76.1(4)
O(5)–Co(2)–N(4)	99.3(4)	O(7)–Co(2)–N(3)	100.8(4)
O(7)–Co(2)–N(4)	77.2(4)	N(3)–Co(2)–N(4)	97.8(5)

Table 2-18. Crystallographic data for [**6**]$(NO_3)_2$.

	[**6**]$(NO_3)_2 \cdot 14H_2O$
Formula	$C_{72}H_{80}Au_4Co_2N_4O_{28}P_4S_4$
Formula weight	2635.26
Crystal color	purple
Crystal size, mm^3	0.06 x 0.06 x 0.02
Crystal system	triclinic
Space group	*P*-1
a, Å	12. 5811(15)
b, Å	12.8788(15)
c, Å	16.1392(19)
α, °	104.679(7)
β, °	105.112(7)°
γ, °	103.499(7)
V, $Å^3$	2313.2(5)
Z	1
ρ(calc), g/cm^3	1.892
*R*1 (*I*>2*σ*(*I*)) [a)]	0.0779
w*R*2 (*I*>2*σ*(*I*)) [b)]	0.1910
*R*1 (all data) [a)]	0.1285
w*R*2 (all data) [b)]	0.2313

a) $R1 = \Sigma|(|F_o|-|F_c|)|/\Sigma(|F_o|)$

b) $wR2 = [\Sigma_w(|F_o|^2-|F_c|^2)^2/\Sigma_w(|F_o|^2)^2]^{1/2}$

Table 2-19. Selected bond distances (Å) and angles (°) for [**6**]$(NO_3)_2$.

		bond distances	
Au(1)-P(1)	2.241(3)	Au(1)-S(1)	2.291(3)
Au(2)-P(2)	2.248(3)	Au(2)-S(2)	2.289(3)
Co(1)-O(3)	1.918(10)	Co(1)-O(1)	1.923(9)
Co(1)-N(1)	1.973(13)	Co(1)-N(2)	1.979(12)
Co(1)-S(2)	2.275(4)	Co(1)-S(1)	2.291(4)
C(11)–C(12)	1.341(17)	Au(1)···Au(2)	3.0189(7)
Co(1)···Co(1)'	12.33		
		angles	
P(1)-Au(1)-S(1)	177.16(12)	P(2)-Au(2)-S(2)	178.35(13)
O(3)-Co(1)-O(1)	176.7(4)	O(3)-Co(1)-N(1)	97.1(5)
O(1)-Co(1)-N(1)	83.2(5)	O(3)-Co(1)-N(2)	81.9(5)
O(1)-Co(1)-N(2)	94.8(5)	N(1)-Co(1)-N(2)	94.5(5)
O(3)-Co(1)-S(2)	91.5(3)	O(1)-Co(1)-S(2)	88.1(3)
N(1)-Co(1)-S(2)	171.0(4)	N(2)-Co(1)-S(2)	84.1(4)
O(3)-Co(1)-S(1)	89.6(3)	O(1)-Co(1)-S(1)	93.8(3)
N(1)-Co(1)-S(1)	83.0(4)	N(2)-Co(1)-S(1)	170.8(4)
S(2)-Co(1)-S(1)	99.67(15)	P(1)-C(11)-C(12)′	125.4(10)
P(2)-C(12)-C(11)′	121.5(10)		

Symmetry codes: (') –x, 1–y, 1–z.

Table 2-20. Crystallographic data for [**6**]$(PF_6)_2$.

	[**6**]$(PF_6)_2$·2EtOH·8H_2O
Formula	$C_{76}H_{92}Au_4Co_2N_4O_{18}P_6S_4F_{12}$
Formula weight	2797.32
Crystal color	purple
Crystal size, mm^3	0.23 x 0.15 x 0.05
Crystal system	triclinic
Space group	*P*-1
a, Å	12.6888(15)
b, Å	12.7235(15)
c, Å	16.4451(19)
α, °	83.710(6)
β, °	73.252(5)
γ, °	85.586(6)
V, $Å^3$	2524.2(5)
Z	1
ρ(calc), g/cm^3	1.840
*R*1 ($I>2\sigma(I)$) [a)]	0.0549
w*R*2 ($I>2\sigma(I)$) [b)]	0.1430
*R*1 (all data) [a)]	0.0738
w*R*2 (all data) [b)]	0.1572

a) $R1 = \Sigma|(|F_o|-|F_c|)|/\Sigma(|F_o|)$

b) $wR2 = [\Sigma_w(|F_o|^2-|F_c|^2)^2/\Sigma_w(|F_o|^2)^2]^{1/2}$

Table 2-21. Selected bond distances (Å) and angles (°) for [**6**]$(PF_6)_2$.

	bond distances		
Au(1)-P(1)	2.2438(18)	Au(1)-S(1)	2.2989(19)
Au(2)-P(2)	2.2485(18)	Au(2)-S(2)	2.3080(19)
C(11)-C(12)'	1.306(9)	C(12)-C(11)'	1.306(9)
Co(1)-O(1)	1.895(6)	Co(1)-O(3)	1.917(6)
Co(1)-N(1)	1.944(8)	Co(1)-N(2)	1.949(8)
Co(1)-S(2)	2.253(2)	Co(1)-S(1)	2.260(2)
Au(1)···Au(2)	3.0671(5)		
	angles		
P(1)-Au(1)-S(1)	176.74(7)	P(2)-Au(2)-S(2)	178.15(7)
C(12)'-C(11)-P(1)	123.6(5)	C(11)'-C(12)-P(2)	121.3(5)
O(1)-Co(1)-O(3)	177.8(3)	O(1)-Co(1)-N(1)	83.5(3)
O(3)-Co(1)-N(1)	95.3(3)	O(1)-Co(1)-N(2)	95.7(3)
O(3)-Co(1)-N(2)	82.6(3)	N(1)-Co(1)-N(2)	94.6(3)
O(1)-Co(1)-S(2)	89.38(19)	O(3)-Co(1)-S(2)	91.7(2)
N(1)-Co(1)-S(2)	172.7(3)	N(2)-Co(1)-S(2)	84.5(2)
O(1)-Co(1)-S(1)	93.3(2)	O(3)-Co(1)-S(1)	88.4(2)
N(1)-Co(1)-S(1)	83.4(3)	N(2)-Co(1)-S(1)	170.5(2)
S(2)-Co(1)-S(1)	98.59(8)		

Symmetry codes: (') 1–x, –y, 1–z.

Table 2-22. Comparison between homochiral and heterochiral $Au^{I}_4Co^{III}_2$ structures.

	homochiral	heterochiral		
	Co^{III}	Co^{II}	Co^{II}	Co^{III}
	[**3**]$(NO_3)_2$	[**5**]	[**5**]'	[**6**]$(NO_3)_2$
Av. Co–S, Å	2.3	2.5	2.5	2.3
Av. Co–O, Å	1.9	2.1	2.1	1.9
Av. Co–N, Å	2.0	2.2	2.1	2.0
Au···Au (shortest), Å	3.6044(5)	3.1214(9)	3.0200(19)	3.0189(7)
Co···Co (in molecule), Å	11.35	12.66	12.31	12.33

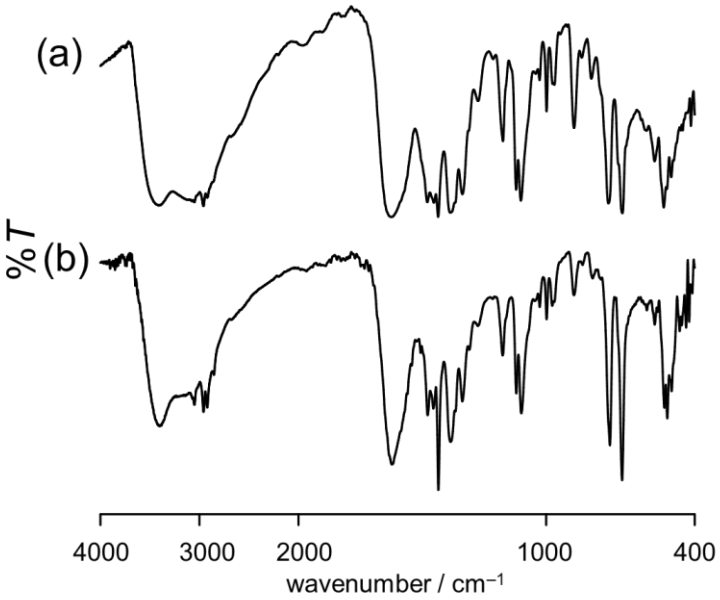

Figure 2-1. IR spectra of (a) D_2-H_2[**2**] and (b) L_2-H_2[**2**] (KBr disk).

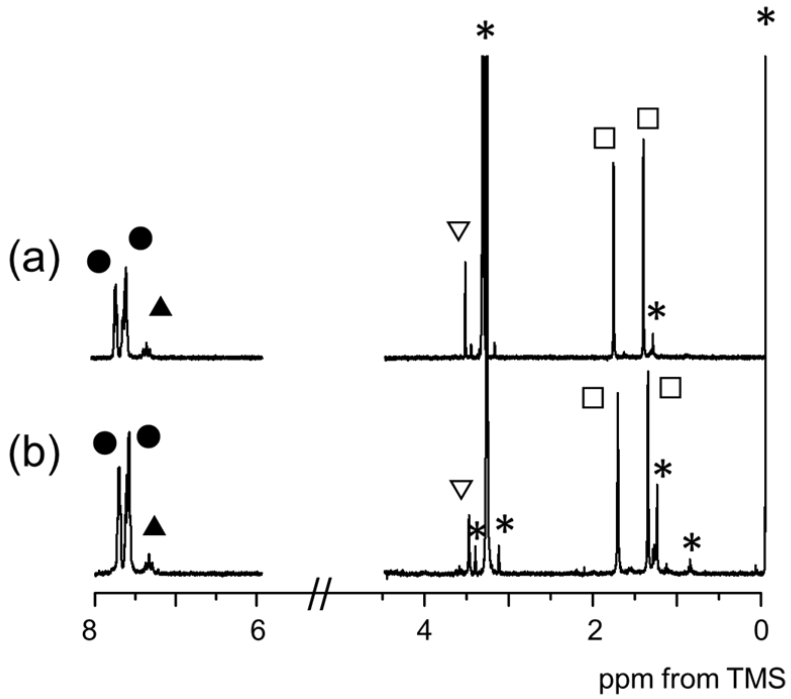

Figure 2-2. ^{1}H NMR spectra of (a) D_2-H_2[**2**] and (b) L_2- H_2[**2**] in CD_3OD. Open squares (□) and triangles (▽) represent the methyl and the methine signals of pen moieties, and filled triangles (▲) and circles (●) represent the vinylene and the phenyl signals of *trans*-dppee moieties. The * marks represent the signals of solvents and TMS signals.

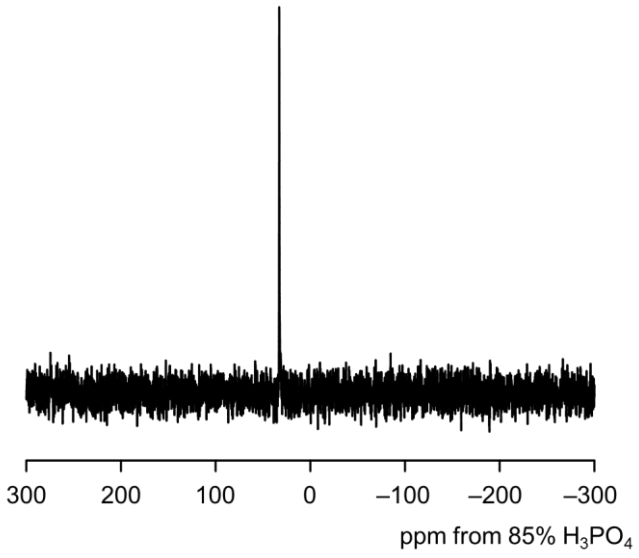

Figure 2-3. ^{31}P NMR spectrum of D_2-H_2[**2**] in CD_3OD.

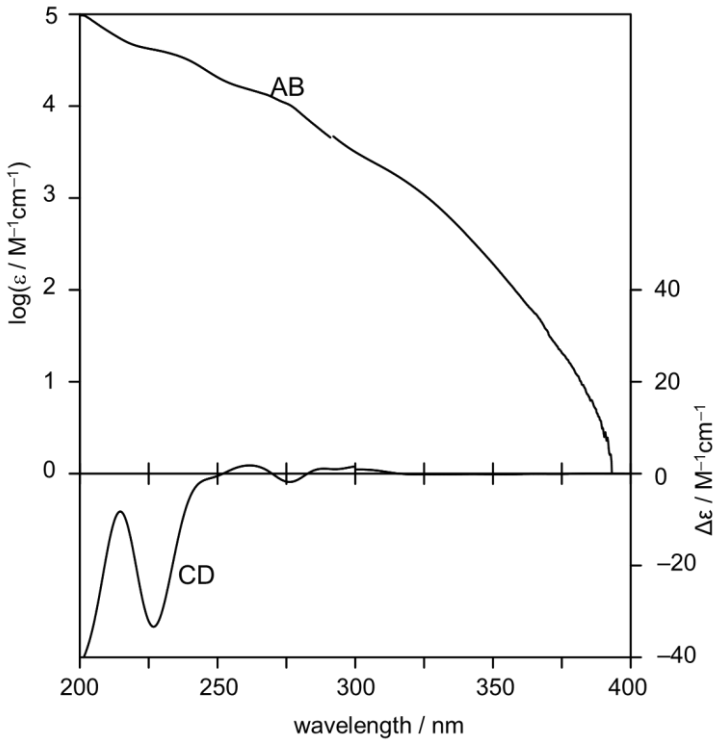

Figure 2-4. Absorption (AB) and CD spectra of D_2-H_2[**2**] in MeOH.

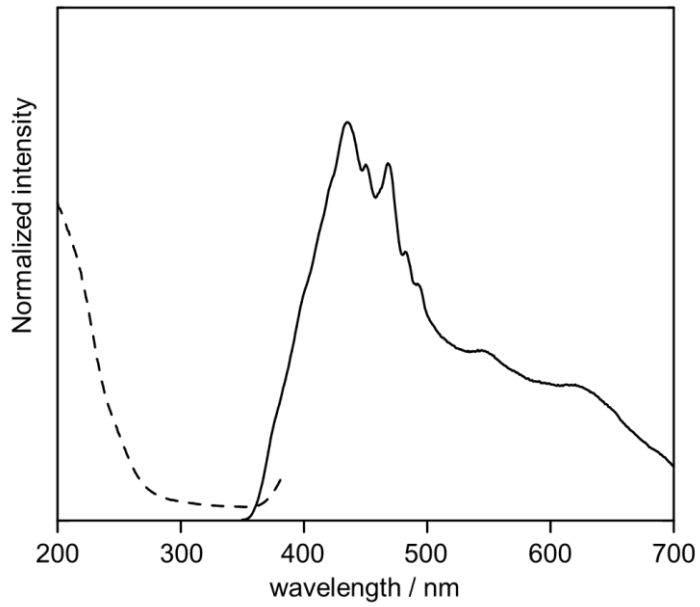

Figure 2-5. Emission and excitation spectra of D_2-H_2[**2**] in the solid state. The solid and dashed lines describe the emission and excitation spectra, respectively.

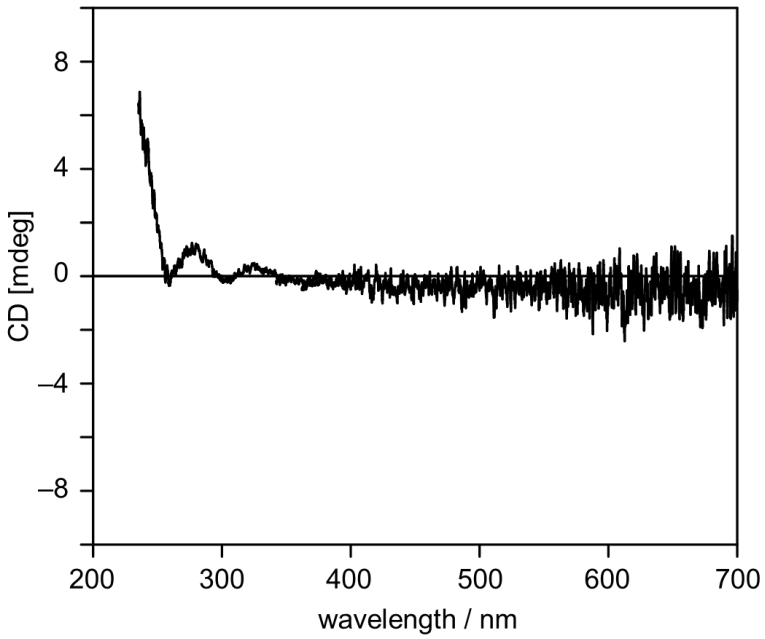

Figure 2-6. CD spectra of L_2-H_2[**2**] in MeOH.

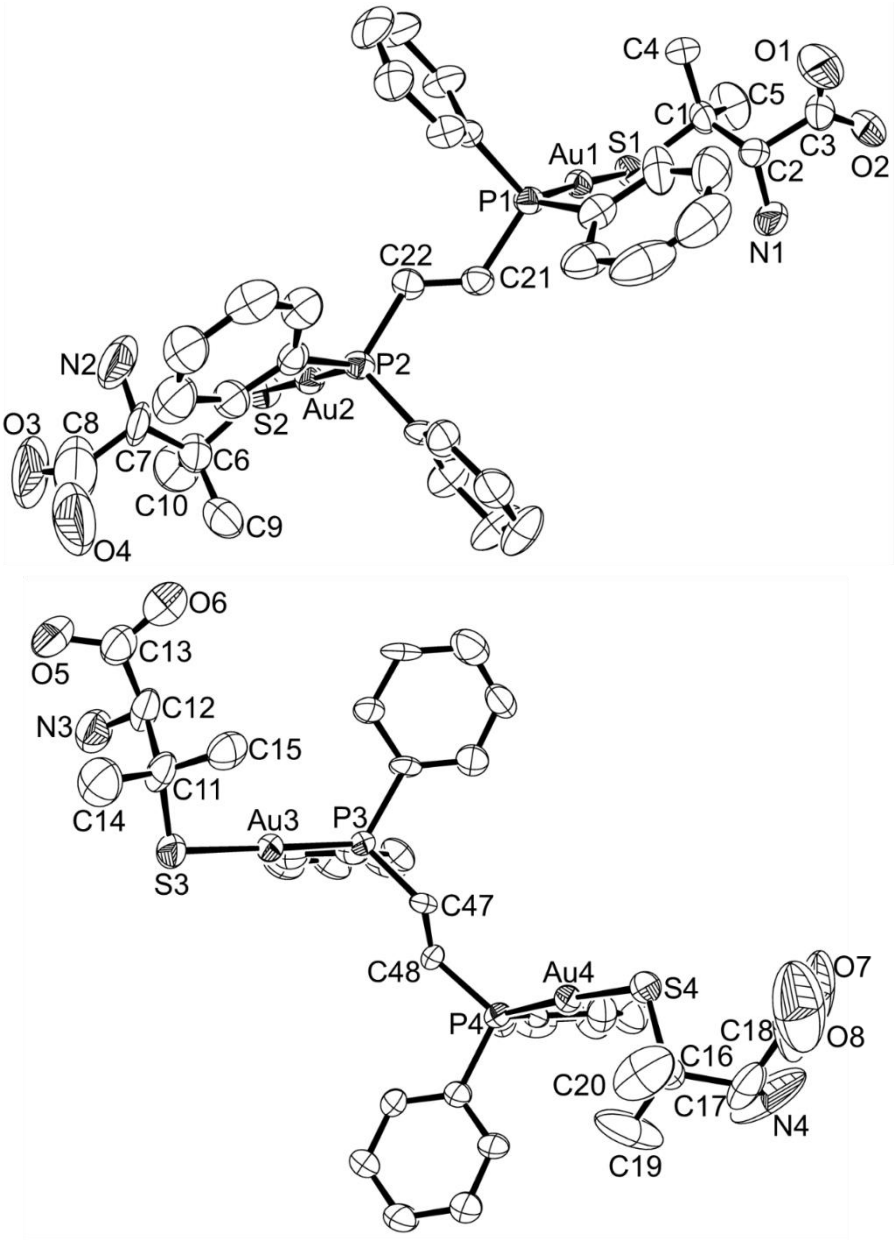

Figure 2-7. Perspective view of metalloligand D_2-H_2[**2**] with the atomic labeling scheme. Hydrogen atoms are omitted for clarity. Thermal ellipsoids were drawn in a 50 % level.

(a)

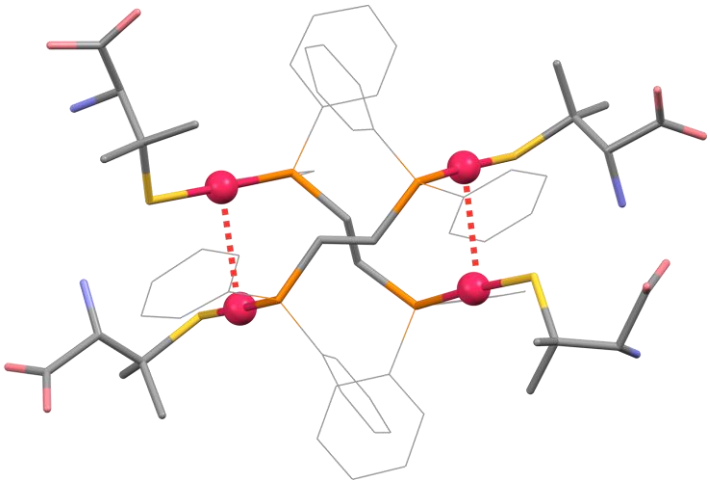

(b)

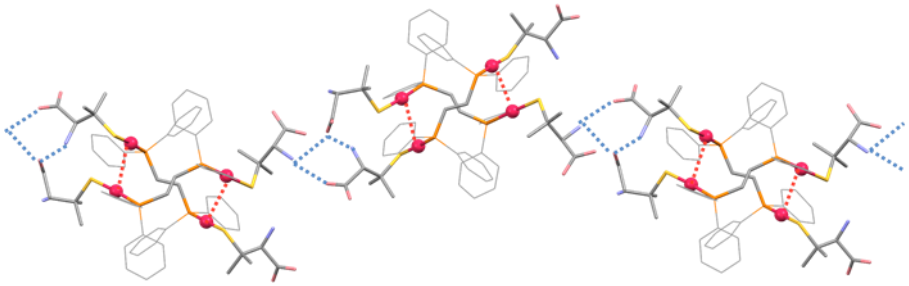

(c)

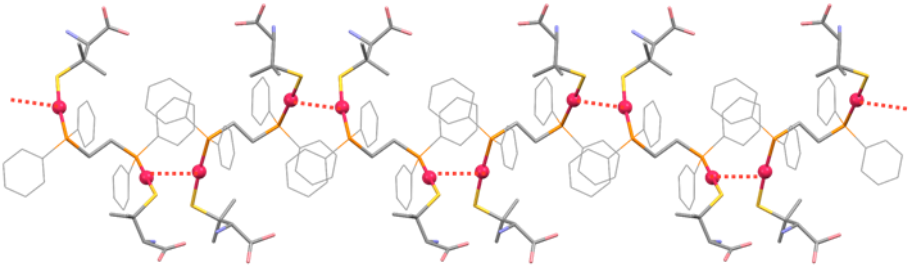

Figure 2-8. Perspective views of (a) dimeric structure connected by aurophilic interaction, (b) 1D chain structure connected by hydrogen bonds in D_2-H_2[**2**], and (c) 1D chain structure connected by aurophilic interactions in [Au_2(dppe)(D-Hpen)$_2$]. Red dotted lines and blue dotted lines represent aurophilic interactions and hydrogen bonding interactions, respectively.

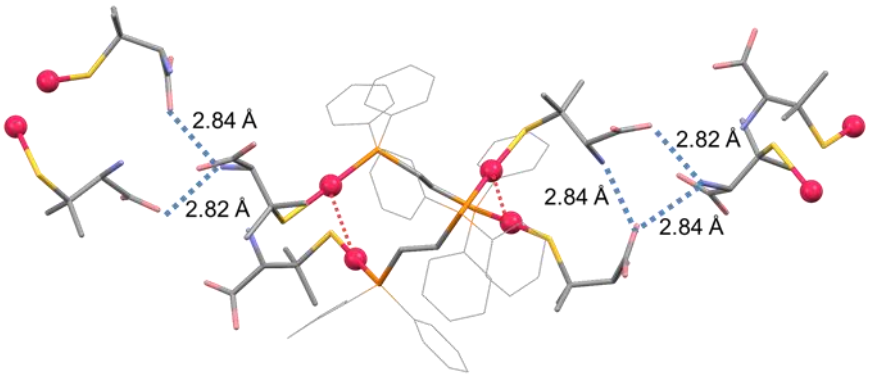

Figure 2-9. Hydrogen bonding interactions in D_2-H_2[**2**]. Red dotted lines and blue dotted lines represent aurophilic interactions and hydrogen bonding interactions, respectively.

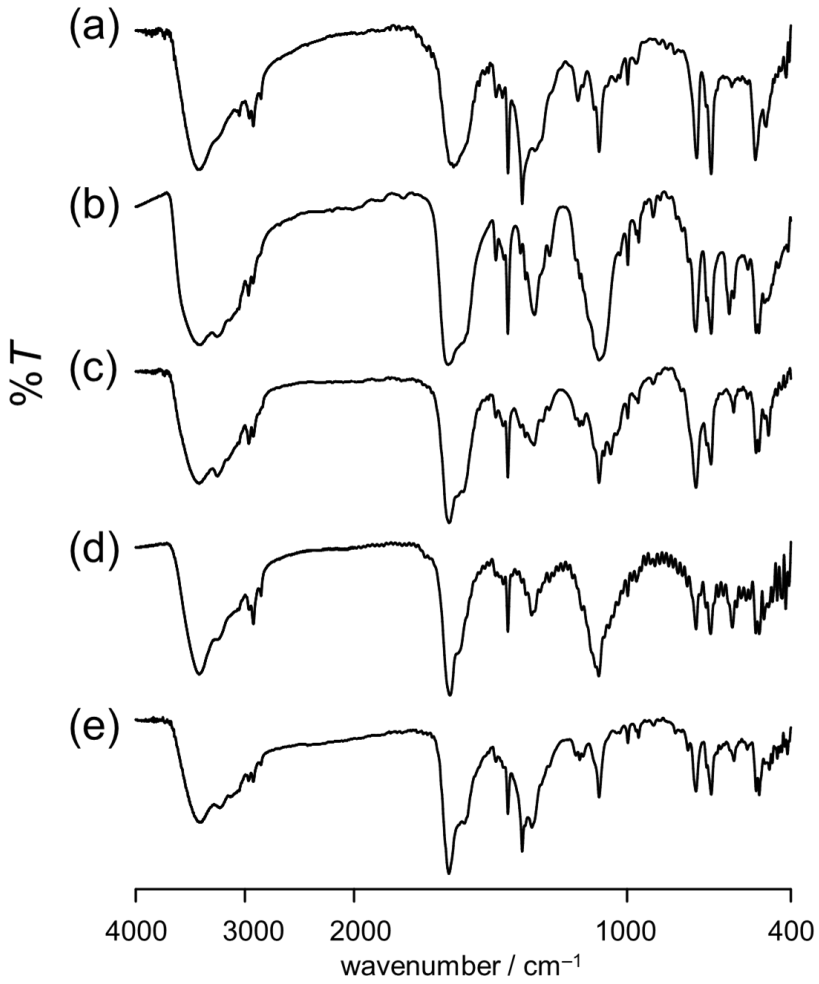

Figure 2-10. IR spectra of (a) [**3**]$(NO_3)_2$, (b) [**3**]$(ClO_4)_2$, (c) [**3**]$(BF_4)_2$, (d) [**3**]SO_4, and (e) [**4**]$(NO_3)_2$ (KBr disk).

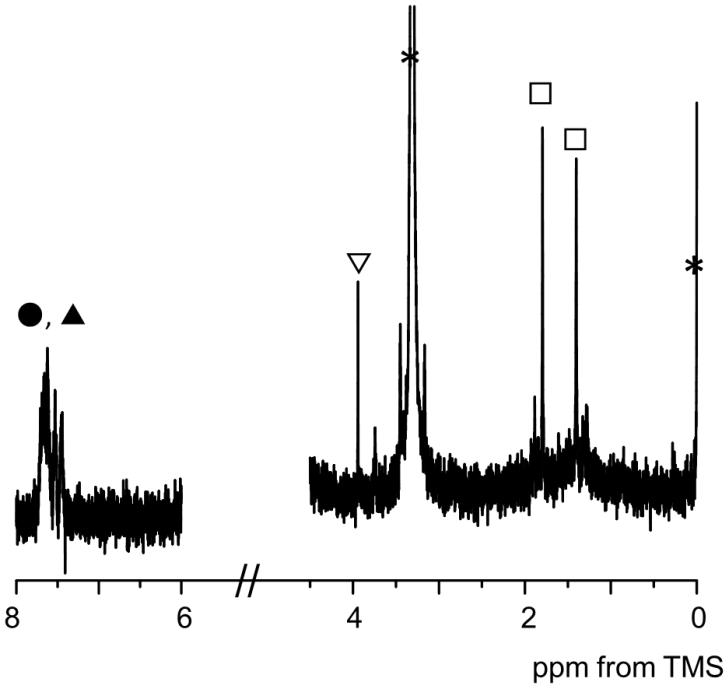

Figure 2-11. ^{1}H NMR spectrum of [**3**]$(NO_3)_2$ in CD_3OD/D_2O (1:2). Open squares (□) and triangles (▽) represent the methyl and the methine signals of pen moieties, and filled triangles (▲) and circles (●) represent the vinylene and the phenyl signals of *trans*-dppee moieties. The * marks represent the signals of solvents and TMS.

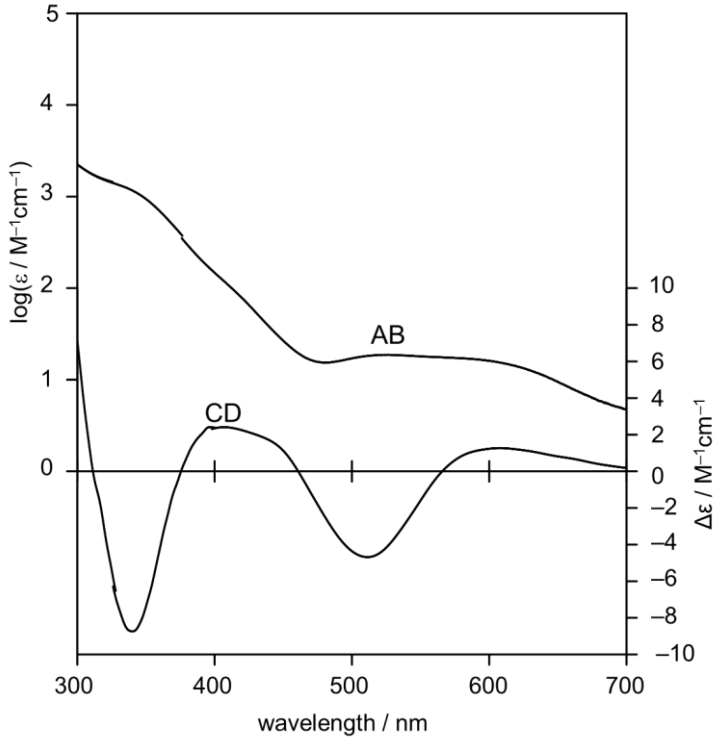

Figure 2-12. Absorption (AB) and CD spectra of [**3**]$(NO_3)_2$ in MeOH.

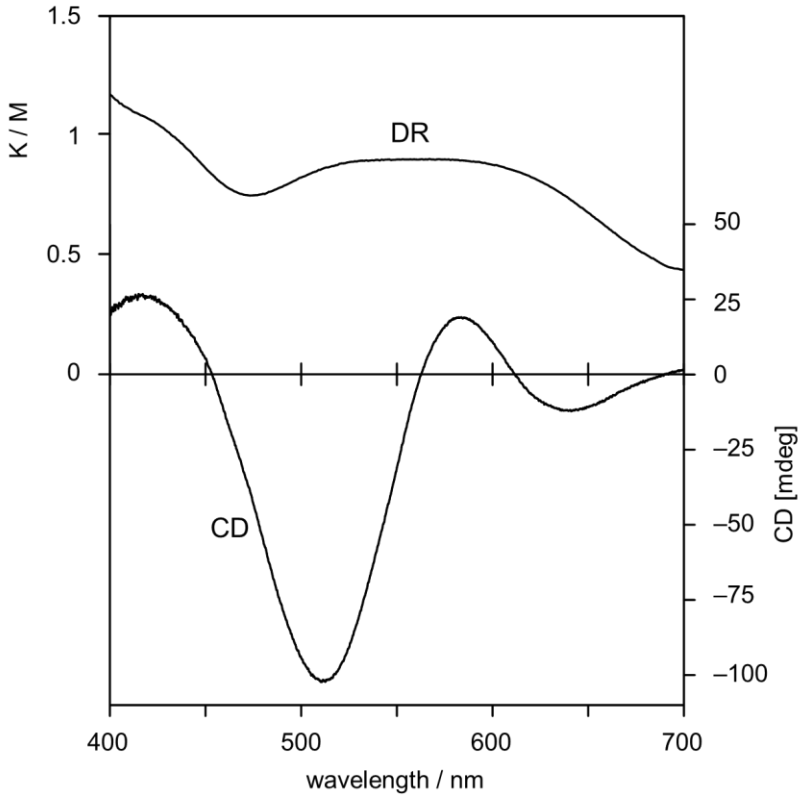

Figure 2-13. Diffuse reflection (DR) and CD spectra of [**3**]$(NO_3)_2$ in the solid state.

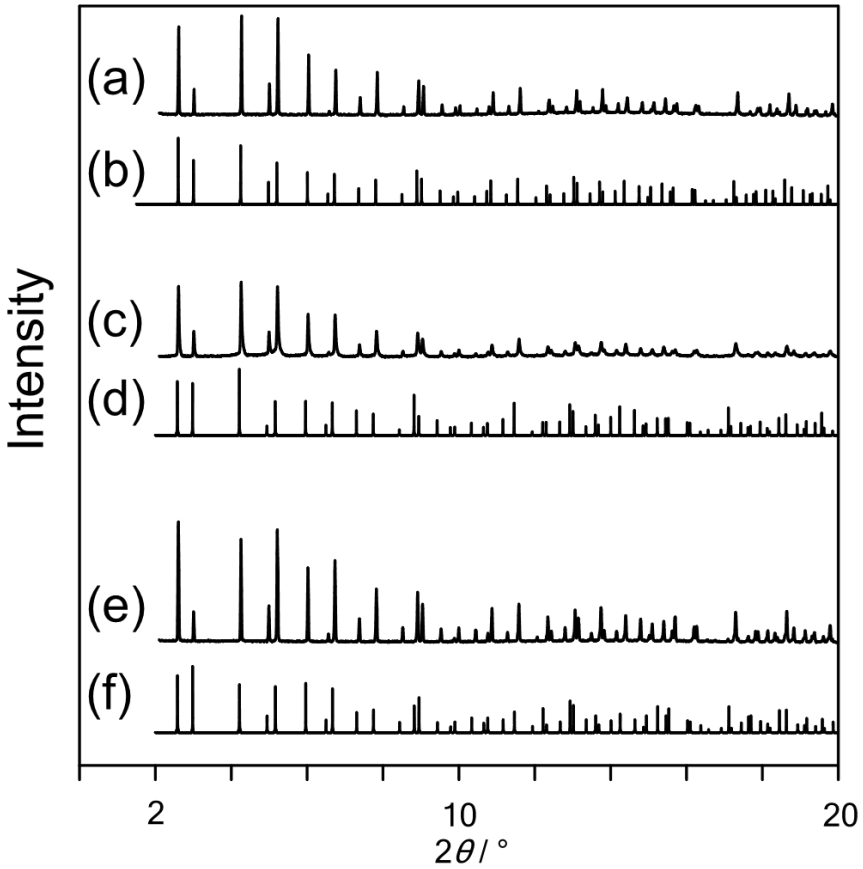

Figure 2-14. Powder X-ray diffraction patterns of (a) [**3**]$(NO_3)_2$, (c) [**3**]$(ClO_4)_2$, and (e) [**3**]$(BF_4)_2$, and the simulated patterns based on the crystal structures of (b) [**3**]$(NO_3)_2$, (d) [**3**]$(ClO_4)_2$, and (f) [**3**]$(BF_4)_2$.

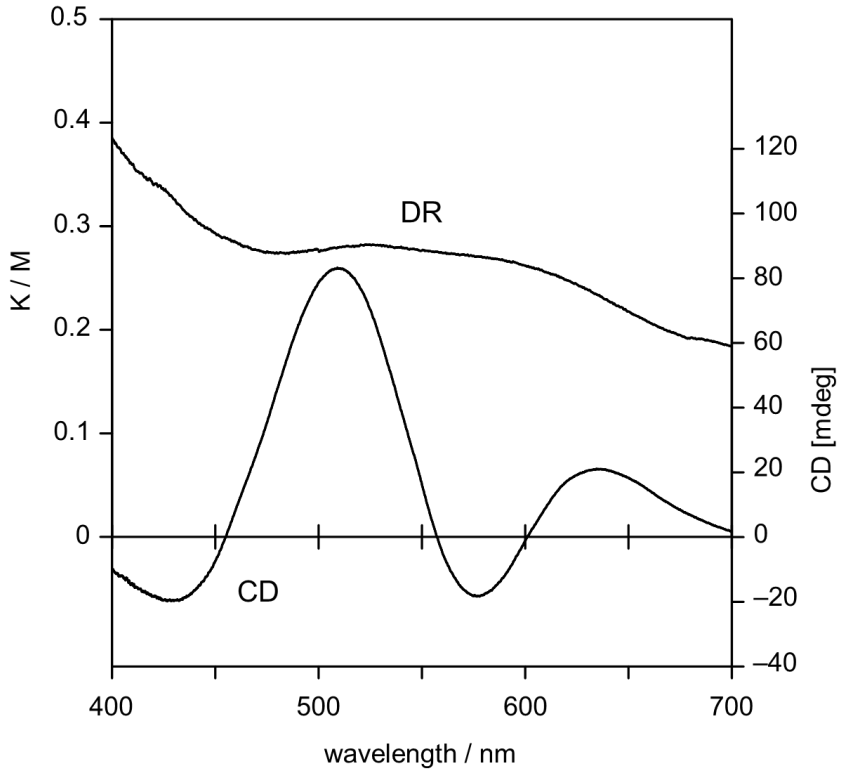

Figure 2-15. Diffuse reflection (DR) and CD spectra of [**4**]$(NO_3)_2$ in the solid state.

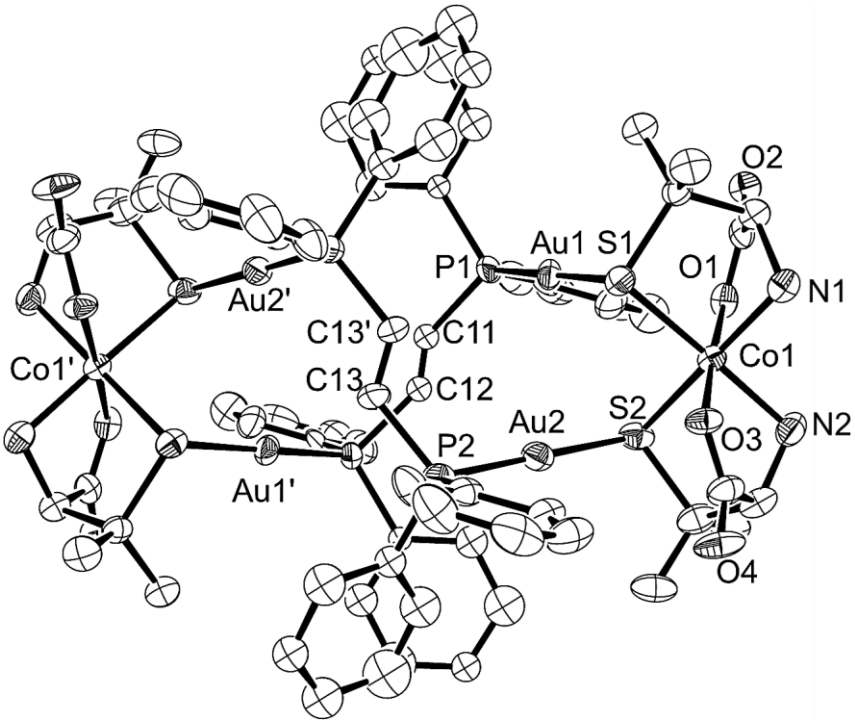

Figure 2-16. An ortep drawing of the complex cation in [**3**]$(NO_3)_2$ with the atomic labeling scheme. Hydrogen atoms are omitted for clarity. Minor part of the disordered atoms is omitted. Symmetry code: (') 3/2–x, 3/2–y, z. Thermal ellipsoids were drawn in a 50 % level.

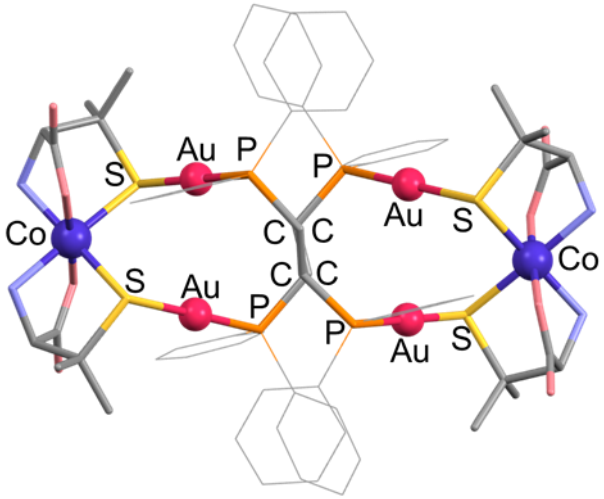

Figure 2-17. Twisted 18-membered metalloring in [**3**]$(NO_3)_2$.

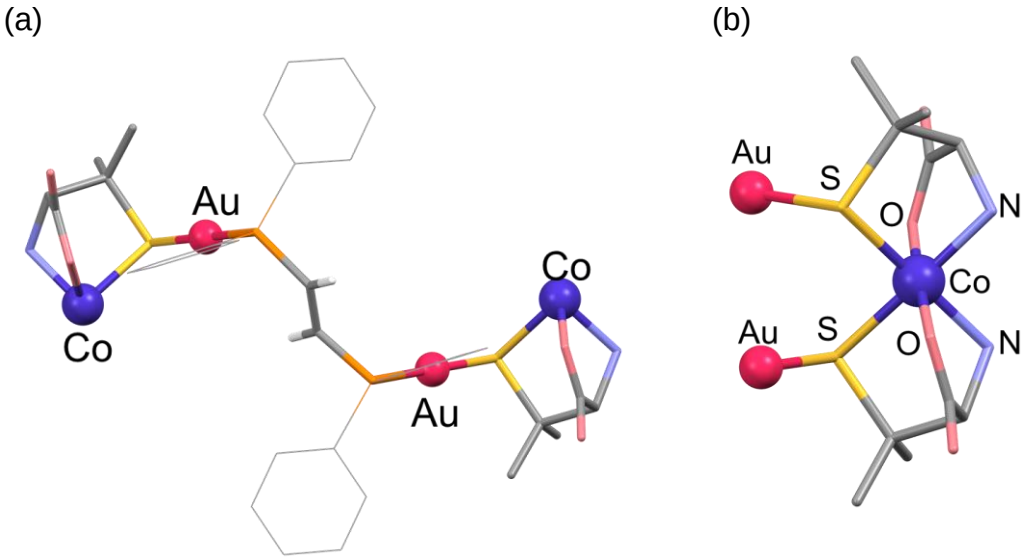

Figure 2-18. (a) Bis(tridentate-*N*,*O*,*S*) coordination mode of the metalloligand and (b) coordination geometry of Co^{III} atom in [**3**]$(NO_3)_2$.

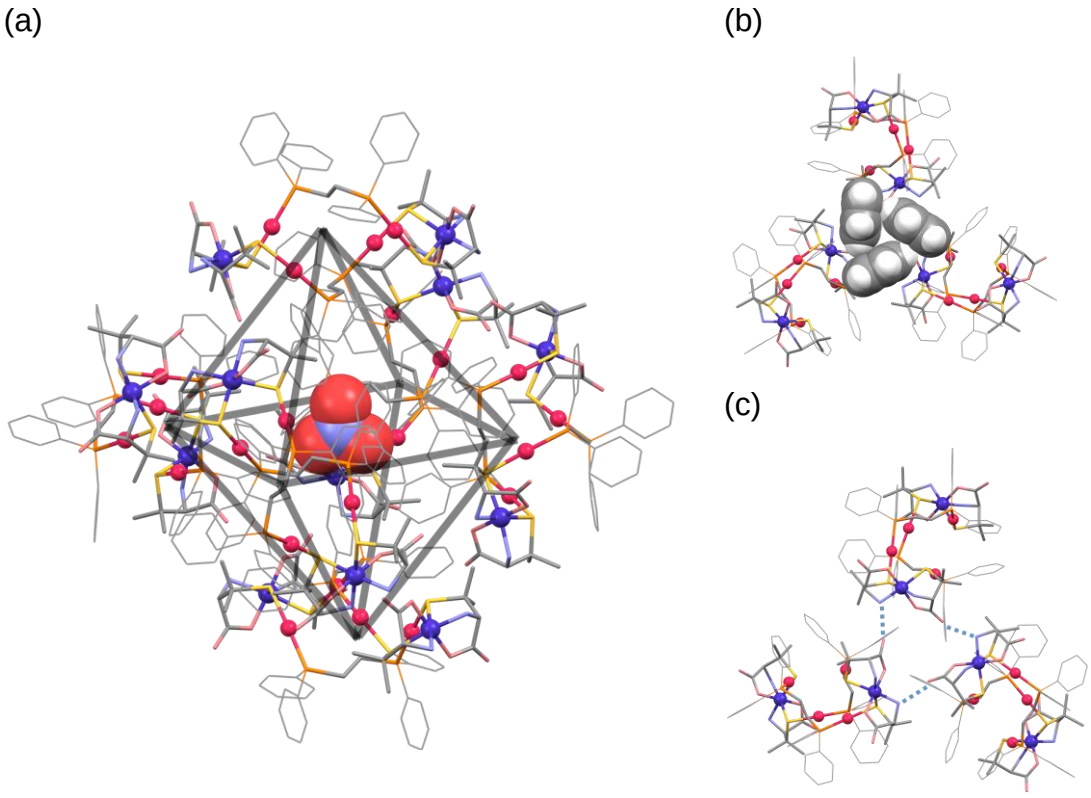

Figure 2-19. (a) Perspective views of the structures of octahedral hexamer accommodating one nitrate anion, (b) a triangular CH···π linkage in the hexamer, and (c) a triangular H_2N···OCO linkage in the hexamer [**3**]$(NO_3)_2$. Dashed lines indicate hydrogen bonds in Figure 2-19c.

(a) (b)

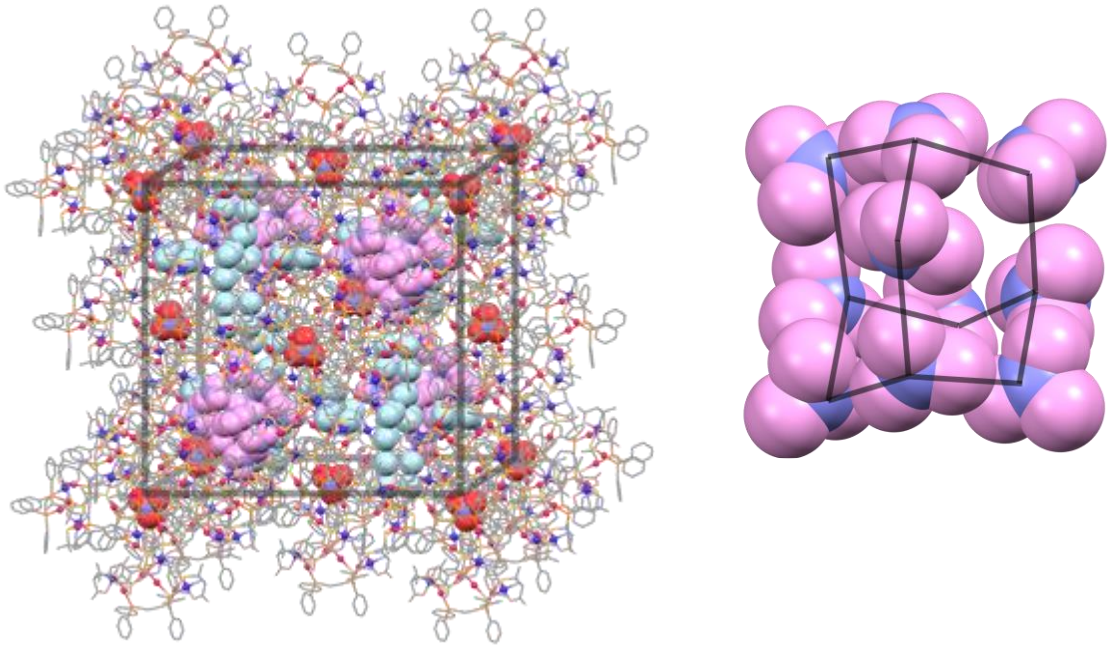

Figure 2-20. Perspective views of (a) the supramolecular structure of [**3**]$(NO_3)_2$, and (b) adamantane-like cluster composed of 10 nitrate anions inside the tetrahedral interstice.

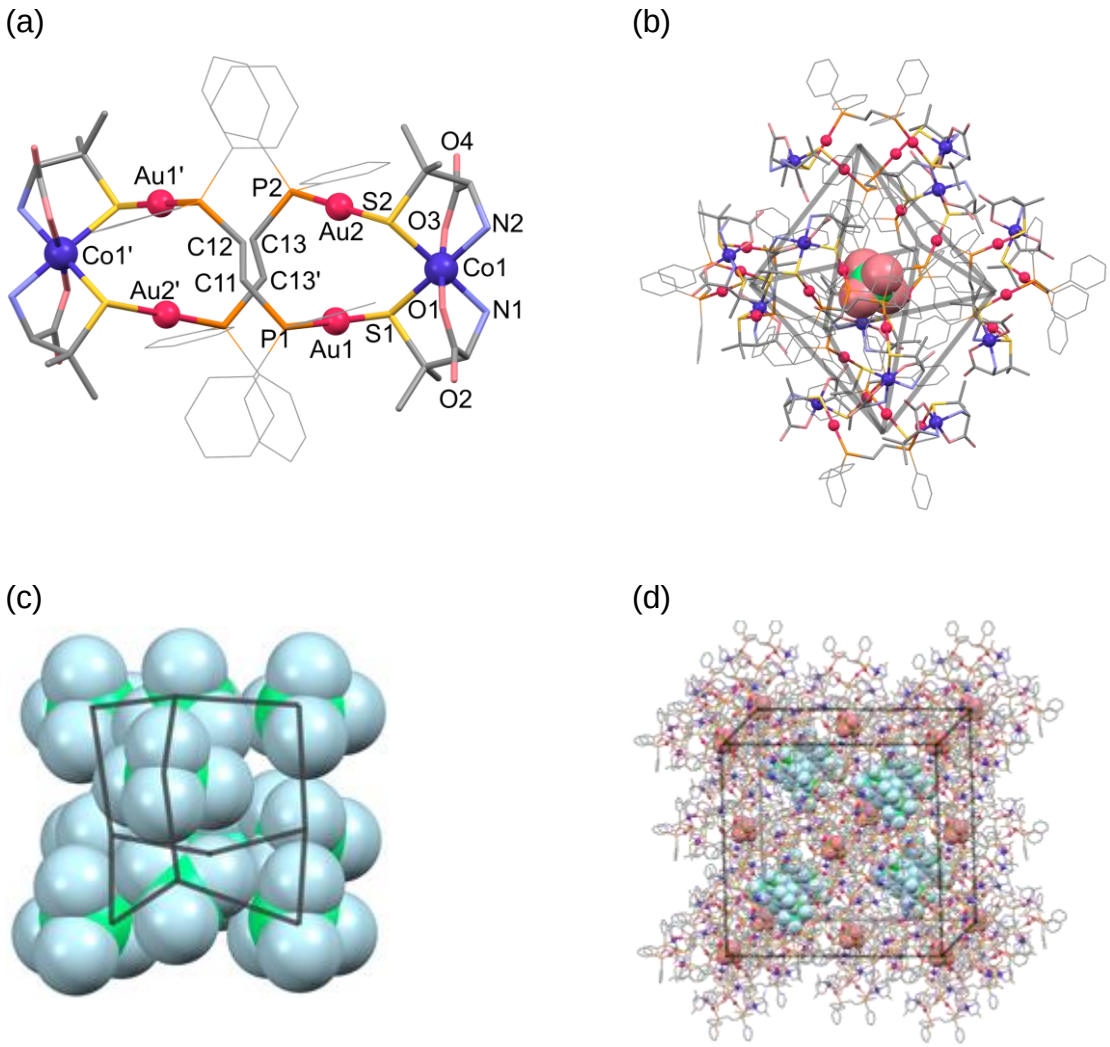

Figure 2-21. Perspective views of (a) complex cation with the atomic labeling scheme, (b) hexameric supramolecular structure of the complex cations accommodating a perchlorate anion, (c) adamantane-like cluster composed of 10 perchlorate anions inside the tetrahedral interstice, and (d) packing structure in [**3**]$(ClO_4)_2$. Symmetry code: (') –x, y, 1–z.

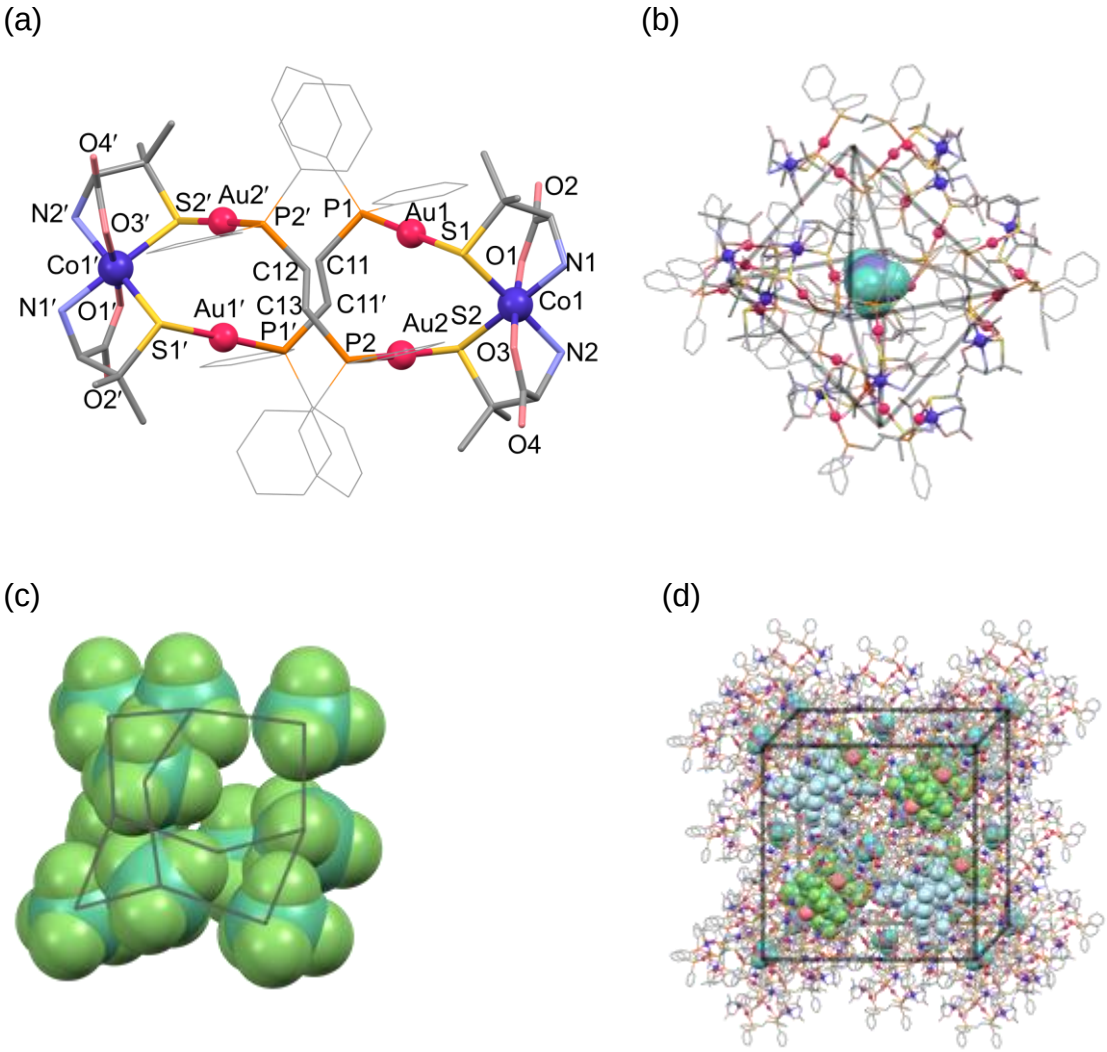

Figure 2-22. Perspective views of (a) complex cation with the atomic labeling scheme, (b) hexameric supramolecular structure of the complex cations accommodating a tetrafluoroborate anion, (c) adamantane-like cluster composed of 10 tetrafluoroborate anions inside the tetrahedral interstice, and (d) packing structure in [**3**]$(BF_4)_2$. Symmetry code: (') 1–x, 1–y, z.

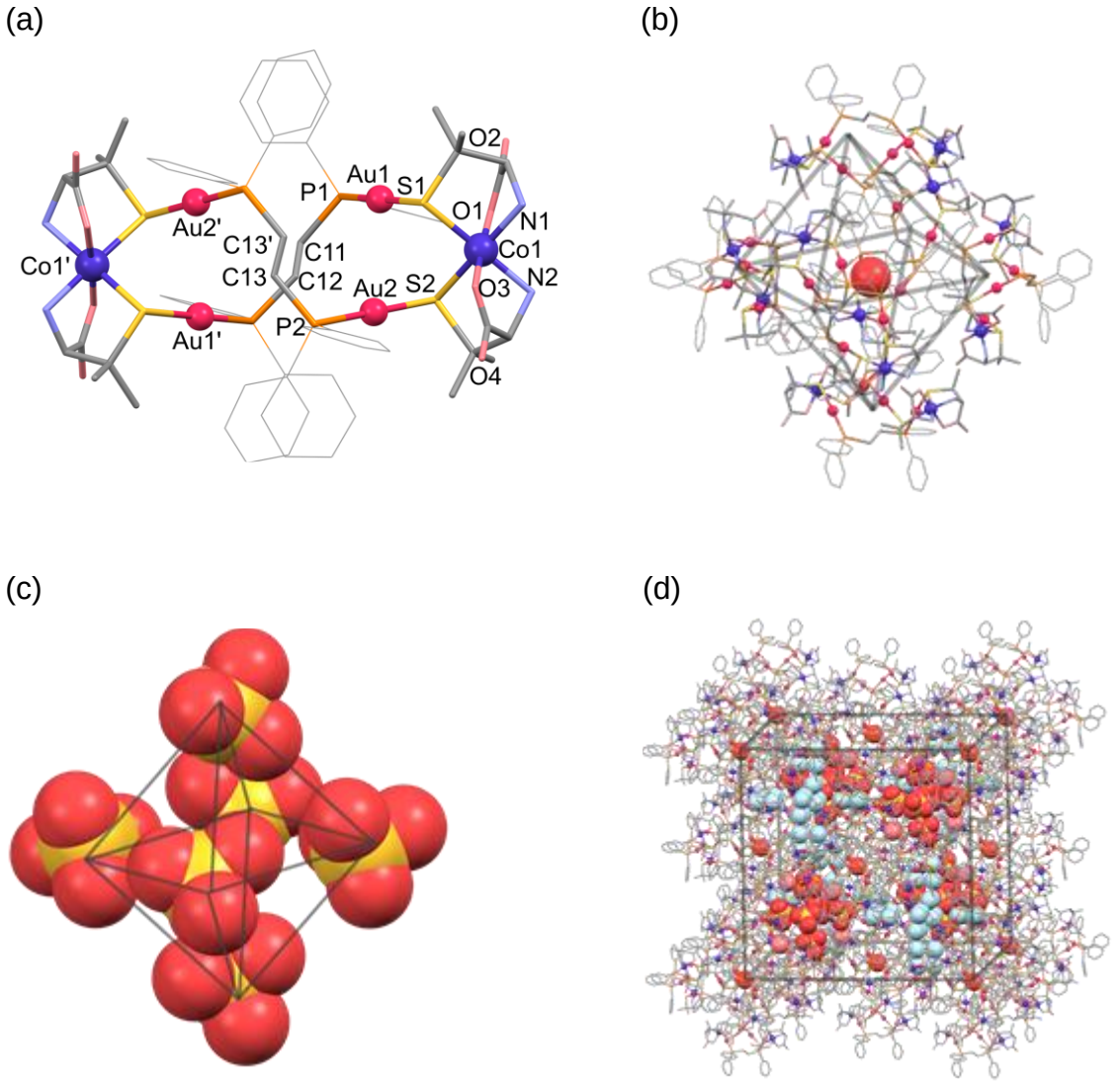

Figure 2-23. Perspective views of (a) complex cation with the atomic labeling scheme, (b) hexameric supramolecular structure of the complex cations accommodating one water molecule, (c) octahedron-like cluster composed of 6 sulfate anions inside the tetrahedral interstice, and (d) packing structure in [**3**]SO_4. Symmetry code: (') 1–x, 1–y, z.

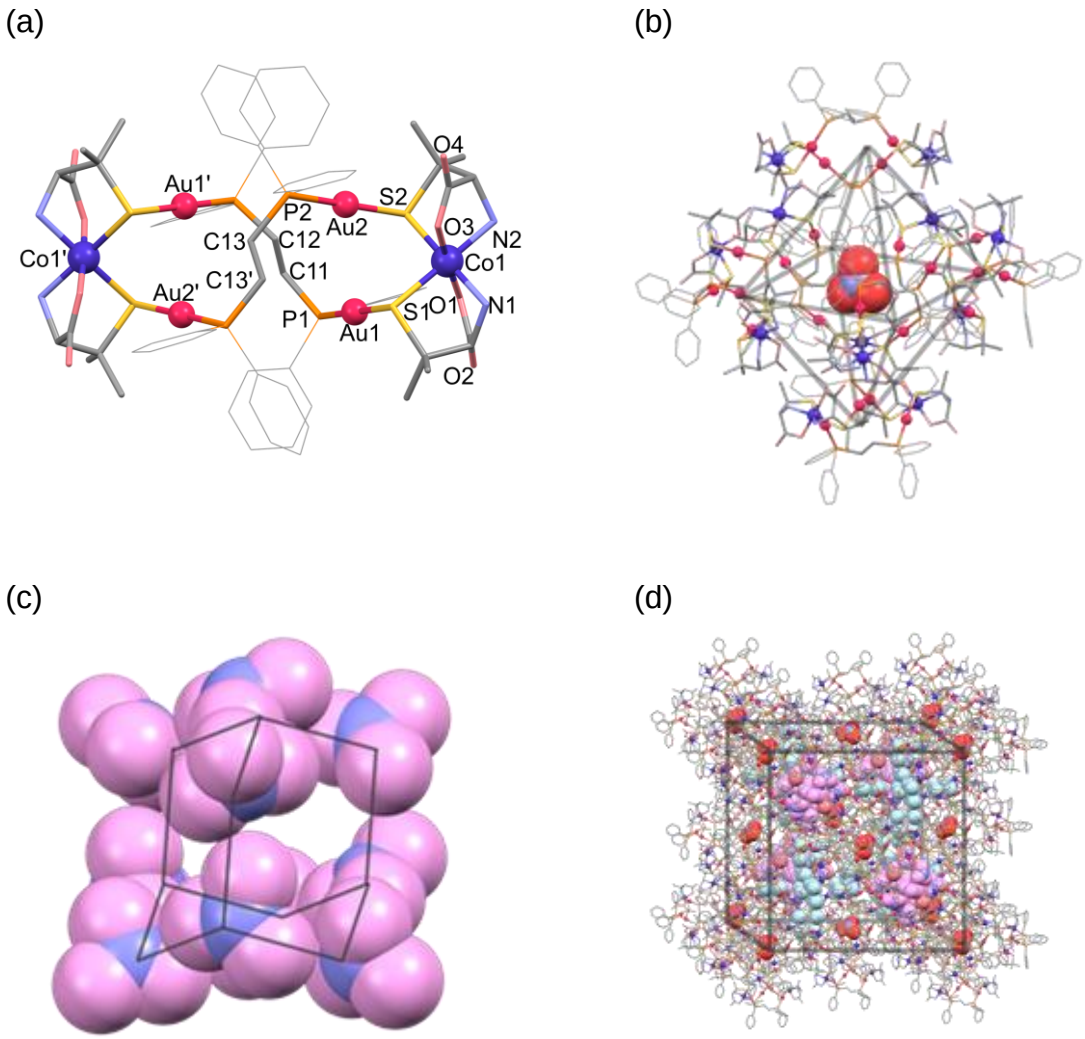

Figure 2-24. Perspective views of (a) complex cation with the atomic labeling scheme, (b) hexameric supramolecular structure of the complex cations accommodating a nitrate anion, (c) adamantane-like cluster composed of 10 nitrate anions inside the tetrahedral interstice, and (d) packing structure in [**4**]$(NO_3)_2$. Symmetry code: (') 1–x, –y, z.

(a)

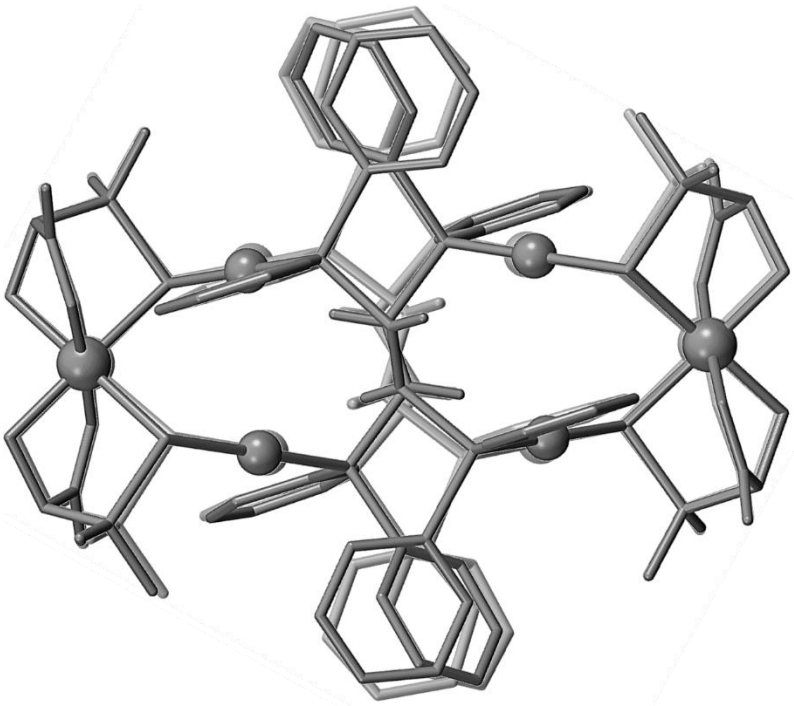

(b)

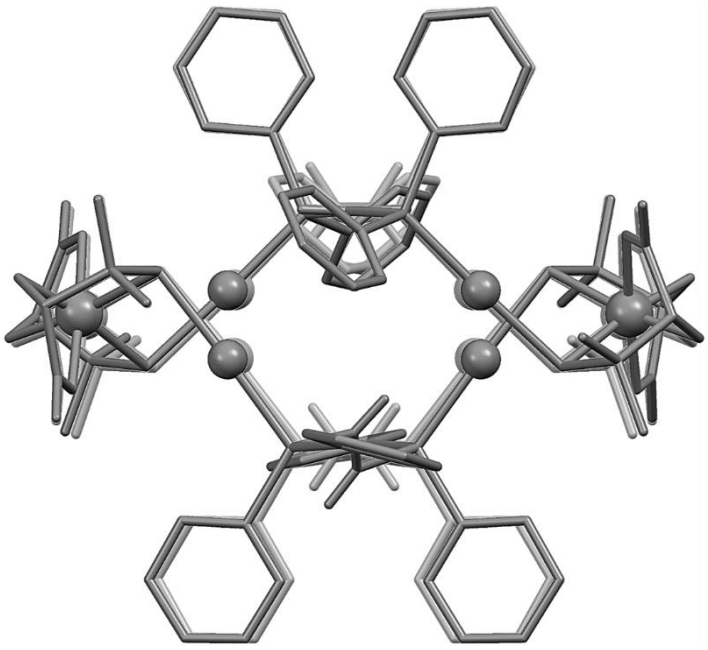

Figure 2-25. Comparison of the hexanuclear structures with dppe and *trans*-dppee. (a) Top view and (b) side view. Dark gray and light gray units represent $[\mathbf{3}]^{2+}$ and $[Au_4Co_2(dppe)_2(D\text{-pen})_4]^{2+}$ in $[\mathbf{3}](NO_3)_2$ and $[Au_4Co_2(dppe)_2(D\text{-pen})_4](NO_3)_2$, respectively.

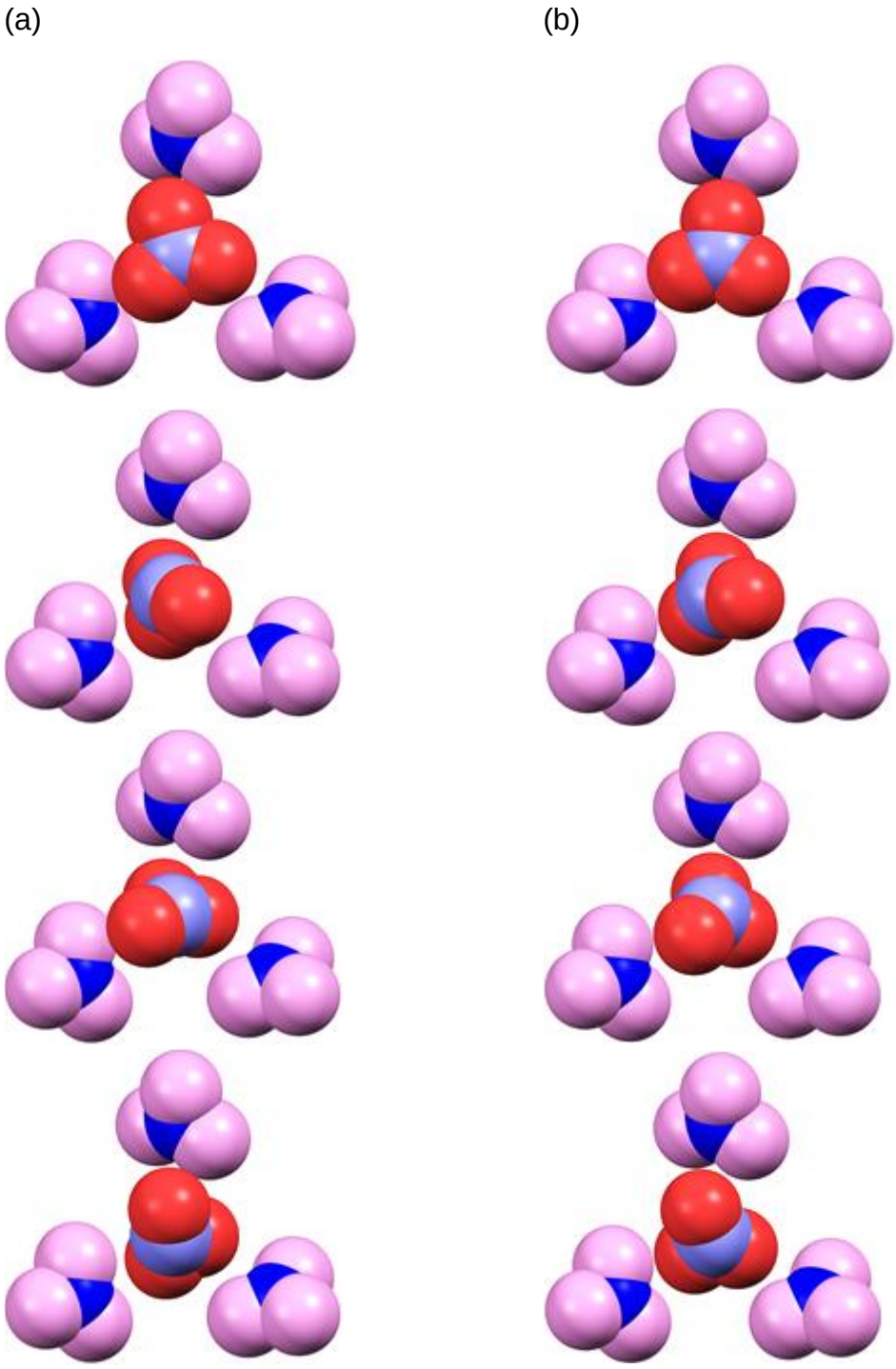

Figure 2-26. Arrangements of four neighboring nitrate anions in the anion supramolecular structure in (a) [**3**]$(NO_3)_2$ and (b) $[Au_4Co_2(dppe)_2(D\text{-}pen)_4](NO_3)_2$. Each of the four disordered anions is shown. The nitrate anions with light gray O atoms and those with dark gray O atoms represent the nitrate anions in the octahedral site and in the tetrahedral site, respectively.

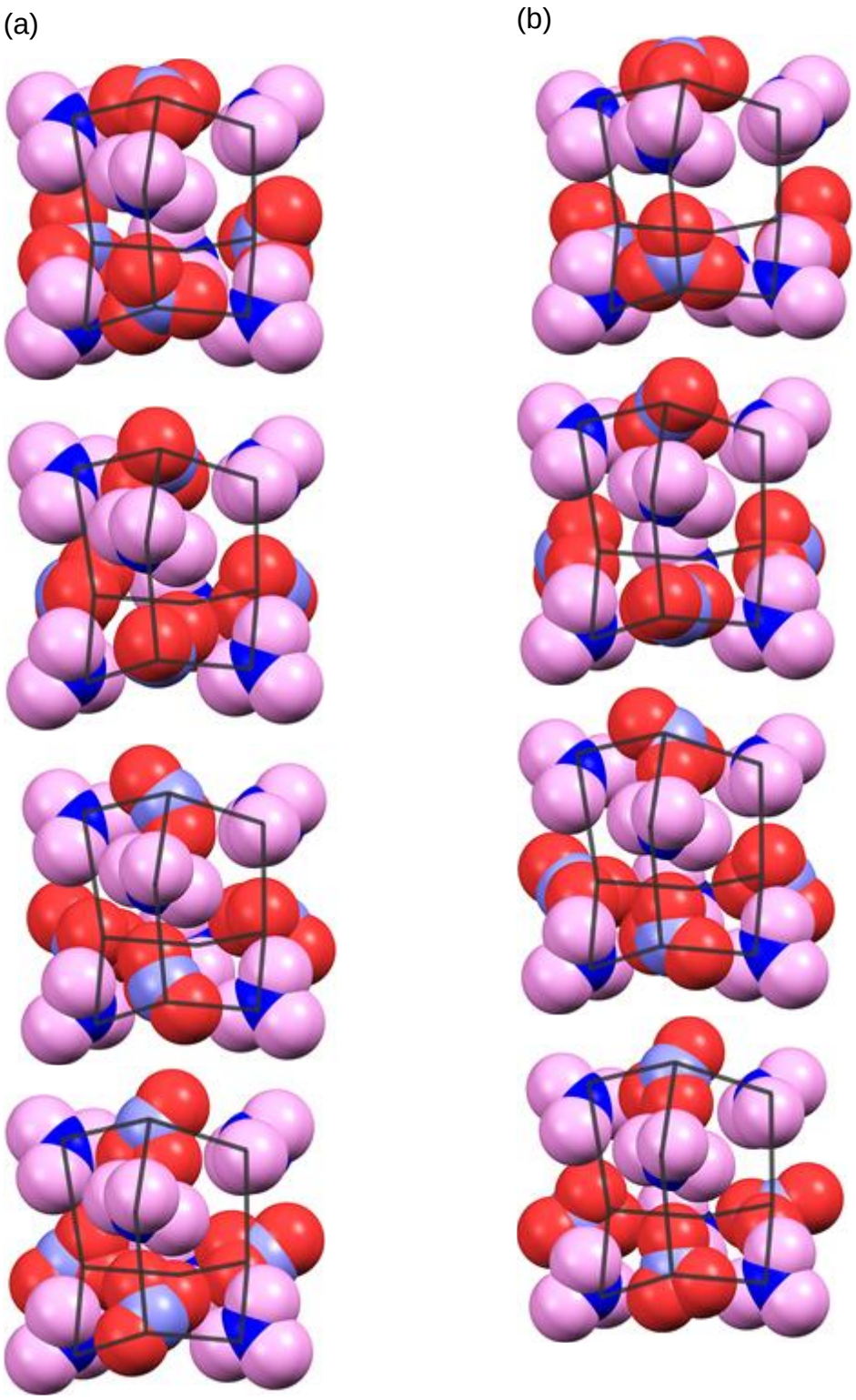

Figure 2-27. Structures of $(NO_3^-)_{10}$ aggregates in (a) [**3**]$(NO_3)_2$ and (b) $[Au_4Co_2(dppe)_2(D\text{-}pen)_4](NO_3)_2$. Each of the four disordered anions are shown. The nitrate anions with light gray O atoms and those with dark gray O atoms represent the nitrate anions in the octahedral site and in the tetrahedral site, respectively.

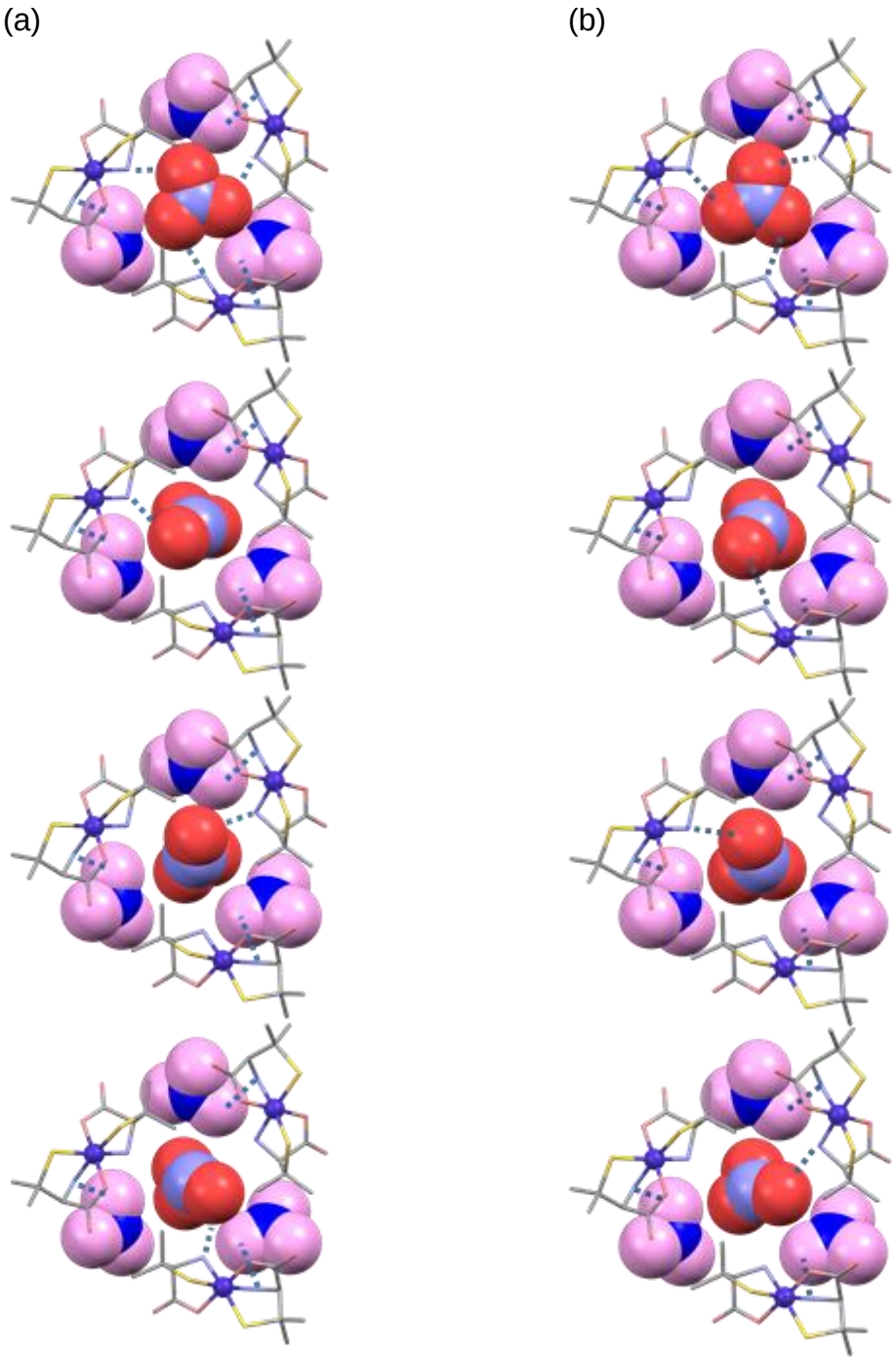

Figure 2-28. The $NH_2\cdots O_{NO3}$ hydrogen bonding interactions between the anions and $[Co(D\text{-pen})_2]^-$ units in (a) [**3**]$(NO_3)_2$ and (b) $[Au_4Co_2(dppe)_2(D\text{-pen})_4](NO_3)_2$. Each of the four disordered anions are shown. The nitrate anions with pink O atoms and those with red O atoms represent the nitrate anions in the octahedral site and in the tetrahedral site, respectively. Dashed lines indicate hydrogen bonds.

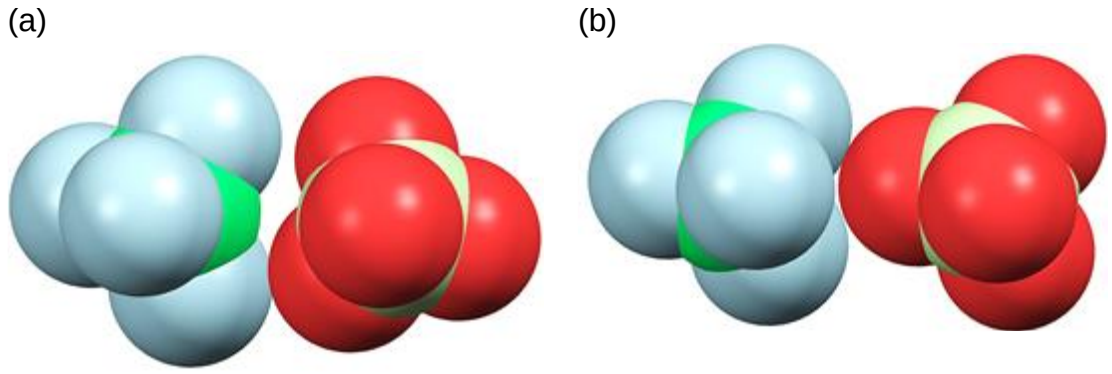

Figure 2-29. (a) Arrangement of two neighboring perchlorate anions in the anion aggregation structure in [**3**]$(ClO_4)_2$ and (b) $[Au_4Co_2(dppe)_2(D\text{-pen})_4](ClO_4)_2$. The perchlorate anions with pale blue O atoms and those with red O atoms represent the perchlorate anions in the octahedral site and in the tetrahedral site, respectively.

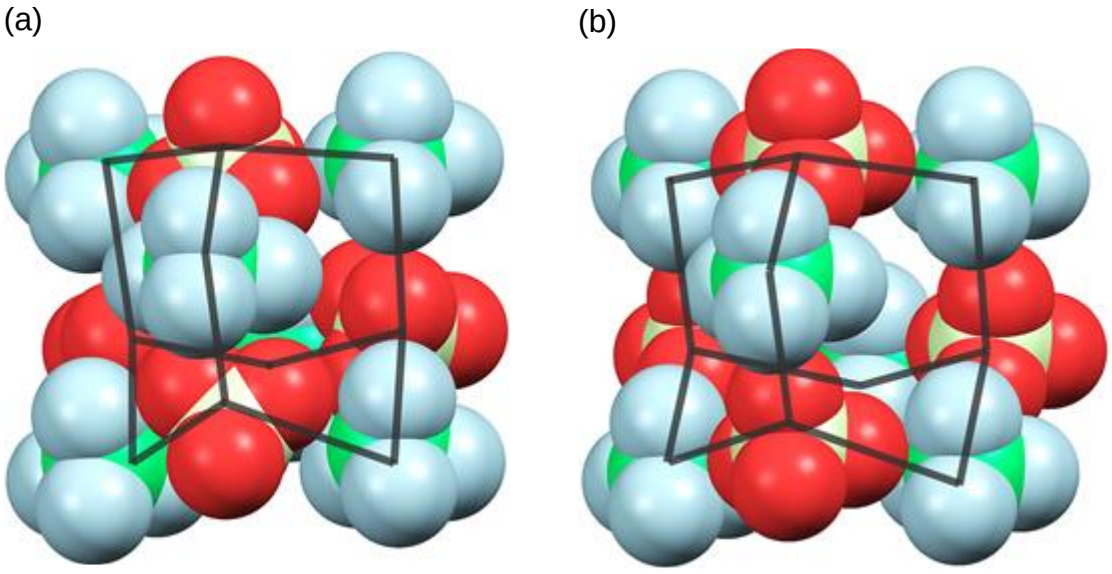

Figure 2-30. Structures of the $(ClO_4^-)_{10}$ aggregates in (a) [**3**]$(ClO_4)_2$ and (b) $[Au_4Co_2(dppe)_2(D\text{-pen})_4](ClO_4)_2$. The perchlorate anions with pale blue O atoms and those with red O atoms represent the perchlorate anions in the octahedral site and in the tetrahedral site, respectively.

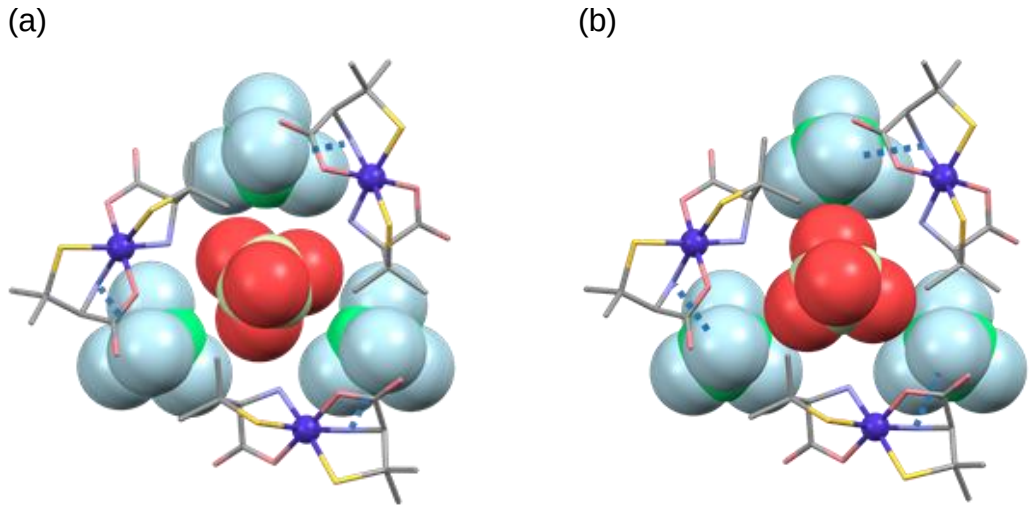

Figure 2-31. The $NH_2\cdots O_{ClO4}$ hydrogen bonding interactions between the anions and the $[Co(D\text{-pen})_2]^-$ units in (a) [**3**]$(ClO_4)_2$ and (b) $[Au_4Co_2(dppe)_2(D\text{-pen})_4](ClO_4)_2$. The perchlorate anions with pale blue O atoms and those with red O atoms represent the perchlorate anions in the octahedral site and in the tetrahedral site, respectively. Dashed lines indicate hydrogen bonds.

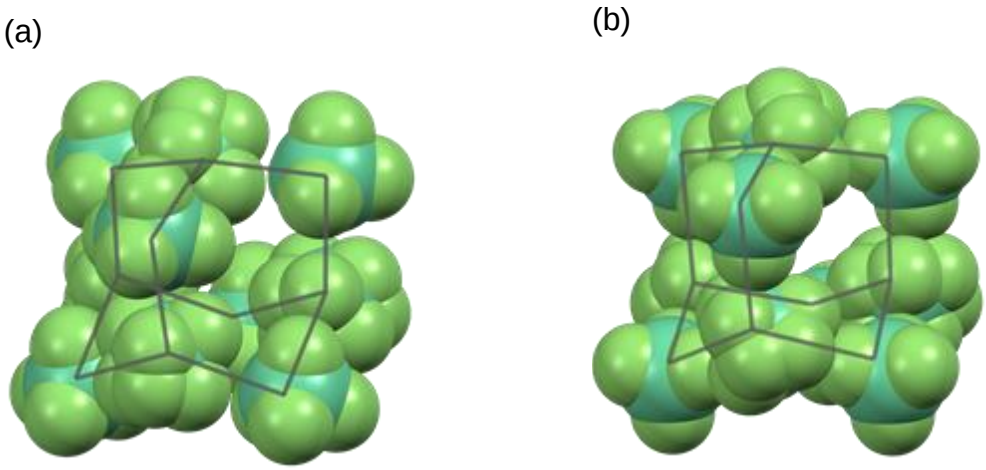

Figure 2-32. Structures of $(BF_4^-)_{10}$ aggregate in (a) [**3**]$(BF_4)_2$ and (b) $[Au_4Co_2(dppe)_2(D\text{-pen})_4](BF_4)_2$. Both of the disordered parts are drawn.

(a) (b)

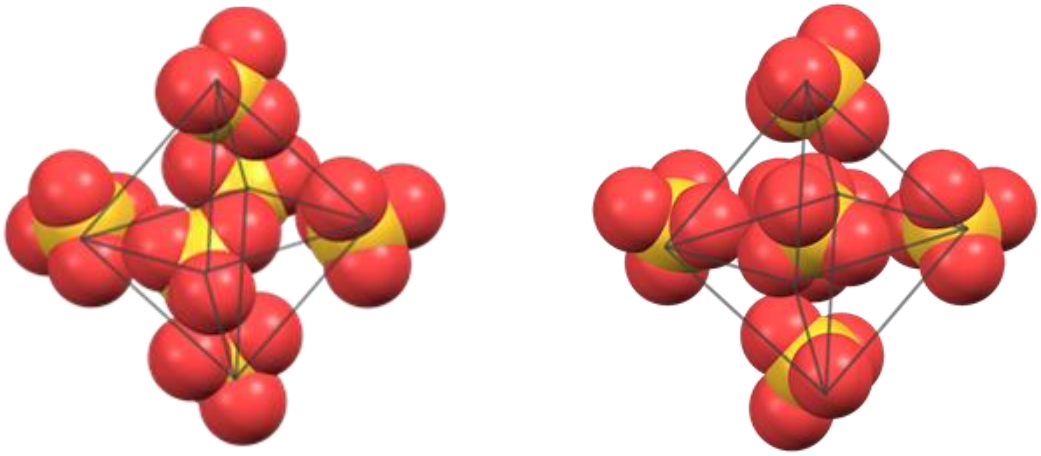

Figure 2-33. Structures of $(SO_4^{2-})_6$ aggregate in (a) [**3**]SO_4 and (b) $[Au_4Co_2(dppe)_2(D\text{-}pen)_4]SO_4$.

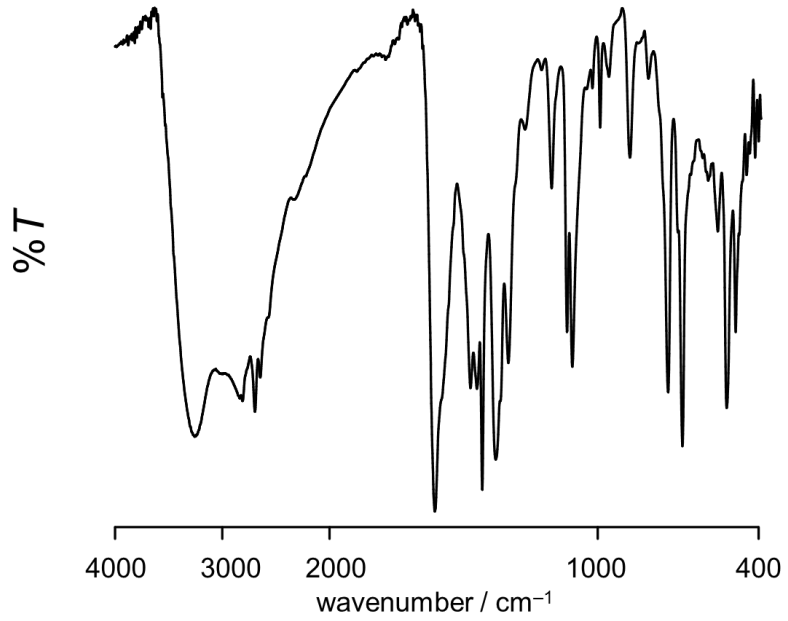

Figure 2-34. IR spectrum of DL-H_2[**2**] (KBr disk).

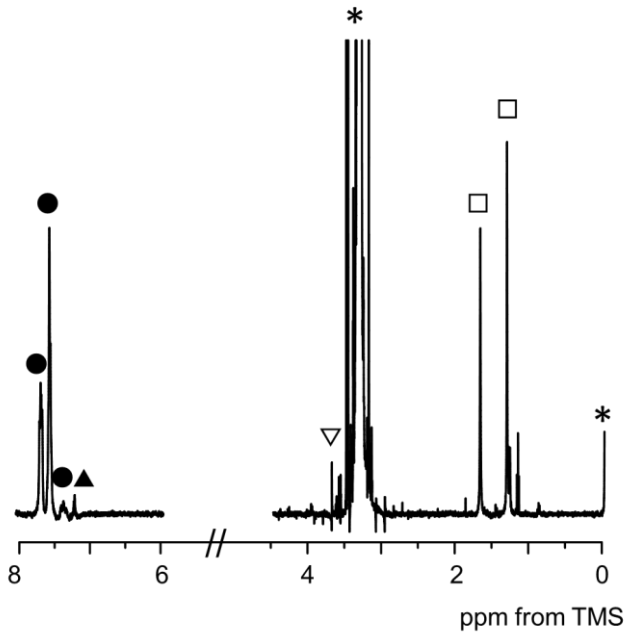

Figure 2-35. ^{1}H NMR spectrum of DL-H_2[**2**] in CD_3OD. Open squares (□) and triangles (▽) represent the methyl and the methine signals of pen moieties, and filled triangles (▲) and circles (●) represent the vinylene and the phenyl signals of *trans*-dppee moieties. The * marks represent the signals of solvents and TMS.

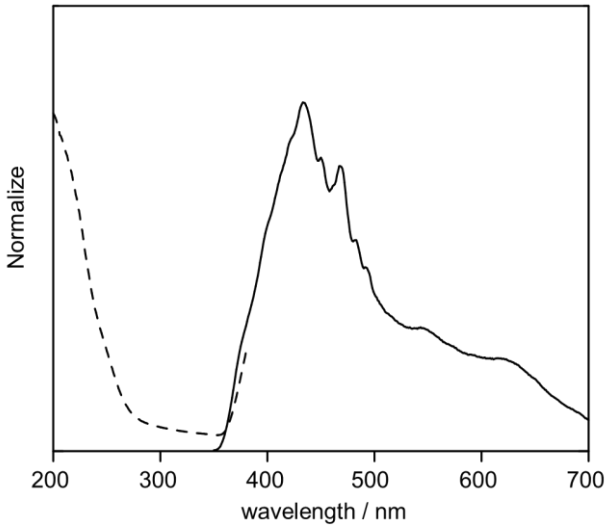

Figure 2-36. Emission and excitation spectra of DL-H_2[**2**] in the solid state. The solid and dashed lines describe the emission and excitation spectra, respectively. The excitation wavelength was 340 nm.

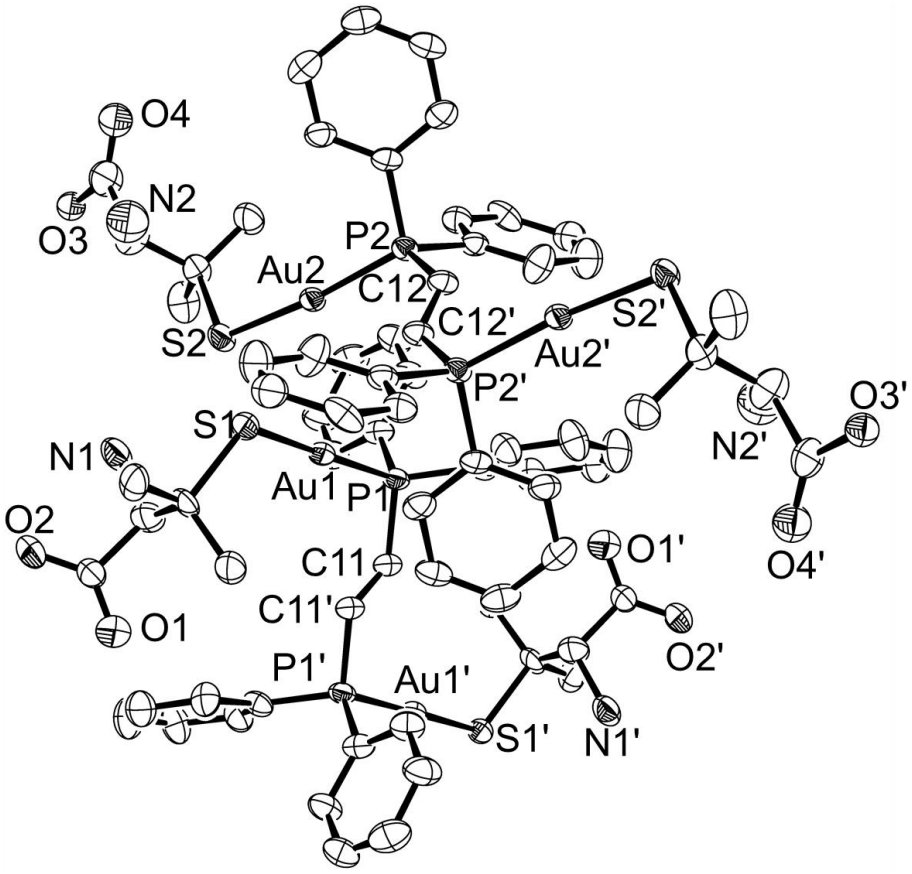

Figure 2-37. Metalloligand DL-H_2[**2**] with the atomic labeling scheme. Hydrogen atoms and the minor part of the disordered atoms are omitted for clarity. Symmetry code: (') 2–x, 1–y, –z. Thermal ellipsoids were drawn in a 50 % level.

(a)

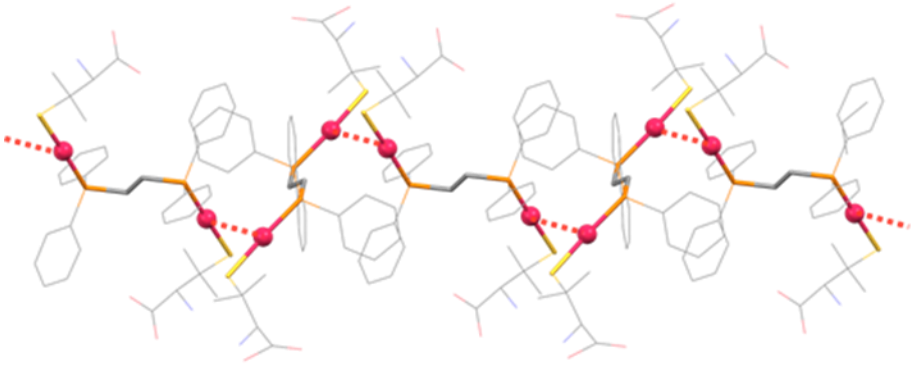

(b)

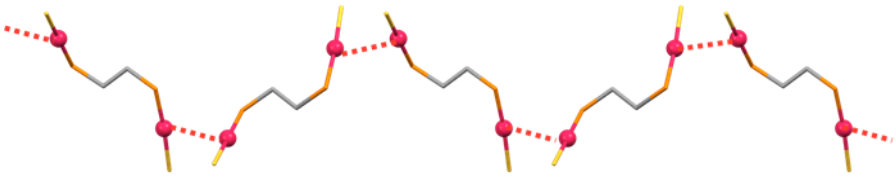

Figure 2-38. Infinite chain structure in (a) DL-H_2[**2**], and (b) [Au_2(dppe)(D-pen)(L-pen)]. Only Au, P, S, and carbon atoms of linker chain are shown for clarity in dppe analogous compound. Red dashed lines indicate aurophilic interactions.

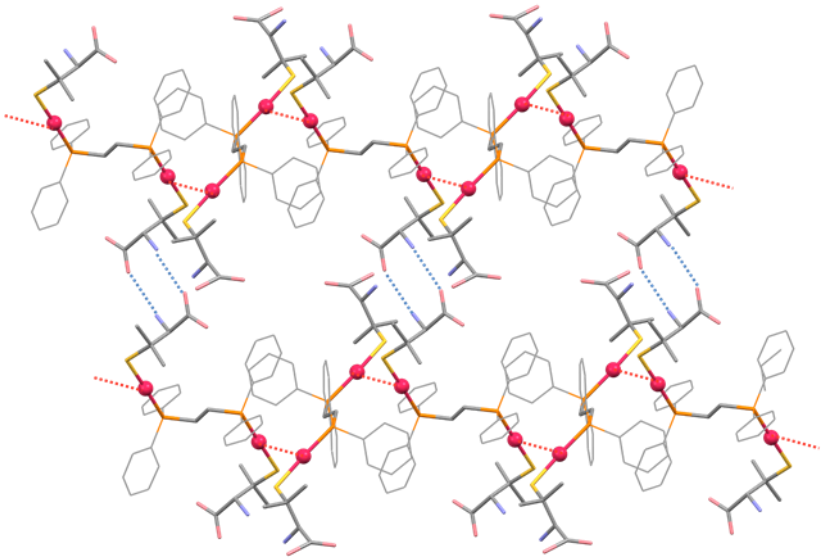

Figure 2-39. Hydrogen bonds between the chain-like aggregates in DL-H_2[**2**]. Red dashed lines indicate aurophilic interactions. Blue dashed lines indicate hydrogen bonds.

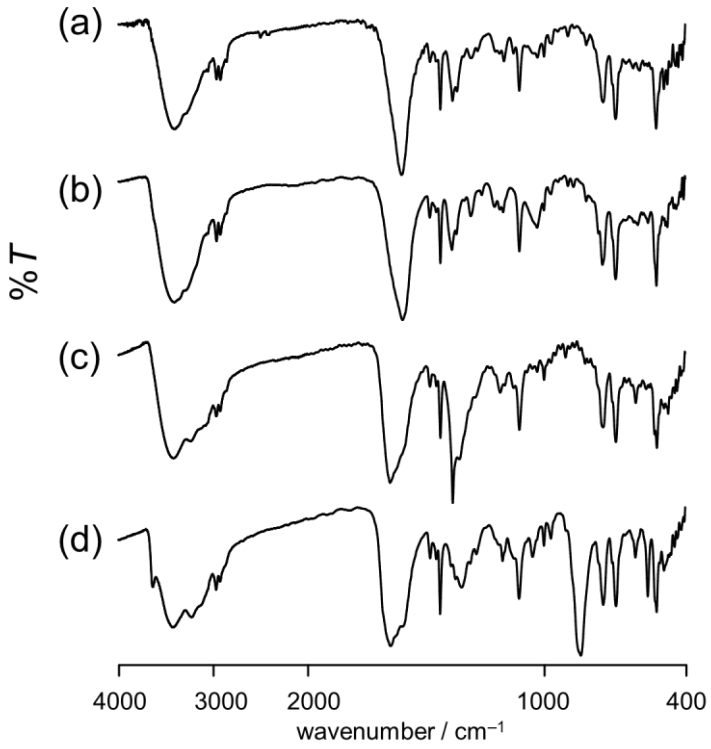

Figure 2-40. IR spectra of (a) [**5**], (b) [**5**]', (c) [**6**]$(NO_3)_2$, and (d) [**6**]$(PF_6)_2$ (KBr disk).

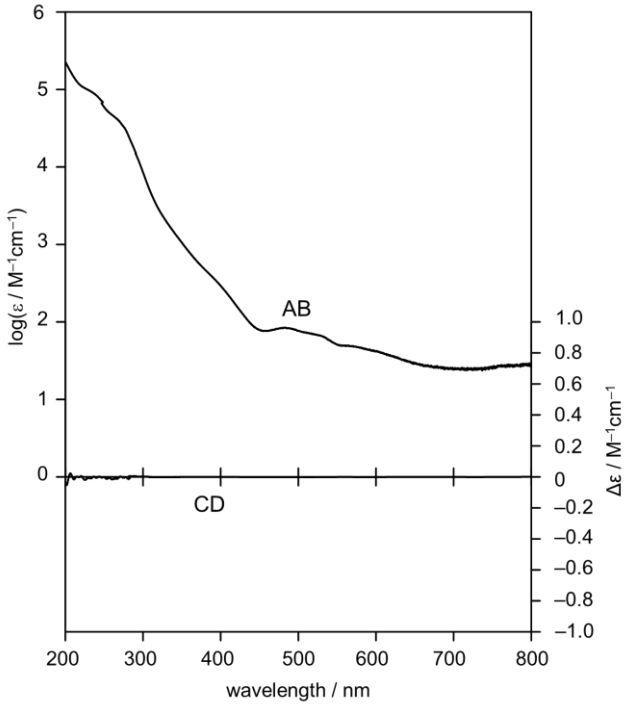

Figure 2-41. Absorption (AB) and CD spectra of [**5**] in MeOH.

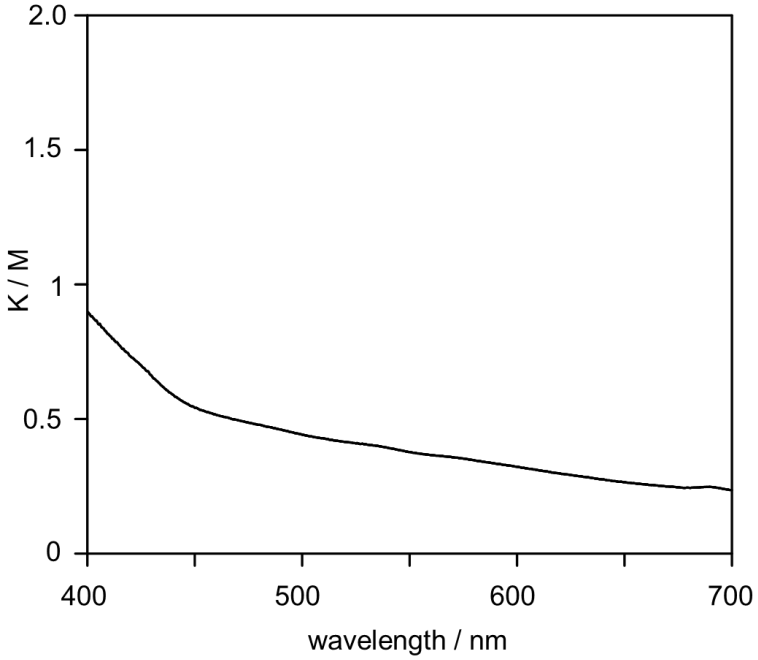

Figure 2-42. Diffuse reflection (DR) spectrum of [**5**] in the solid state.

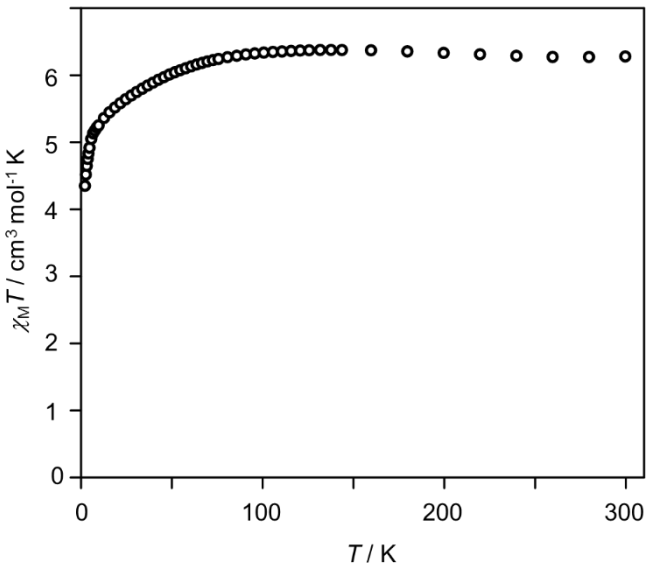

Figure 2-43. Plots of $X_M T$ vs T for $[Au^{I}_4Co^{II}_2(\textit{trans}\text{-dppee})_2(\text{D-pen})_2(\text{L-pen})_2]$ ([**5**]).

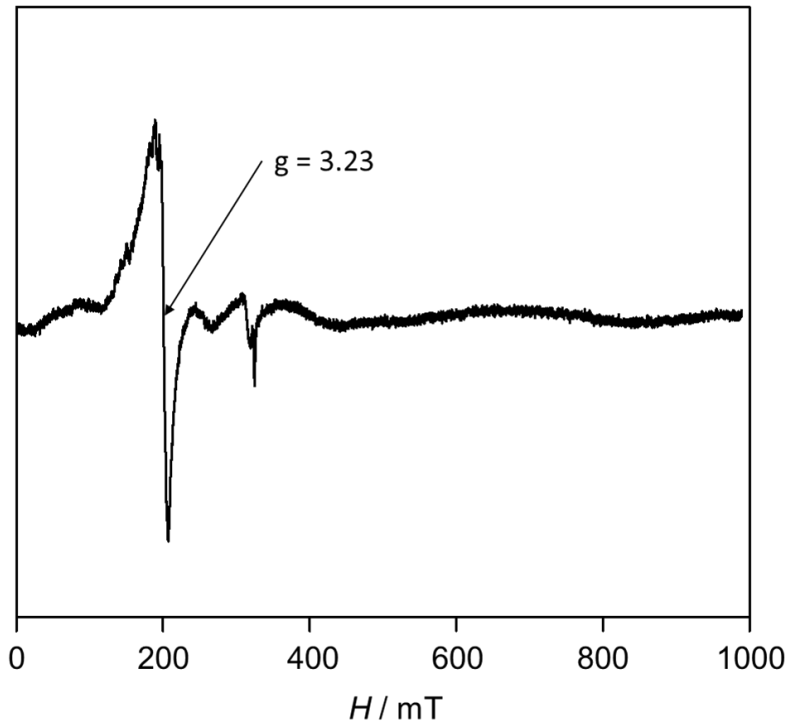

Figure 2-44. The ESR spectrum of [**5**].

(a)

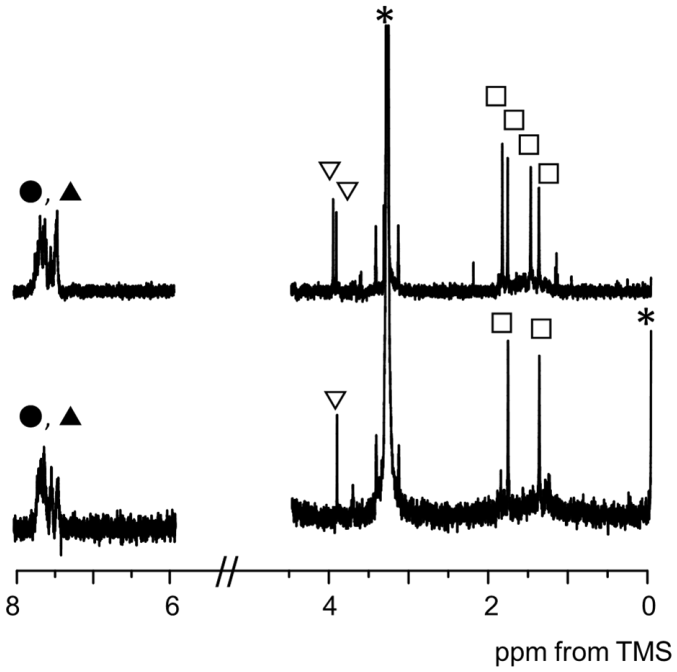

(b)

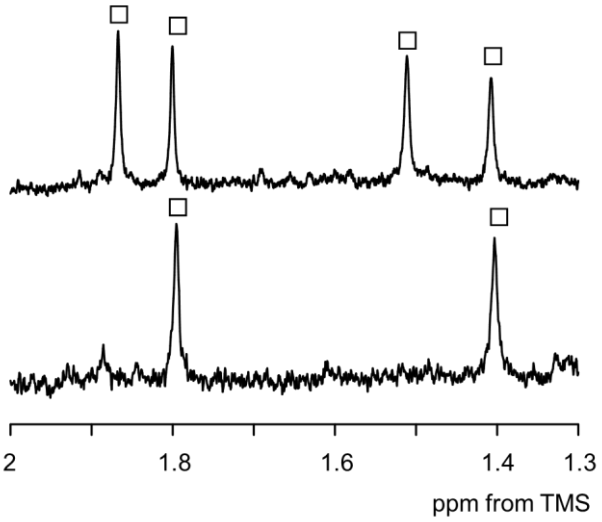

Figure 2-45. ^{1}H NMR spectra of [**6**]$(NO_3)_2$ (upper) and [**3**]$(NO_3)_2$ (bottom) in CD_3OD solution (a) in the 0-8 ppm region and (b) in the methyl region. Open squares (□) and triangles (▽) represent the methyl and the methine signals of pen moieties, and filled triangles (▲) and circles (●) represent the vinylene and the phenyl signals of *trans*-dppee moieties. The * marks represent the signals of solvents and TMS.

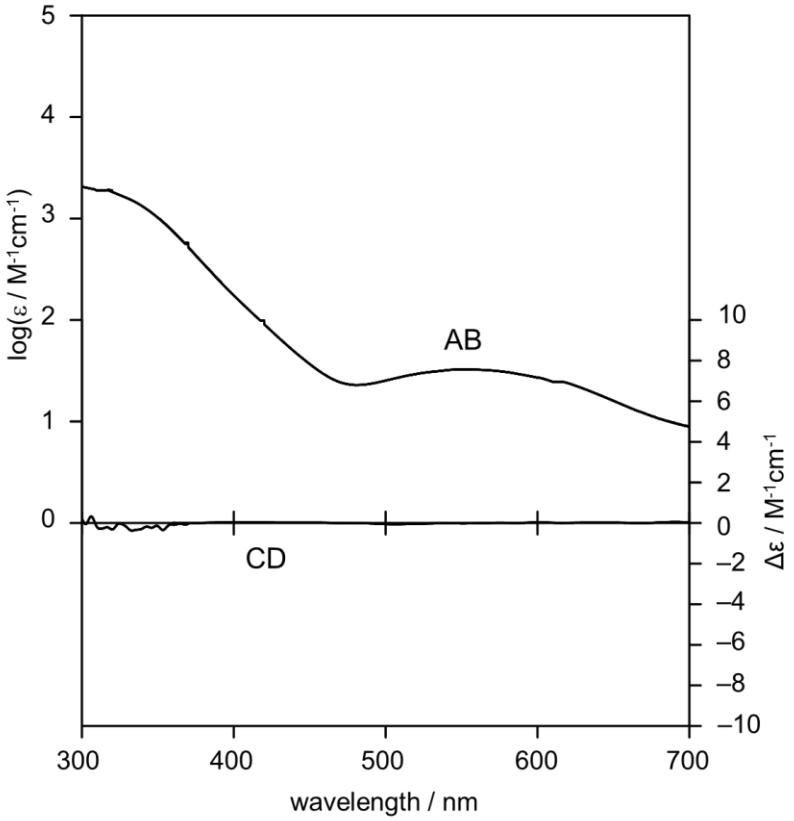

Figure 2-46. Absorption (AB) and CD spectra of [**6**]$(NO_3)_2$ in MeOH.

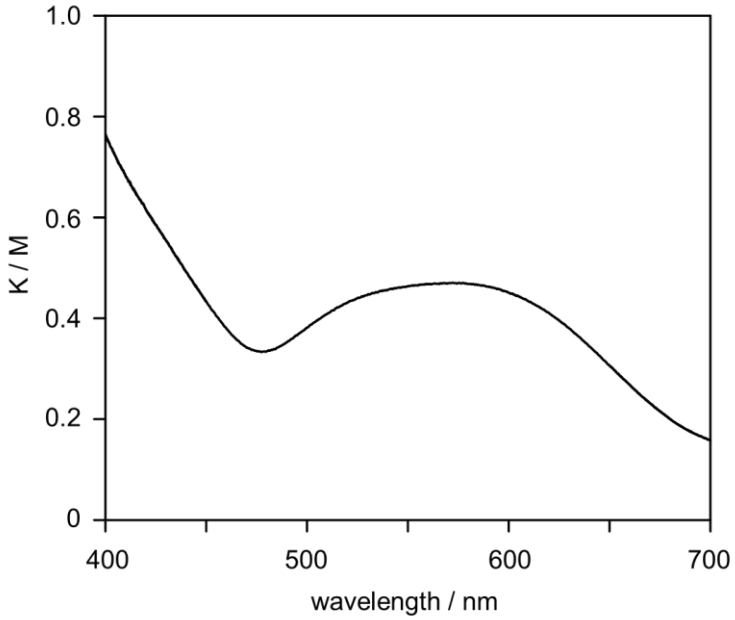

Figure 2-47. Diffuse reflection (DR) spectrum of [**6**]$(NO_3)_2$ in the solid state.

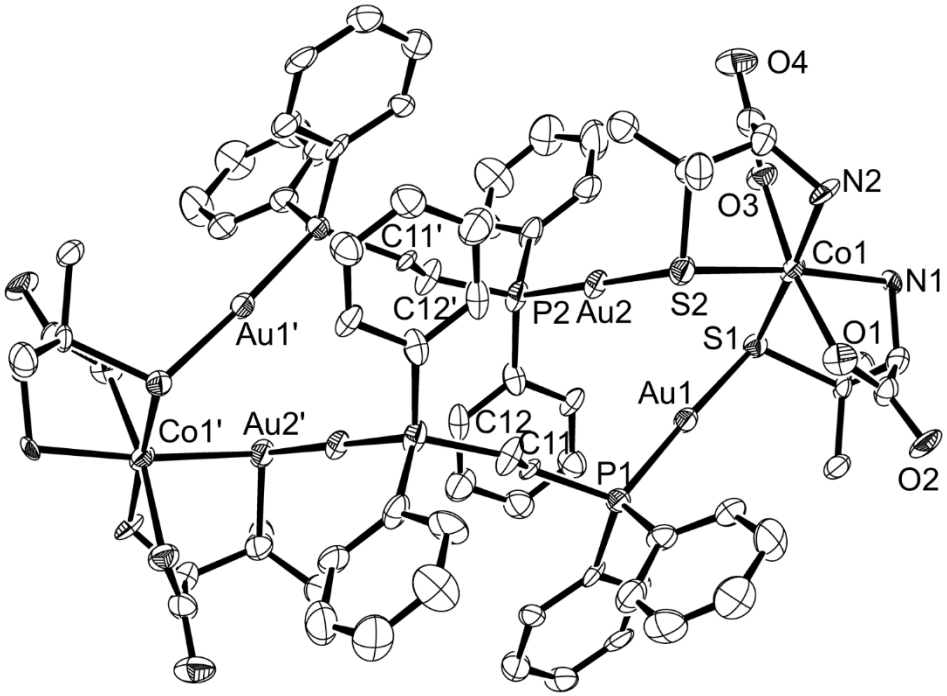

Figure 2-48. An ortep drawing of the complex molecule in [**5**] with the atomic labeling scheme. Hydrogen atoms are omitted for clarity. Symmetry code: (') 1–x, 1–y, 1–z. Thermal ellipsoids were drawn in a 50 % level.

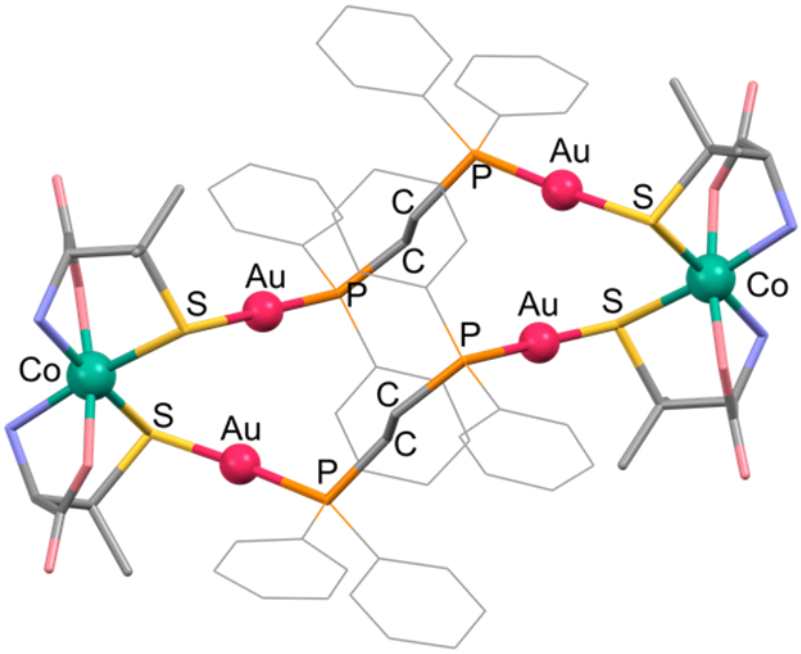

Figure 2-49. An 18-membered metalloring in [**5**].

(a)

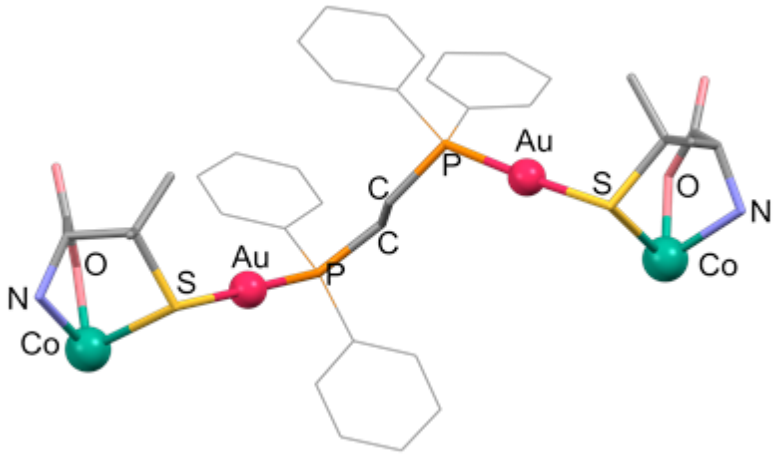

(b)

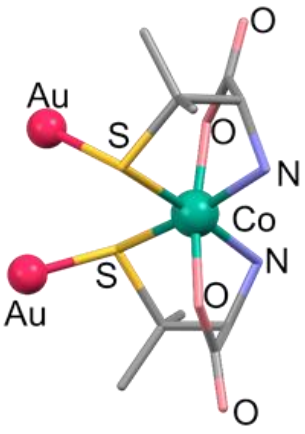

Figure 2-50. (a) Bis(tridentate-*N*,*O*,*S*) coordination mode of the metalloligand and (b) coordination geometry of Co^{II} atom.

(a)

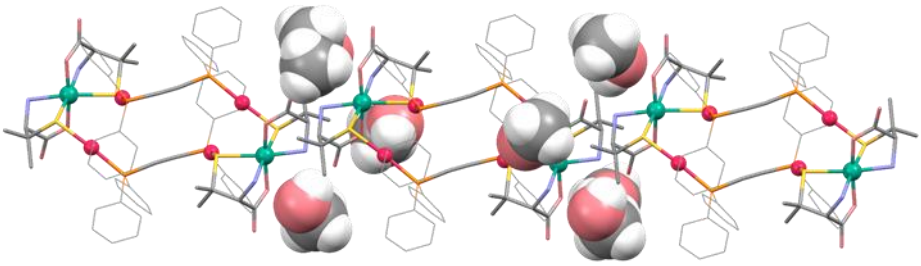

(b)

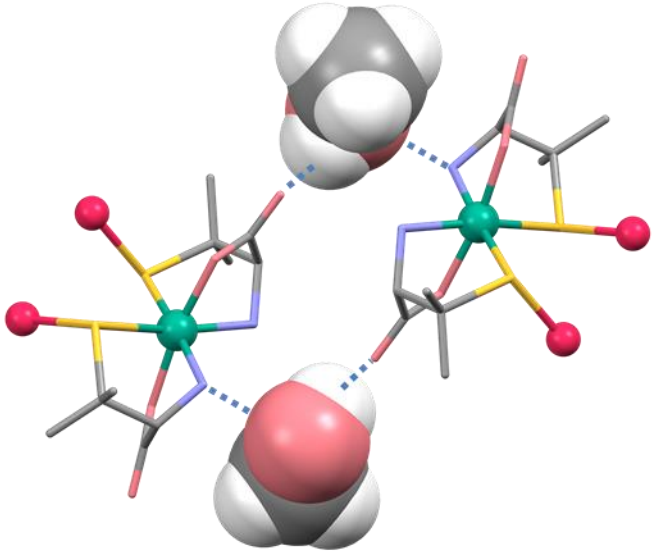

Figure 2-51. (a) 1D straight chain supramolecular structure of [**5**] and (b) hydrogen bonding mode mediated by MeOH molecules.

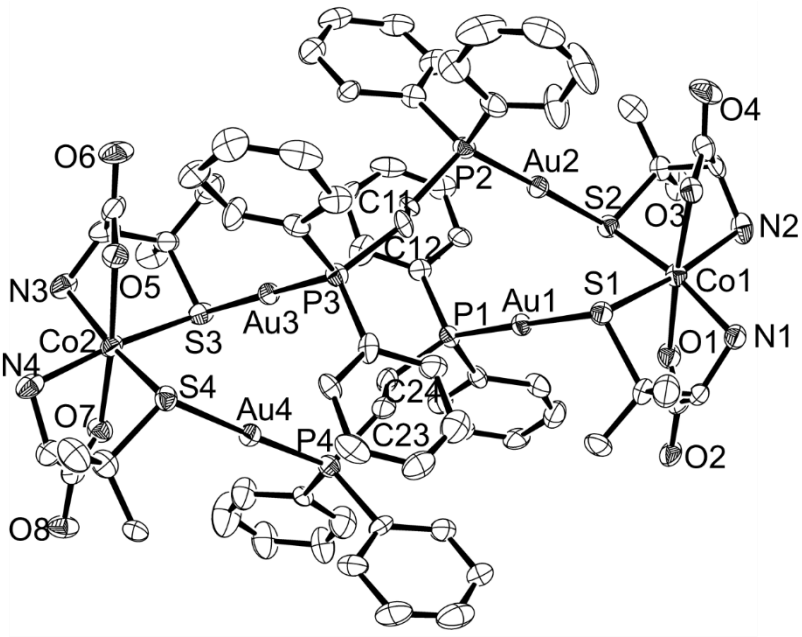

Figure 2-52. An ortep drawing of the complex cation in [**5**]' with the atomic labeling scheme. Hydrogen atoms are omitted for clarity. Thermal ellipsoids were drawn in a 50 % level.

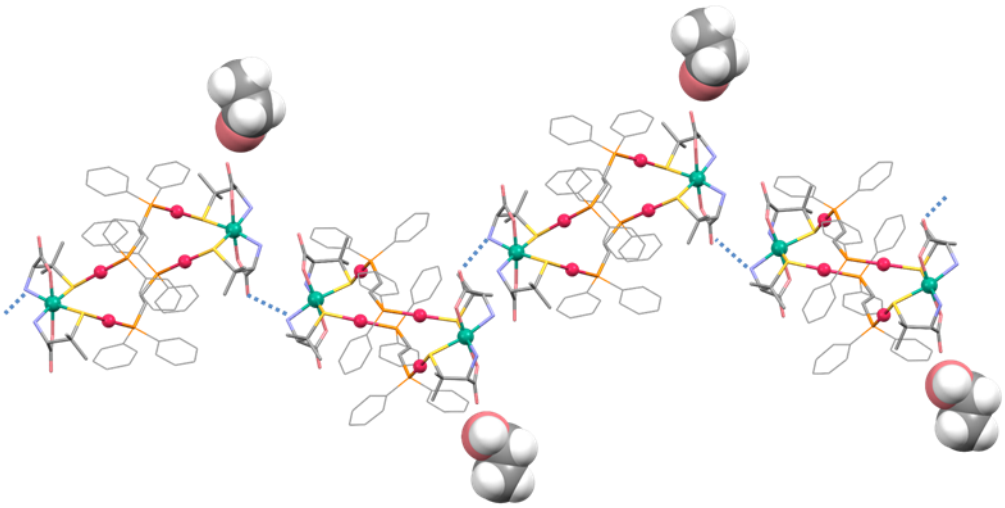

Figure 2-53. 1D zigzag chain structure of [**5**]'.

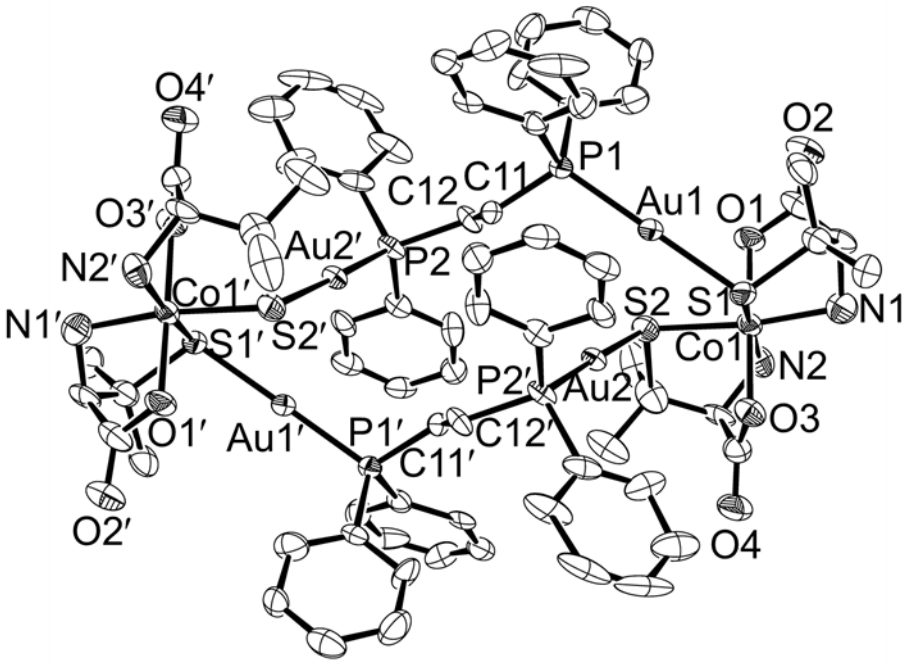

Figure 2-54. An ortep drawing of the complex cation in [**6**]$(NO_3)_2$ with the atomic labeling scheme. Hydrogen atoms are omitted for clarity. Symmetry code: (') –x, 1–y, 1–z. Thermal ellipsoids were drawn in a 50 % level.

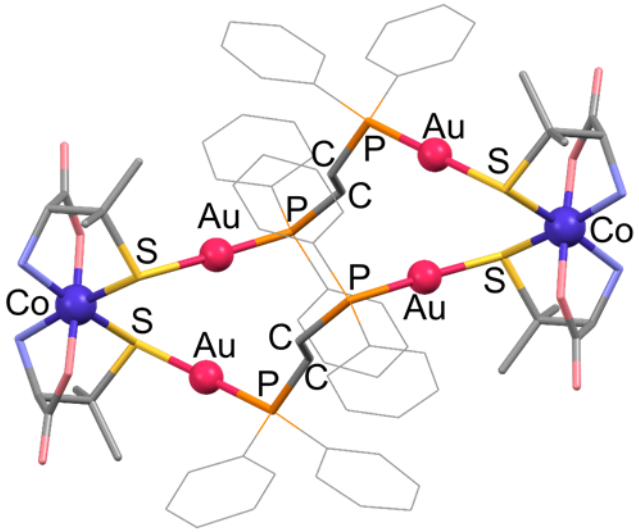

Figure 2-55. 18-Membered metalloring in [**6**]$(NO_3)_2$.

(a)

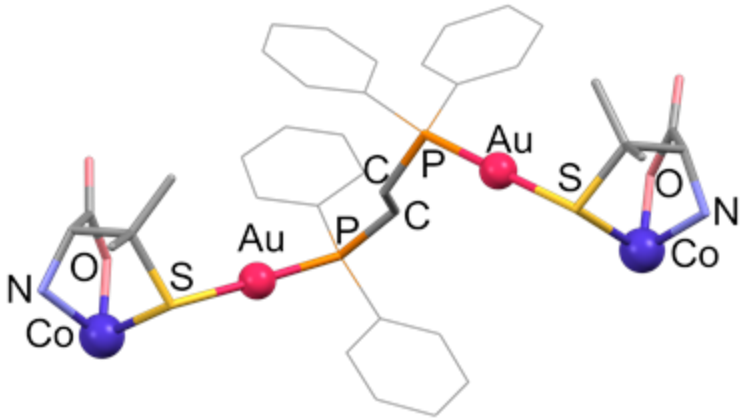

(b)

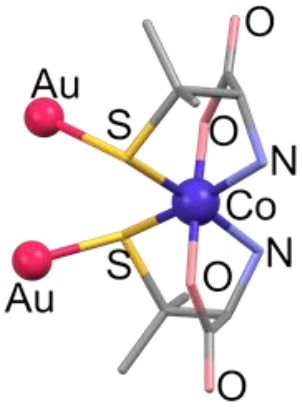

Figure 2-56. (a) Bis(tridentate-*N*,*O*,*S*) coordination mode of the metalloligand and (b) coordination geometry of Co^{III} atom in [**6**]$(NO_3)_2$.

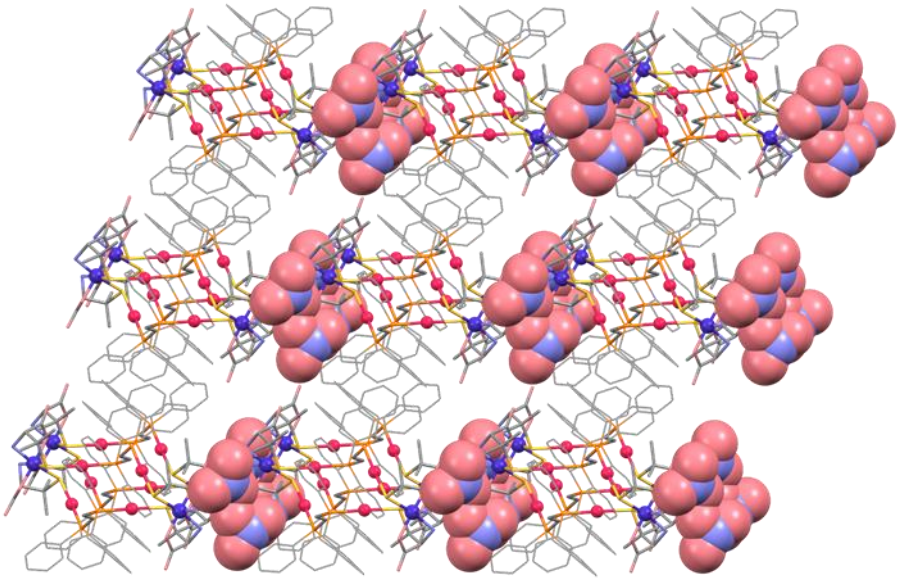

Figure 2-57. A packing structure of [**6**]$(NO_3)_2$.

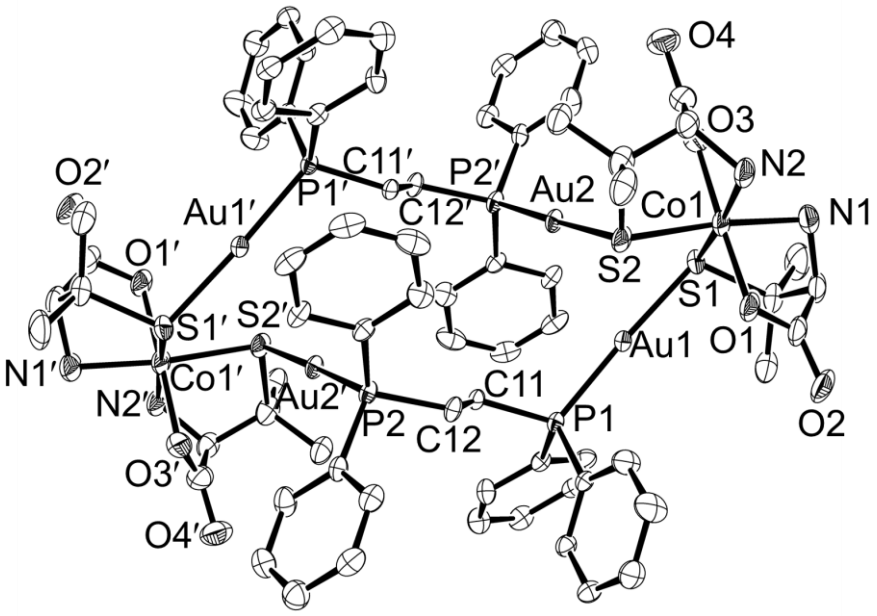

Figure 2-58. An ortep drawing of the complex cation in [**6**]$(PF_6)_2$ with the atomic labeling scheme. Hydrogen atoms are omitted for clarity. Symmetry code: (') 1–x, –y, 1–z. Thermal ellipsoids were drawn in a 50 % level.

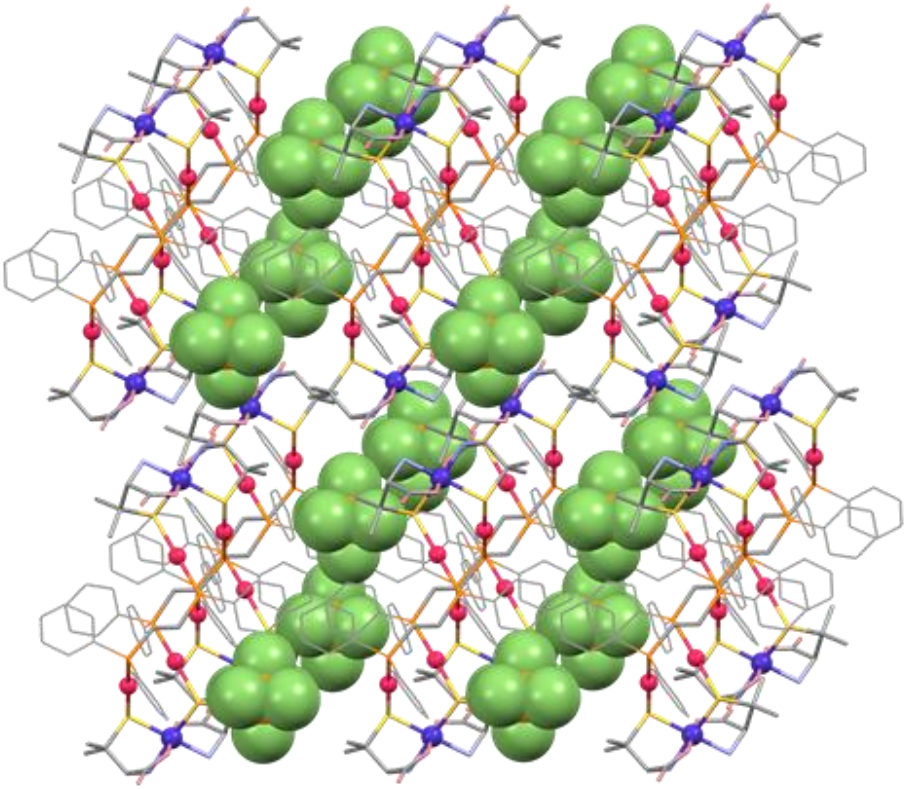

Figure 2-59. A packing structure of [**6**]$(PF_6)_2$.

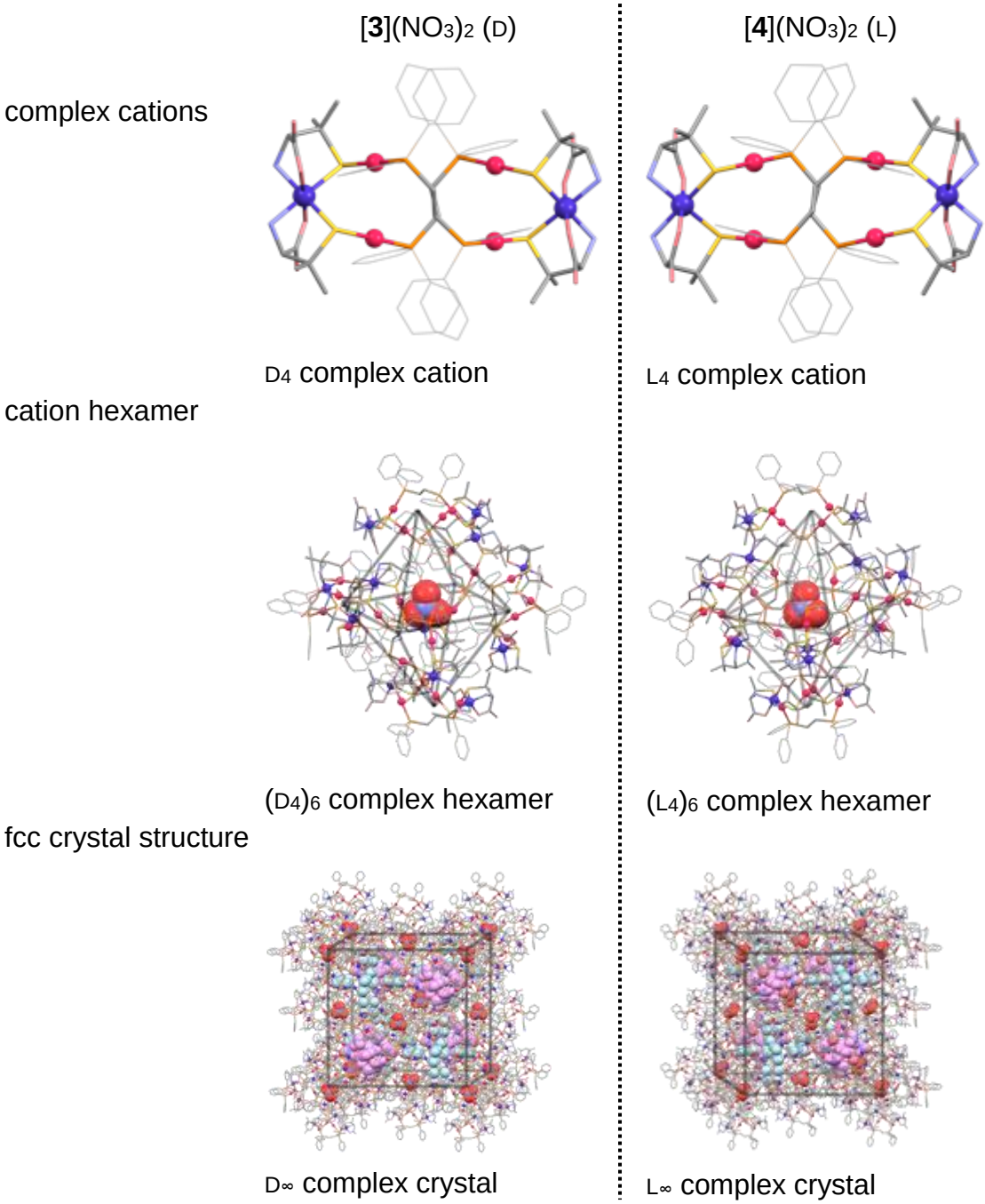

Figure 2-60. Stepwise aggregation behavior in homochiral complex [**3**]$(NO_3)_2$, [**4**]$(NO_3)_2$.

(a)

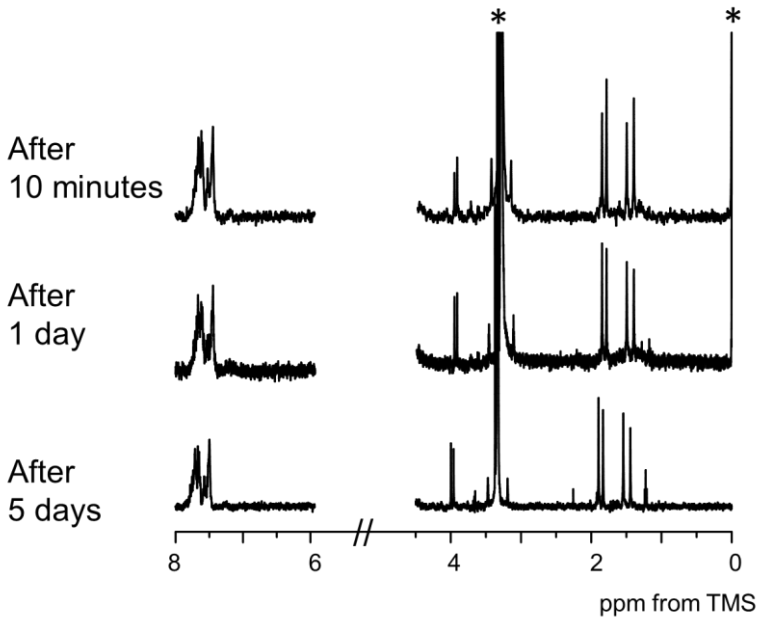

(b)

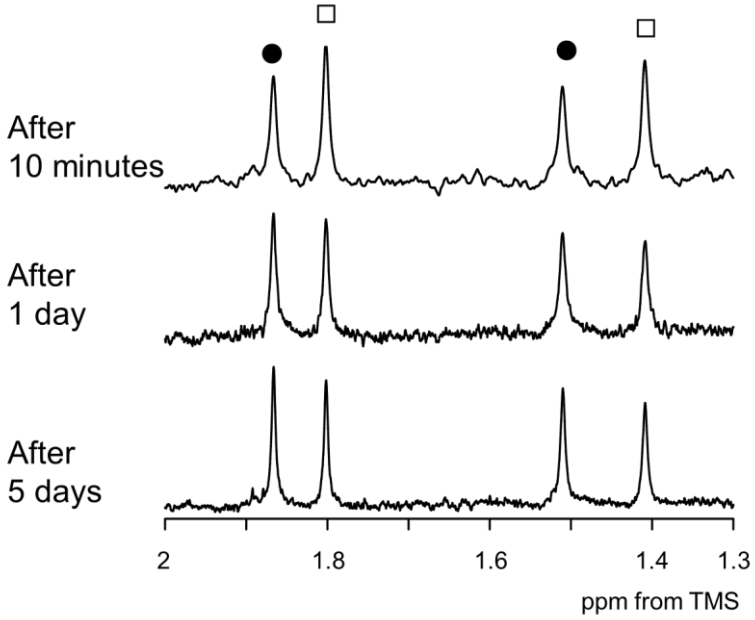

Figure 2-61. ^{1}H NMR spectral change of a 1:1 mixture of homochiral enantiomers ([**3**](NO$_3$)$_2$ + [**4**](NO$_3$)$_2$) in CD$_3$OD/D$_2$O (2:1) solution (a) in 0-8 ppm region and (b) in methyl region. Open squares (□) represent the signals of homochiral species and filled circles (●) represent the signals of heterochiral species. The * marks represent the signals of solvents and TMS.

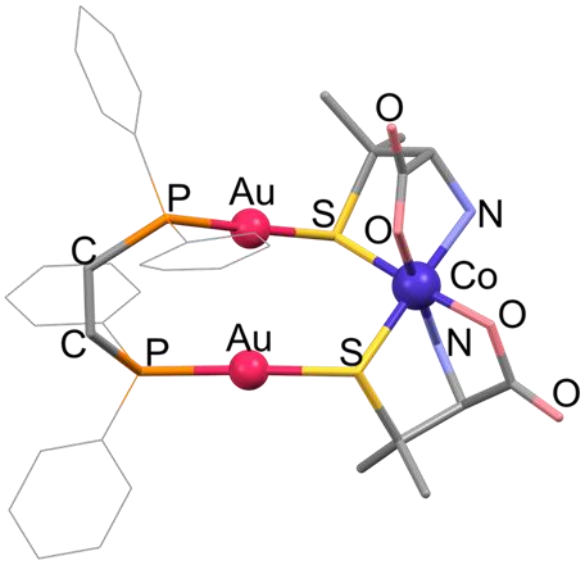

Figure 2-62. The molecular structure of $[Au^{I}_{2}Co^{III}(dppe)(D\text{-pen})(L\text{-pen})]^{+}$ complex cation.[7c]

(a)

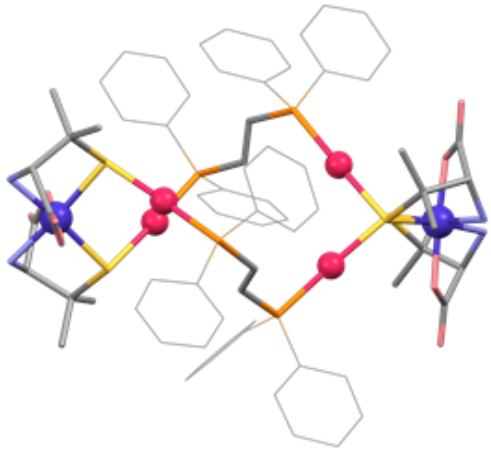

(b)

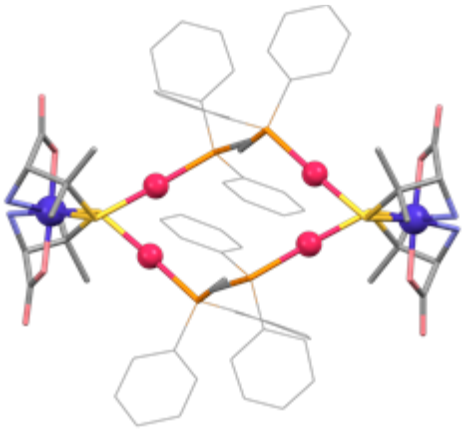

Figure 2-63. Comparison of homochiral and heterochiral hexanuclear $[Au^{I}_{4}Co^{III}_{2}]^{2+}$ cation structures. Structures of (a) homochiral $[Au^{I}_{4}Co^{III}_{2}]^{2+}$ cation and (b) heterochiral $[Au^{I}_{4}Co^{III}_{2}]^{2+}$ cation.

Chapter III. Preparation and Aggregation Behavior of $Au^{I}Ni^{II}$ Complexes.

III-1. Introduction.

In Chapter II, the reaction of [Au_2(*trans*-dppee)(D-Hpen)$_2$] with Co^{II} in air was investigated. The resulting cationic complex, [$Au^{I}_4Co^{III}_2$(*trans*-dppee)$_2$(D-pen)$_4$]$^{2+}$, crystallized in the unique supramolecular structure showing separate aggregation of cationic complexes and inorganic anions. The molecular and supramolecular structures were similar to those found in the dppe analogous crystal, [$Au^{I}_4Co^{III}_2$(dppe)$_2$(D-pen)$_4$]$^{2+}$, but the slight change of the linker unit affected the orientation of anions in the aggregate. In the dppe system, not only the cationic $Au^{I}_4Co^{III}_2$ complex but also the neutral $Au^{I}_4Ni^{II}_2$ complex, [$Au^{I}_4Ni^{II}_2$(dppe)$_2$(D-pen)$_4$], which had a similar hexanuclear structure to that of $Au^{I}_4Co^{III}_2$ complex was reported.[6,9]. Therefore, the $Au^{I}_4Ni^{II}_2$ complex molecules formed the hydrogen-bonded 1D chain arrangement and did not form the charge-separated structure like the $Au^{I}_4Co^{III}_2$ complex.

In this chapter, to get the insight into the effect of the bridging diphosphine linkers on the supramolecular structure, the reactions of [Au_2(*trans*-dppee)(D-Hpen)$_2$] (D$_2$-H$_2$[**2**], *trans*-dppee = *trans*-1,2-bis(diphenylphosphino)ethylene, D-H$_2$pen = D-penicillamine) with Ni^{II} were examined. Interestingly, a unique example of the strong-acid-templated construction of a metallosupramolecular structure based on the digold(I) metalloligand, (D$_2$-H$_2$[**2**]) was found (Scheme 2-1). Whereas the reaction of D$_2$-H$_2$[**2**] with basic Ni(OAc)$_2$ in methanol yielded the infinite {$Au^{I}_2Ni^{II}$}$_n$ 1D coordination polymer, i.e. [Ni{Au_2(*trans*-dppee)(D-pen)$_2$}]$_n$, a similar reaction with acidic Ni(ClO$_4$)$_2$ or Ni(NO$_3$)$_2$ produced the discrete hexanuclear $Au^{I}_4Ni^{II}_2$ complex, i.e. [Ni$_2$\{Au_2(*trans*-dppee)(D-pen)$_2$\}$_2$] ([**7**]), which co-crystallized with HClO$_4$ or HNO$_3$ to yield [**7**]·2HClO$_4$ or [**7**]·4/3HNO$_3$, respectively (Scheme 3-1 and 3-2). In [**7**]·2HClO$_4$, six $Au^{I}_4Ni^{II}_2$ hexanuclear molecules were self-assembled into a neutral {[$Au^{I}_4Ni^{II}_2$]}$_6$ supramolecular octahedron, and ten ClO_4^- ions were aggregated into an anionic {ClO_4^-}$_{10}$ adamantane-like arrangement. A similar aggregation of inorganic anions was also found in [**7**]·4/3HNO$_3$. Remarkably, [**7**]·2HClO$_4$ was found to absorb NH$_3$ molecules and converted into [**7**]·2NH$_4$ClO$_4$ when the crystals of [**7**]·2HClO$_4$ were soaked in aqueous ammonia, with retention of its single crystallinity (Scheme 3-1). Such a construction of the acidic supramolecular structure templated by a strong Brønsted acid and its single-crystal-to-single-crystal conversion to a neutral structure via absorption of base molecules are unprecedented. The reverse, single-crystal-to-single-crystal conversion from [**7**]·2NH$_4$ClO$_4$ to [**7**]·2HClO$_4$ also occurred when the crystals of [**7**]·2NH$_4$ClO$_4$ were soaked in aqueous HClO$_4$.

III-2. Experimental Section.

III-2-1. Materials.

The starting complexes (D$_2$-H$_2$[**2**], L$_2$-H$_2$[**2**], and DL-H$_2$[**2**]) were prepared by the methods described in Chapter II. Synthesis of [Au$_2$(dppe)(D-Hpen)$_2$]·8H$_2$O has been described in the previous paper.[6] The reagents were commercially available and used without further purification. All experiments were performed in the air.

III-2-2. Preparation of $Au^{I}Ni^{II}$ Complexes.

III-2-2-1a. [Au$_4$Ni$_2$(*trans*-dppee)$_2$(D-pen)$_4$]·2HClO$_4$ ([**7**]·2HClO$_4$).

To a white suspension containing 0.050 g (0.043 mmol) of D$_2$-H$_2$[**2**] in MeOH (20 mL) was added 0.019 g (0.052 mmol) of Ni(ClO$_4$)$_2$·4H$_2$O, which was stirred at room temperature for 1 h. To the resulting pale yellow solution, an NH$_3$ aqueous solution (1 M, 0.1 mL) was added followed by standing at room temperature for 9 weeks with slow evaporation to give green crystals of [**7**]·2HClO$_4$, which were collected by filtration and washed with water and MeOH. Yield: 0.022 g (39%). Anal. Calcd for [Au$_4$Ni$_2$(*trans*-dppee)$_2$(D-pen)$_4$]·2HClO$_4$·6H$_2$O = $C_{72}H_{94}N_4Au_4Cl_2Ni_2O_{22}P_4S_4$: C, 33.31; H, 3.65; N, 2.16; Cl, 2.73%. Found: C, 33.20; H, 3.72; N, 2.35; Cl, 2.48%. IR spectrum (cm^{-1}, KBr disk): 1718 (shoulder, ν_{CO}), 1591 (ν_{CO}), 1101 (ν_{ClO4}), 746-691 (ν_{Ph}), and 623 (ν_{ClO4}).

III-2-2-1b. [Au$_4$Ni$_2$(*trans*-dppee)$_2$(D-pen)$_4$]·4/3HNO$_3$ ([**7**]·4/3HNO$_3$).

To a white suspension containing 0.050 g (0.043 mmol) of D$_2$-H$_2$[**2**] in MeOH (20 mL) was added 0.016 g (0.055 mmol) of Ni(NO$_3$)$_2$·6H$_2$O, which was stirred at room temperature for 1 h. To the resulting pale yellow solution, an NH$_3$ aqueous solution (1 M, 0.1 mL) was added followed by standing at room temperature for 9 weeks with slow evaporation to give green crystals and green crystalline precipitate of [**7**]·4/3HNO$_3$, which were collected by filtration and washed with water and MeOH. Yield: 0.043 g (82%). Anal. Calcd for [Au$_4$Ni$_2$(*trans*-dppee)$_2$(D-pen)$_4$]·4/3HNO$_3$·4H$_2$O = $C_{72}H_{89.33}N_{5.33}$ $Au_4Ni_2O_{16}P_4S_4$: C, 35.40; H, 3.69; N, 3.06%. Found: C, 35.38; H, 3.79; N, 3.23%. IR spectrum (cm^{-1}, KBr disk): 1720 (shoulder, ν_{CO}), 1591 (ν_{CO}), 1385 (ν_{NO3}), and.746-691 (ν_{Ph}).

III-2-2-2. [Au$_4$Ni$_2$(dppe)$_2$(D-pen)$_4$]·2HClO$_4$ ([**8**]·2HClO$_4$).

To a white suspension containing 0.050 g (0.040 mmol) of [Au(dppe)(D-Hpen)$_2$]·8H$_2$O in MeOH (10 mL) was added 0.018 g (0.048 mmol) of Ni(ClO$_4$)$_2$·6H$_2$O. To the resulting pale red solution, an NH$_3$ aqueous solution (1 M, 0.04 mL) was added to give a green solution followed by standing at room temperature for 5 weeks with slow evaporation to give green crystals of [**8**]·2HClO$_4$ and green residue. The crystals were picked up by hand

and washed with water and MeOH. Yield: 0.005 g (9%). Anal. Calcd for $[Au_4Ni_2(dppe)_2(D\text{-pen})_4]\cdot 2HClO_4\cdot 6H_2O$ = $C_{72}H_{98}N_4Au_4Cl_2Ni_2O_{22}$ P_4S_4: C, 33.26; H, 3.80; N, 2.15%. Found: C, 33.15; H, 3.86; N, 2.34%. IR spectrum (cm^{-1}, KBr disk): 1590 (ν_{CO}), 1105 (ν_{ClO4}), 733-691 (ν_{Ph}), and 624 (ν_{ClO4}).

III-2-2-3. [Au_2Ni(*trans*-dppee)(D-pen)$_2$]$_\infty$ ([9]).

To a white suspension containing 0.01 g (0.009 mmol) of D_2-H_2[**2**] in MeOH (1.5 mL) was added 0.003 g (0.01 mmol) of $Ni(OAc)_2\cdot 4H_2O$. Green plate-like crystals suitable for X-ray analysis were obtained via the slow diffusion of MeCN vapor into the resulting green solution. The crystals were collected via filtration and washed with MeOH. Yield: 0.009 g (82%). Anal. Calcd for $[Au_2Ni(trans\text{-dppee})(D\text{-pen})_2]\cdot 7H_2O$ = $C_{36}H_{54}N_2Au_2NiO_{11}P_2S_2$: C, 34.06; H, 4.29; N, 2.21%. Found: C, 34.04; H, 4.11; N, 2.25%. IR spectrum (cm^{-1}, KBr disk): 1593 (ν_{CO}), 1102 (ν_{PC}), and 745-691 (ν_{Ph}).

III-2-2-4. Treatment of Acidic Crystals with Aqueous Basic Solution.

Reaction A-1

Freshly prepared crystals of [**7**]$\cdot 2HClO_4$ (20 mg) were soaked in an aqueous solution of NH_3 (0.1 M, 50 mL) and were subsequently allowed to stand at room temperature overnight. The green crystals were collected via filtration and washed with water. Anal. Calcd for $[Au_4Ni_2(trans\text{-dppee})_2(D\text{-pen})_4]\cdot 2NH_4ClO_4\cdot 6H_2O$ = $C_{72}H_{100}N_6Au_4Cl_2Ni_2O_{22}$ P_4S_4: C, 32.88; H, 3.83; N, 3.20%. Found: C, 33.04; H, 3.88; N, 2.89%. IR spectrum (cm^{-1}, KBr disk): 1579 (ν_{CO}), 1102 (ν_{ClO4}), 745-691 (ν_{Ph}), and 624 (ν_{ClO4}).

Reaction A-2

Freshly prepared crystals of [**7**]$\cdot 2HClO_4$ (10 mg) were soaked in an aqueous solution of $MeNH_2$ (0.1 M, 25 mL) and were subsequently allowed to stand at room temperature overnight. The green precipitate was collected via filtration and washed with water. Anal. Calcd for $[Au_4Ni_2(trans\text{-dppee})_2(D\text{-pen})_4]\cdot 13H_2O$ = $C_{72}H_{106}N_6Au_4Ni_2O_{21}P_4S_4$: C, 34.30; H, 4.24; N, 2.22%. Found: C, 34.23; H, 4.07; N, 2.26%. IR spectrum (cm^{-1}, KBr disk): 1595 (ν_{CO}), and 742-689 (ν_{Ph}).

Reaction B

Freshly prepared crystals of [**7**]$\cdot 4/3HNO_3$ (10 mg) were soaked in an aqueous solution of NH_3 (0.1 M, 25 mL) and were subsequently allowed to stand at room temperature for a day. The green precipitate was collected via filtration and washed with water. Anal. Calcd for $[Au_4Ni_2(trans\text{-dppee})_2(D\text{-pen})_4]\cdot 5H_2O$ = $C_{72}H_{90}N_4Au_4Ni_2O_{13}P_4S_4$: C, 36.38; H, 3.82; N, 2.36%. Found: C, 36.26; H, 4.04; N, 2.24%. IR spectrum (cm^{-1}, KBr disk): 1590 (ν_{CO}) and 744-692 (ν_{Ph}).

Reaction C

Freshly prepared crystals of [**8**]·2$HClO_4$ (5 mg) were soaked in an aqueous solution of NH_3 (0.1 M, 12.5 mL) and were subsequently allowed to stand at room temperature for a day. The green precipitate was collected via filtration and washed with water. Anal. Calcd for [Au_4Ni_2(dppe)$_2$(D-pen)$_4$]·12H_2O = $C_{72}H_{108}N_4Au_4Ni_2O_{20}P_4S_4$: C, 34.49; H, 4.34; N, 2.23%. Found: C, 34.58; H, 4.18; N, 2.24%. IR spectrum (cm^{-1}, KBr disk): 1590 (ν_{CO}) and 727-690 (ν_{Ph}).

Reaction D

Crystalline powder of [**9**] (10 mg) were soaked in an aqueous solution of NH_3 (0.1 M, 12.5mL) and were subsequently allowed to stand at room temperature overnight. The green precipitate was collected via filtration and washed with water. Anal. Calcd for [Au_2Ni(*trans*-dppee)(D-pen)]·9H_2O = $C_{36}H_{54}N_2Au_2NiO_{11}P_2S_2$: C, 34.06; H, 4.29; N, 2.21%. Found: C, 33.98; H, 4.24; N, 2.27%. IR spectrum (cm^{-1}, KBr disk): 1598 (ν_{CO}) and 744-691 (ν_{Ph}).

Reaction E

Crystals of [**3**](ClO_4)$_2$ (5 mg) were soaked in an aqueous solution of NH_3 (0.1 M, 12.5mL) and were subsequently allowed to stand at room temperature overnight. The purple crystals were collected via filtration and washed with water. Anal. Calcd for [Au_4Co_2(*trans*-dppee)$_2$(D-pen)$_4$](ClO_4)$_2$·9H_2O = $C_{72}H_{98}N_4Au_4Cl_2Co_2O_{25}P_4S_4$: C, 32.65; H, 3.73; N, 2.12%. Found: C, 32.74; H, 3.93; N, 2.20%. IR spectrum (cm^{-1}, KBr disk): 1646 (ν_{CO}), 1102 (ν_{ClO4}), 747-691 (ν_{Ph}), and 625 (ν_{ClO4}).

III-2-2-5. Treatment of Acidic Crystals with Basic Gas.

Reaction A

Freshly prepared crystals of [**7**]·2$HClO_4$ (5 mg) were allowed to be kept with 4 mL of concentrated aqueous solution of ammonia and 3 g of magnesium sulfate for absorbing excess moisture in a vial at room temperature. The green crystals were collected after standing for a week. Anal. Calcd for [Au_4Ni_2(*trans*-dppee)$_2$(D-pen)$_4$]·2NH_4ClO_4·5H_2O = $C_{72}H_{98}N_6Au_4Ni_2O_{21}P_4S_4Cl_2$: C, 33.11; H, 3.78; N, 3.22%. Found: C, 33.20; H, 3.94; N, 3.18%. IR spectrum (cm^{-1}, KBr disk): 1593 (ν_{CO}), 1100 (ν_{ClO4}), 743-690 (ν_{Ph}), and 625 (ν_{ClO4}).

Reaction B

Freshly prepared crystals of [**7**]·4/3HNO_3 (5 mg) were allowed to be kept with 4 mL of concentrated aqueous solution of ammonia and 3 g of magnesium sulfate for absorbing excess moisture in a vial at room temperature. The green crystals were collected after standing for a week. Anal. Calcd for [Au_4Ni_2(*trans*-dppee)$_2$(D-pen)$_4$] ·4/3NH_4NO_3·H_2O =

$C_{72}H_{87.33}N_{6.67}Au_4Ni_2O_{13}P_4S_4$: C, 35.86; H, 3.65; N, 3.87%. Found: C, 35.98; H, 3.82; N, 3.74%. IR spectrum (cm^{-1}, KBr disk): 1588 (ν_{CO}), 1385 (ν_{NO3}), and 746-692 (ν_{Ph}).

Reaction C

Freshly prepared crystals of [**8**]·$2HClO_4$ (5 mg) were allowed to be kept with 4 mL of concentrated aqueous solution of ammonia and 3 g of magnesium sulfate for absorbing excess moisture in a vial at room temperature. The green crystals were collected after standing for a week. Anal. Calcd for $[Au_4Ni_2(dppe)_2(D\text{-pen})_4]\cdot 2NH_4ClO_4\cdot 4H_2O$ = $C_{72}H_{100}N_6Au_4Ni_2O_{20}P_4S_4Cl_2$: C, 33.29; H, 3.88; N, 3.23%. Found: C, 33.24; H, 4.05; N, 3.13%. IR spectrum (cm^{-1}, KBr disk): 1577 (ν_{CO}), 1105(ν_{ClO4}), 732-692 (ν_{Ph}), and 625 (ν_{ClO4}).

III-2-2-7. Treatment of Neutralized Crystals with Acidic Solution.

Freshly prepared crystals of [**7**]·$2NH_4ClO_4$ (2 mg) were soaked in an aqueous solution of $HClO_4$ (0.01 M, 5 mL) and was subsequently allowed to stand at room temperature overnight. The green crystals were collected via filtration and washed with water. Anal. Calcd for $[Au_4Ni_2(\textit{trans}\text{-dppee})_2(D\text{-pen})_4]\cdot 2HClO_4\cdot 6H_2O$ = $C_{72}H_{94}Au_4Cl_2N_4Ni_2O_{22}P_4S_4$: C, 33.31; H, 3.65; N, 2.16%. Found: C, 33.13; H, 3.81; N, 2.38%. IR spectrum (cm^{-1}, KBr disk): 1716 (shoulder, ν_{CO}), 1590 (ν_{CO}), 1103 (ν_{ClO4}), 746-691 (ν_{Ph}), and 624 (ν_{ClO4}).

III-2-2-4. [Au_4Ni_2(*trans*-dppee)$_2$(D-pen)$_2$(L-pen)$_2$] ([10]).

To a white suspension containing 0.050 g (0.045 mmol) of DL-H_2[**2**] in EtOH (2.5 mL) and water (2.5 mL) was added 0.013 g (0.050 mmol) of $Ni(OAc)_2\cdot 4H_2O$, which was stirred at room temperature for 30 min to give a green solution. Green crystals of [**10**] were obtained by slow evaporation at room temperature for 1 week, which were collected by filtration and washed with water and EtOH. Yield: 0.020 g (38%). Anal. Calcd for $[Au_4Ni_2(\textit{trans}\text{-dppee})_2(D\text{-pen})_2(L\text{-pen})_2]\cdot 14H_2O$ = $C_{72}H_{108}N_4Au_4Ni_2O_{22}P_4S_4$: C, 34.06; H, 4.29; N, 2.21%. Found: C, 33.86; H, 4.01; N, 2.10%. IR spectrum (cm^{-1}, KBr disk): 1599 (ν_{CO}) and 746-693 (ν_{Ph}).

III-2-3. Physical Measurements.

The elemental analyses (C/H/N) were performed at Osaka University using a YANACO CHN Coda MT-5 and MT-6 analyzers. The elemental analyses (Cl) were

performed at Kyoto University. The IR spectra were recorded on a JASCO FT/IR-4100 infrared spectrometer with a KBr disk at room temperature. Diffuse reflection spectra were recorded on a JASCO V-570 spectrometer, and the solid CD spectra were recorded on a JASCO J-840 or a JASCO J-820 spectropolarimeter at room temperature. The X-ray fluorescence spectrometries were performed on HORIBA MESA-500 spectrometer or SHIMADZU EDX-720. Normal-quality powder X-ray diffraction patterns were recorded on Bruker D2-PHASER X-ray diffractometer system at room temperature in reflection mode [Cu Kα (λ = 1.5418 Å); 2θ range = 0−60°; step width = 0.01°; data collection time = 0.5 h]. High-quality powder X-ray diffraction patterns were recorded at room temperature in transmission mode [synchrotron radiation, λ = 0.999115(18) Å; 2θ range = 0–78°; step width = 0.01°; data collection time = 5 min for [**9**] and 3 min for [**7**]·2$HClO_4$ or [**7**]·2NH_4ClO_4] with a diffractometer equipped with a white imaging plate detector at the SPring-8 BL02B2 beamline; these experiments were conducted with the approval of the Japan Synchrotron Radiation Research Institute (JASRI). The crystals were placed into 0.3 mm glass capillary tubes, which were rotated during the measurements. The diffraction patterns were collected with a large Debye-Scherrer camera. The powder simulation patterns were generated from the single-crystal X-ray structures using the Mercury 3.5.1 program.

III-2-4 X-ray Structural Determination.

The single-crystal X-ray diffraction measurements for [**7**]·2$HClO_4$, [**7**]·4/3HNO_3, [**8**]·2$HClO_4$, [**7**]·2NH_4ClO_4, and [**7**]·4/3NH_4NO_3 were performed at 100 K with a Rigaku Mercury 2 CCD detector with synchrotron radiation (λ =0.7000 Å) at the BL02B1 beamline in "SPring-8," with the approval of the Japan Synchrotron Radiation Research Institute (JASRI). The single-crystal X-ray diffraction measurements for [**9**] and [**8**]·2NH_4ClO_4 were performed at 100 K with an ADSC Q210 CCD area detector with synchrotron radiation (λ =0.7000 Å for [**9**] and λ =0.6300 Å for [**8**]·2NH_4ClO_4) at the 2D beamline at the Pohang Accelerator Laboratory (PAL). The intensity data was processed using the HKL3000 program.

The collected diffraction data was processed with the Rapid Auto software program. The structures of the complexes were solved via direct methods using the SHELXS2014 program.[21] The structure refinements were carried out using full-matrix least-squares (SHELXL2014).[21] All calculations were performed using the Yadokari-XG software package.

For [**7**]·2$HClO_4$, a half of [$Au^{I}_4Ni^{II}_2$(*trans*-dppee)$_2$(D-pen)$_4$] units, water, oxonium cations, and four disordered ClO_4^- molecules were crystallographically independent. One

phenyl ring was disordered. Three of the phenyl rings, one vinylene linker and perchlorate anions were fixed. All non-hydrogen atoms except the C atoms of the disordered region and O atoms of 2 water molecules were refined anisotropically. Hydrogen atoms were included in calculated positions except those of water molecules, oxonium cations, and one vinylene linker.

For [**7**]·4/3HNO_3, a half of [$Au^{I}_4Ni^{II}_2$(*trans*-dppee)$_2$(D-pen)$_4$] units, water, and three NO_3^- molecules were crystallographically independent. One phenyl ring was disordered. Three of the phenyl rings, one vinylene linker, nitrate anions, and water molecules were fixed. All non-hydrogen atoms except the C atoms of the disordered region and a vinylene linker unit, N and O atoms of nitrate anions were refined anisotropically. Hydrogen atoms were included in calculated positions except those of water molecules, oxonium cations, and one vinylene linker.

For [**8**]·2$HClO_4$, a half of [$Au^{I}_4Ni^{II}_2$(dppe)$_2$(D-pen)$_4$] units, water, oxonium, and four disordered ClO_4^- molecules were crystallographically independent. All of the anions were fixed. All non-hydrogen atoms except the Cl atoms of perchlorate molecules and O atoms of perchlorate and water molecules were refined anisotropically. Hydrogen atoms were included in calculated positions except those of water molecules and oxonium cations.

For [**7**]·2NH_4ClO_4 in section III-2-2-5, a half of [$Au^{I}_4Ni^{II}_2$(*trans*-dppee)$_2$(D-pen)$_4$] units, 2 ammonium cations, water, and four disordered ClO_4^- molecules were crystallographically independent. One phenyl ring was disordered. Three of the phenyl rings, one vinylene linker and perchlorate anions were fixed. All non-hydrogen atoms except the C atoms of the disordered region N atoms of ammonium cations, and O atoms of water molecules were refined anisotropically. Hydrogen atoms were included in calculated positions except those of water molecules, ammonium cations, and one vinylene linker.

For [**7**]·4/3NH_4NO_3, a half of [$Au^{I}_4Ni^{II}_2$(*trans*-dppee)$_2$(D-pen)$_4$] units, 2 ammonium cations, water, and three disordered NO_3^- molecules were crystallographically independent. One phenyl ring was disordered. The disordered phenyl ring, one vinylene linker, and perchlorate anions were fixed. All non-hydrogen atoms except the C atoms of the disordered region and a vinylene linker, N and O atoms of 2 of the nitrate molecules were refined anisotropically. Hydrogen atoms were included in calculated positions except those of water molecules and ammonium cations.

For [**8**]·2NH_4ClO_4, a half of [$Au^{I}_4Ni^{II}_2$(dppe)$_2$(D-pen)$_4$] units, 2 ammonium cations, water, and four disordered ClO_4^- molecules were crystallographically independent. One of the perchlorate anion was so highly disordered that the thermal ellipsoid was much higher than other perchlorate anions. All of the anions were fixed. All non-hydrogen

atoms except the Cl atoms of perchlorate molecules, N atoms of ammonium cations, and O atoms of perchlorate and water molecules were refined anisotropically. Hydrogen atoms were included in calculated positions except those of water molecules and ammonium cations.

For [**7**]·2$HClO_4$ reverted from [**7**]·2NH_4ClO_4 in section III-2-2-7, a half of [$Au^{I}_4Ni^{II}_2$(*trans*-dppee)$_2$(D-pen)$_4$] units, water, oxonium cations, and four disordered ClO_4^- molecules were crystallographically independent. One of the perchlorate anion was so highly disordered to find all of the oxygen atoms on it. All of the phenyl rings and the perchlorate anions were fixed. All non-hydrogen atoms except the C atoms of the disordered region, Cl and O atoms of the two perchlorate anions and O atoms of water molecules were refined anisotropically. Hydrogen atoms were included in calculated positions except those of water molecules and oxonium cations.

For [**9**], 3 of [$Au^{I}_2Ni^{II}$(*trans*-dppee)(D-pen)$_2$] units, water, and eleven MeOH molecules were crystallographically independent. 3 of phenyl rings and all of MeOH molecules were fixed. All non-hydrogen atoms except the C atoms and O atoms of the solvent molecules were refined anisotropically. Hydrogen atoms were included in calculated positions except those of solvent molecules.

For [**10**], one [$Au^{I}_4Ni^{II}_2$(*trans*-dppee)$_2$(D-pen)$_2$(L-pen)$_2$] units, water, and two EtOH molecules were crystallographically independent. All non-hydrogen atoms except the O atoms of water molecules were refined anisotropically. Hydrogen atoms were included in calculated positions except those of water molecules.

III-3. Results and Discussion.

III-3-1. Synthesis and Characterization of [Au_4Ni_2(*trans*-dppee)$_2$(D-pen)$_4$]·HX (HX = $2HClO_4$ or $4/3HNO_3$).

Reaction of multidentate metalloligand D-H_2[**2**] with $Ni(ClO_4)_2·4H_2O$ in a 1:1 ratio in MeOH at room temperature gave a yellow solution. The addition of a diluted NH_3 aqueous solution to it led to the color change from yellowish green to green, from which trigonal-pyramidal green crystals ([**7**]·$2HClO_4$) were isolated (Scheme 3-2). X-ray fluorescence spectroscopy indicated the presence of Au, Ni, and Cl atoms in [**7**]·$2HClO_4$, and its elemental analytical data was in agreement with a formula consisting of [Au_2(*trans*-dppee)(D-pen)$_2$]$^{2-}$ (D-[**2**]$^{2-}$) , Ni^{2+}, and $HClO_4$ in a 2:2:1 ratio. The IR spectrum showed the presence of D-pen and *trans*-dppee ligands based on the bands of COO^- and P–Ph groups at 1591 and 746-691 cm^{-1}, respectively, and also showed the presence of ClO_4^- based on the bands at 1101 and 623 cm^{-1} (Figure 3-1). Notably, a small shoulder at ca. 1718 cm^{-1} was observed, and this was assigned as the band for protonated carboxylate group. This was explained by the strong hydrogen bond between carboxylate groups and oxonium cations inside the crystal as discussed below.

When $Ni(NO_3)_2·6H_2O$ was used instead of $Ni(ClO_4)_2·4H_2O$, trigonal-pyramidal green crystals ([**7**]·$4/3HNO_3$) were produced (Scheme 3-2). For [**7**]·$4/3HNO_3$ the X-ray fluorescence spectroscopy indicated the presence of Au and Ni, and its elemental analytical data was in agreement with a formula consisting of [Au_2(*trans*-dppee) (D-pen)$_2$]$^{2-}$ (D-[**2**]$^{2-}$) , Ni^{2+}, and HNO_3 in a 2:2:4/3 ratio. In the IR spectrum, a C=O stretching band for deprotonated carboxylate groups of D-pen at 1591 cm^{-1}, an N–O stretching band for nitrate anion at 1385 cm^{-1}, and P–Ph stretching bands at 746-691 cm^{-1} were observed (Figure 3-1). The shoulder for protonated carboxylate groups was also detected at 1727 cm^{-1} as well as [**7**]·$2HClO_4$.

Single-crystal X-ray analysis revealed that [**7**] was a hexanuclear neutral complex, [$Au^I_4Ni^{II}_2$(*trans*-dppee)$_2$(D-pen)$_4$], in which two [Au^I_2(*trans*-dppee)(D-pen)$_2$]$^{2-}$ moieties were bridged by two Ni^{II} centers. The supramolecular structure resembles to that of [**3**]$^{2+}$ salts and the inorganic anion clusters (NO_3^- or ClO_4^-) were found, and considering the charge compensation, oxonium cations also supposed to be incorporated into the flame. The anions and the oxonium cations mediate the hydrogen bonds between the hexanuclear molecules and work as a template (*vide infra*). These complexes were almost insoluble to common solvents, and the spectral measurements in solution could not be performed. Diffuse reflection spectra of [**7**]·$2HClO_4$ and [**7**]·$4/3HNO_3$ in the solid state in the region of 1200-400 nm showed two bands assignable to $^3T_{2g}\leftarrow{}^3A_{2g}$ and $^3T_{1g}\leftarrow{}^3A_{2g}$ transitions for the octahedral Ni^{II} center at 1021 and 595 nm for [**7**]·$2HClO_4$, 1049 and 598 nm for

[**7**]·4/3HNO_3, respectively (Figures 3-2 and 3-3), which were similar to those observed for [$Au^I_4Ni^{II}_2$(dppe)$_2$(D-pen)$_4$] in previous papers showing the bands at 1034 and 601 nm (Figure 3-4).[9] Solid state CD spectrum of [**7**]·2$HClO_4$ in the region of 850-400 nm showed a positive band at 679 nm and a negative band at 580 nm, which were also similar to those of the dppe analogous compound showing positive and negative bands at 627 and 554 nm, respectively (Figure 3-5). In the syntheses for [**7**]·2$HClO_4$ and [**7**]·4/3HNO_3, the aqueous NH_3 was used as a base for deprotonating the carboxyl groups in the metalloligand to form a hexa-coordinated Ni species, and after the deprotonation, NH_3 was gradually volatilized into the atmosphere by standing the solution for a long time. This volatilization was probably the reason why the crystals did not contain ammonia and/or ammonium cations, and makes pH value suitable for both the incorporation of perchlorate acid molecules and keeping the carboxylate groups deprotonated. The powder X-ray diffraction patterns matched the patterns that were simulated from the crystal structures determined by SC-XRD results well, and denoted the samples' purity in terms of crystallography (Figures 3-6, 3-7).

Many attempts to obtain single crystals of the complex by the similar crystallization condition as [$Au^I_4Ni^{II}_2$(dppe)$_2$(D-pen)$_4$] afforded only crystalline powder, probably because of the lower solubility of the complex caused by the rigidness of *trans*-dppee unit.

III-3-2. Synthesis and Characterization of [Au_4Ni_2(dppe)$_2$(D-pen)$_4$]·2$HClO_4$ ([8]·2$HClO_4$).

Reaction of multidentate metalloligand with dppe linker unit, [Au_2(dppe)(D-Hpen)$_2$], with $Ni(ClO_4)_2$·6H_2O in a 1:1 ratio in MeOH at room temperature gave a yellow solution. The addition of a diluted NH_3 aqueous solution to it led to the color change from yellow to green, from which trigonal-pyramidal green crystals ([**8**]·2$HClO_4$) were isolated (Scheme 3-3). X-ray fluorescence spectroscopy indicated the presence of Au and Ni atoms in [**8**]·2$HClO_4$. In the IR spectrum, a C=O stretching band for deprotonated carboxylate groups of D-pen at 1590 cm^{-1}, Cl–O stretching bands for perchlorate anion at 1105 and 624 cm^{-1}, and P–Ph stretching bands at 733-691 cm^{-1} were observed (Figure 3-8). Single-crystal X-ray analysis revealed that [**8**] was a hexanuclear neutral complex, [$Au^I_4Ni^{II}_2$(dppe)$_2$(D-pen)$_4$], in which two [Au^I_2(dppe)(D-pen)$_2$]$^{2-}$ moieties were bridged by two Ni^{II} centers, and the perchlorate anions existed in their interstice (*vide infra*). This complex was almost insoluble to common solvents, and the spectral measurements in solution could not be performed. Diffuse reflection spectra of [**8**]·2$HClO_4$ in the region of 1200-400 nm in the solid state showed two bands assignable to $^3T_{2g}\leftarrow{}^3A_{2g}$ and $^3T_{1g}\leftarrow{}^3A_{2g}$ transitions for the octahedral Ni^{II} center at 1035 and 594 nm (Figure 3-8), which were similar to those observed for [$Au^I_4Ni^{II}_2$(dppe)$_2$(D-pen)$_4$] without

incorporation of acid showing the bands at 1034 and 601 nm (Figure 3-9). Solid state CD spectrum of [**7**]·2$HClO_4$ in the region of 850-400 nm showed a positive band at 658 nm and a negative band at 567 nm, which were also similar to those of the analogous crystal without incorporation of acid showing positive and negative bands at 627 and 554 nm, respectively (Figure 3-10). The powder X-ray diffraction pattern matched with the patterns simulated from the single-crystal X-ray structures well, and denoted the sample's purity in terms of crystallography (Figure 3-11).

III-3-3. Synthesis and Characterization of [Au_2Ni(*trans*-dppee)(D-pen)$_2$]$_\infty$ ([9]).

Reaction of multidentate metalloligand D$_2$-H_2[**2**] with $Ni(OAc)_2 \cdot 4H_2O$ in a 1:1 ratio in MeOH at room temperature gave a green solution. Green crystals with a plate-like shape ([**9**]) were isolated from the reaction solution, after the diffusion of acetonitrile (Scheme 3-2). X-ray fluorescence spectroscopy indicated the presence of Au and Ni atoms in [**9**], and its elemental analytical data was in agreement with a formula consisting of [Au_2(*trans*-dppee)(D-pen)$_2$]$^{2-}$ (D$_2$-[**2**]$^{2-}$) , Ni^{2+} in a 1:1 ratio. In the IR spectrum, a C=O stretching band for deprotonated carboxylate groups of D-pen at 1593 cm^{-1}, and P–Ph stretching bands at 745-691 cm^{-1} were observed (Figure 3-12).

Single-crystal X-ray analysis revealed that [**9**] was an infinite neutral chain complex, [$Au^{I}_2Ni^{II}$(*trans*-dppee)(D-pen)$_2$]$_\infty$, in which [Au^{I}_2(*trans*-dppee)(D-pen)$_2$]$^{2-}$ moieties and Ni^{II} centers arranged alternately, and the solvent molecules were found in the crystal (*vide infra*). This complex was almost insoluble to common solvents, and the spectral measurements in solution could not be performed. Diffuse reflection spectrum in the region of 1200-400 nm in the solid state showed two bands assignable to $^3T_{2g} \leftarrow {}^3A_{2g}$ and $^3T_{1g} \leftarrow {}^3A_{2g}$ transitions for the octahedral Ni^{II} center at 1025 and 599 nm, which were similar to those observed for [$Au^{I}_4Ni^{II}_2$(dppe)$_2$(D-pen)$_4$] (Figure 3-13). Solid state CD spectrum in the region of 850-400 nm showed a positive band at 688 nm and a negative band at 591 nm (Figures 3-10, 3-14), which were also similar to these for [$Au^{I}_4Ni^{II}_2$(dppe)$_2$(D-pen)$_4$]. The powder X-ray diffraction pattern matched with the patterns simulated from the single-crystal X-ray structures well, and no contamination of the crystalline phase that was isostructural to [**7**]·2$HClO_4$ was observed (Figure 3-15).

III-3-4. Synthesis and Characterization of [Au_4Ni_2(*trans*-dppee)$_2$(D-pen)$_4$]·NH_4X ([7]·NH_4X, NH_4X = 2NH_4ClO_4 or 4/3NH_4NO_3).

To investigate whether [**7**]·2$HClO_4$ exhibits absorption capability with respect to base molecules, green single crystals of [**7**]·2$HClO_4$ were soaked in a 0.1 M aqueous solution of NH_3 overnight to give the crystals of [**7**]·2NH_4ClO_4 (Scheme 3-4). The shapes of the

crystals remained unchanged, and the PXRD pattern of the crystals after this treatment was essentially the same as those of [**7**]·2$HClO_4$ (Figure 3-6). X-ray fluorescence spectroscopy indicated the presence of Au, Ni, and Cl atoms in [**7**]·2NH_4ClO_4, and its elemental analytical data was in agreement with a formula consisting of [Au_2(*trans*-dppee)(D-pen)$_2$]$^{2-}$ (D$_2$-[**2**]$^{2-}$) , Ni^{2+}, NH_4^+, and ClO_4^- in a 2:2:1:1 ratio. However, the elemental analysis data showed that the observed weight % of nitrogen was smaller than the calculated value by 0.31%. This result was explained by the release of a small amount of the incorporated ammonia in [**7**]·2NH_4ClO_4 during the filtration and washing with water. Indeed, the elemental analysis data of [**7**]·2NH_4ClO_4 which was exposed to the ammonia gas was good agreement with the hexahydrate form due to the avoidance of the release of ammonia during the above processes (*vide infra*). The IR spectrum showed the presence of D-pen and *trans*-dppee ligands based on the bands of COO^- and P–Ph group at 1591 and 746-691 cm^{-1}, respectively, and also showed the presence of ClO_4^- based on the bands at 1101 and 623 cm^{-1} but no shoulder for C=O stretching as observed in the spectrum of [**7**]·2$HClO_4$ (Figure 3-1). Diffuse reflection spectra of [**7**]·2NH_4ClO_4 in the region of 1200-400 nm in the solid state showed two bands assignable to $^3T_{2g}\leftarrow{}^3A_{2g}$ and $^3T_{1g}\leftarrow{}^3A_{2g}$ transitions for the octahedral Ni^{II} center at 1037 and 599 nm (Figure 3-16), which were similar to those observed for [**7**]·2$HClO_4$ showing the bands at 1035 and 594 nm (Figure 3-2). Solid state CD spectrum of [**7**]·2NH_4ClO_4 in the region of 850-400 nm showed a positive band at 646 nm and a negative band at 557 nm (Figure 3-17), which were also similar to those of [**7**]·2$HClO_4$ showing positive and negative bands at 658 and 567 nm, respectively. These similarities indicated the maintenance of the molecular conformation. By single-crystal X-ray analysis, the single-crystal-to-single-crystal (SCSC) incorporation of ammonia into [**7**]·2$HClO_4$ was confirmed (*vide infra*).

Standing the crystals of [**7**]·4/3HNO_3 in ammonia atmosphere for a week led to the incorporation of ammonia into the crystal lattice. X-ray fluorescence spectroscopy indicated the presence of Au, and Ni atoms in [**7**]·4/3NH_4NO_3, and its elemental analytical data was in agreement with a formula consisting of [Au_2(*trans*-dppee)(D-pen)$_2$]$^{2-}$ (D$_2$-[**2**]$^{2-}$) , Ni^{2+}, NH_4^+, and NO_3^- in a 2:2:4/3:4/3 ratio. The IR spectrum showed the presence of D-pen and *trans*-dppee ligands based on the bands of COO^- and P–Ph group at 1588 and 746-692 cm^{-1}, respectively, and also showed the presence of NO_3^- based on the band at 1385 cm^{-1} but no band for C=O stretching shoulder observed in the spectrum of [**7**]·4/3HNO_3 (Figure 3-1). Its powder X-ray diffraction pattern (Figure 3-7c) and the result of single crystal X-ray diffraction experiment indicated that the ammonia molecules were incorporated into the crystals in a SCSC manner (*vide infra*).

III-3-5. Synthesis and Characterization of [Au_4Ni_2(dppe)$_2$(D-pen)$_4$]·2NH_4ClO_4 ([**8**]·

2NH_4ClO_4).

Standing the crystals of [**8**]·2$HClO_4$ in ammonia atmosphere for a week led to the incorporation of ammonia into the crystal lattice. X-ray fluorescence spectroscopy indicated the presence of Au, Ni, and Cl atoms in [**8**]·2NH_4ClO_4, and its elemental analytical data was in agreement with a formula consisting of [Au_2(*trans*-dppee)(D-pen)$_2$]$^{2-}$ (D_2-[**2**]$^{2-}$) , Ni^{2+}, NH_4^+, and ClO_4^- in a 2:2:1:1 ratio. The IR spectrum showed the presence of D-pen and *trans*-dppee ligands based on the bands of COO^- and P–Ph group at 1577 and 732-692 cm^{-1}, respectively, and also showed the presence of ClO_4^- based on the bands at 1105 and 625 cm^{-1} (Figure 3-8). Its powder X-ray diffraction pattern indicated the retention of crystallinity after the ammonia molecules were incorporated into the crystals (Figure 3-11, *vide infra*).

III-3-6. Reverse Ammonia Desorption Reaction for [Au_4Ni_2(*trans*-dppee)$_2$(D-pen)$_4$]·2NH_4ClO_4

Immersing [**7**]·2NH_4ClO_4 crystals into an aqueous solution of $HClO_4$ (0.01 M) overnight led to the desorption of ammonia and reverted [**7**]·2$HClO_4$ crystals were obtained in a SCSC manner (Scheme 3-4). X-ray fluorescence spectroscopy indicated the presence of Au, Ni, and Cl atoms in reverted [**7**]·2$HClO_4$, and its elemental analytical data was in agreement with a formula consisting of [Au_2(*trans*-dppee)(D-pen)$_2$]$^{2-}$ (D_2-[**2**]$^{2-}$) , Ni^{2+}, and $HClO_4$ in a 2:2:1 ratio. The IR spectrum showed the presence of D-pen and *trans*-dppee ligands based on the bands of COO^- and P–Ph group at 1590 and 746-691 cm^{-1}, respectively, and also showed the presence of ClO_4^- based on the bands at 1103 and 624 cm^{-1} (Figure 3-1). A small shoulder at ca. 1716 cm^{-1} re-appeared after the treatment and this could be assigned as the band for protonated carboxylate group as in the initial [**7**]·2$HClO_4$. Its powder X-ray diffraction pattern was essentially same as that of initial [**7**]·2$HClO_4$ (Figure 3-6e). The single crystal X-ray analysis was also carried out, and some features in the crystal structure specific for [**7**]·2$HClO_4$ were also found through the data was not good enough (*vide infra*) .

III-3-7. Synthesis and Characterization of [Au_4Ni_2(*trans*-dppee)$_2$(D-pen)$_2$(L-pen)$_2$] ([10]).

Reaction of a racemic mixture of metalloligands, D_2-H_2[**2**] and L_2-H_2[**2**], with Ni(OAc)$_2$·4H_2O in a 1:1 ratio in EtOH/water (1:1) at room temperature gave a green solution, from which green crystals with a block shape ([**10**]) were isolated by standing for a week (Scheme 3-5). X-ray fluorescence spectroscopy indicated the presence of Au and Ni atoms in [**10**], and its elemental analytical data was in agreement with a formula

consisting of $[Au_2(\textit{trans}\text{-dppee})(pen)_2]^{2-}$ ($[\mathbf{2}]^{2-}$) and Ni^{2+} in a 1:1 ratio. In the IR spectrum, a C=O stretching band for deprotonated carboxylate groups of pen at 1599 cm^{-1}, and P–Ph stretching bands at 746-693 cm^{-1} were observed (Figure 3-18). Diffuse reflection spectrum in the region of 1200-400 nm in the solid state showed two bands assignable to $^3T_{2g}\leftarrow{}^3A_{2g}$ and $^3T_{1g}\leftarrow{}^3A_{2g}$ transitions for the octahedral Ni^{II} center at 1060 and 601 nm (Figure 3-19), which were similar to those observed for the homochiral compounds. Solid state CD spectrum in the region of 850-400 nm was silent, indicating that [**10**] was a meso complex or a racemic mixture of two enantiomers (Figure 3-20). Single-crystal X-ray analysis revealed that [**10**] was a hexanuclear neutral complex, $[Au^I_4Ni^{II}_2(\textit{trans}\text{-dppee})_2(\text{D-pen})_2(\text{L-pen})_2]$, in which two $[Au^I_2(\textit{trans}\text{-dppee})(\text{D-pen})(\text{L-pen})]^{2-}$ moieties were bridged by two Ni^{II} centers (*vide infra*). This complex was almost insoluble to common solvents, and the spectral measurements in solution could not be performed.

III-3-8. Crystal Structures of $[Au_4Ni_2(\textit{trans}\text{-dppee})_2(\text{D-pen})_4]\cdot HX$ ([**7**]·HX, HX = $2HClO_4$ or $4/3HNO_3$).

The crystal structure of [**7**]·$2HClO_4$ was determined by single-crystal X-ray crystallography using synchrotron-radiation X-ray. Molecular and packing structures are shown in Figures 3-21, 3-22, 3-23, 3-24, 3-25, and 3-26. The crystallographic data are summarized in Table 3-1, and the selected bond distances and angles are listed in Table 3-2. Crystal [**7**]·$2HClO_4$ contained a half of $[Au_4Ni_2(\textit{trans}\text{-dppee})_2(\text{D-pen})_4]$ unit, 4 ClO_4^- ions with an occupancy of 1/2, 1/3, 1/12, and 1/12, respectively, and 14/3 solvated water molecules in the asymmetric unit. As shown in Figure 3-22, the neutral complex molecule had an S-bridged $Au^I_4Ni^{II}_2$ hexanuclear structure consisting of two $[Au_2(\textit{trans}\text{-dppee})(\text{D-pen})_2]^{2-}$ metalloligands that linked two Ni^{II} atoms to form a twisted 18-membered ring structure composed of Au, Ni, S, P, and C atoms like the cationic homochiral $Au^I_4Co^{III}_2$ complexes described in Chapter II. The coordination geometry of each Au^I atoms was nearly linear bound with P and S atoms (Av. Au–S = 2.31 Å, Au–P = 2.25 Å, P–Au–S = 178.4°). The two D_2-$[\mathbf{2}]^{2-}$ metalloligands each bound to two Ni^{II} atoms in a bis(tridentate-*N,O,S*) mode such that each Ni^{II} atoms was in a *cis*(*N*)*trans*(*O*)*cis*(*S*)-$N_2O_2S_2$ octahedral environment (Av. Ni–S = 2.45 Å, Ni–O = 2.06 Å, Ni–N = 2.08 Å, S–Ni–S = 100.6°, O–Ni–O = 174.9°, N–Ni–N = 96.5°) (Figure 3-23a, b). All S atoms adopted an *R* configuration. The $Au^I_4Ni^{II}_2$ hexanuclear structure in [**7**]·$2HClO_4$ was very similar to that found in previously reported $[Au_4Ni_2(dppe)_2(\text{D-pen})_4]$ crystal incorporating no inorganic acid (intramolecular Ni···Ni = 11.263(3) Å for [**7**]·$2HClO_4$, 11.38 Å for $[Au_4Ni_2(dppe)_2(\text{D-pen})_4]$, Figure 3-4). [6,9] However, the aggregation mode of the $Au^I_4Ni^{II}_2$ hexanuclear molecules in [**7**]·$2HClO_4$ differed substantially from that in $[Au_4Ni_2(dppe)_2(\text{D-pen})_4]$.

That was, the hexanuclear molecules in [**7**]·2$HClO_4$ were self-assembled into a supramolecular octahedron of {[$Au^I_4Ni^{II}_2$]}$_6$ through 24 CH···π (C···Ph = 3.43 Å and 4.46 Å) and 12 NH_2···OCO (N···O = 2.99 Å) hydrogen-bonding interactions, accommodating a ClO_4^- ion in the center (Figure 3-24a), whereas the $Au^I_4Ni^{II}_2$ hexanuclear molecules in [Au_4Ni_2(dppe)$_2$(D-pen)$_4$] were connected with another through intermolecular H_2N···OCO hydrogen bonds, thus forming a 1D chain (Figure 3-4b, c).[9] In [**7**]·2$HClO_4$, the supramolecular octahedra were closely packed in a face-centered cubic (fcc) structure by forming intercluster CH···π interactions (Figure 3-24c). A similar fcc structure composed of {[$Au^I_4Co^{III}_2$]$^{2+}$}$_6$ supramolecular octahedra has been found in inorganic salts of the cationic $Au^I_4Co^{III}_2$ complex, i.e., [Au_4Co_2(*trans*-dppee)$_2$(D-pen)$_4$]$^{2+}$ ([**3**]$^{2+}$) or [Au_4Co_2(dppe)$_2$(D-pen)$_4$]$^{2+}$.[6,7] The fcc structure involved a type of octahedral interstice and two types of larger tetrahedral interstices, with one being hydrophilic, surrounded by amine and carboxylate groups, and with the other being hydrophobic, surrounded by phenyl and methyl groups (Figures 3-25a 3-26a). In [**7**]·2$HClO_4$, each octahedral interstice, hydrophilic tetrahedral interstice, and hydrophobic tetrahedral interstice accommodated a ClO_4^- ion, ten ClO_4^- ions that formed an adamantane-like arrangement, and a number of water molecules that formed a large water cluster, respectively (Figures 3-25b, 3-26b).

A detailed inspection of the structure of [**7**]·2$HClO_4$ revealed the presence of oxygen atoms on each of the four trigonal faces of the {[$Au^I_4Ni^{II}_2$]}$_6$ octahedron, forming strong hydrogen bonds (O···O = 2.69 Å) with three D-pen carboxylate groups from three different $Au^I_4Ni^{II}_2$ complex molecules (Figure 3-27a). Because of the strong hydrogen bond, each carboxylate group had asymmetric C–O bonds (1.23 Å, 1.27 Å), consistently with the IR spectral features. Moreover, four oxygen atoms were found inside each {ClO_4^-}$_{10}$ adamantane (Figure 3-28 b), each of which was hydrogen-bonded (O···O = 2.71 Å) with three oxygen atoms from three different ClO_4^- ions located at the octahedral site (site **A**) of the adamantane (Figure 3-28a), rather than from those located at its tetrahedral site (site **B**). The aforementioned oxygen atoms that formed hydrogen bonds with three adjacent O atoms were assumed to be protonated to form H_3O^+ ions. The existence of additional four protons was required to compensate for the negative charge of the ClO_4^- ions in [**7**]·2$HClO_4$. We speculate that these protons were involved in the water cluster. Although this crystal had similar crystal structure to that of [**3**](ClO_4)$_2$, closer look of the anion adamantane structure revealed that the ClO_4^- anions were more closely packed in the structure of [**7**]·2$HClO_4$ than that of [**3**](ClO_4)$_2$ (minimum Cl···Cl = 4.31 Å for [**7**]·2$HClO_4$, 4.50 Å for [**3**](ClO_4)$_2$), and this result might be related to the

presence of the oxonium in the $\{ClO_4^-\}_{10}$ adamantane that weaken the coulombic repulsion inside the anion aggregate.

The crystal structure of [**7**]·4/3HNO_3, obtained by the similar reaction using $Ni(NO_3)_2·6H_2O$ instead of $Ni(ClO_4)_2·6H_2O$, was similar to that of [**7**]·2HNO_3. Crystal [**7**]·4/3HNO_3 contained a half of [Au_4Ni_2(*trans*-dppee)$_2$(D-pen)$_4$] unit, three NO_3^- ions with an occupancy of 1/2, 1/12, and 1/12, and 31/6 solvated water molecules in the asymmetric unit. In [**7**]·4/3HNO_3, the $Au^I_4Ni^{II}_2$ hexanuclear structure, the hexameric octahedrally aggregated neutral structure, and the fcc packing structure similar to those of [**7**]·2$HClO_4$ were formed (Table 3-3, Figures 3-29a, b, d). However, the number of anions in the tetrahedral interstices was not 10 but 6, lacking anions in site **B**, which resulted in the different number of incorporated Brønsted acid per one complex molecule (Figure 3-29c). This result was explained by the hydrophobic nature of ClO_4^- anion. The hydrophobic methyl groups of D-pen moieties existed near site **B** in the tetrahedral interstices, which indicated the hydrophobicity of the site **B**, and we could suppose that nitrate anions were less stabilized than more hydrophobic perchlorate anions, therefore nitrate anions could not be accommodated in site **B**. As in the case of [**7**]·2$HClO_4$, there were oxygen atoms on the four trigonal faces of the $\{[Au^I_4Ni^{II}_2]\}_6$ octahedron, forming hydrogen bonds (O···O = 2.88 Å) with three D-pen carboxylate groups from three different $Au^I_4Ni^{II}_2$ complex molecules, and these oxygen atoms were assumed to be protonated to form H_3O^+ ions as [**7**]·2$HClO_4$. In the tetrahedral interstices, 8 oxygen atoms were found inside each $\{NO_3^-\}_6$ hexamer including these at site **B,** forming weak hydrogen bonding (O···O = 3.48 Å) with three oxygen atoms from three different NO_3^- ions located at the octahedral site. For compensating for the negative charge of the NO_3^- anions, other 4 protons were needed, and the possibility that some of these oxygen atoms inside the $\{NO_3^-\}_6$ hexamer were protonated for weakening the Coulombic repulsion between the nitrate anions was unneglectable.

III-3-9. Crystal Structure of [Au_4Ni_2(dppe)$_2$(D-pen)$_4$]·2$HClO_4$ ([**8**]·2$HClO_4$)

The crystal structure of [**8**]·2$HClO_4$, obtained by the similar reaction using [Au_2(dppe)(D-Hpen)$_2$] instead of D$_2$-H$_2$[**2**] was isomorphous with that of [**7**]·2$HClO_4$. Molecular and packing structures are shown in Figure 3-30. The crystallographic data are summarized in Table 3-1, and the selected bond distances and angles are listed in Table 3-4. Crystal [**8**]·2$HClO_4$ contained a half of [Au_4Ni_2(dppe)$_2$(D-pen)$_4$] unit, five disordered ClO_4^- ions with an occupancy of 1/2, 1/3, 1/12, and 1/12 and 8/3 solvated water molecules in the asymmetric unit. In [**8**]·2$HClO_4$, the $Au^I_4Ni^{II}_2$ hexanuclear structure, the hexameric octahedrally aggregated neutral structure, and the fcc packing structure similar to those

of [**7**]·2$HClO_4$ were found (Figures 3-30a, b, d). In the hydrophilic tetrahedral interstice, ten ClO_4^- ions were accommodated in an adamantane-like structure with the oxonium cations inside it like [**7**]·2$HClO_4$ ($H_3O^+\cdots O_{ClO4}$ = 2.76 Å, minimum Cl···Cl = 4.25 Å, O···O = 2.64 Å. Figure 3-30c). As described before, from the reaction of Ni^{II} and [Au_2(dppe)(D-Hpen)$_2$] without inorganic acid, crystals with same hexanuclear [Au_4Ni_2(dppe)$_2$(D-pen)$_4$] structure were already obtained by our group, while their aggregation was quite different from that of [**8**]·2$HClO_4$, and this fact supported the importance of the inorganic anions as a template for the face-centered-cubic supramolecular structures of [**7**].

III-3-10. Crystal Structure of [Au_2Ni(*trans*-dppee)(D-pen)$_2$]$_\infty$ ([9]).

The crystal structure of [**9**] was determined by single-crystal X-ray crystallography. Molecular and packing structures are shown in Figures 3-31, 3-32, 3-33, and 3-34. The crystallographic data are summarized in Table 3-5, and the selected bond distances and angles are listed in Table 3-6. Crystal [**9**] contained three of [Au_2Ni(*trans*-dppee)(D-pen)$_2$] unit, eleven solvated methanol molecules, and three solvated water molecules in the asymmetric unit. As shown in Figure 3-32, the complex had an S-bridged $Au^I_2Ni^{II}$ 1D chain structure, in which [Au_2(*trans*-dppee)(D-pen)$_2$]$^{2-}$ metalloligands and Ni^{II} atoms were arranged in an alternate manner. The coordination geometry of each Au^I atoms was nearly linear bound with P and S atoms (Av. Au–S = 2.30 Å, Au–P = 2.25 Å, P–Au–S = 175.3°, Au···Au = 3.26 Å). The two D$_2$-[**2**]$^{2-}$ metalloligands each bound to two Ni^{II} atoms in a bis(tridentate-*N*,*O*,*S*) mode such that each Ni^{II} atoms was in a *cis*(*N*)*trans*(*O*)*cis*(*S*)-$N_2O_2S_2$ octahedral environment (Av. Ni–S = 2.44 Å, Ni–O = 2.07 Å, Ni–N = 2.08 Å, S–Ni–S = 99.8°, O–Ni–O=172.7°, N–Ni–N = 98.4°) (Figure 3-33a, b). All S atoms adopted an *R* configuration. In the crystal structure, the $Au^I_2Ni^{II}$ infinite chains were connected to each other through the methanol and water mediated hydrogen bonding interactions to form a 3D network structure, accommodating solvate molecules between them (Figure 3-34). This infinite polymer structure in [**9**] containing open-bridged metalloligand was in sharp contrast to the charge-separated supramolecular structure in the crystal of [**7**]·HX, in which the metalloligands had closed-bridging mode, thus forming a discrete $Au^I_4Ni^{II}_2$ hexanuclear structure (Scheme 3-1).

III-3-11. Crystal Structures of [Au_4Ni_2(*trans*-dppee)$_2$(D-pen)$_4$]·NH_4X ([7]·NH_4X, NH_4X = 4/3NH_4NO_3 or 2NH_4ClO_4).

The crystal structure of [**7**]·2NH_4ClO_4 was determined by single-crystal X-ray crystallography using synchrotron-radiation X-ray. Molecular and packing structures are

shown in Figures 3-35. The crystallographic data are summarized in Table 3-1, and the selected bond distances and angles are listed in Table 3-7. Crystal [**7**]·2NH_4ClO_4 contained a half of [Au_4Ni_2(*trans*-dppee)$_2$(D-pen)$_4$] unit, four ClO_4^- ions with occupancy of 1/2, 1/3, 1/12, and 1/12, respectively, two ammonium cations with occupancy of 1/3 and 1/3, and 61/24 solvated water molecules in the asymmetric unit. The overall structure in [**7**]·2NH_4ClO_4 was very similar to that in [**7**]·2$HClO_4$, having an fcc structure comprising the $\{[Au^I_4Ni^{II}_2]\}_6$ supramolecular octahedra (Figure 3-35b, 3-35c). Moreover, the octahedral interstices, the hydrophilic tetrahedral interstices, and the hydrophobic tetrahedral interstices in [**7**]·2NH_4ClO_4 each accommodated one ClO_4^- ion, ten ClO_4^- ions with an adamantane-like arrangement, and a water cluster, respectively. However, in [**7**]·2NH_4ClO_4, the orientation of four ClO_4^- anions located at site **B** of the $\{ClO_4^-\}_{10}$ adamantane appeared to be opposite that in [**7**]·2$HClO_4$ (Figures 3-28a, 3-28c). Four nitrogen atoms inside the $\{ClO_4^-\}_{10}$ adamantane were also found as the oxygen atoms in the perchlorate cluster in the crystal structure of [**7**]·2$HClO_4$. However, each nitrogen was hydrogen-bonded not only with the ClO_4^- ions at site **A** (N···O = 2.95 Å) but also with those at site **B** (N···O = 2.77 Å) (Figures 3-28b, 3-28d). This structural feature was rationalized by the replacement of the H_3O^+ ions inside the $\{ClO_4^-\}_{10}$ adamantane with symmetrical NH_4^+ ions, which allowed for the formation of flexible hydrogen-bonding interactions with all of the surrounding ClO_4^- ions. A detailed structural comparison between [**7**]·2$HClO_4$ and [**7**]·2NH_4ClO_4 also revealed that the hydrogen-bond distances between the H_3O^+ ion and the three D-pen carboxylate groups in [**7**]·2$HClO_4$ (H_3O^+···O = 2.69 Å) were elongated in [**7**]·2NH_4ClO_4 (NH_4^+···O = 2.81 Å) (Figure 3-27). This elongation suggested that H_3O^+ was replaced with NH_4^+ given that N-H···O hydrogen bonds are commonly weaker than O-H···O bonds.[19] The disappearance of the C=O stretching shoulder in the IR spectrum of [**7**]·2NH_4ClO_4 was consistent with this possibility.

The crystal structure of [**7**]·4/3NH_4NO_3 was determined by single-crystal X-ray crystallography using synchrotron-radiation X-ray. Molecular and packing structures are shown in Figure 3-36. The crystallographic data are summarized in Table 3-1, and the selected bond distances and angles are listed in Table 3-8. Crystal [**7**]·4/3NH_4NO_3 contained a half of [Au_4Ni_2(*trans*-dppee)$_2$(D-pen)$_4$] unit, three NO_3^- ions with an occupancy of 1/2, 1/12, and 1/12, respectively, two ammonium cations with an occupancy of 1/3 and 1/3, and two solvated water molecules in the asymmetric unit. The overall structure in [**7**]·4/3NH_4NO_3 was also very similar to that in [**7**]·4/3HNO_3 (Figures 3-36a, b, d). However, in [**7**]·4/3NH_4NO_3, there was no anions at site **B** and the change of the orientation of anions located was not remarkable (Figure 3-36c), the same tendency was

found as [**7**]·2$HClO_4$ for the hydrogen bond distance and the hydrogen-bond distances between the H_3O^+ ion and the three D-pen carboxylate groups in [**7**]·4/3HNO_3 (O···O = 2.88 Å) were elongated in [**7**]·4/3NH_4NO_3 (N···O = 2.92 Å).

III-3-12. Crystal Structures of [Au_4Ni_2(dppe)$_2$(D-pen)$_4$]·2NH_4ClO_4 ([**8**]·2NH_4ClO_4).

The crystal structure of [**8**]·2NH_4ClO_4 was determined by single-crystal X-ray crystallography using synchrotron-radiation X-ray. Molecular and packing structures are shown in Figure 3-37. The crystallographic data are summarized in Table 3-1, and the selected bond distances and angles are listed in Table 3-9. Crystal [**8**]·2NH_4ClO_4 contained a half of [Au_4Ni_2(dppe)$_2$(D-pen)$_4$] unit, four disordered ClO_4^- ions with an occupancy of 1/2, 1/3, 1/12, and 1/12, two ammonium molecules with an occupancy of 1/3, and one solvated water molecule in the asymmetric unit. In [**8**]·2NH_4ClO_4, the $Au^I_4Ni^{II}_2$ hexanuclear structure, the hexameric octahedrally aggregated neutral structure, and the fcc packing structure similar to those of [**7**]·2$HClO_4$ were formed (Figure 3-37a, b, d). In the hydrophilic tetrahedral interstice, ten ClO_4^- ions were accommodated in an adamantane-like structure with four ammonium cations mediating the hydrogen bonding between them, like [**7**]·2NH_4ClO_4 ($NH_4^+\cdots O_{ClO4}$ = 2.79, 2.76 Å, minimum Cl···Cl = 4.12 Å, O···O = 2.59 Å. Figure 3-37c). The shorter Cl···Cl length might be resulted from the stronger hydrogen bonding ability of ammonium cation than that of oxonium cation.

III-3-13. Crystal Structure of reverted [Au_4Ni_2(*trans*-dppee)$_2$(D-pen)$_4$]·2$HClO_4$ ([**7**]·2$HClO_4$).

The crystal structure of reverted [**7**]·2$HClO_4$ after the desorption of ammonia was also investigated via single-crystal X-ray crystallography using synchrotron-radiation X-ray. The crystallographic data are summarized in Table 3-1, and the selected bond distances and angles are listed in Table 3-9. Molecular and packing structures are shown in Figure 3-38. While the single-crystal-to-single-crystal reverse conversion was proved, the data was not so good and the oxygen atoms on perchlorate anions in site **B** could not be found perfectly. Despite the comparably low data quality, the hydrogen-bond distances between the oxonium cation and the three D-pen carboxylate groups in reversed [**7**]·2$HClO_4$ ($H_3O^+\cdots O$ = 2.71 Å) were shorter than the distance between ammonium and carboxylate in [**7**]·2NH_4ClO_4 ($NH_4^+\cdots O$ = 2.81 Å), and similar to that in initial [**7**]·2$HClO_4$ ($H_3O^+\cdots O$ = 2.69 Å), indicating that reverse conversion occurred successfully (Figure 3-27).

III-3-14. Crystal Structure of [Au_4Ni_2(*trans*-dppee)$_2$(D-pen)$_2$(L-pen)$_2$] ([**10**]).

The crystal structure of [**10**] was determined by single-crystal X-ray crystallography. Molecular and packing structures are shown in Figures 3-39, 3-40, 3-41, and 3-42. The crystallographic data are summarized in Table 3-10, and the selected bond distances and angles are listed in Table 3-11. Crystal [**10**] contained one [Au_4Ni_2(*trans*-dppee)$_2$ (D-pen)$_2$(L-pen)$_2$] unit, two EtOH molecules, and 18 solvated water molecules in the asymmetric unit. As shown in Figure 3-40, the complex molecule had an S-bridged $Au^I_4Ni^{II}_2$ hexanuclear structure consisting of two heterochiral [Au_2(*trans*-dppee)(D-pen)(L-pen)]$^{2-}$ metalloligands that linked two Ni^{II} atoms to form an 18-membered ring structure composed of Au, Ni, S, P, and C atoms. The coordination geometry of each Au^I atoms was nearly linear bound with P and S atoms (Av. Au–S = 2.32 Å, Au–P = 2.25 Å, P–Au–S = 176.8°). The two DL-[**2**]$^{2-}$ metalloligands each bound to two Ni^{II} atoms in a bis(tridentate-*N*,*O*,*S*) mode such that each Ni^{II} atoms was in a *cis*(*N*)*trans*(*O*)*cis*(*S*)-$N_2O_2S_2$ octahedral environment (Av. Ni–S = 2.45 Å, Ni–O = 2.06 Å, Ni–N = 2.07 Å, S–Ni–S = 99.9°, O–Ni–O= 173.8°, N–Ni–N = 99.8°) (Figures 3-41a, b). The intramolecular aurophilic interactions were found in the complex molecule (Au···Au = 3.0334(10), 3.0157(10) Å) and these interactions probably stabilize the whole hexanuclear heterochiral complex structure and prevent the formation of homochiral hexanuclear and homochiral 1D chain structures. In [**10**], no direct hydrogen bonds between the complex molecules were found, and the complex molecule arranged in parallel fashion (Figure 3-42).

III-3-15. Aggregation Behavior of the Au^INi^{II} Complexes.

In the reactions using homochiral *trans*-dppee metalloligand D$_2$-H$_2$[**2**], two kinds of crystals with totally different structures were obtained depending on the presence of acid; the 1D infinite chain structure incorporating no acid ([**9**]) and the discrete hexanuclear complex with a hexameric supramolecular structure incorporating $HClO_4$ or HNO_3 molecules ([**7**]·2$HClO_4$ and [**7**]·4/3HNO_3). In [**7**]·HX, the acid was incorporated separately as an anionic form (NO_3^- and ClO_4^-) and a protonated oxonium form. The inorganic anions formed an adamantane-like decameric or an octahedron-like hexameric supramolecular structure and were accommodated in the tetrahedral interstices in the fcc structure constructed by the hexamer of the neutral $Au^I_4Ni^{II}_2$ complex molecules. Each of the anion was hydrogen bonded with amine groups of different complex molecules so as to connect neighboring complex hexamers (Figures 3-43a, b, c). The presence of the anions might contribute to the stabilization of this crystal structure as template. Such behaviors that introducing strong Brønsted acid as a template have been scarcely reported; only weak acids, such as boronic acids and protonated nucleobases, have been used as a

template,[20] while the acid-incorporated materials have been proposed to be highly applicable as acid catalysts, base scavengers and base-responsive sensors.[21] On the other hand, in [**9**], no acid was incorporated even though the acetate anions from the nickel source $Ni(OAc)_2$ had a possibility for the incorporation. Such differences might come from the acidity of coexisting acids. The weaker acid (AcOH) might be in a protonated form in the reaction solution, whereas the strong acids (HNO_3 and $HClO_4$) were dissociated to form H_3O^+ and the anions. Acetic acid does not have the same hydrogen bonding ability as strong acids, enabling to act as a template for [**7**]·nHX.

In the case of homochiral dppe metalloligand, the molecular structure of the $Au^{I}Ni^{II}$ complexes was the same $Au^{I}_4Ni^{II}_2$ 18-membered twisted ring structure for both the crystal with acid ([**8**]·$2HClO_4$) and without acid ([**8**]·$0.5EtOH·0.5Et_2O·7.25H_2O$) which was obtained by the reaction of [Au_2(dppe)(D-Hpen)$_2$] and $Ni(OAc)_2$ without any additional acid.[6] Although their molecular structures were same, their supramolecular structures were completely different. In the previously reported complex, [**8**]·$0.5EtOH·0.5Et_2O$ ·$7.25H_2O$, which incorporated no acid molecules, the hexanuclear units were connected to each other only through the hydrogen bonds between the amine and carboxylate groups to form a hydrogen bonded 1D chain-like arrangement (Figures 3-4a, b, c), On the other hand, in [**8**]·$2HClO_4$, the hexanuclear units were connected to each other through the CH···π and hydrogen-bonding interactions to form the hexameric structure and the closely packed fcc structure incorporating the anions in its tetrahedral interstice. These facts indicated the importance of the coexisting acid in the reaction solution on the crystallization process. Similar to the *trans*-dppee case, the presence of the suitable inorganic anions might stabilize the above-mentioned unique supramolecular structure. In addition, the difference between the 1D coordination polymer of [**9**] with *trans*-dppee ligands and the discrete hexanuclear structure of [**8**]·$0.5EtOH·0.5Et_2O·7.25H_2O$ with dppe ligands. Due to the rigidness of *trans*-dppee, it was assumed that metalloligands prefer a possible linear shaped structure. Furthermore, stronger Au···Au interactions could be recognized in [**9**] (Av. Au···Au = 3.26 Å) than in [**8**]·$0.5EtOH·0.5Et_2O·7.25H_2O$ (Av. Au···Au = 3.42 Å). This stabilization also contributed to form the coordination polymer structure in [**9**].

In the dppe heterochiral system, the homochiral $Au^{I}_4Ni^{II}_2$ hexanuclear complexes in [Au_4Ni_2(dppe)$_2$(D-pen)$_4$] and [Au_4Ni_2(dppe)$_2$(L-pen)$_4$] were formed, and these structures were crystallized together to form a racemic crystal.[7c] In the crystal, the dimer structure was formed through hydrogen bonds between the amine and carboxylate groups, which were further connected through hydrogen bonds mediated by water molecules to construct a chain structure (Figure 3-44a, b), which was different from that in the

homochiral [**8**]·2$HClO_4$ crystals. For the heterochiral $Au^I_4Ni^{II}_2$ complex ([**10**]) with *trans*-dppee ligands, the complexes formed a hydrogen-bonding 1D chain arrangement structure which is, again, sharp contrast to the supramolecular structure found in homochiral systems ([**7**]). These results indicated the importance of chirality for the formation of the supramolecular structure, because the unique separate aggregation behavior of complex molecules and anions were found only in homochiral crystals of [**7**]·2$HClO_4$ and [**8**]·2$HClO_4$.

III-3-16. Reaction Behavior of the Acidic Au^INi^{II} Crystals toward Base

The immersion of the crystals of [**7**]·2$HClO_4$ into an aqueous NH_3 solution led to the SCSC incorporation of ammonia into [**7**]·2$HClO_4$ giving [**7**]·2NH_4ClO_4 as reported in **III-3-3**. Notably, [**7**]·2NH_4ClO_4 easily reverted back to [**7**]·2$HClO_4$, with the retention of crystallinity, by soaking the crystals in an aqueous solution of $HClO_4$ overnight (**III-3-5**). These results indicated the robust crystal framework of [**7**]·2$HClO_4$.

Next, the absorption behavior to the methylamine ($MeNH_2$) molecule was examined in the similar conditions (**III-2-2-4-A-2**). Unlike the treatment with NH_3, the crystallinity was lost during the treatment, confirmed by PXRD measurement of the obtained pale green powder. The IR spectra indicated no existence of ClO_4^- anions (Figures 3-45a, 3-46a). Since the tetrahedral interstices in [**7**]·2$HClO_4$ were infinitely connected *via* very narrow gates (2.90 x 0.97 $Å^2$), which were capped by two water molecules (Figure 3-47a), it was conceivable that the $MeNH_2$ molecule (diameter ca. 3~4 Å)[22] cannot pass through the crystal lattice. Only on the surface of the crystals, the neutralization occurred leading to the proton transportation through the gate, which resulted in the collapse of the crystal lattice caused by the large Coulombic repulsion among ClO_4^- ions in the adamantine-like aggregate.

The 1D coordination polymer in [**9**] did not absorb NH_3 molecules by the same treatment as [**7**]·2$HClO_4$ (**III-2-2-4-D**) based on the elemental analytical data. The same result was also obtained when the $Au^I_4Co^{III}_2$ complex of [**3**]$(ClO_4)_2$ was treated with an aqueous NH_3, although [**3**]$(ClO_4)_2$ had nearly the same fcc structure as [**7**]·2$HClO_4$ (**III-2-2-4-E**). Thus, the presence of H_3O^+ ions was essential for the absorption of NH_3 molecules in [**7**]·2$HClO_4$.

The NH_3 absorption behavior was also examined for [**7**]·4/3HNO_3 (**III-2-2-4-B**) with the treatment in aqueous NH_3. Based on the IR spectrum, elemental analysis, and powder X-ray diffraction, the green powder was found to incorporate neither nitrate nor ammonia with the loss of crystallinity (Figures 3-45b, 3-46b). This result is explained by the size difference between perchlorate and nitrate anions; the nitrate anion is smaller than

perchlorate and the elusion of nitrate anion though the above-mentioned narrow gates takes place more easily than perchlorate (Figure 3-46a). Eventually, the loss of inorganic anions mediating the interaction between the complex molecules led to the loss of its crystallinity.

Based on the failure of NH_3 incorporation experiment from an aqueous solution, the incorporation of gaseous ammonia was undergone as described above (**III-3-3**). The gaseous reaction led to the incorporation of ammonia into [**7**]·4/3HNO_3 crystals to be [**7**]·4/3NH_4NO_3 with the retention of the crystallinity.

The incorporation of ammonia from gaseous phase was also successful in the case of [**7**]·2$HClO_4$, which was confirmed by elemental analysis, IR spectra, and powder X-ray diffraction pattern (**III-2-2-5-A**, Figures 3-45c, 3-46c).

The NH_3 absorption behavior of [**8**]·2$HClO_4$ in an aqueous solution was also examined (**III-2-2-4-C**). Based on the IR spectrum, elemental analysis, and powder X-ray diffraction, the green powder was found to incorporate neither perchlorate nor ammonia with the loss of crystallinity (Figures 3-45d, 3-46d). This result was sharp contrast to the SCSC conversion of [**7**]·2$HClO_4$ with *trans*-dppee units. It was possible to explain the difference by the flexibility of the diphosphine linker units; the dppe unit is less rigid than *trans*-dppee unit. (Figure 3-47b) The narrow gate in [**7**]·2$HClO_4$ bearing rigid *trans*-dppee units did not allow the perchlorate anion to be eluted, while the gate in [**8**]·2$HClO_4$ with dppe would flexibly open the gate for the pathway of perchlorate anions. Eventually, the elusion of inorganic anions that mediate the hydrogen bonding interactions between the complex molecules led to the loss of the crystallinity.

The incorporation of gaseous ammonia was also undergone (previously explained in **III-3-3**). This experiment also led to the isolation of [**8**]·2NH_4ClO_4 with the retention of its single-crystallinity.

III-4. Summary.

In this chapter, the $Au^{I}_4Ni^{II}_2$ hexanuclear complexes, $[Au^{I}_4Ni^{II}_2(\textit{trans}\text{-dppee})_2(\text{D-pen})_4]\cdot HX$ ([**7**]·HX; HX = 4/3HNO_3, 2$HClO_4$), and the $Au^{I}_2Ni^{II}$ 1D chain coordination polymer, $[Au^{I}_2Ni^{II}(\textit{trans}\text{-dppee})(\text{D-pen})_2]_\infty$ ([**9**]), were synthesized by the reactions of the chiral metalloligand, $[Au^{I}_2(\textit{trans}\text{-dppee})(\text{D-Hpen})_2]$ (D_2-H_2[**2**]), with Ni^{II} with and without strong Brønsted acids. In these complexes, the metalloligand, D_2-H_2[**2**], coordinated to two Ni^{II} centers in a bis(tridentate-*N*,*O*,*S*) mode to form a twisted metalloring structure in [**7**]·HX and a chain structure in [**9**]. In the crystal structures of [**7**]·HX, the six complex molecules were aggregated into a large octahedron-shaped supramolecular structure through multiple interactions, and these hexameric supramolecular octahedrons were packed in a face-centered cubic (fcc) structure. Remarkably, inorganic anions (10ClO_4^-, or 6NO_3^-) were aggregated in each hydrophilic tetrahedral interstice in a fcc structure in spite of the neutral nature of [**7**]. It is assumed that some of solvated water molecules are protonated to balance the charge. The formation of the crystals by the incorporation of acids indicates the importance of the inorganic anions during the crystallization process. Its importance was also indicated by the successful crystallization of the isomorphous dppe analogue ([**8**]·2$HClO_4$), of which molecular structure was similar to the previously reported crystal of $[Au^{I}_4Ni^{II}_2(\text{dppe})_2(\text{D-pen})_4]$, but its aggregation behavior was totally different.

These crystals accommodating an inorganic acid showed a reversible reactivity toward basic molecules, where the incorporation of NH_3 molecules underwent with the retention of the single crystallinity. [**7**]·2$HClO_4$ absorbed NH_3 molecules from an aqueous ammonia and produced [**7**]·2NH_4ClO_4, which was easily reverted back to [**7**]·2$HClO_4$ in a single-crystal-to-single-crystal conversion manner. The removal of ammonia from aqueous media is an important issue in environmental and biological sciences.[23] However, to our best of knowledge, the system reported in this thesis represented the first example of a coordination system that exhibits reversible absorption/desorption of NH_3 molecules in aqueous media; the reported incorporation of NH_3 molecules into metal-organic frameworks has been achieved only from gaseous ammonia.[24]

In the absence of inorganic acids in the synthetic conditions, the 1D chain coordination polymer was formed in [**9**]. Such an infinite chain structure has never been found for the $Au^{I}Co^{III}$ and $Au^{I}Ni^{II}$ analogous crystals.

In this chapter, the effect of the chirality on the molecular and supramolecular structures of $Au^{I}Ni^{II}$ complexes was also investigated. The reaction of a racemic mixture of the chiral metalloligands $[Au^{I}_2(\textit{trans}\text{-dppee})(\text{D or L-Hpen})_2]$ (D_2-H_2[**2**], L_2-H_2[**2**]) with Ni^{II} gave the $Au^{I}_4Ni^{II}_2$ heterochiral complex, $[Au^{I}_4Ni^{II}_2(\textit{trans}\text{-dppee})_2(\text{D-pen})_2(\text{L-pen})_2]$

([**10**]). In [**10**], the heterochiral metalloligand (DL-H_2[**2**]) was formed through the scrambling of the racemic metalloligands in solution, which links two Ni ions in a bis(tridentate-*N*,*O*,*S*) mode to make the 18-membered ring structure. The crystal packing did not show the charge-separated type of supramolecular structure, indicating the importance of chirality on the unique supramolecular aggregation. Thus, the study in this chapter clarified the useful role of the *trans*-dppee units in the crystallinity, the rigidity, and the novel SCSC conversion.

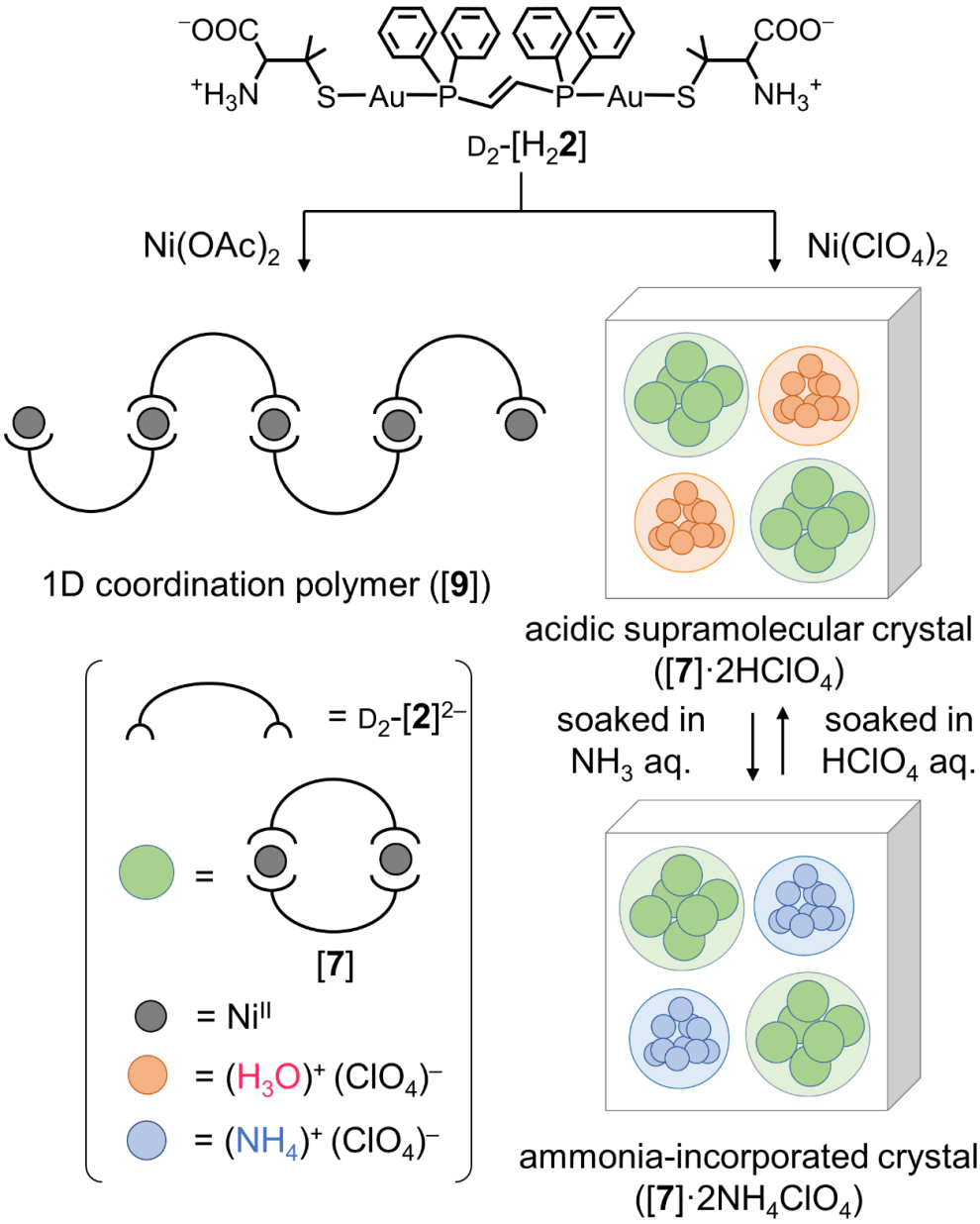

Scheme 3-1. Schematic of the formation of the 1D structure in [**9**] and the acidic supramolecular structure in [**7**]·2$HClO_4$, showing reversible conversion to [**7**]·2NH_4ClO_4 in aqueous media.

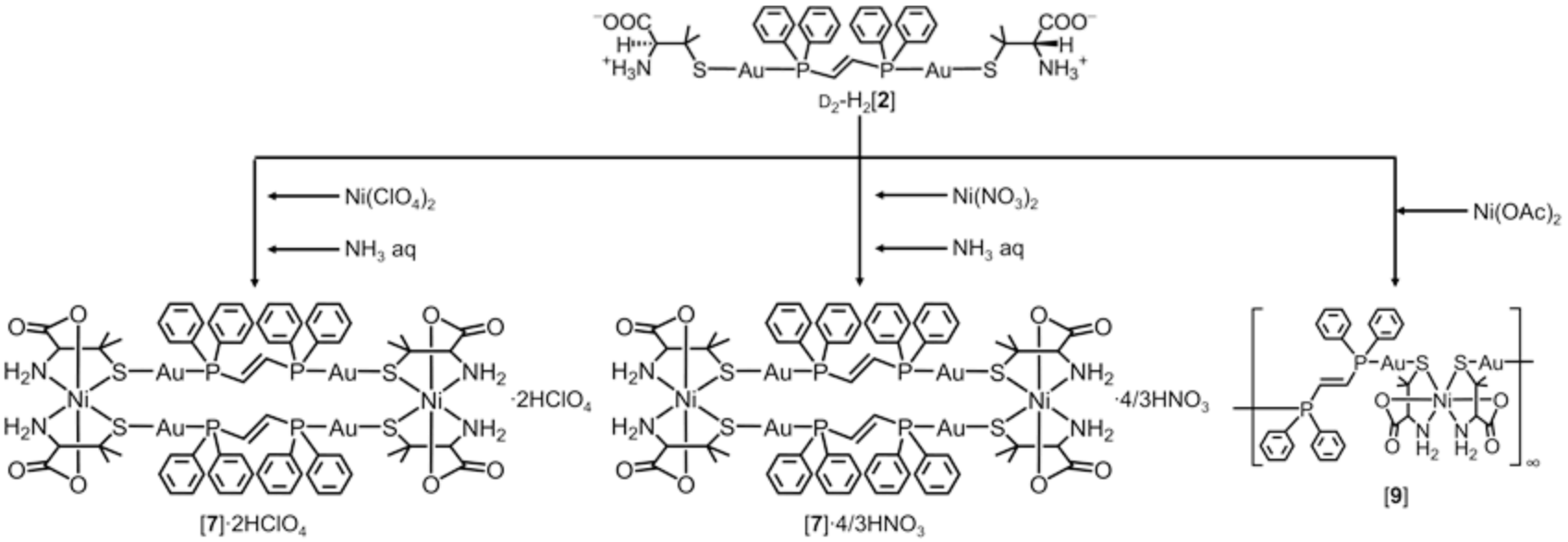

Scheme 3-2. Synthesis of $Au^{I}_{4}Ni^{II}_{2}$ complexes, [**7**]·2$HClO_4$ and [**7**]·4/3HNO_3, and 1D polymer $Au^{I}_{2}Ni^{II}$ complex, [**9**].

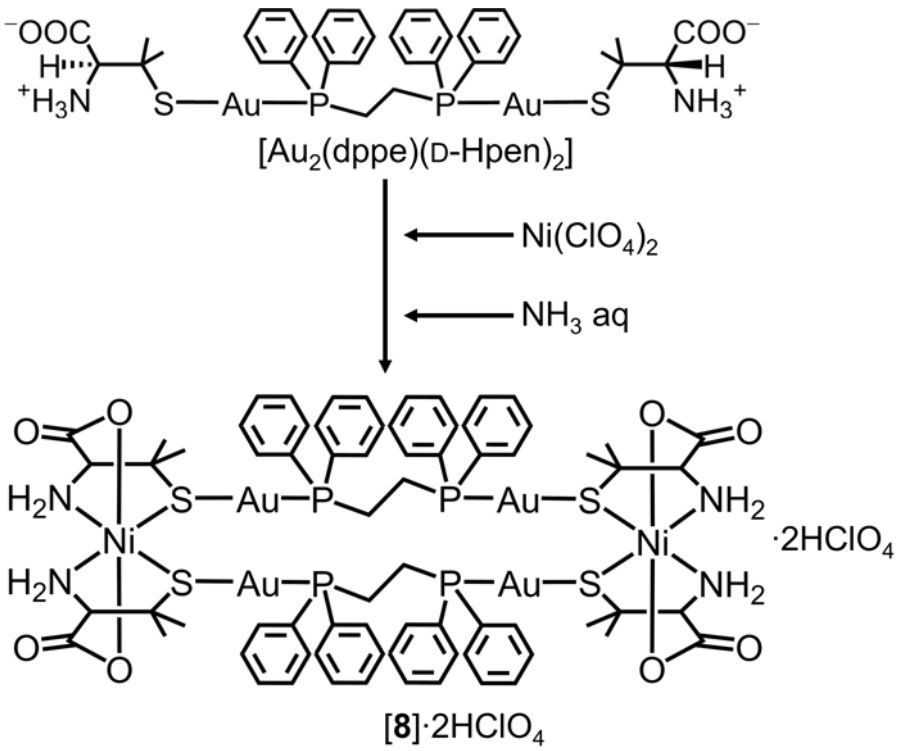

Scheme 3-3. Synthesis of $Au^{I}_{4}Ni^{II}_{2}$ complex with dppe linker unit, [**8**]·2$HClO_4$.

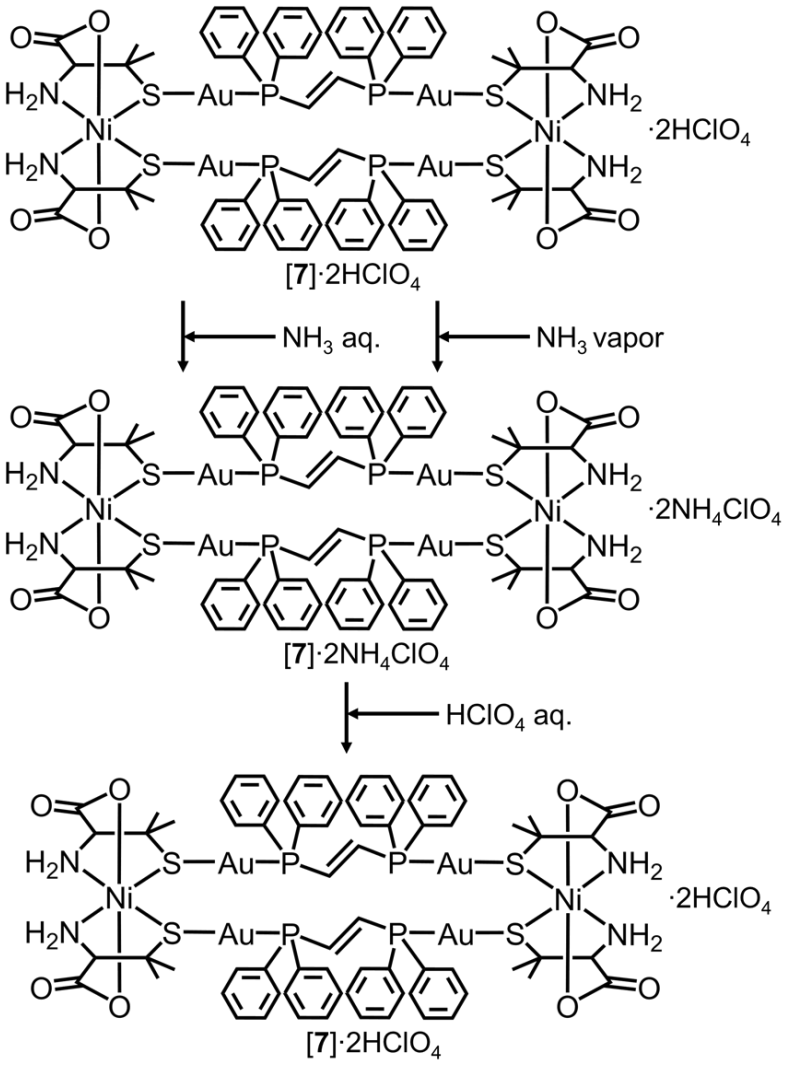

Scheme 3-4. Reaction of ammonia and acidic crystals in aqueous solution or gaseous phase for [**7**]·2$HClO_4$ and the desorption of ammonia from the resulted ammonia incorporated crystals of [**7**]·2NH_4ClO_4.

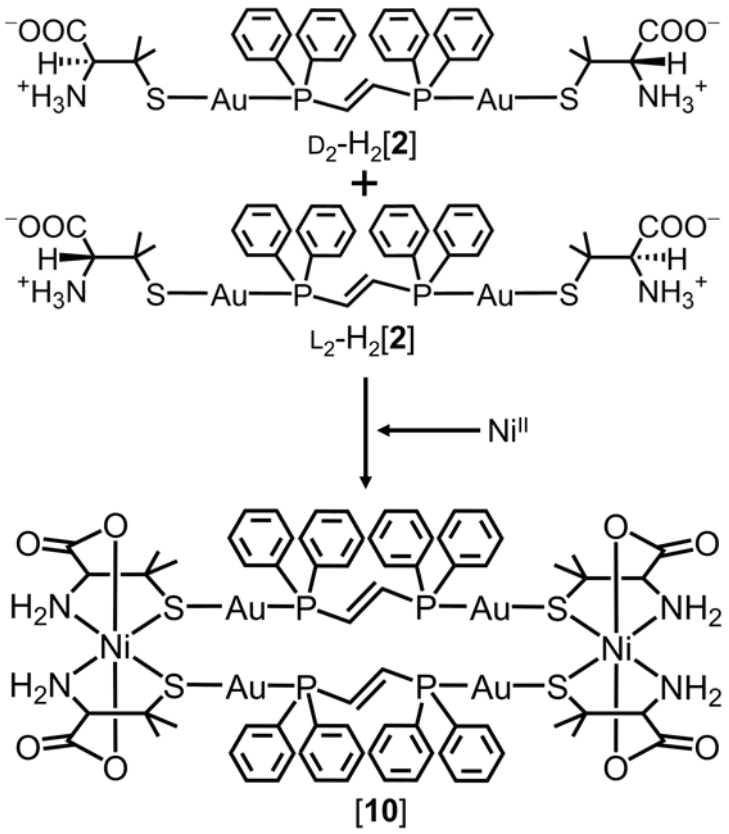

Scheme 3-5. Synthesis of heterochiral $Au^{I}_{4}Ni^{II}_{2}$ complex [**10**].

Table 3-1. Crystallographic data for [**7**]·HX (HX = $2HClO_4$ or $4/3HNO_3$), [**8**]·$2HClO_4$, [**7**]·NH_4X (NH_4X = $2NH_4ClO_4$ or $4/3NH_4NO_3$) and [**8**]·$2NH_4ClO_4$.

	[**7**]·$2NH_4ClO_4$·$5.08H_2O$	[**7**]·$4/3NH_4NO_3$·$4H_2O$	[**8**]·$2NH_4ClO_4$·$2H_2O$	reverted [**7**]·$2HClO_4$·$4H_2O$
Formula	$C_{72}H_{76}Au_4Ni_2Cl_2$ $N_{5.33}O_{21.08}P_4S_4$	$C_{72}H_{80}Au_4Ni_2$ $N_{6.67}O_{216}P_4S_4$	$C_{72}H_{84}Au_4Ni_2Cl_2$ $N_{5.33}O_{18}P_4S_4$	$C_{72}H_{80}Au_4Ni_2Cl_2$ $N_4O_{18.67}P_4S_4$
Formula weight	2581.68	2452.16	2540.41	2528.37
Crystal color	green	green	green	green
Crystal size, mm^3	0.12 x 0.07 x 0.05	0.16 x 0.13 x 0.03	0.15x 0.08 x 0.06	0.10 x 0.10 x 0.10
Crystal system	cubic	cubic	cubic	cubic
Space group	*F*23	*F*23	*F*23	*F*23
a, Å	37.938(14)	37.755(8)	37.9065(3)	37.702(13)
V, $Å^3$	54604(59)	53816(34)	54468.0(13)	53591(56)
Z	24	24	24	24
ρ(calc), g/cm^3	1.884	1.816	1.859	1.880
*R*1 ($I>2\sigma(I)$) [a]	0.0727	0.0648	0.0510	0.0765
w*R*2 ($I>2\sigma(I)$) [b]	0.1686	0.1247	0.1230	0.1570
*R*1 (all data) [a]	0.1031	0.1275	0.0552	0.1593
w*R*2 (all data) [b]	0.1896	0.1459	0.1273	0.1880

a) $R1 = \Sigma|(|F_o|-|F_c|)|/\Sigma(|F_o|)$

b) $wR2 = [\Sigma_w(|F_o|^2-|F_c|^2)^2/\Sigma_w(|F_o|^2)^2]^{1/2}$

Table 3-1. Crystallographic data for [**7**]·HX (HX = $2HClO_4$ or $4/3HNO_3$), [**8**]·$2HClO_4$, [**7**]·NH_4X (NH_4X = $2NH_4ClO_4$ or $4/3NH_4NO_3$) and [**8**]·$2NH_4ClO_4$.

	[**7**]·$2HClO_4$·$4.67H_2O$	[**7**]·$4/3HNO_3$·$8.83H_2O$	[**8**]·$2HClO_4$·$4.67H_2O$
Formula	$C_{72}H_{80}Au_4Ni_2Cl_2N_4O_{20.67}P_4S_4$	$C_{72}H_{72}Au_4Ni_2N_{5.33}O_{20.83}P_4S_4$	$C_{72}H_{84}Au_4Ni_2Cl_2N_4O_{20.67}P_4S_4$
Formula weight	2560.37	2502.75	2564.40
Crystal color	green	green	green
Crystal size, mm^3	0.20 x 0.10 x 0.02	0.14 x 0.12 x 0.03	0.25 x 0.24 x 0.08
Crystal system	cubic	cubic	cubic
Space group	*F*23	*F*23	*F*23
a, Å	38.052(3)	37.902(11)	37.935(4)
V, $Å^3$	55097(15)	54446(46)	54591(19)
Z	24	24	24
ρ(calc), g/cm^3	1.852	1.832	1.872
*R*1 ($I>2\sigma(I)$) [a)]	0.0640	0.0667	0.0289
w*R*2 ($I>2\sigma(I)$) [b)]	0.1430	0.1219	0.0828
*R*1 (all data) [a)]	0.0874	0.1277	0.0320
w*R*2 (all data) [b)]	0.1571	0.1432	0.0862

a) $R1 = \Sigma|(|F_o|-|F_c|)|/\Sigma(|F_o|)$

b) $wR2 = [\Sigma_w(|F_o|^2-|F_c|^2)^2/\Sigma_w(|F_o|^2)^2]^{1/2}$

Table 3-2. Selected bond distances (Å) and angles (°) for [**7**]·2$HClO_4$.

		distances	
Au(1)-P(1)	2.252(6)	Au(1)-S(1)	2.305(5)
Au(2)-P(2)	2.251(4)	Au(2)-S(2)	2.306(4)
Ni(1)-O(3)	2.041(9)	Ni(1)-N(2)	2.069(13)
Ni(1)-O(1)	2.081(9)	Ni(1)-N(1)	2.096(12)
Ni(1)-S(1)	2.437(4)	Ni(1)-S(2)	2.463(4)
C(23)-C(23)′	1.262(18)	C(36)-C(36)′	1.25(3)
		angles	
P(1)-Au(1)-S(1)	178.59(16)	P(2)-Au(2)-S(2)	178.19(13)
O(3)-Ni(1)-N(2)	79.6(5)	O(3)-Ni(1)-O(1)	174.9(4)
N(2)-Ni(1)-O(1)	98.2(5)	O(3)-Ni(1)-N(1)	97.3(4)
N(2)-Ni(1)-N(1)	96.5(5)	O(1)-Ni(1)-N(1)	78.4(4)
O(3)-Ni(1)-S(1)	91.8(3)	N(2)-Ni(1)-S(1)	171.0(4)
O(1)-Ni(1)-S(1)	90.3(3)	N(1)-Ni(1)-S(1)	82.0(4)
O(3)-Ni(1)-S(2)	90.1(3)	N(2)-Ni(1)-S(2)	82.1(4)
O(1)-Ni(1)-S(2)	94.0(3)	N(1)-Ni(1)-S(2)	172.0(3)
S(1)-Ni(1)-S(2)	100.60(16)	C(23)′-C(23)-P(1)	141(2)
C(36)′-C(36)-P(2)	122.3(18)		

Symmetry code: (') x, 1–y, 1–z.

Table 3-3. Selected bond distances (Å) and angles (°) for [**7**]·4/3HNO_3.

		distances	
Au(1)-P(1)	2.231(7)	Au(1)-S(1)	2.305(6)
Au(2)-P(2)	2.251(6)	Au(2)-S(2)	2.307(6)
Ni(1)-O(3)	2.043(13)	Ni(1)-N(2)	2.045(18)
Ni(1)-N(1)	2.088(15)	Ni(1)-O(1)	2.089(13)
Ni(1)-S(1)	2.446(6)	Ni(1)-S(2)	2.466(6)
C(23)-C(23)′	1.280(15)	C(36)-C(36)′	1.297(15)
		angles	
P(1)-Au(1)-S(1)	178.5(2)	P(2)-Au(2)-S(2)	178.5(2)
O(3)-Ni(1)-N(2)	81.0(7)	O(3)-Ni(1)-N(1)	97.4(6)
N(2)-Ni(1)-N(1)	96.4(6)	O(3)-Ni(1)-O(1)	175.8(6)
N(2)-Ni(1)-O(1)	97.9(6)	N(1)-Ni(1)-O(1)	78.6(5)
O(3)-Ni(1)-S(1)	90.7(4)	N(2)-Ni(1)-S(1)	170.9(5)
N(1)-Ni(1)-S(1)	81.0(4)	O(1)-Ni(1)-S(1)	90.1(4)
O(3)-Ni(1)-S(2)	90.1(4)	N(2)-Ni(1)-S(2)	82.3(5)
N(1)-Ni(1)-S(2)	172.1(5)	O(1)-Ni(1)-S(2)	93.8(4)
S(1)-Ni(1)-S(2)	101.5(2)	C(23)′-C(23)-P(1)	129(3)
C(36)′-C(36)-P(2)	120.8(18)		

Symmetry code: (') 1–x, y, 1–z.

Table 3-4. Selected bond distances (Å) and angles (°) for [**8**]·2$HClO_4$.

		distances	
Au(1)-P(1)	2.261(2)	Au(1)-S(1)	2.311(2)
Au(2)-P(2)	2.251(2)	Au(2)-S(2)	2.312(2)
Ni(1)-O(1)	2.039(6)	Ni(1)-O(3)	2.080(6)
Ni(1)-N(1)	2.069(8)	Ni(1)-N(2)	2.090(7)
Ni(1)-S(2)	2.432(2)	Ni(1)-S(1)	2.459(2)
C(11)-C(11)′	1.521(17)	C(12)-C(12)′	1.52(2)
		angles	
P(1)-Au(1)-S(1)	177.98(8)	P(2)-Au(2)-S(2)	177.73(8)
O(1)-Ni(1)-O(3)	173.6(3)	O(1)-Ni(1)-N(1)	79.4(3)
O(3)-Ni(1)-N(1)	97.2(3)	O(1)-Ni(1)-N(2)	96.6(3)
O(3)-Ni(1)-N(2)	78.2(3)	N(1)-Ni(1)-N(2)	96.7(3)
O(1)-Ni(1)-S(2)	92.7 (2)	O(3)-Ni(1)-S(2)	90.5 (2)
N(1)-Ni(1)-S(2)	171.9(3)	N(2)-Ni(1)-S(2)	82.2(2)
O(1)-Ni(1)-S(1)	89.89(19)	O(3)-Ni(1)-S(1)	95.05(19)
N(1)-Ni(1)-S(1)	81.6(2)	N(2)-Ni(1)-S(1)	172.9(2)
S(2)-Ni(1)-S(1)	100.42(8)	C(11)′-C(11)-P(1)	110.5 (8)
C(12)′-C(12)-P(2)	110.7(8)		

Symmetry code: (') x, 3/2–y, 3/2–z.

Table 3-5. Crystallographic data for [**9**].

	[**9**]·11MeOH·5H_2O
Formula	$C_{39.67}H_{40}Au_2NiN_2O_{9.33}P_2S_2$
Formula weight	1272.77
Crystal color	green
Crystal size, mm^3	0.14 x 0.14 x 0.05
Crystal system	orthorhombic
Space group	$P2_12_12_1$
a, Å	11.96520(10)
b, Å	31.3254(2)
c, Å	37.5942(2)
V, $Å^3$	14090.86(17)
Z	12
ρ(calc), g/cm^3	1.800
*R*1 ($I>2\sigma(I)$) [a)]	0.0781
w*R*2 ($I>2\sigma(I)$) [b)]	0.2090
*R*1 (all data) [a)]	0.0897
w*R*2 (all data) [b)]	0.2202

a) $R1 = \Sigma(|(|F_o|-|F_c|)|/\Sigma(|F_o|)$

b) $wR2 = [\Sigma_w(|F_o|^2-|F_c|^2)^2/\Sigma_w(|F_o|^2)^2]^{1/2}$

Table 3-6. Selected bond distances (Å) and angles (°) for [**9**].

		distances	
P(1)-Au(1)	2.242(5)	S(1)-Au(1)	2.318(4)
P(3)-Au(2)	2.247(4)	S(2)-Au(2)	2.301(4)
P(4)-Au(3)	2.250(4)	S(3)-Au(3)	2.297(4)
P(5)-Au(4)	2.244(5)	S(4)-Au(4)	2.304(5)
P(6)-Au(5)	2.251(5)	S(5)-Au(5)	2.288(5)
P(2)-Au(6)′	2.258(5)	S(6)-Au(6)	2.308(4)
Ni(1)-O(5)	2.059(16)	Ni(1)-O(7)	2.089(16)
Ni(1)-N(3)	2.102(16)	Ni(1)-N(4)	2.044(16)
Ni(1)-S(3)	2.435(5)	Ni(1)-S(4)	2.450(5)
O(1)-Ni(2)	2.087(14)	O(3)-Ni(2)	2.060(13)
N(1)-Ni(2)	2.057(19)	N(2)-Ni(2)	2.104(18)
S(1)-Ni(2)	2.429(6)	S(2)-Ni(2)	2.413(6)
Ni(3)-O(9)	2.072(10)	Ni(3)-O(11)	2.049(12)
Ni(3)-N(5)	2.078(16)	Ni(3)-N(6)	2.079(13)
Ni(3)-S(5)	2.448(5)	Ni(3)-S(6)	2.457(5)
C(55)-C(56)	1.22(4)	C(81)-C(82)	1.30(2)
C(107)-C(108)	1.19(4)	Au(1)-Au(2)	3.3094(11)
Au(3)-Au(4)	3.2019(10)	Au(5)-Au(6)	3.2772(11)
		angles	
P(1)-Au(1)-S(1)	172.3(2)	P(3)-Au(2)-S(2)	174.69(14)
P(4)-Au(3)-S(3)	172.08(15)	P(5)-Au(4)-S(4)	177.71(19)
P(6)-Au(5)-S(5)	176.68(18)	P(2)″-Au(6)-S(6)	178.2(2)
N(4)-Ni(1)-O(5)	96.5(7)	N(4)-Ni(1)-O(7)	79.1(7)
O(5)-Ni(1)-O(7)	173.8(6)	N(4)-Ni(1)-N(3)	96.6(6)
O(5)-Ni(1)-N(3)	78.5(7)	O(7)-Ni(1)-N(3)	97.6(7)
N(4)-Ni(1)-S(3)	171.6(5)	O(5)-Ni(1)-S(3)	91.3(5)
O(7)-Ni(1)-S(3)	92.8(4)	N(3)-Ni(1)-S(3)	81.8(5)
N(4)-Ni(1)-S(4)	82.2(5)	O(5)-Ni(1)-S(4)	90.9(4)
O(7)-Ni(1)-S(4)	92.8(4)	N(3)-Ni(1)-S(4)	169.1(6)
S(3)-Ni(1)-S(4)	100.90(17)	N(1)-Ni(2)-O(3)	94.9(6)
N(1)-Ni(2)-O(1)	81.0(7)	O(3)-Ni(2)-O(1)	173.2(6)
N(1)-Ni(2)-N(2)	99.3(8)	O(3)-Ni(2)-N(2)	79.7(6)

O(1)-Ni(2)-N(2)	95.5(7)	N(1)-Ni(2)-S(2)	172.8(5)
O(3)-Ni(2)-S(2)	91.9(4)	O(1)-Ni(2)-S(2)	91.9(6)
N(2)-Ni(2)-S(2)	79.6(5)	N(1)-Ni(2)-S(1)	82.6(6)
O(3)-Ni(2)-S(1)	94.4(5)	O(1)-Ni(2)-S(1)	90.5(6)
N(2)-Ni(2)-S(1)	173.9(5)	S(2)-Ni(2)-S(1)	99.22(17)
O(11)-Ni(3)-O(9)	171.2(6)	O(11)-Ni(3)-N(5)	93.2(6)
O(9)-Ni(3)-N(5)	79.3(5)	O(11)-Ni(3)-N(6)	79.9(5)
O(9)-Ni(3)-N(6)	96.8(5)	N(5)-Ni(3)-N(6)	99.4(6)
O(11)-Ni(3)-S(5)	93.3(4)	O(9)-Ni(3)-S(5)	90.1(3)
N(5)-Ni(3)-S(5)	81.7(4)	N(6)-Ni(3)-S(5)	173.1(4)
O(11)-Ni(3)-S(6)	91.0(5)	O(9)-Ni(3)-S(6)	96.5(3)
N(5)-Ni(3)-S(6)	175.7(4)	N(6)-Ni(3)-S(6)	80.2(4)
S(5)-Ni(3)-S(6)	99.33(16)	C(56)-C(55)-P(1)	121.6(18)
C(55)-C(56)-P(2)	121.2(14)	C(82)-C(81)-P(3)	123.4(12)
C(81)-C(82)-P(4)	121.4(12)	C(108)-C(107)-P(5)	128(2)
C(107)-C(108)-P(6)	132(2)		

Symmetry codes: (') –x–1/2, –y, z–1/2, (") –x–1/2, –y, z+1/2.

Table 3-7. Selected bond distances (Å) and angles (°) for [**7**]·2NH_4ClO_4.

		distances	
Au(1)-P(1)	2.255(7)	Au(1)-S(1)	2.313(7)
Au(2)-P(2)	2.250(5)	Au(2)-S(2)	2.306(5)
Ni(1)-O(1)	2.053(11)	Ni(1)-O(3)	2.070(11)
Ni(1)-N(1)	2.075(17)	Ni(1)-N(2)	2.081(15)
Ni(1)-S(1)	2.444(5)	Ni(1)-S(2)	2.486(5)
C(23)-C(23)′	1.287(19)	C(36)-C(36)′	1.19(3)
		angles	
P(1)-Au(1)-S(1)	177.98(18)	P(2)-Au(2)-S(2)	178.20(16)
O(1)-Ni(1)-O(3)	175.2(5)	O(1)-Ni(1)-N(1)	78.8(5)
O(3)-Ni(1)-N(1)	97.9(5)	O(1)-Ni(1)-N(2)	96.5(5)
O(3)-Ni(1)-N(2)	80.3(5)	N(1)-Ni(1)-N(2)	98.3(6)
O(1)-Ni(1)-S(1)	91.2(3)	O(3)-Ni(1)-S(1)	91.8(3)
N(1)-Ni(1)-S(1)	81.2(5)	N(2)-Ni(1)-S(1)	172.0(4)
O(1)-Ni(1)-S(2)	94.4(3)	O(3)-Ni(1)-S(2)	88.7(4)
N(1)-Ni(1)-S(2)	172.9(4)	N(2)-Ni(1)-S(2)	80.2(4)
S(1)-Ni(1)-S(2)	101.3(2)	C(23)′-C(23)-P(1)	139(3)
C(36)′-C(36)-P(2)	123.4(18)		

Symmetry code: (') x, 1–y, 1–z.

Table 3-8. Selected bond distances (Å) and angles (°) for [**7**]·4/3NH_4NO_3.

		distances	
Au(1)-P(1)	2.253(6)	Au(1)-S(1)	2.318(6)
Au(2)-P(2)	2.246(7)	Au(2)-S(2)	2.303(6)
Ni(1)-O(1)	2.048(13)	Ni(1)-N(1)	2.048(18)
Ni(1)-O(3)	2.078(12)	Ni(1)-N(2)	2.083(18)
Ni(1)-S(2)	2.448(6)	Ni(1)-S(1)	2.472(6)
C(11)-C(11)′	1.25(4)	C(12)-C(12)′	1.13(4)
		angles	
P(1)-Au(1)-S(1)	178.55(19)	P(2)-Au(2)-S(2)	178.4(2)
O(1)-Ni(1)-N(1)	80.6(7)	O(1)-Ni(1)-O(3)	177.1(6)
N(1)-Ni(1)-O(3)	98.7(6)	O(1)-Ni(1)-N(2)	99.5(6)
N(1)-Ni(1)-N(2)	96.3(7)	O(3)-Ni(1)-N(2)	77.8(6)
O(1)-Ni(1)-S(2)	90.6(5)	N(1)-Ni(1)-S(2)	170.4(5)
O(3)-Ni(1)-S(2)	89.9(4)	N(2)-Ni(1)-S(2)	81.4(5)
O(1)-Ni(1)-S(1)	89.3(4)	N(1)-Ni(1)-S(1)	82.0(5)
O(3)-Ni(1)-S(1)	93.4(4)	N(2)-Ni(1)-S(1)	170.7(5)
S(2)-Ni(1)-S(1)	101.7(2)	C(11)′-C(11)-P(1)	124(2)
C(12)′-C(12)-P(2)	140(5)		

Symmetry code: (') 1–x, 1–y, z.

Table 3-8. Selected bond distances (Å) and angles (°) for [**8**]·2NH_4ClO_4.

		distances	
Au(1)-P(1)	2.253(3)	Au(1)-S(1)	2.310(3)
Au(2)-P(2)	2.251(3)	Au(2)-S(2)	2.320(3)
Ni(1)-O(3)	2.038(9)	Ni(1)-O(1)	2.048(9)
Ni(1)-N(1)	2.052(13)	Ni(1)-N(2)	2.076(12)
Ni(1)-S(2)	2.439(3)	Ni(1)-S(1)	2.478(3)
C(11)-C(11)′	1.52(2)	C(12)-C(12)′	1.55(3)
		angles	
P(1)-Au(1)-S(1)	178.21(10)	P(2)-Au(2)-S(2)	177.80(12)
O(3)-Ni(1)-O(1)	175.2(4)	O(3)-Ni(1)-N(1)	96.4(5)
O(1)-Ni(1)-N(1)	80.9(5)	O(3)-Ni(1)-N(2)	78.6(4)
O(1)-Ni(1)-N(2)	97.7(4)	N(1)-Ni(1)-N(2)	97.3(5)
O(3)-Ni(1)-S(2)	90.8(3)	O(1)-Ni(1)-S(2)	91.8(3)
N(1)-Ni(1)-S(2)	172.5(4)	N(2)-Ni(1)-S(2)	81.9(4)
O(3)-Ni(1)-S(1)	94.3(3)	O(1)-Ni(1)-S(1)	89.2(3)
N(1)-Ni(1)-S(1)	80.7(4)	N(2)-Ni(1)-S(1)	172.5(3)
S(2)-Ni(1)-S(1)	101.06(12)	C(11)′-C(11)-P(1)	111.5(11)
C(12)′-C(12)-P(2)	113.2(12)		

Symmetry code: (') x, 3/2–y, 1/2–z.

Table 3-9. Selected bond distances (Å) and angles (°) for reverted [**7**]·2HClO$_4$.

		distances	
Au(1)-P(1)	2.232(9)	Au(1)-S(1)	2.301(8)
Au(2)-P(2)	2.253(7)	Au(2)-S(2)	2.303(8)
Ni(1)-O(3)	2.061(17)	Ni(1)-O(1)	2.070(16)
Ni(1)-N(2)	2.09(2)	Ni(1)-N(1)	2.09(2)
Ni(1)-S(1)	2.436(8)	Ni(1)-S(2)	2.467(8)
C(23)-C(23)′	1.03(5)	C(36)-C(36)′	1.25(4)
		angles	
P(1)-Au(1)-S(1)	178.3(3)	P(2)-Au(2)-S(2)	178.5(3)
O(3)-Ni(1)-O(1)	175.6(8)	O(3)-Ni(1)-N(2)	80.2(9)
O(1)-Ni(1)-N(2)	99.0(9)	O(3)-Ni(1)-N(1)	97.8(8)
O(1)-Ni(1)-N(1)	78.0(8)	N(2)-Ni(1)-N(1)	96.2(8)
O(3)-Ni(1)-S(1)	90.3(6)	O(1)-Ni(1)-S(1)	90.1(5)
N(2)-Ni(1)-S(1)	170.1(8)	N(1)-Ni(1)-S(1)	82.1(6)
O(3)-Ni(1)-S(2)	90.5(6)	O(1)-Ni(1)-S(2)	93.7(5)
N(2)-Ni(1)-S(2)	82.4(6)	N(1)-Ni(1)-S(2)	171.3(6)
S(1)-Ni(1)-S(2)	100.7(3)	C(23)′-C(23)-P(1)	142(4)
C(36)′-C(36)-P(2)	123(3)		

Symmetry code: (') x, 1–y, 1–z.

Table 3-10. Crystallographic data for [**10**].

	[**10**]·2EtOH·18H_2O
Formula	$C_{76}H_{128}Au_4Ni_2N_4O_{28}P_4S_4$
Formula weight	2703.23
Crystal color	green
Crystal size, mm^3	0.24 x 0.15 x 0.03
Crystal system	triclinic
Space group	*P*-1
a, Å	12.873(3)
b, Å	13.023(3)
c, Å	31.145(7)
α, °	96.530(7)
β, °	96.972(7)
γ, °	105.031(7)
V, $Å^3$	4948(2)
Z	2
ρ(calc), g/cm^3	1.815
*R*1 (*I*>2*σ*(*I*)) [a)]	0.1000
w*R*2 (*I*>2*σ*(*I*)) [b)]	0.2272
*R*1 (all data) [a)]	0.1723
w*R*2 (all data) [b)]	0.2620

a) $R1 = \Sigma|(|F_o|-|F_c|)|/\Sigma(|F_o|)$

b) $wR2 = [\Sigma_w(|F_o|^2-|F_c|^2)^2/\Sigma_w(|F_o|^2)^2]^{1/2}$

Table 3-11. Selected bond distances (Å) and angles (°) for [**10**].

		distances	
Au(1)–S(1)	2.287(4)	Au(2)–S(2)	2.310(4)
Au(3)–S(3)	2.283(4)	Au(4)–S(4)	2.309(4)
Au(1)–P(1)	2.253(4)	Au(2)–P(2)	2.245(4)
Au(3)–P(3)	2.239(4)	Au(4)–P(4)	2.256(4)
Au(1)···Au(2)	3.0333(10)	Au(3)···Au(4)	3.0157(10)
C(11)–C(12)	1.280(17)	C(23)–C(24)	1.312(19)
Ni(1)–S(1)	2.479(4)	Ni(1)–S(2)	2.437(4)
Ni(1)–O(1)	2.068(10)	Ni(1)–O(3)	2.040(11)
Ni(1)–N(1)	2.062(11)	Ni(1)–N(2)	2.068(11)
Ni(2)–S(3)	2.446(5)	Ni(2)–S(4)	2.439(5)
Ni(2)–O(5)	2.057(12)	Ni(2)–O(7)	2.069(11)
Ni(2)–N(3)	2.101(15)	Ni(2)–N(4)	2.080(14)
Ni(1)···Ni(2)	12.1356(37)		
		angles	
P(1)–Au(1)–S(1)	176.01(14)	P(2)–Au(2)–S(2)	176.46(14)
P(3)–Au(3)–S(3)	175.85(15)	P(4)–Au(4)–S(4)	178.81(14)
P(2)–C(11)–C(12)	127.5(11)	P(3)–C(12)–C(11)	120.7(11)
P(4)–C(23)–C(24)	124.7(12)	P(1)–C(24)–C(23)	121.9(11)
S(1)–Ni(1)–S(2)	98.67(13)	S(1)–Ni(1)–O(1)	92.7(3)
S(1)–Ni(1)–O(3)	92.5(3)	S(1)–Ni(1)–N(1)	79.8(3)
S(1)–Ni(1)–N(2)	171.2(3)	S(2)–Ni(1)–O(1)	92.2(3)
S(2)–Ni(1)–O(3)	90.7(3)	S(2)–Ni(1)–N(1)	170.9(3)
S(2)–Ni(1)–N(2)	81.9(3)	O(1)–Ni(1)–O(3)	173.6(4)
O(1)–Ni(1)–N(1)	78.9(4)	O(1)–Ni(1)–N(2)	96.0(4)
O(3)–Ni(1)–N(1)	98.4(4)	O(3)–Ni(1)–N(2)	78.7(4)
N(1)–Ni(1)–N(2)	101.0(4)	S(3)–Ni(2)–S(4)	101.06(14)
S(3)–Ni(2)–O(5)	93.6(4)	S(3)–Ni(2)–O(7)	90.3(4)
S(3)–Ni(2)–N(3)	79.7(4)	S(3)–Ni(2)–N(4)	169.3(4)
S(4)–Ni(2)–O(5)	92.0(4)	S(4)–Ni(2)–O(7)	91.3(4)
S(4)–Ni(2)–N(3)	171.1(4)	S(4)–Ni(2)–N(4)	81.9(5)
O(5)–Ni(2)–O(7)	174.4(5)	O(5)–Ni(2)–N(3)	79.2(5)
O(5)–Ni(2)–N(4)	96.6(5)	O(7)–Ni(2)–N(3)	97.5(6)
O(7)–Ni(2)–N(4)	79.3(5)	N(3)–Ni(2)–N(4)	99.0(6)

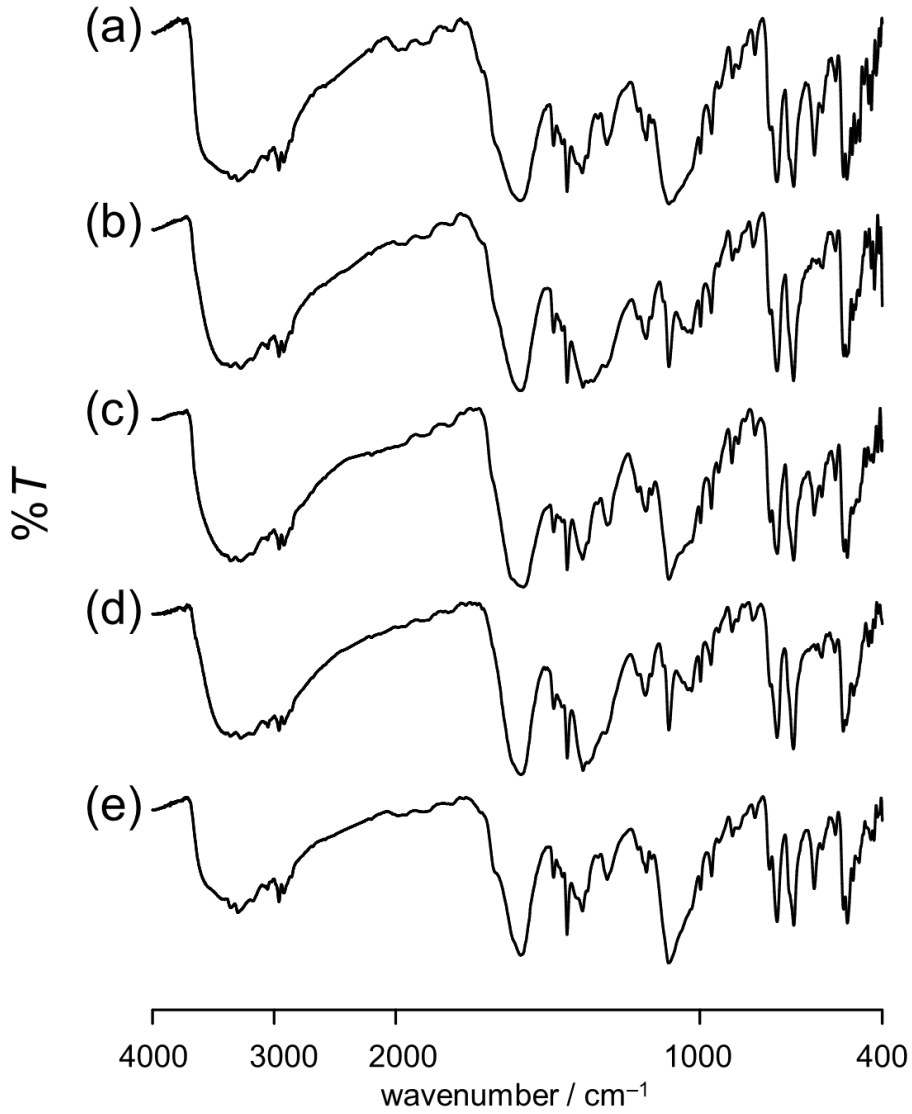

Figure 3-1. IR spectra of (a) [**7**]·2$HClO_4$, (b) [**7**]·4/3HNO_3, (c) [**7**]·2NH_4ClO_4, (d) [**7**]·4/3NH_4NO_3, and (e) reverted [**7**]·2$HClO_4$ (KBr disk).

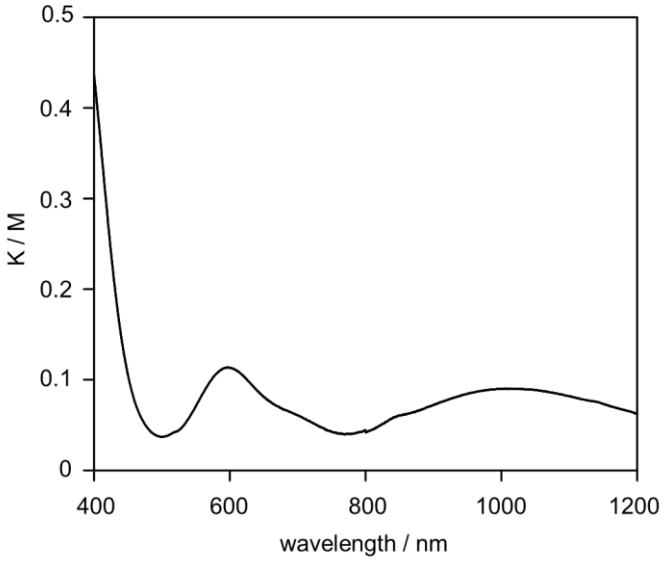

Figure 3-2. Diffuse reflection (DR) spectrum of [**7**]·2$HClO_4$ in the solid state.

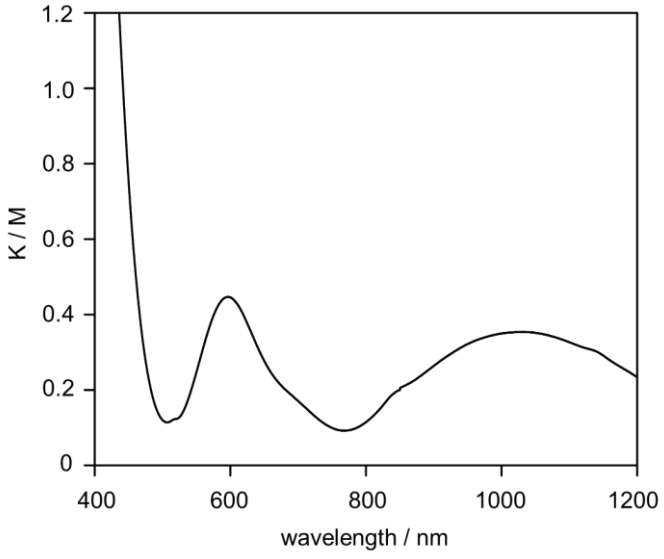

Figure 3-3. Diffuse reflection (DR) spectrum of [**7**]·4/3HNO_3 in the solid state.

(a)

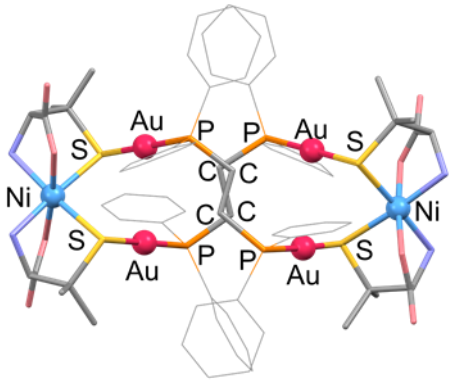

(b)

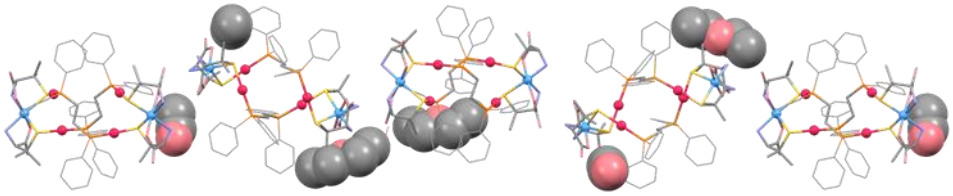

(c)

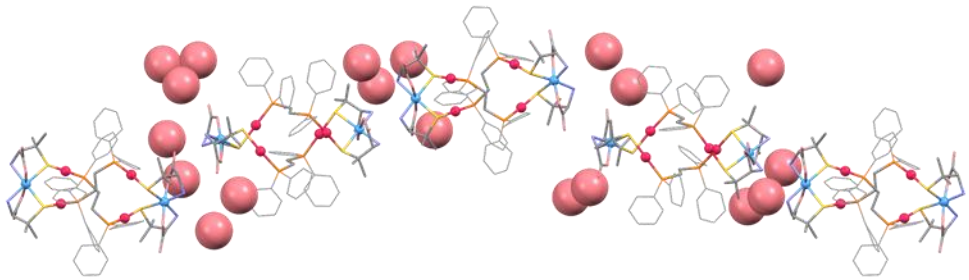

Figure 3-4. Perspective views of (a) complex molecule $[Au^{I}_{4}Ni^{II}_{2}(dppe)_2(D\text{-pen})_4]$, (b) supramolecular structure in $[Au_4Ni_2(dppe)_2(D\text{-pen})_4]\cdot 0.5EtOH\cdot 0.5Et_2O\cdot 25H_2O$ crystal, and (c) $[Au_4Ni_2(dppe)_2(D\text{-pen})_4]\cdot 16H_2O$ in previously reported paper. The molecules shown in space-filling models are the solvent molecules found in the crystal structure (ethanol and diethyl ether molecules for Figure 3-4b and water for Figure 3-4c, respectively).

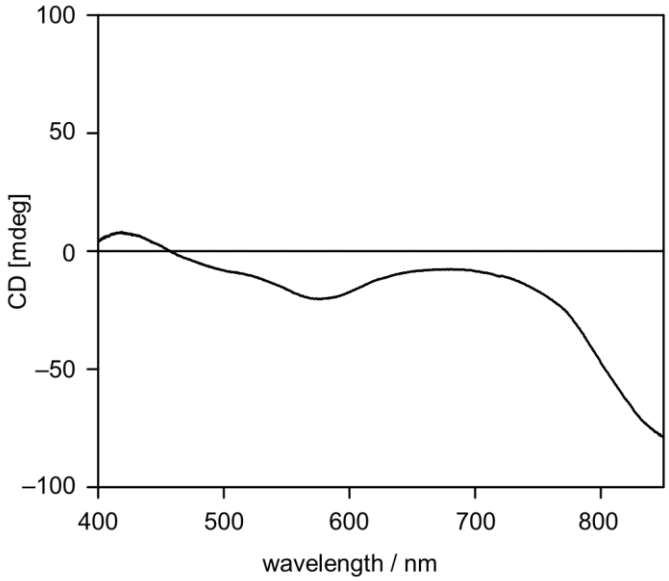

Figure 3-5. CD spectrum of [**7**]·2$HClO_4$ in the solid state.

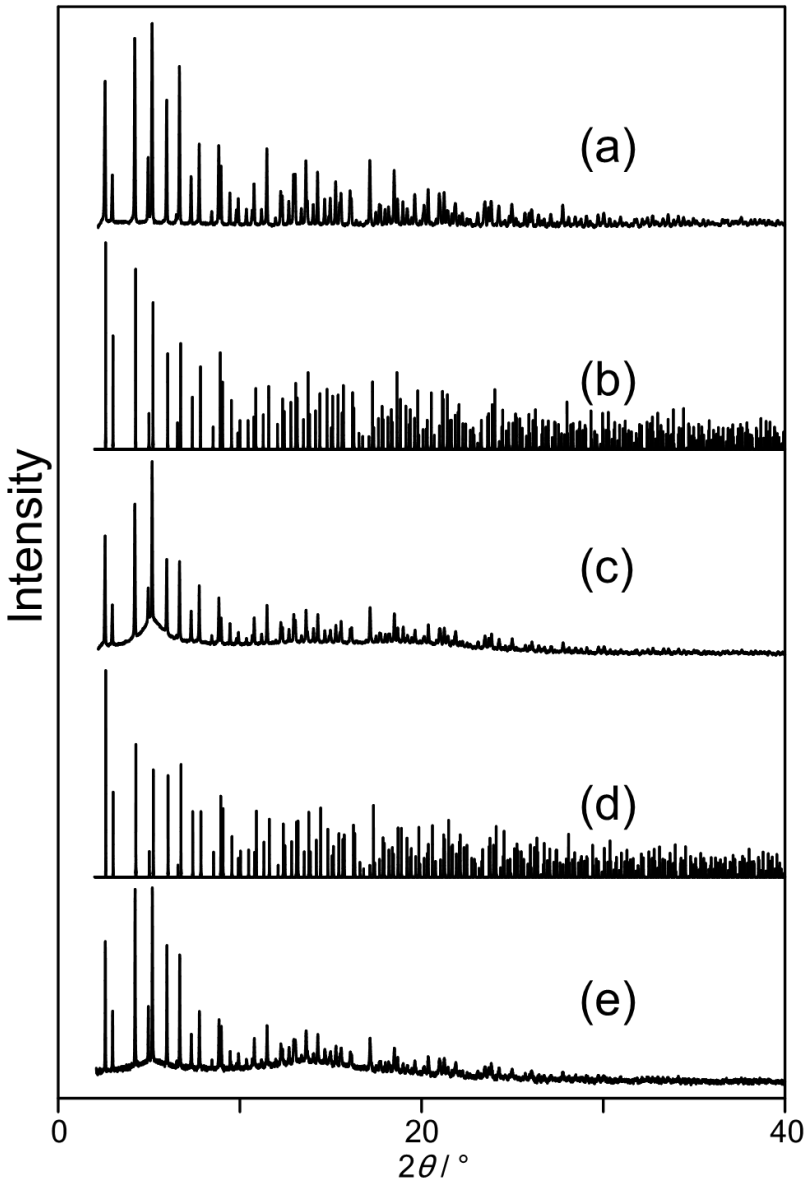

Figure 3-6. High resolution powder X-ray diffraction patterns of (a) [**7**]·2$HClO_4$, (c) [**7**]·2NH_4ClO_4, and (e) reverted [**7**]·2$HClO_4$, with simulated patterns calculated for the crystal structure of (b) [**7**]·2$HClO_4$ and (d) [**7**]·2NH_4ClO_4.

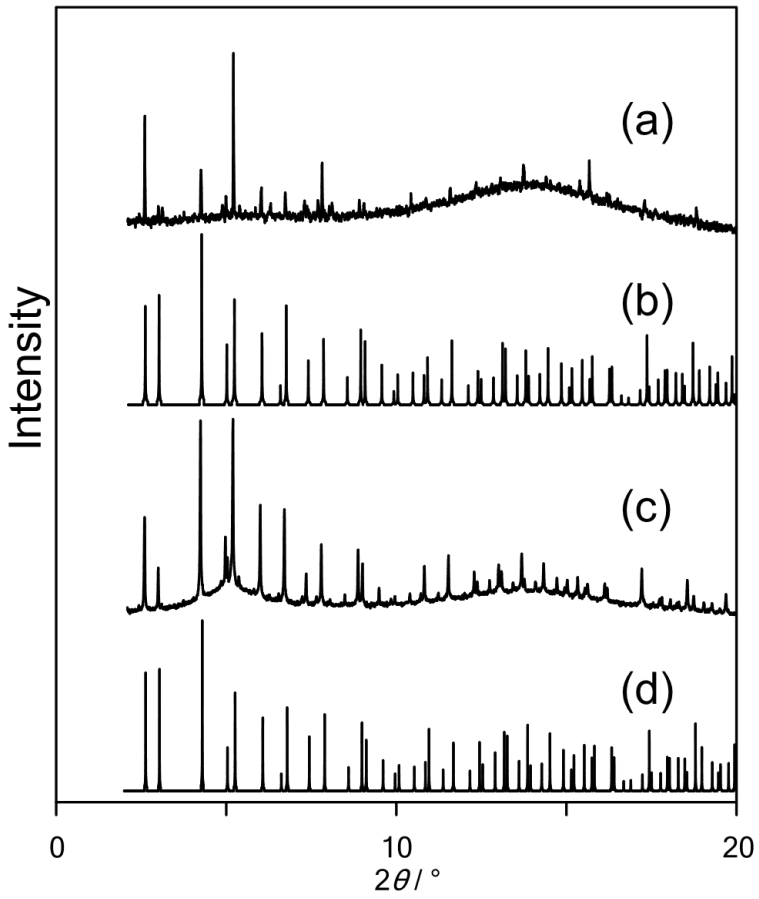

Figure 3-7. Powder X-ray diffraction patterns of (a) [**7**]·4/3HNO_3 and (c) [**7**]·4/3NH_4NO_3, with simulated patterns calculated for the crystal structure of (b) [**7**]·4/3HNO_3 and (d) [**7**]·4/3NH_4NO_3.

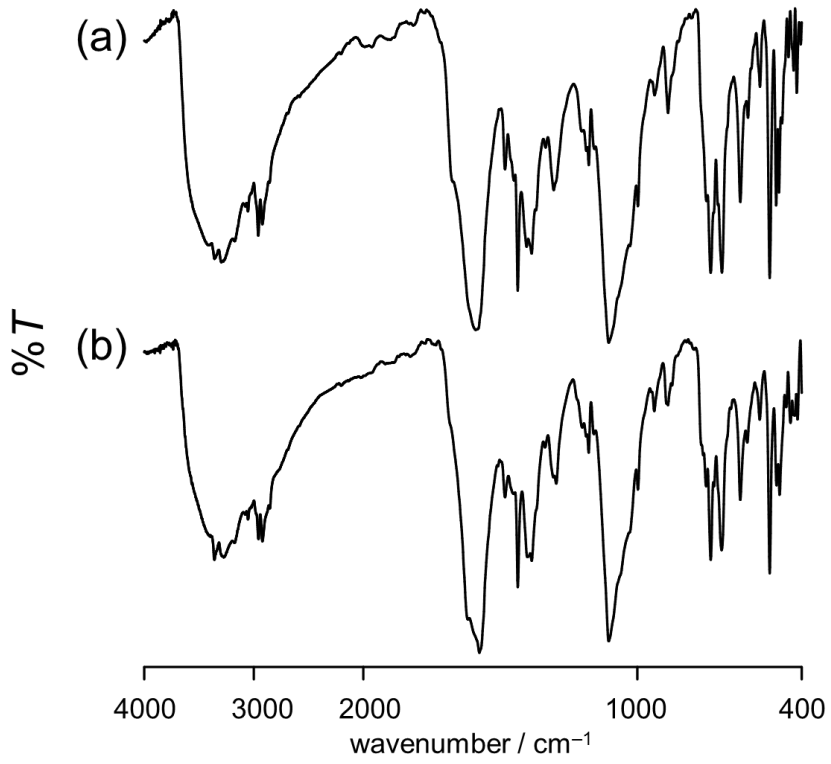

Figure 3-8. IR spectra of (a) [**8**]·2$HClO_4$ and (b) [**8**]·2NH_4ClO_4 (KBr disk).

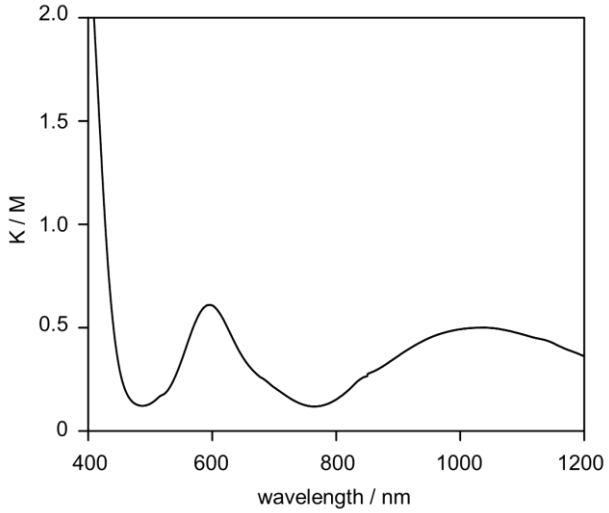

Figure 3-9. Diffuse reflection (DR) spectrum of [**8**]·2$HClO_4$ in the solid state.

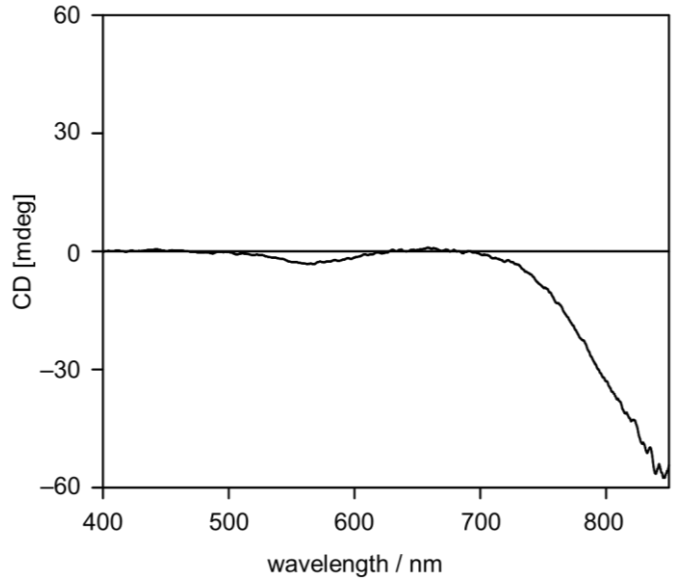

Figure 3-10. CD spectrum of [**8**]·2$HClO_4$ in the solid state.

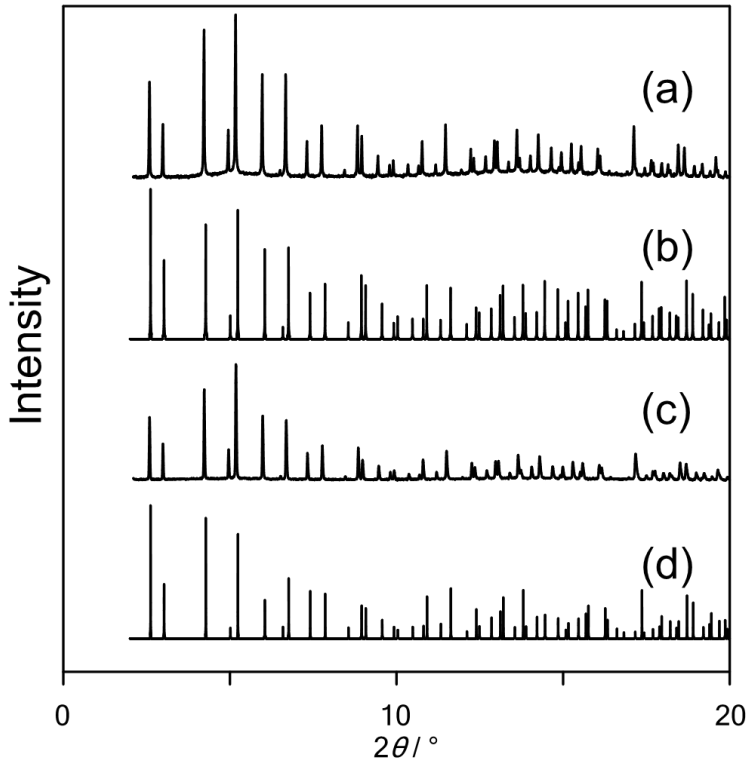

Figure 3-11. Powder X-ray diffraction patterns of (a) [**8**]·2$HClO_4$ and (c) [**8**]·2NH_4ClO_4, with simulated pattern calculated for the crystal structure of (b) [**8**]·2$HClO_4$ and (d) [**8**]·2NH_4ClO_4.

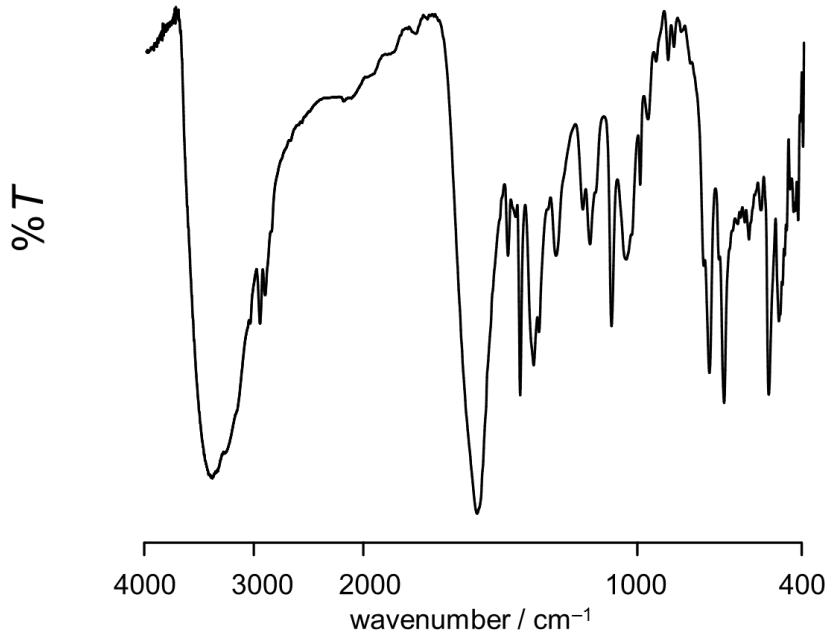

Figure 3-12. IR spectrum of [**9**] (KBr disk).

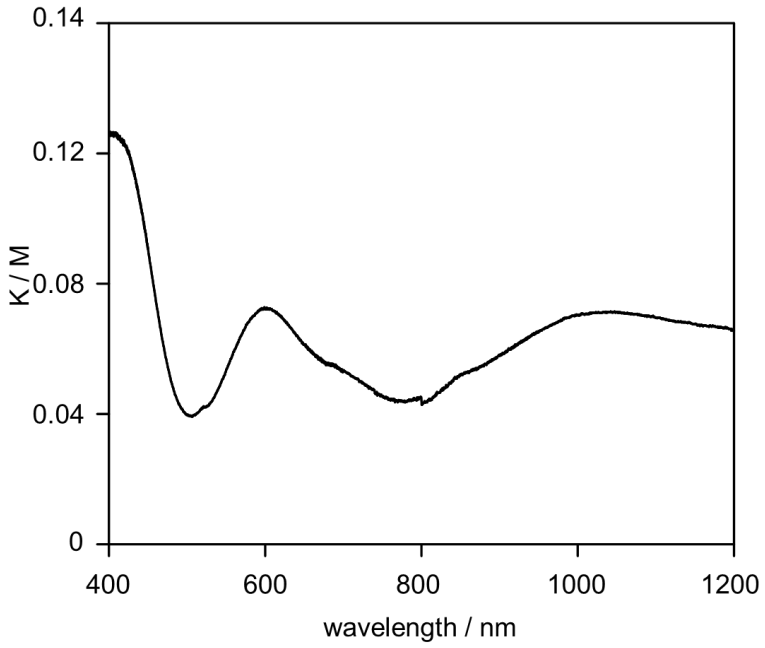

Figure 3-13. Diffuse reflection (DR) spectrum of [**9**] in the solid state.

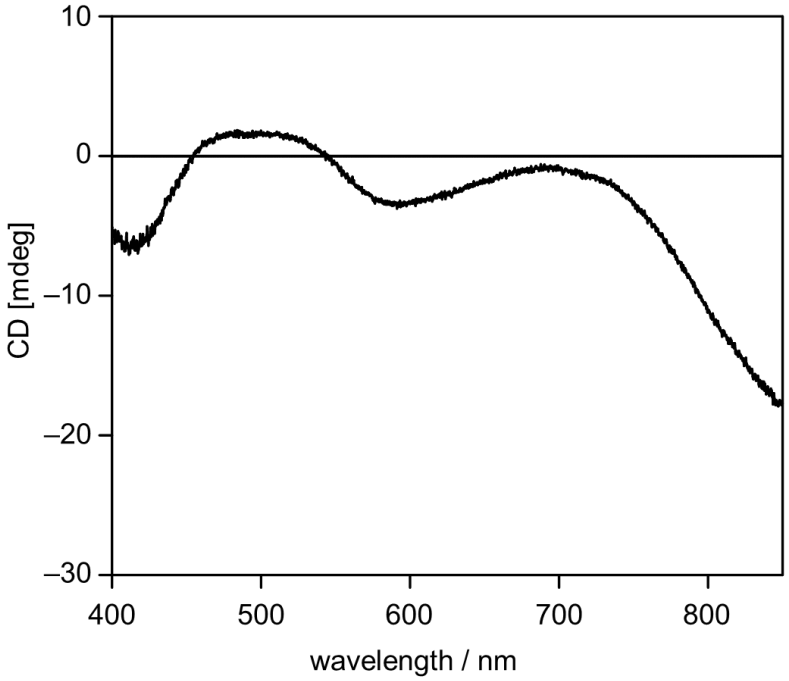

Figure 3-14. CD spectrum of [**9**] in the solid state.

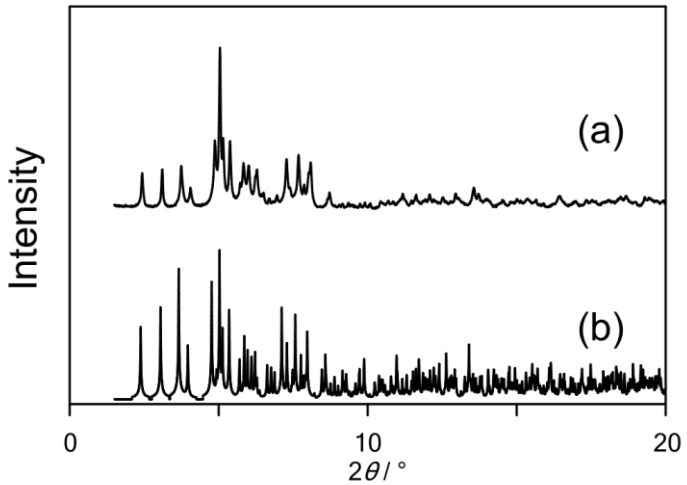

Figure 3-15. Powder X-ray diffraction patterns (a) observed for [**9**] with (b) simulated patterns calculated for the crystal structure of [**9**].

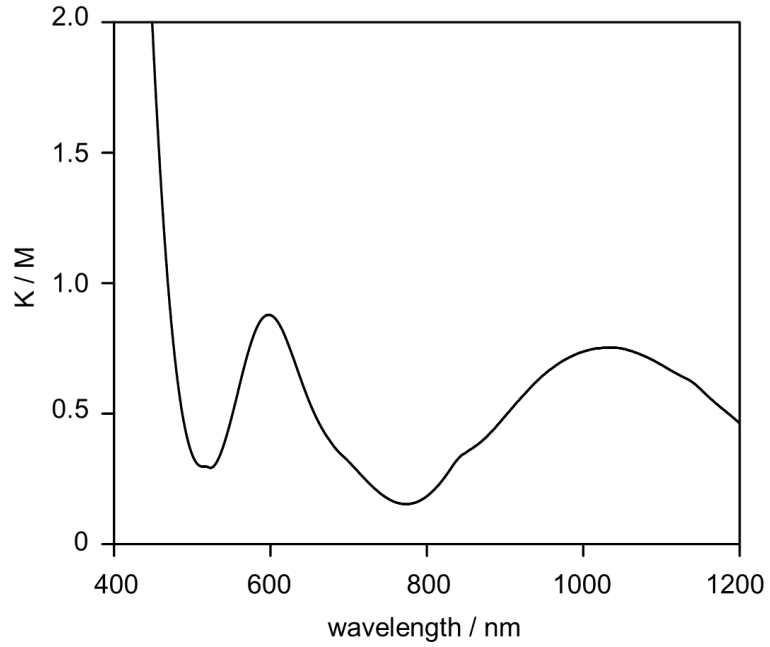

Figure 3-16. Diffuse reflection (DR) spectrum of [**7**]·2NH_4ClO_4 in the solid state.

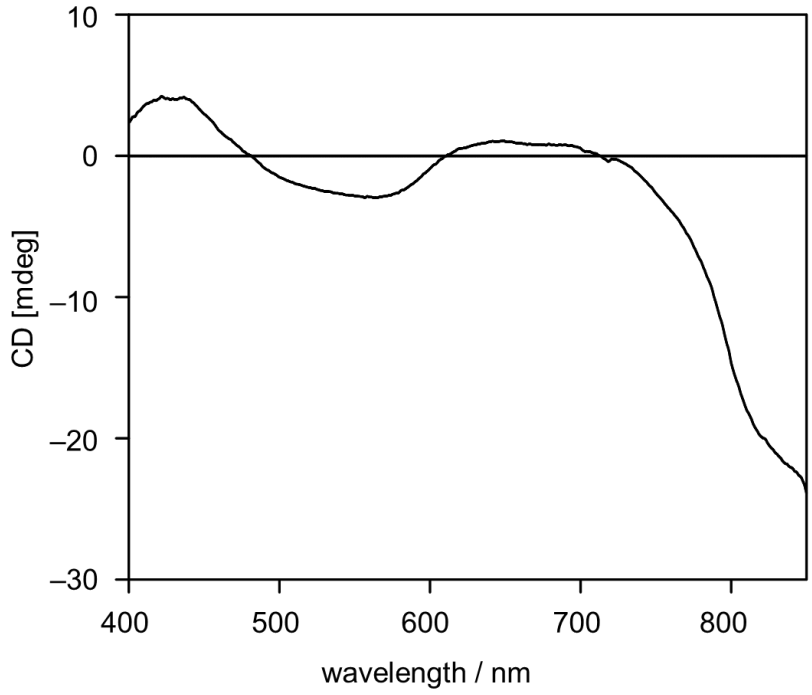

Figure 3-17. CD spectrum of [**7**]·2NH_4ClO_4 in the solid state.

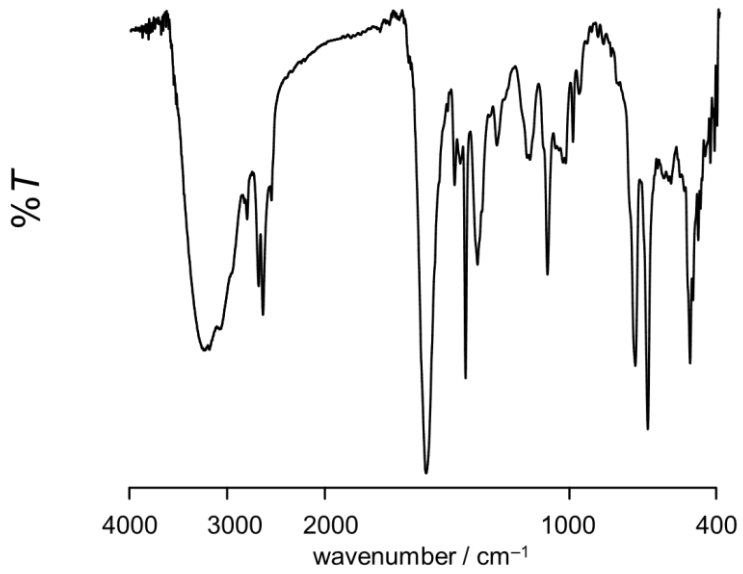

Figure 3-18. IR spectrum of [**10**] (KBr disk).

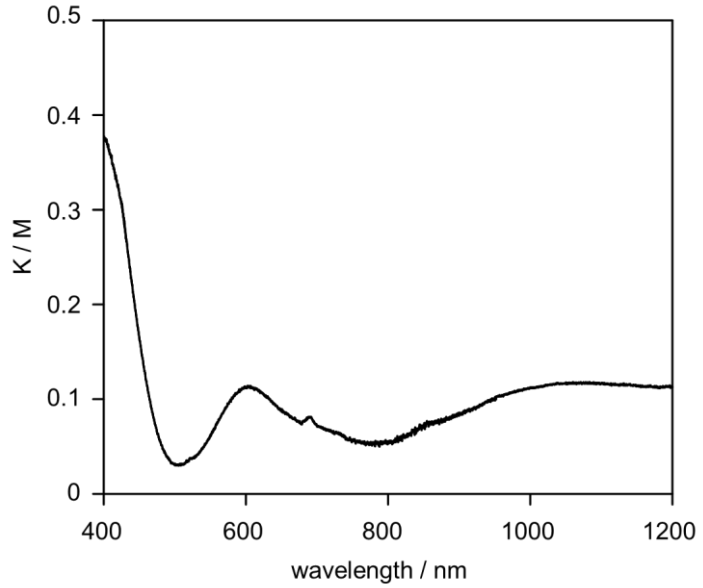

Figure 3-19. Diffuse reflection (DR) spectrum of [**10**] in the solid state.

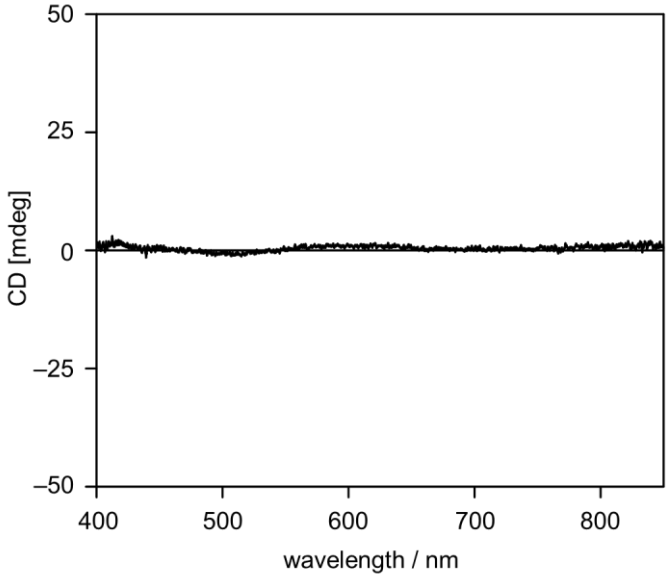

Figure 3-20. CD spectrum of [**10**] in the solid state.

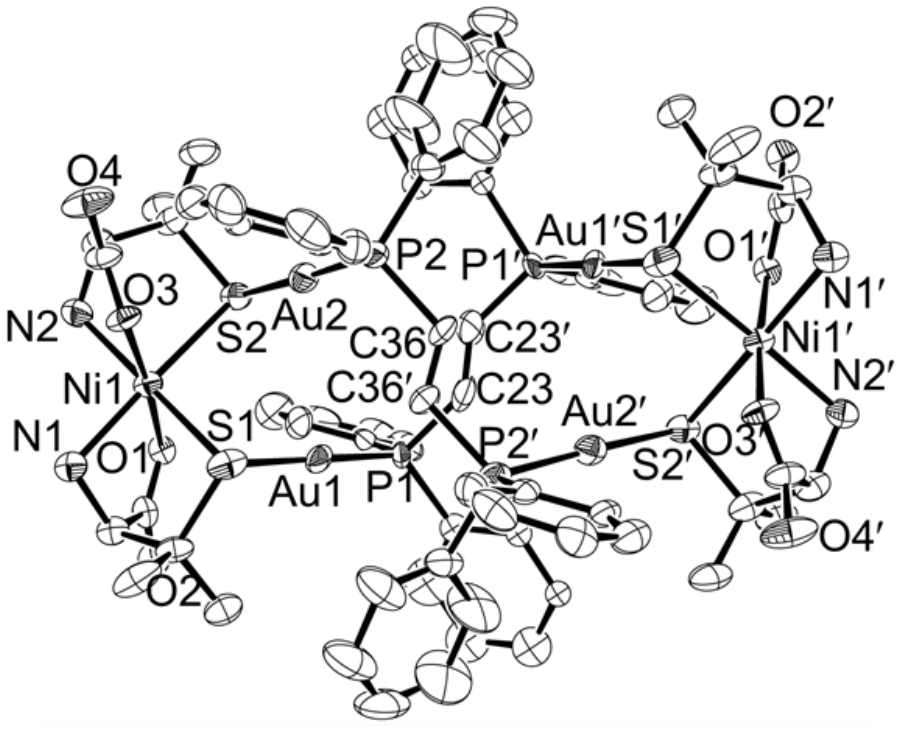

Figure 3-21. An ortep drawing of complex molecule in [**7**]·2$HClO_4$ with the atomic labeling scheme. Hydrogen atoms are omitted for clarity. One part of the disordered atoms is omitted. Symmetry code: (') x, 1–y, 1–z. Thermal ellipsoids were drawn in a 50 % level.

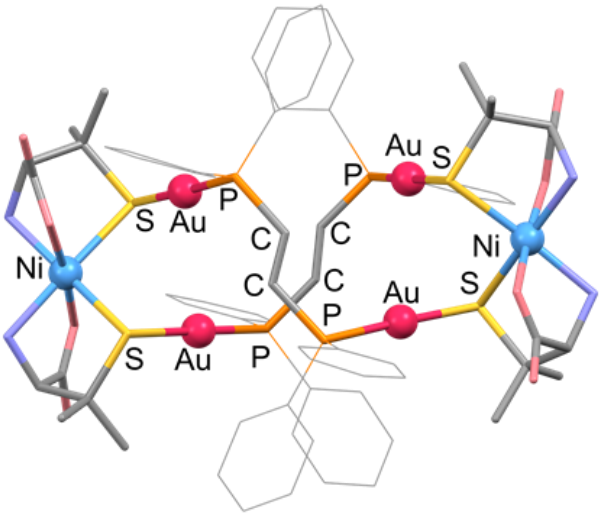

Figure 3-22. Twisted 18-membered metalloring in [**7**]·2HClO$_4$.

(a)

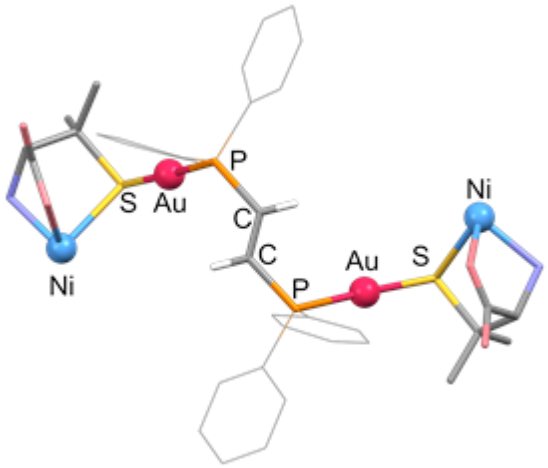

(b)

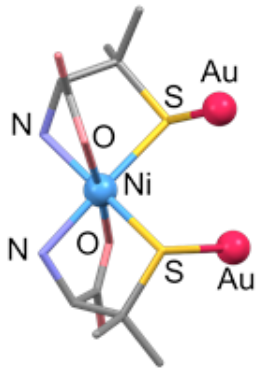

Figure 3-23. (a) Bis(tridentate-*N*,*O*,*S*) coordination mode of the metalloligand and (b) coordination geometry of Ni^{II} atom in [**7**]·2HClO$_4$.

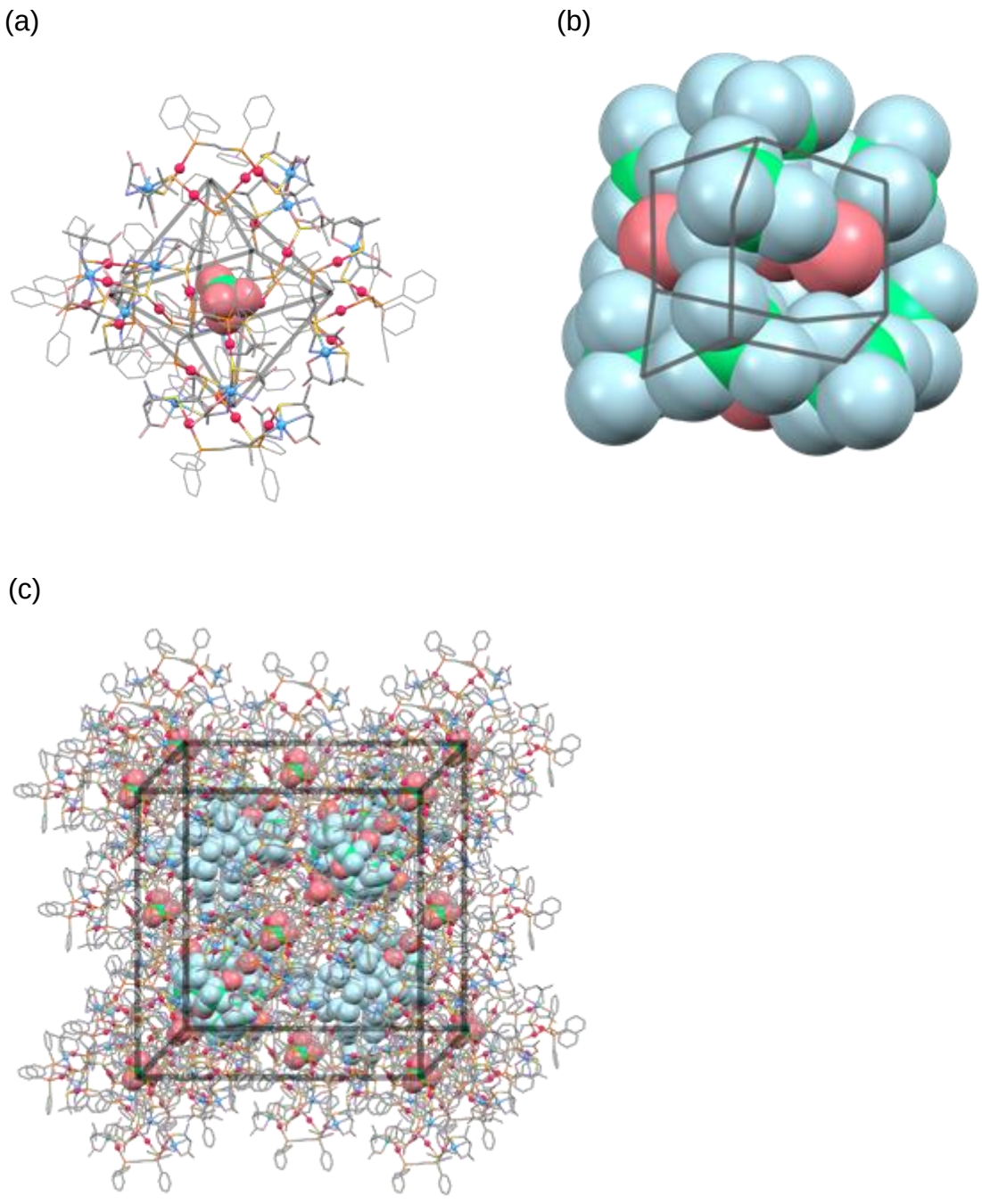

Figure 3-24. Perspective views of (a) hexameric supramolecular structure of the complex molecules accommodating one perchlorate anion, (b) adamantane-like cluster composed of 10 perchlorate anions with 4 oxonium cations inside the tetrahedral interstice, and (c) packing structure in [**7**]·2$HClO_4$.

(a) (b)

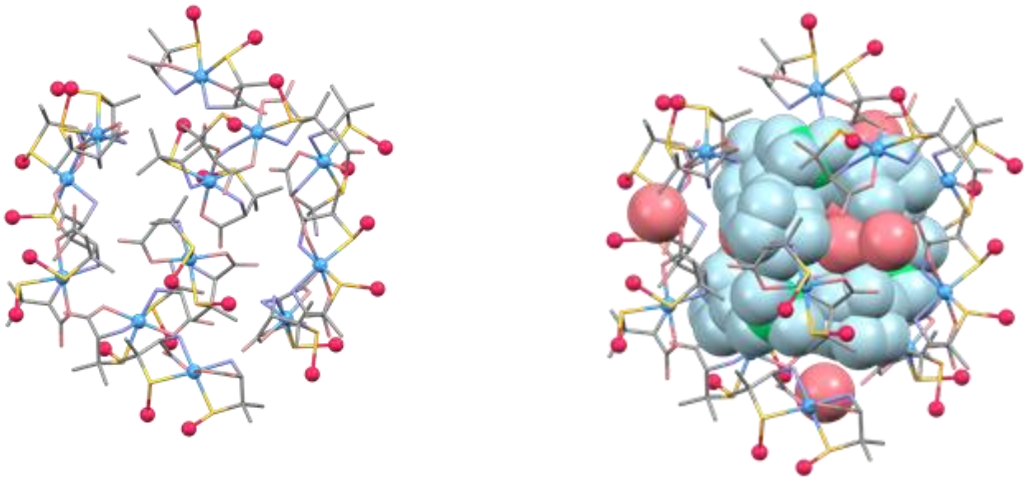

Figure 3-25. Perspective views of hydrophilic tetrahedral interstice (a) without accommodated molecules and (b) with accommodated molecules in the crystal structure of [**7**]·2$HClO_4$.

(a) (b)

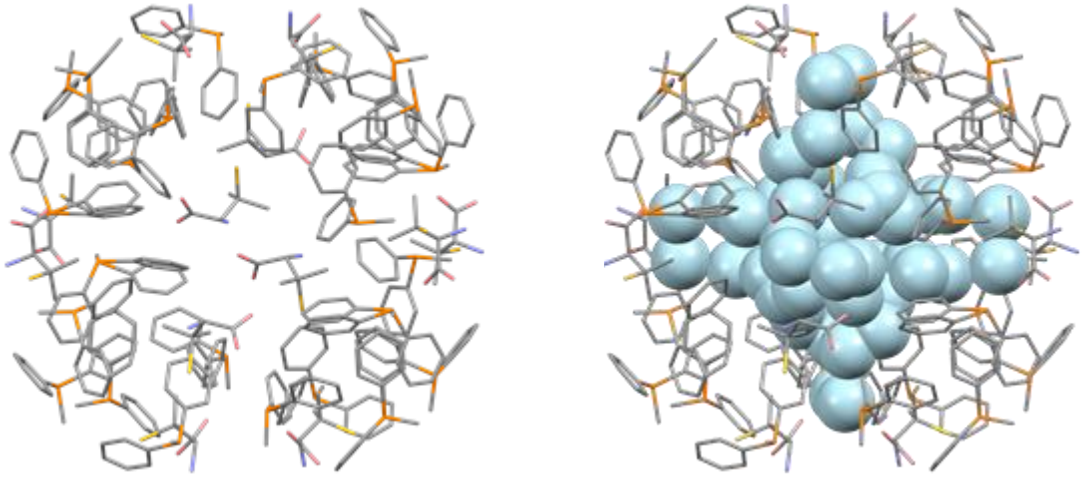

Figure 3-26. Perspective views of hydrophobic tetrahedral interstice (a) without accommodated molecules and (b) with accommodated water molecules in the crystal structure of [**7**]·2$HClO_4$.

(a) (b)

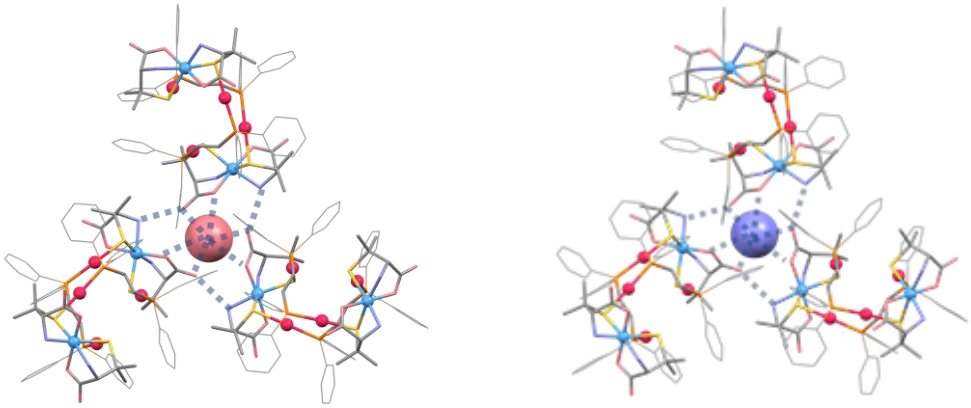

Figure 3-27. Perspective views of the hydrogen bonds on the face of supramolecular octahedron ({[**7**]}$_6$) in the crystal structure of (a) [**7**]·2HClO$_4$, and (b) [**7**]·2NH$_4$ClO$_4$.

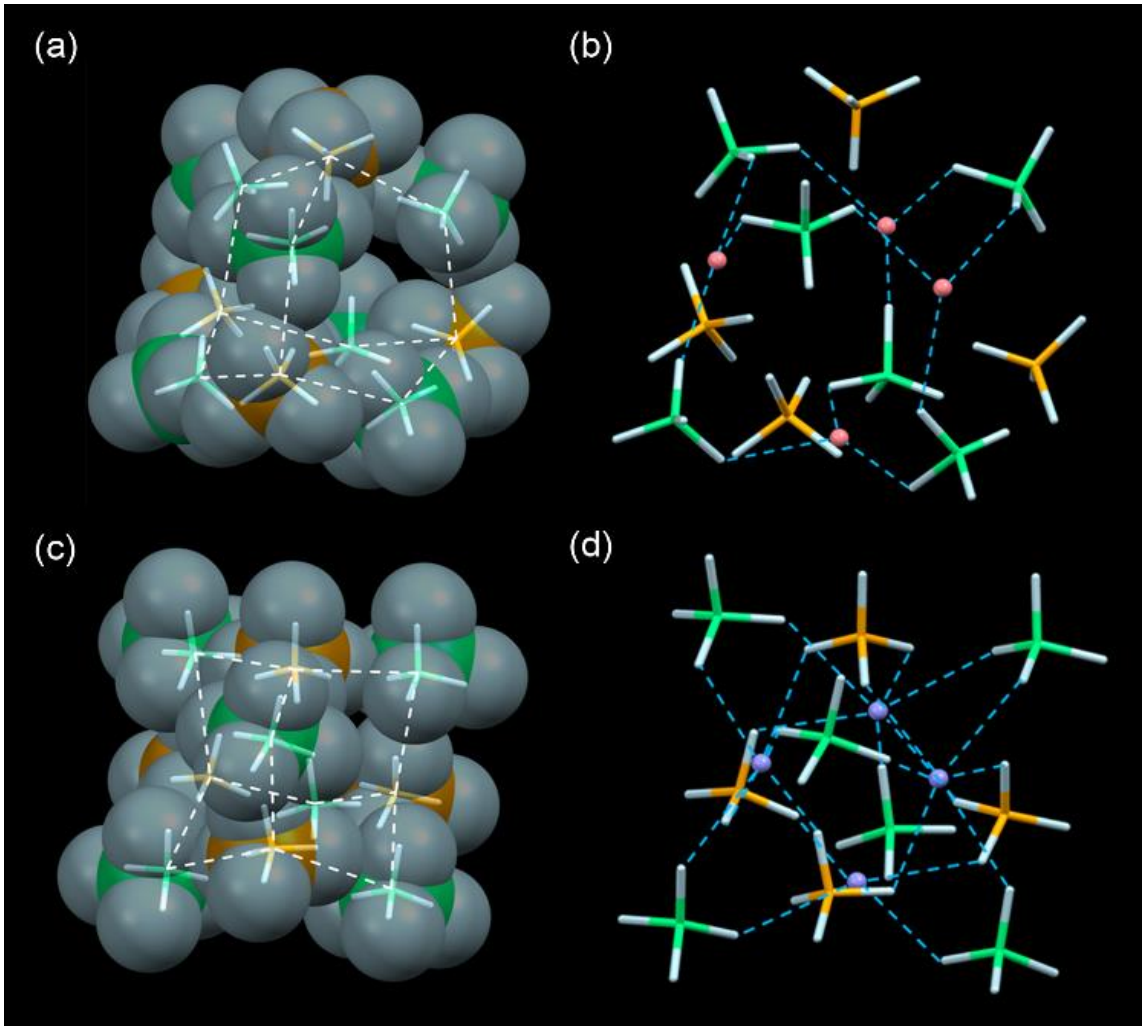

Figure 3-28. Perspective views of (a) the $\{ClO_4^-\}_{10}$ adamantane (space-filling and stick models) and (b) the $\{ClO_4^-\}_{10}$ adamantane with H_3O^+ ions (pink balls) in [**7**]·2$HClO_4$. Perspective views of (c) the $\{ClO_4^-\}_{10}$ adamantane (space-filling and stick models) and (d) the $\{ClO_4^-\}_{10}$ adamantane with NH_4^+ ions (blue balls) in [**7**]·2NH_4ClO_4. The Cl atoms of ClO_4^- ions at site **A** and site **B** are green and orange, respectively.

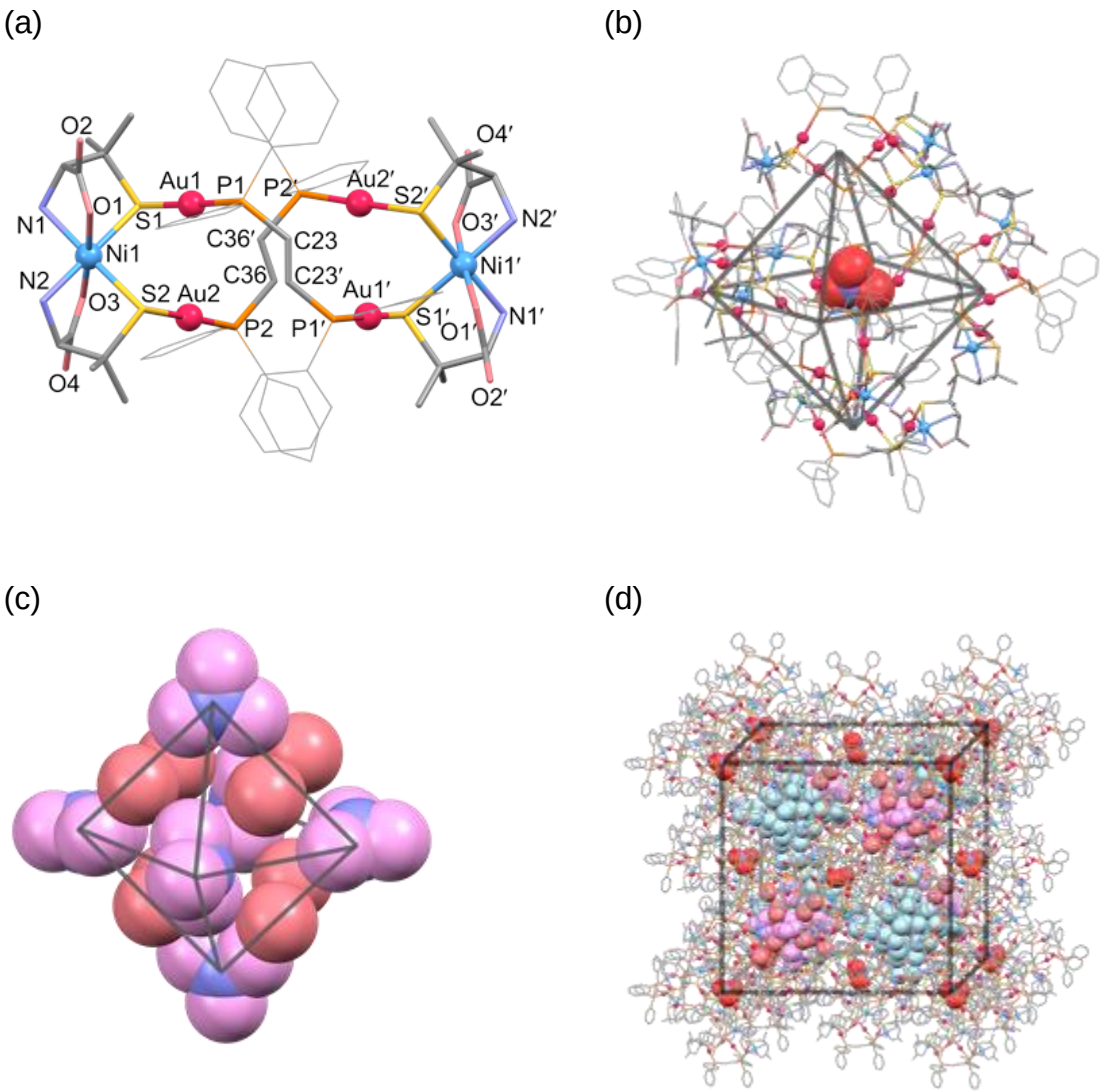

Figure 3-29. Perspective views of (a) complex molecule with some of the atomic labeling scheme, (b) hexameric supramolecular structure of the complex molecules accommodating one nitrate anion, (c) octahedron-like cluster composed of 6 nitrate anions and 8 oxonium cations / water molecules inside the tetrahedral interstice, and (d) packing structure in [**7**]·4/3HNO_3. Symmetry code: (') 1–x, y, 1–z.

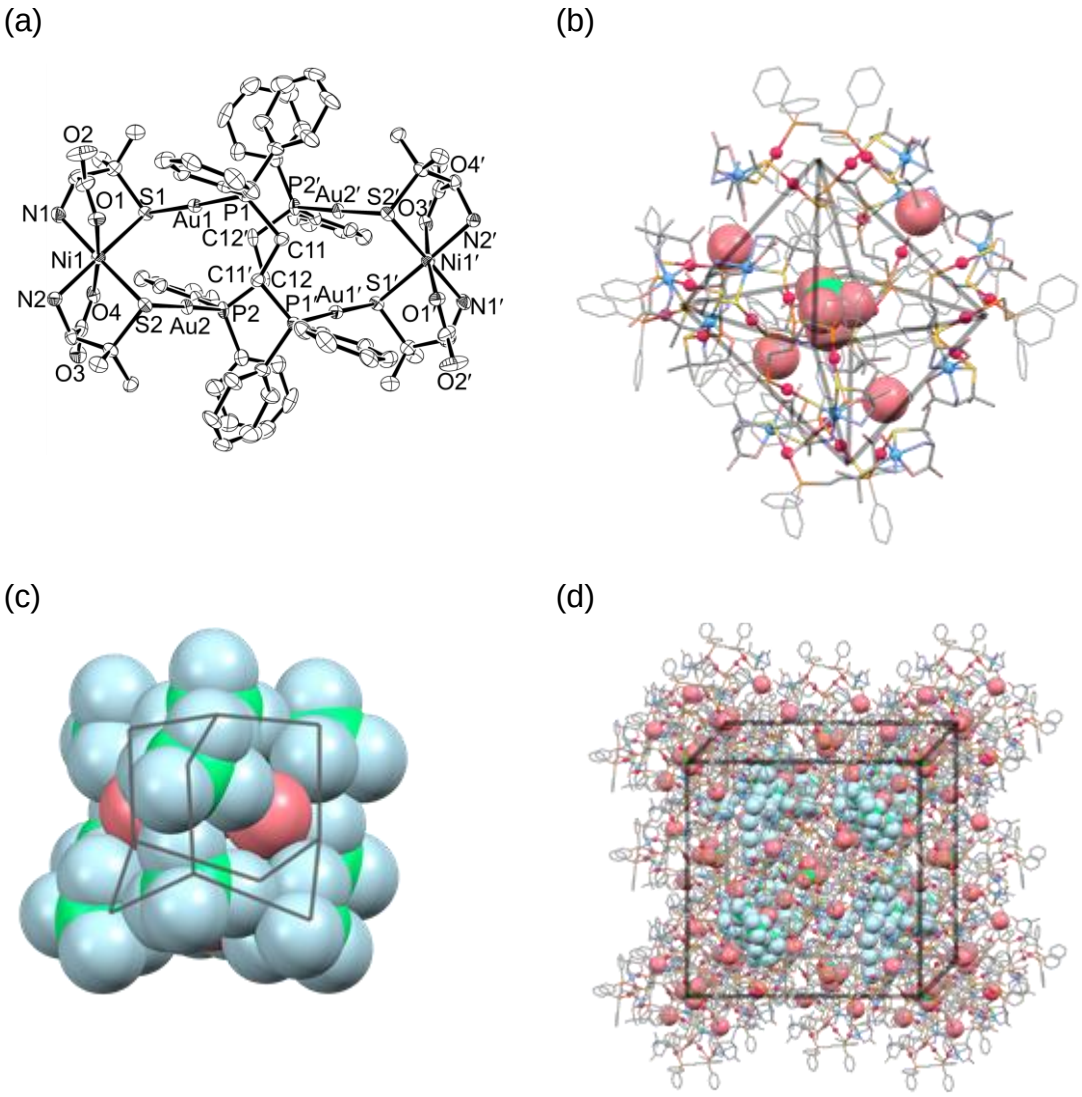

Figure 3-30. Perspective views of (a) complex molecule with the atomic labeling scheme, (b) hexameric supramolecular structure of complex molecules accommodating one water molecule, (c) adamantane-like cluster composed of 10 perchlorate anions inside the tetrahedral interstice with accommodated oxonium cations, and (d) packing structure in [**8**]·2HClO$_4$. Symmetry code: (') x, 3/2–y, 3/2–z. Thermal ellipsoids were drawn in a 50 % level.

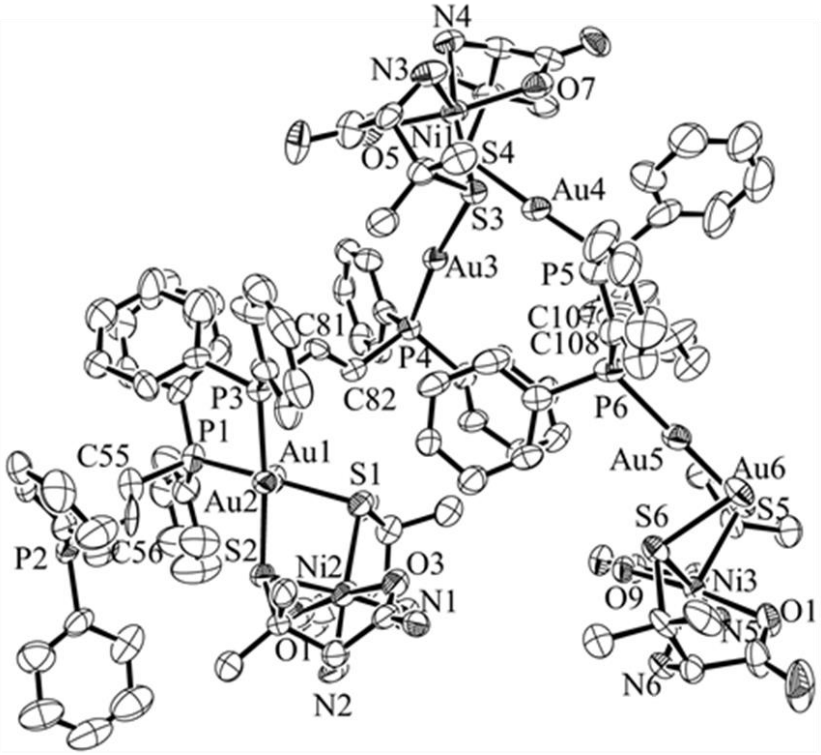

Figure 3-31. An ortep drawing of complex chain in [**9**] with the atomic labeling scheme. Hydrogen atoms are omitted for clarity. Thermal ellipsoids were drawn in a 50 % level.

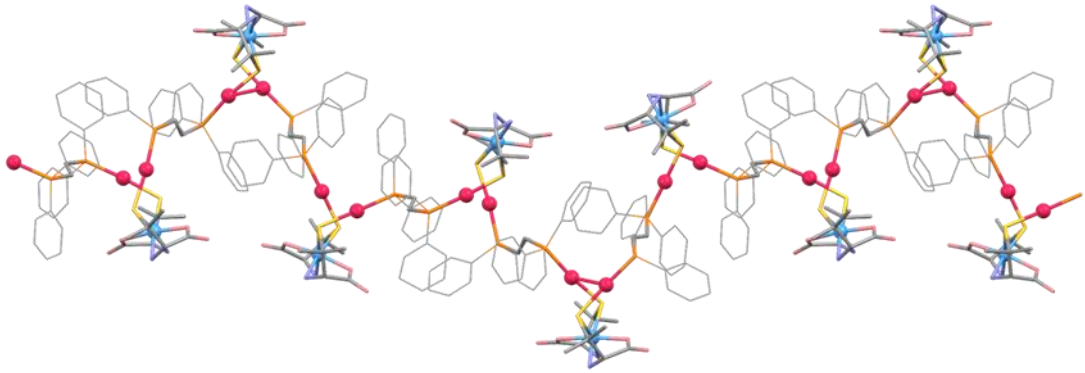

Figure 3-32. S-Bridged $Au^{I}_{2}Ni^{II}$ 1D chain structure in [**9**].

(a)

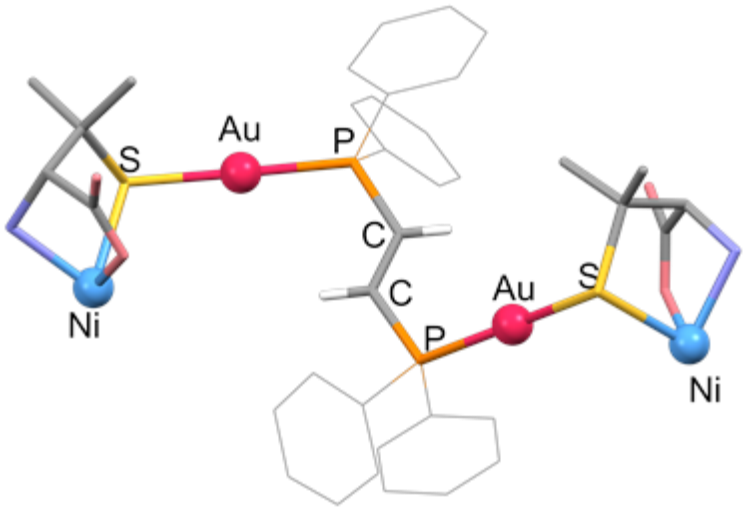

(b)

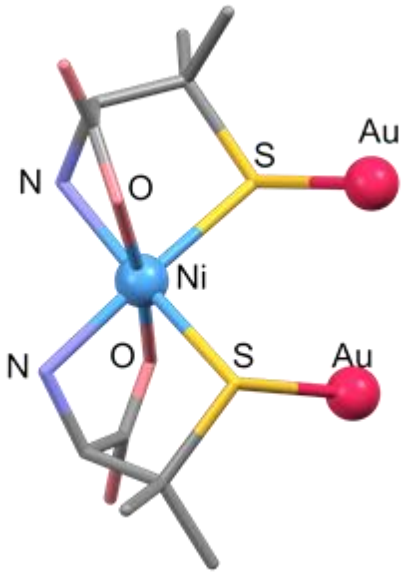

Figure 3-33. (a) Bis(tridentate-*N*,*O*,*S*) coordination mode of the metalloligand, and (b) coordination geometry of Ni^{II} atom in [**9**].

(a)

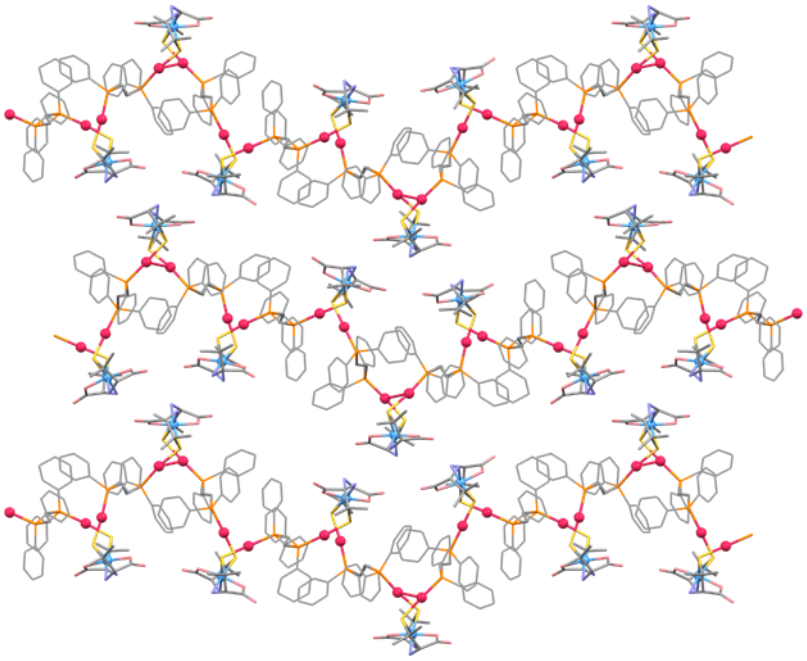

(b)

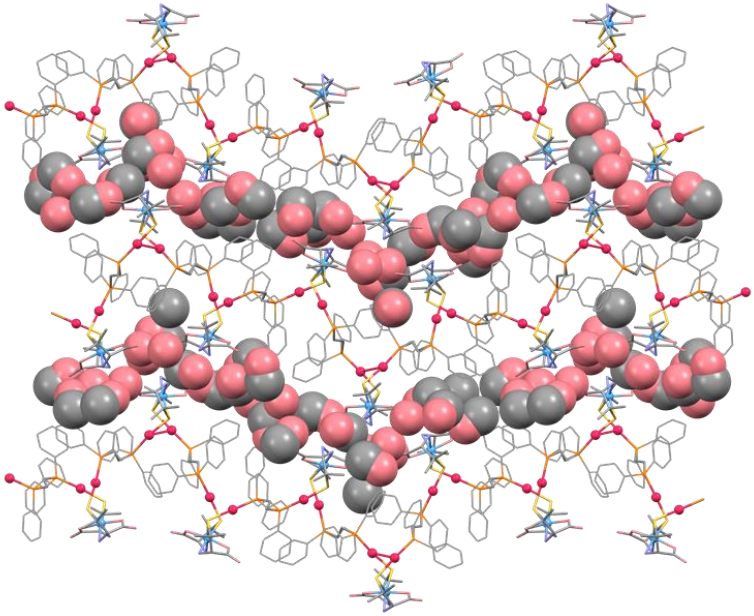

Figure 3-34. Supramolecular structure of the complex chain in [**9**] (a) without solvated molecules and (b) with solvated molecules in space filling model.

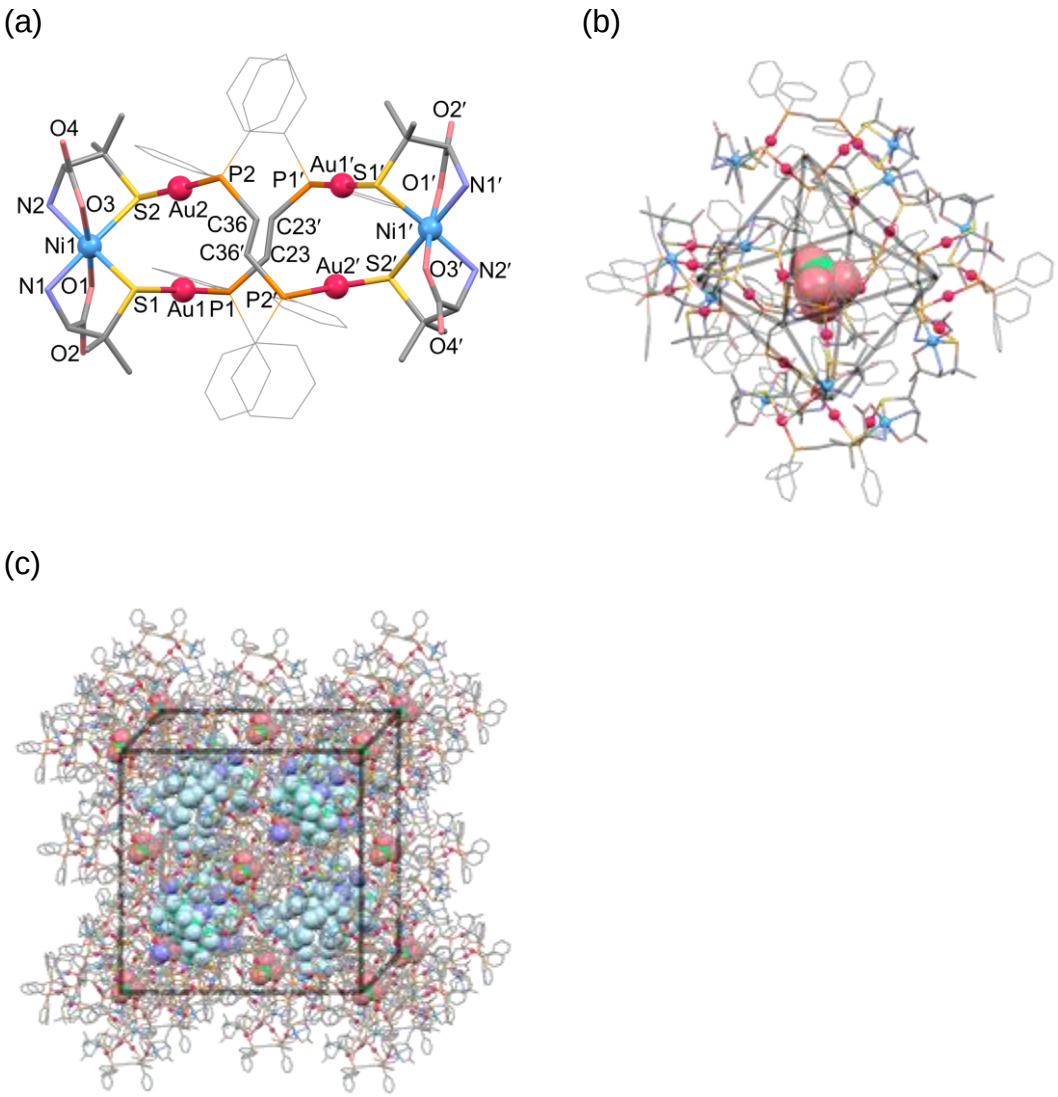

Figure 3-35. Perspective views of (a) complex molecule with the atomic labeling scheme, (b) hexameric supramolecular structure of complex molecules accommodating one perchlorate anion, and (c) packing structure in [**7**]·2NH_4ClO_4. Symmetry code: (′) x, 1–y, 1–z.

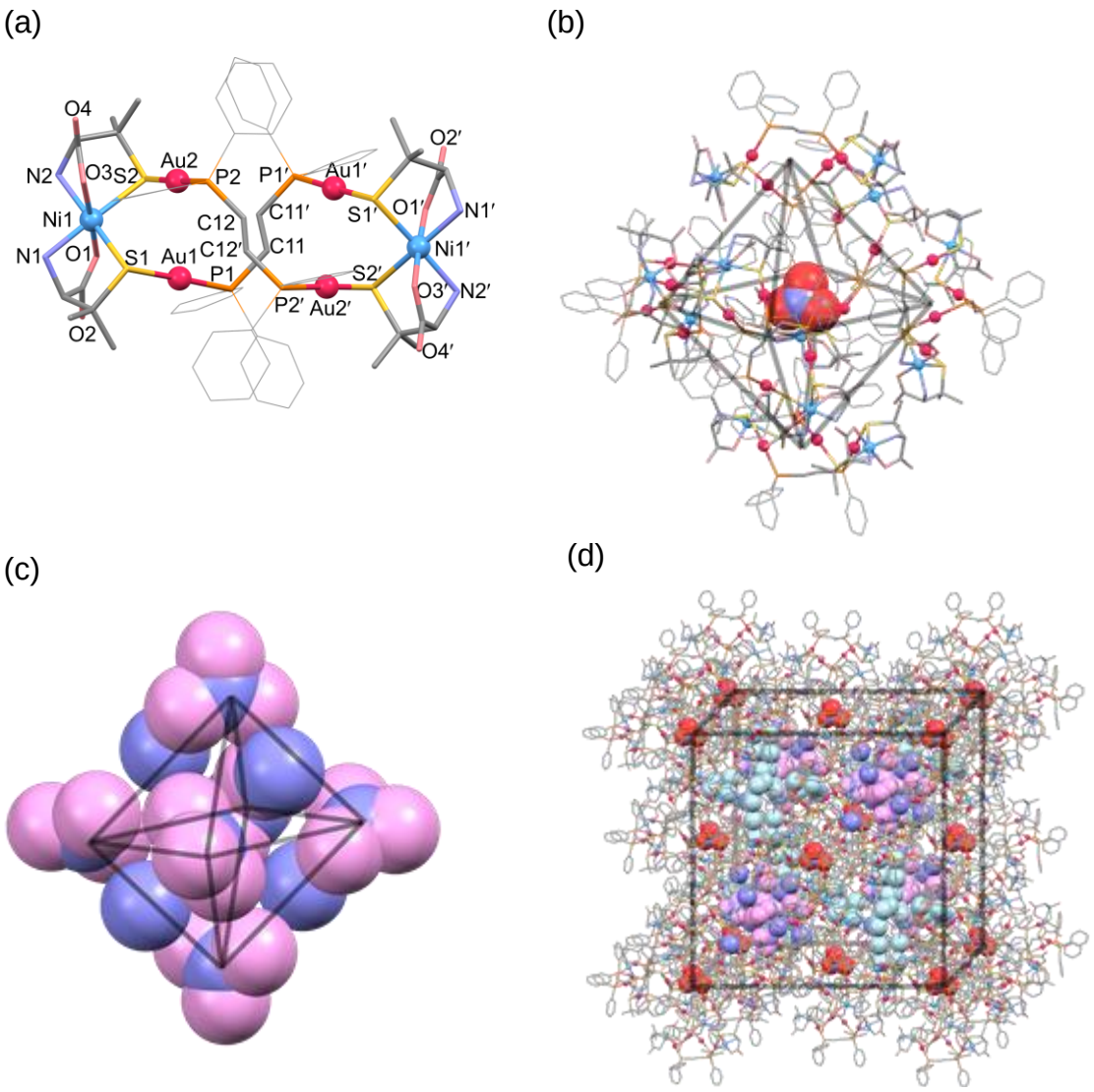

Figure 3-36. Perspective views of (a) complex molecule with the atomic labeling scheme, (b) hexameric supramolecular structure of complex molecules accommodating one nitrate anions, (c) octahedron-like cluster composed of 6 nitrate anions inside the tetrahedral interstice with ammonium cations, and (d) packing structure in [**7**] $\cdot 4/3NH_4NO_3$. Symmetry code: (') 1–x, 1–y, z.

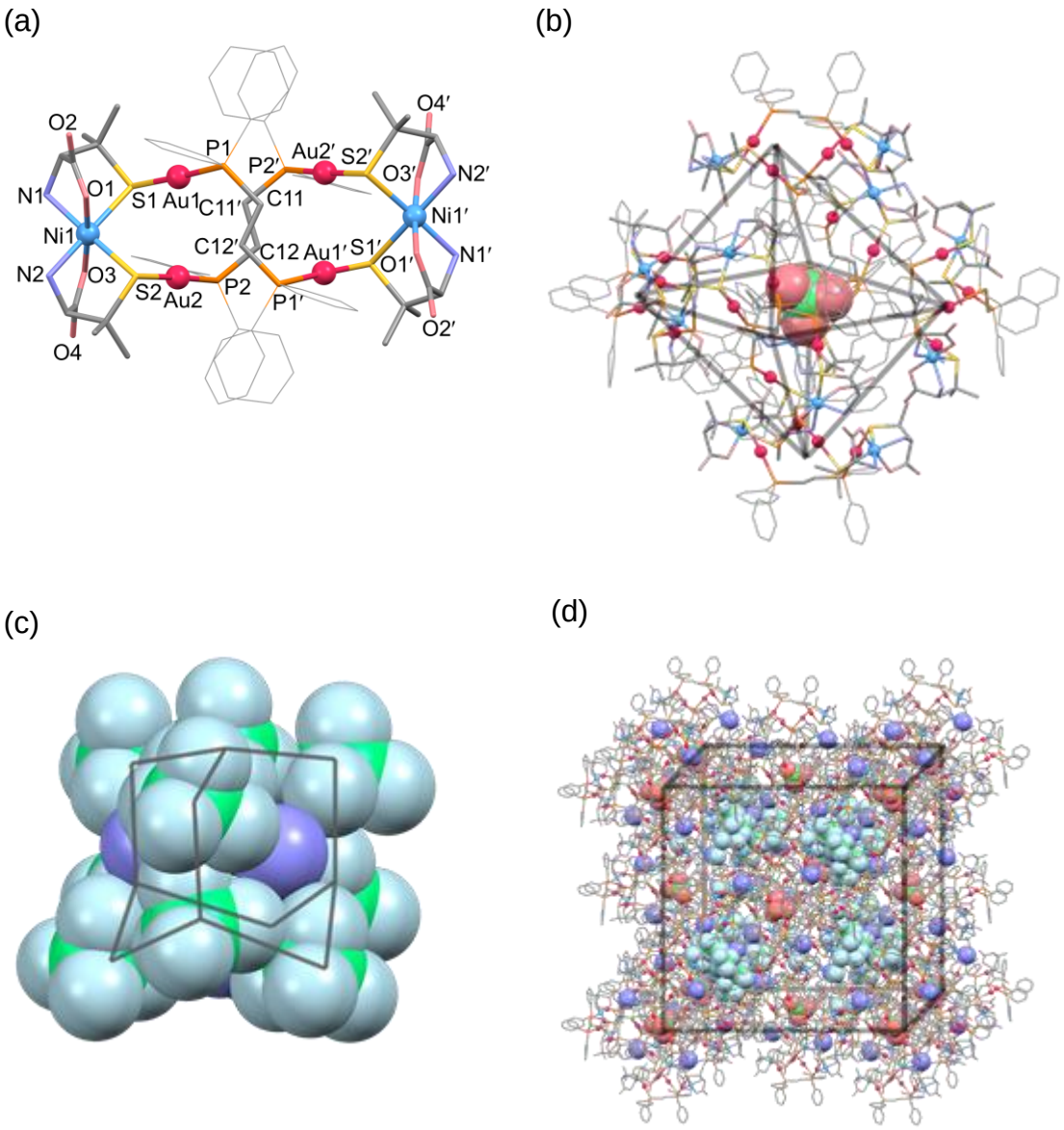

Figure 3-37. Perspective views of (a) complex molecule with the atomic labeling scheme, (b) hexameric supramolecular structure of complex molecules accommodating one perchlorate anions, (c) adamantane-like cluster composed of 10 perchlorate anions inside the tetrahedral interstice with accommodated ammonium cations, and (d) packing structure in [**8**]·2NH_4ClO_4. Symmetry code: (') x, 3/2–y, 1/2–z.

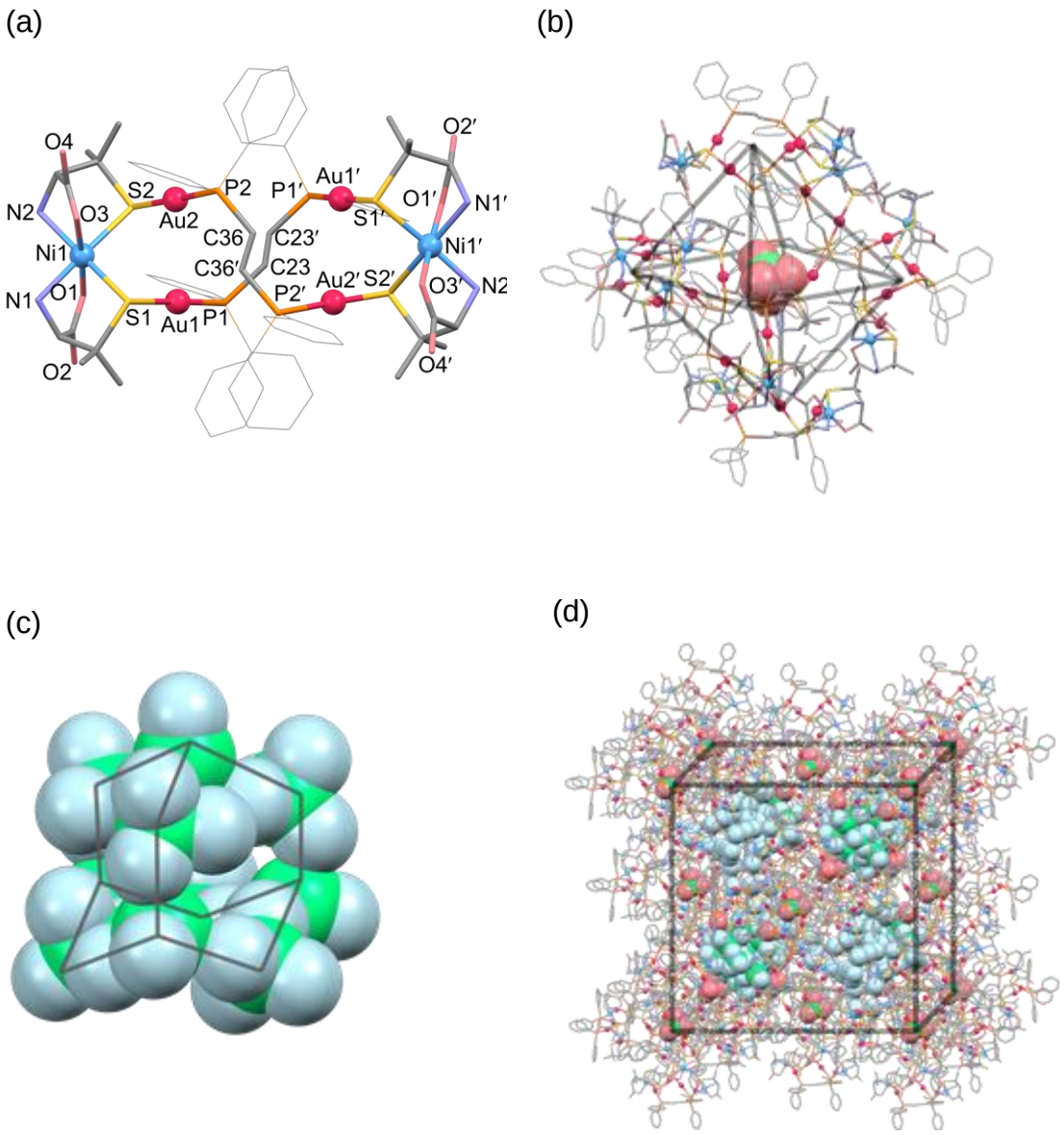

Figure 3-38. Perspective views of (a) complex molecule with the atomic labeling scheme, (b) hexameric supramolecular structure of complex molecules accommodating one perchlorate anions, (c) adamantane-like cluster composed of 10 perchlorate anions inside the tetrahedral interstice, and (d) packing structure in reverted [**7**]·2HClO$_4$. Symmetry code: (') x, 1–y, 1–z.

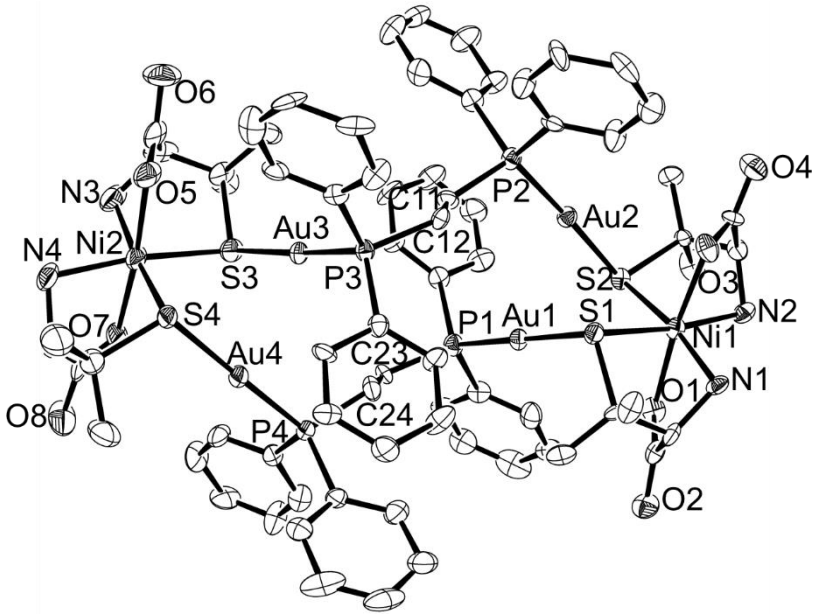

Figure 3-39. An ortep drawing of complex molecule in [**10**] with the atomic labeling scheme. Hydrogen atoms and solvent molecules are omitted for clarity. Thermal ellipsoids were drawn in a 50 % level.

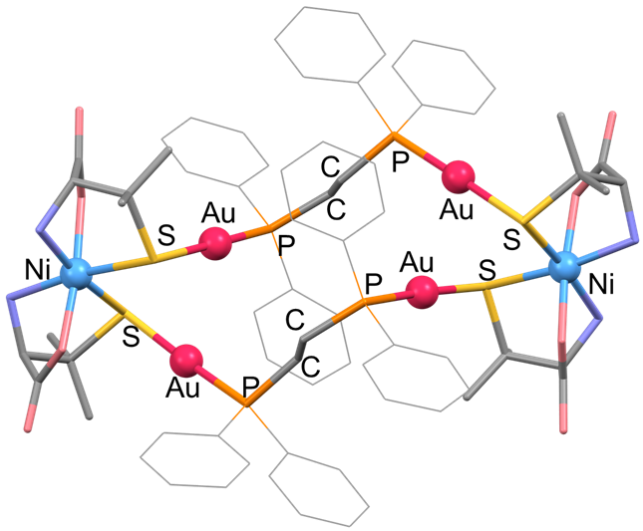

Figure 3-40. 18-Membered metalloring in [**10**].

(a)

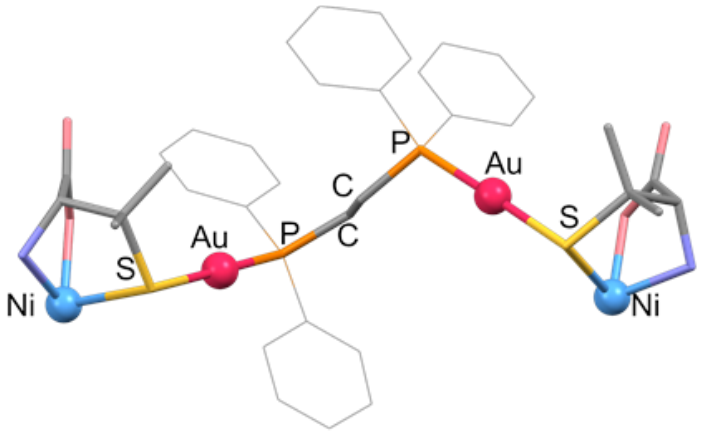

(b)

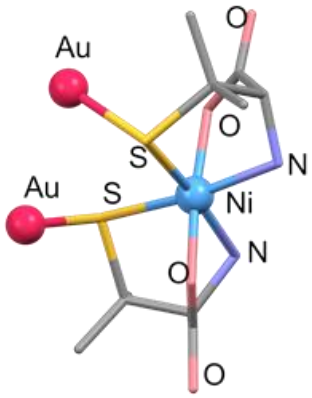

Figure 3-41. (a) Bis(tridentate-*N*,*O*,*S*) coordination mode of the metalloligand, (b) coordination geometry of Ni^{II} atom in [**10**].

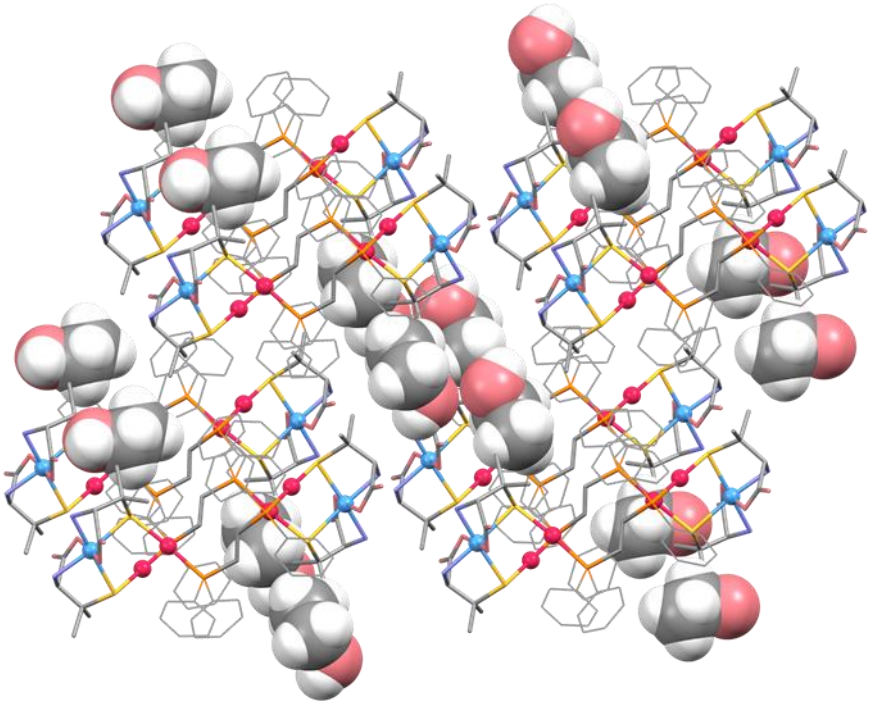

Figure 3-42. A packing structure of [**10**]. The EtOH molecules are represented as a space fill model.

(a)

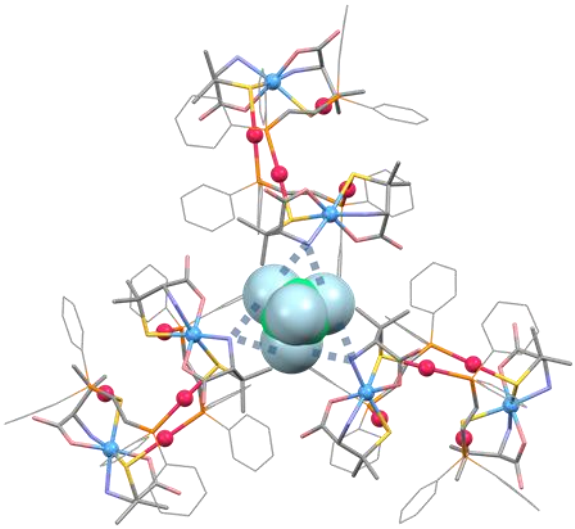

(b)

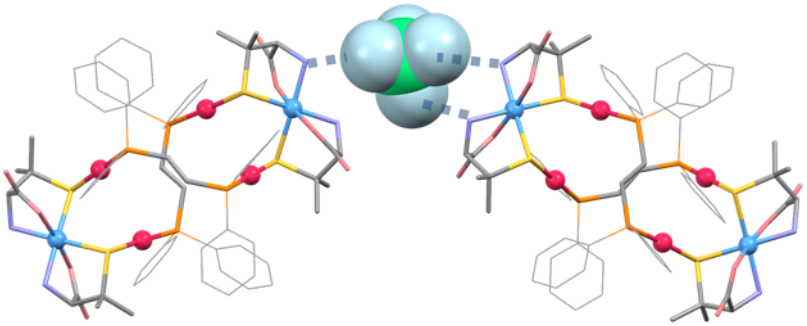

(c)

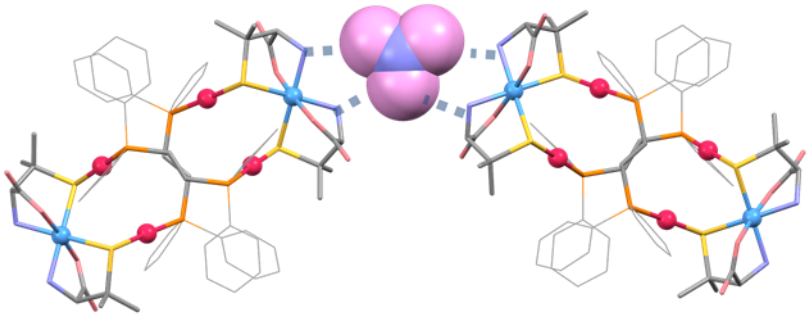

Figure 3-43. Hydrogen bonds between the complex molecules and the anions (a) at octahedral site (site **A**) in [**7**]·2$HClO_4$ ($H_2N\cdots O_{ClO4}$ = 2.997(19), 2.996(19) Å), (b) at tetrahedral site (site **B**) in [**7**]·2$HClO_4$ ($H_2N\cdots O_{ClO4}$ = 2.97(3), 3.15(3), 3.11(4) Å), and (c) in [**7**]·4/3HNO_3 ($H_2N\cdots O_{NO3}$ = 3.01(3), 3.07(3) Å). Only one part of the disordered region is drawn.

(a)

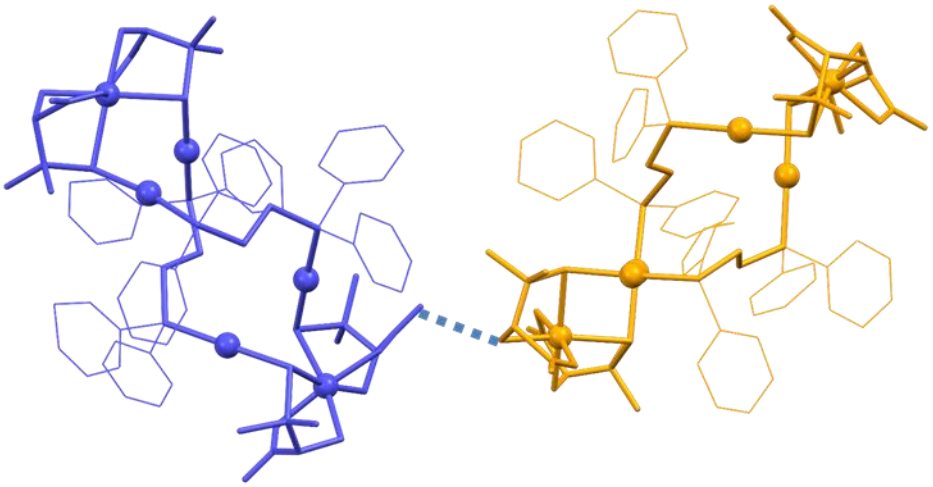

(b)

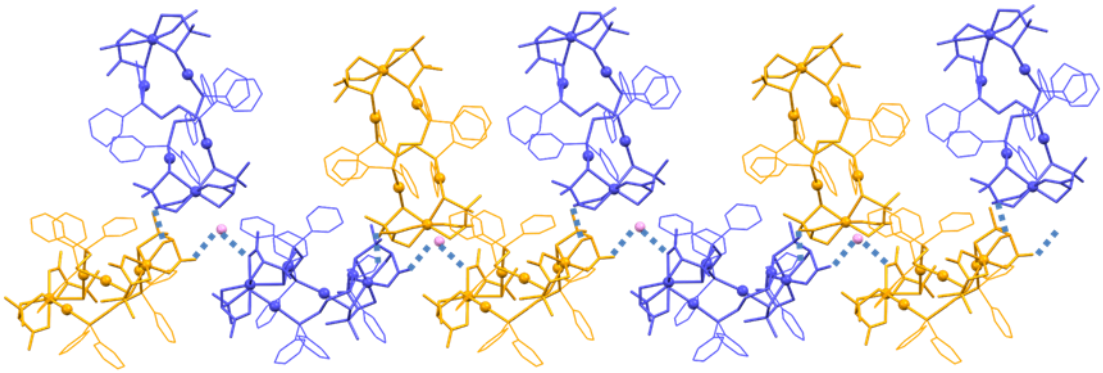

Figure 3-44. Perspective views of previously synthesized $[Au_4Ni_2(dppe)_2(D\text{-pen})_4][Au_4Ni_2(dppe)_2(L\text{-pen})_4]\cdot 15H_2O$.[7c] (a) Dimer structure constructed by hydrogen bonds between the amine and carboxylate groups, and (b) chain structure constructed by hydrogen bonds between the complex dimer and the water molecule.

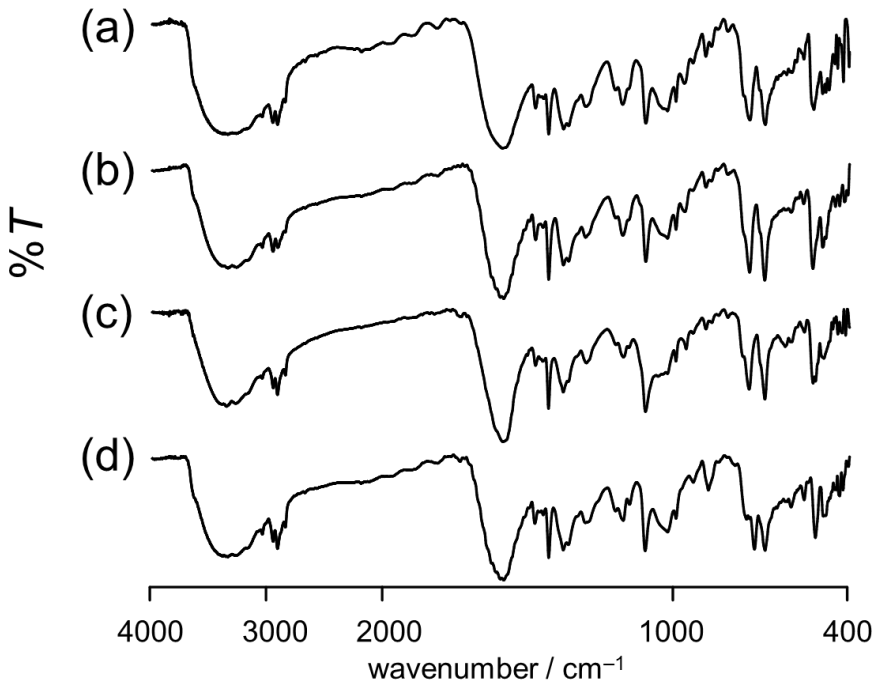

Figure 3-45. IR spectra of (a) green powder after reaction of [**7**]·2HClO$_4$ and aqueous methylamine solution, (b) green powder after reaction of [**7**]·4/3HNO$_3$ and aqueous ammonia solution, (c) green crystals after reaction of [**7**]·2HClO$_4$ and ammonia in gaseous phase, and (d) green powder after reaction of [**8**]·2HClO$_4$ and aqueous ammonia solution (KBr disk).

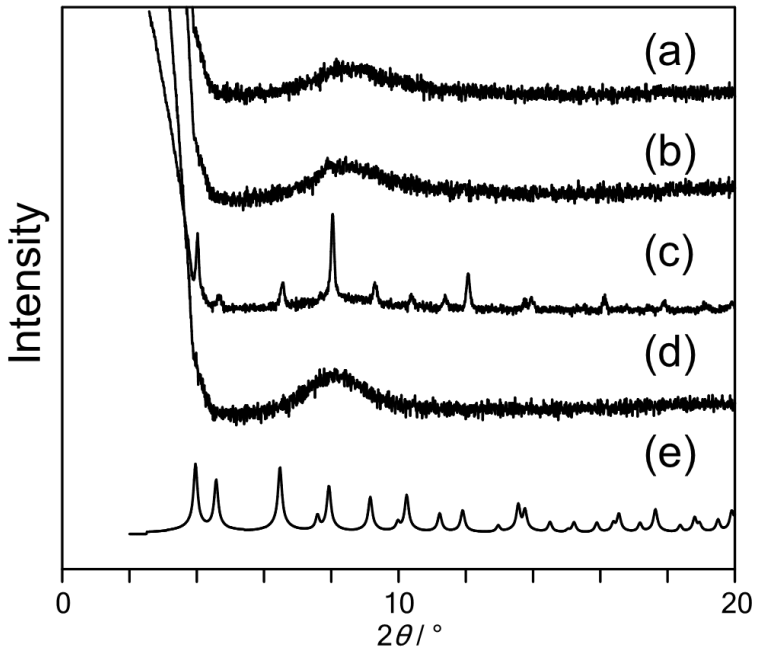

Figure 3-46. Powder X-ray diffraction patterns of (a) green powder after reaction of [**7**]·2$HClO_4$ and aqueous methylamine solution, (b) green powder after reaction of [**7**]·4/3HNO_3 and aqueous ammonia solution, (c) green crystals after reaction of [**7**]·2$HClO_4$ and ammonia in gaseous phase, (d) green powder after reaction of [**8**]·2$HClO_4$ and aqueous ammonia solution, and (e) simulated pattern calculated for the crystal structure of [**7**]·2$HClO_4$.

(a)

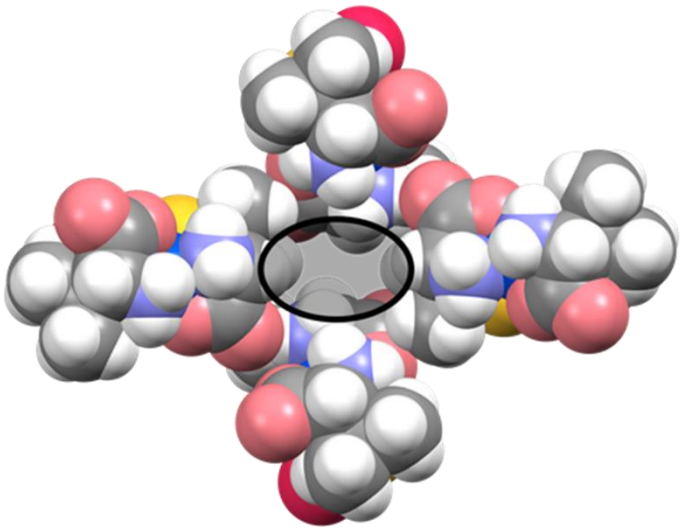

(b)

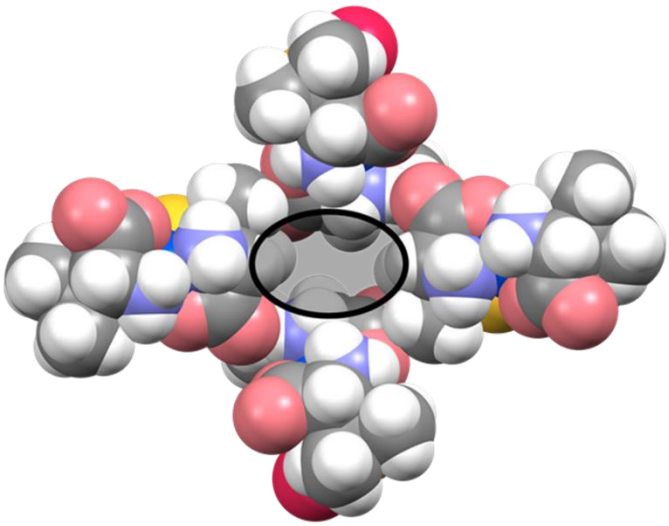

Figure 3-47. The narrow channel connecting the tetrahedral interstices in the crystal structure of (a) [**7**]·2$HClO_4$, and (b) [**8**]·2$HClO_4$.

Chapter IV. Coordination Behavior of Digold(I) Metalloligand with dcpe toward Co^{II} / Ni^{II}

IV-1. Introduction.

In this chapter, the effect of the functional groups on the phosphorus atoms is discussed. To figure out the role of the substituent, dcpe (1,2-bis(dicyclohexylphosphino)ethane) was chosen as the alternative bridging diphosphine which has cyclohexyl groups instead of phenyl groups in dppe. The molecular structures and physical properties of the complexes bearing dcpe units have often been compared with the dppe analogous complexes.[25] The introduction of a bulky substituent (cyclohexyl group) instead of phenyl rings on the phosphorus atoms must cause a steric hindrance,[26] which in turn, might make the conformation of the metalloligand more constrained. Moreover, the loss of the phenyl rings on the phosphorus atoms must change the complex arrangement drastically because of the lack of intermolecular π···π and CH···π interactions on the phenyl rings, which contribute to the aggregation.

In this context, two kinds of metalloligands, $[Au_2(dcpe)(D\text{-}Hpen)_2]$ (D_2-H_2[**12**]) and $[Au_2(dcpe)(D\text{-}Hpen)(L\text{-}Hpen)]$ (DL-H_2[**12**]) were newly designed and prepared, from a precursor $[Au_2(dcpe)Cl_2]$ ([**11**]). The reaction of the homochiral metalloligand (D_2-H_2[**12**]) with Co^{II} led to the crystallization of $[Au_4Co_2(dcpe)_2(D\text{-}pen)_4]^{2+}$ ([**13**]$^{2+}$) as a nitrate salt. The structure of the homochiral $Au^{I}_4Co^{III}_2$ complex cation [**13**]$^{2+}$ was topologically the same as the dppe analogous complex, $[Au_4Co_2(dppe)_2(D\text{-}pen)_4]^{2+}$, but the configuration of the complex was different, and [**13**]$^{2+}$ had a bent molecular structure. In the crystal structure of [**13**]$(NO_3)_2$, inorganic anions were not aggregated, which is different from the dppe system.

By the reaction of the heterochiral metalloligand, $[Au_2(dcpe)(D\text{-}Hpen)(L\text{-}Hpen)]$ (DL-H_2[**12**]), with cobalt(II) and nickel(II), $[Au_2Co(dcpe)(D\text{-}pen)(L\text{-}pen)]^+$ ([**14**]$^+$) and $[Au_2Ni(dcpe)(D\text{-}pen)(L\text{-}pen)]$ ([**15**]) were isolated, respectively. These two complexes had essentially the same molecular structures as that of the heterochiral dppe system, $[Au_2Co(dppe)(D\text{-}pen)(L\text{-}pen)]^+$, which had a chirality on the secondary metal center (Co^{III} or Ni^{II}). While the molecular structures were similar to each other, the chiral aggregation behavior is quite distinct. The cationic Co^{III} complex [**14**]$^+$ led to the achiral crystal packing as expected for the heterochiral nature of the reaction solution. On the other hand, the neutral nickel(II) complex [**15**] showed a unique chiral crystal packing consisting of the heterochiral *meso* molecules by the spontaneous resolution (Scheme 4-1, 4-4). The previous examples of the chiral crystallization of the discrete molecules consisting of *meso* molecules are very limited and categorized into 2 types; one is the

spontaneous resolution of purely organic *meso* isomeric species,[28] and another is the spontaneous resolution of metal complexes that have *meso* isomeric ligands.[29] However, in both cases, the *meso* molecule is an organic ligand, and the chiral scrambling is hardly possible due to the requirement of the cleavage of covalent bonds. The use of the *meso* isomeric metalloligand ([D–M–L]), which has one or more pairs of chiral ligands (D or L, respectively) for the reaction with metal ions is an interesting idea, because the metalloligand can show chiral scrambling behavior by the cleavage of relatively weak coordination bonds (2[D–M–L] $\rightleftarrows$ [D–M–D] + [L–M–L]), and two kinds of spontaneous resolution are possible after the reaction with the secondary metal ions (M′): one is the spontaneous resolution of the homochiral complexes with *in situ* produced homochiral metalloligands (M′[D–M–D] + M′[L–M–L]) as observed in the previous dppe system,[8] and the other is the spontaneous resolution of the heterochiral complex with heterochiral metalloligands, which has a chirality on the secondary metal site (M′*[D–M–L] + M′*[L–M–D]). However, the metalloligand approach have rarely been utilized for the spontaneous resolution.[30] The first example of the spontaneous resolution of the heterochiral molecules composed of an enantiomeric pair of chiral subunits was provided by this work.

IV-2. Experimental Section.

IV-2-1. Materials.

All starting materials were commercially available and used without further purification. All experiments were performed in the air.

IV-2-2. Preparation of dcpe Complexes.

IV-2-2-1 [Au_2Cl_2(dcpe)] ([11]).

To a yellow solution containing 1.25 g (3.04 mmol) of $HAuCl_4 \cdot 2H_2O$ in 10 mL of MeOH and 2.5 mL of H_2O was added to an 8 M $S(C_2H_4OH)_2$ solution in methanol (1.5 mL, 12 mmol). The mixture was added to a colorless solution containing 0.50 g (1.18 mmol) of dcpe in $CHCl_3$ (5 mL). The mixture was stirred at room temperature for 1 h. in the dark after the addition of MeOH (4 mL) to give a white precipitate. The resulting white precipitate of [**11**] was collected by filtration and washed with H_2O and MeOH. Yield 0.89 g (85%). Anal. Calcd for $[Au_2Cl_2(dcpe)] \cdot 0.5H_2O = C_{26}H_{49}Au_2P_2Cl_2O_{0.5}$: C, 34.84; H, 5.51 %. Found: C, 34.86; H, 5.35 %. IR spectrum (cm^{-1}, KBr disk): 2926, 2849 (ν_{CH2}), 1447 (ν_{PC}). ^1H NMR spectrum in $CDCl_3$ (δ, ppm from TMS): 2.02-1.75 (m, 24H), 1.57 (s, 4H), 1.42-1.25 (m, 18H). ^{31}P NMR spectrum in $CDCl_3$ (δ, ppm from H_3PO_4): 48.8 (s). MS (ESI-neg) in MeOH, Calcd. for $C_{26}H_{44}Au_2Cl_3P_2$ [[**11**] + Cl^-]: *m*/*z* = 921.1623, Found.: *m*/*z* = 921.1753 (100%).

Crystals suitable for single crystal X-ray analysis were obtained by the recrystallization from CH_2Cl_2 solution.

IV-2-2-2. [Au_2(dcpe)(D-Hpen)$_2$] (D$_2$-H$_2$[12]).

To a white suspension containing 0.50 g (0.55 mmol) of [**11**] in EtOH (100 mL) was added 0.25 g (1.7 mmol) of D-H_2pen and 0.5 M aqueous NaOH solution (3.4 mL, 1.7 mmol). The mixture was stirred at room temperature for 10 min. in the dark to give a colorless solution. The colorless solution was evaporated to dryness. The resulting white crystalline residue of D_2-H_2[**12**] was washed with H_2O. Yield 0.56 g (88%). Anal. Calcd for $[Au_2(dcpe)(D\text{-}Hpen)_2] \cdot 3H_2O = C_{36}H_{74}Au_2N_2O_7P_2S_2$: C, 37.05; H, 6.39; N, 2.40 %. Found: C, 37.04; H, 6.38; N, 2.34 %. IR spectrum (cm^{-1}, KBr disk): 2925, 2850 (ν_{CH2}), 1628 (ν_{CO}), 1448 (ν_{PC}). ^1H NMR spectrum in CD_3OD (δ, ppm from TMS): 3.47 (s, 2H), 1.77 (s, 6H), 1.36 (s, 6H), 2.46–1.28 (m). ^{31}P NMR spectrum in $CDCl_3$ (δ, ppm from H_3PO_4): 47.2 (s). MS (ESI-neg) in MeOH, Calcd. for $C_{36}H_{63}Au_2N_2O_4P_2S_2$ [D_2-H_2[**12**] – H^+]: *m*/*z* = 1111.3343, Found.: *m*/*z* = 1111.2707 (100%).

IV-2-2-3. [Au_2(dcpe)(D-Hpen)(L-Hpen)] (DL-H_2[12]).

To a white suspension containing 0.50 g (0.55 mmol) of [Au_2Cl_2(dcpe)] in EtOH (100 mL) was added 0.25 g (1.7 mmol) of DL-H_2pen and 0.5 M aqueous NaOH solution (3.4 mL, 1.7 mmol). The mixture was stirred at room temperature for 10 min. in the dark to give a colorless solution. The colorless solution was evaporated to dryness. The resulting white crystalline residue of DL-H_2[**12**] was washed with H_2O. Yield 0.55 g (87%). Anal. Calcd for [Au_2(dcpe)(DL-Hpen)$_2$]·3H_2O = $C_{36}H_{74}Au_2N_2O_7P_2S_2$: C, 37.05; H, 6.39; N, 2.40%. Found: C, 37.04; H, 6.52; N, 2.34%. IR spectrum (cm^{-1}, KBr disk): 2925, 2849 (ν_{CH2}), 1626 (ν_{CO}), 1447 (ν_{PC}). ^{1}H NMR spectrum in CD_3OD (δ, ppm from TMS): 3.47, 3.48 (d, 2H), 1.76 (s, 6H), 1.35, 1.37 (d, 6H), 2.35–1.16 (m). ^{31}P NMR spectrum in $CDCl_3$ (δ, ppm from H_3PO_4): 47.3 (s). MS (ESI-neg) in MeOH, Calcd. for $C_{36}H_{63}Au_2N_2O_4P_2S_2$ [DL-H_2[**12**] – H^+]: *m*/*z* = 1111.3343, Found.: *m*/*z* = 1111.3455 (100%).

By the recrystalzation of DL-H_2[**12**] from solution in methanol after the addition of 0.1 equivalent of $HClO_4$ aq. , a racemic crystal suitable for single crystal X-ray analysis (D$_2$/L$_2$-H_3[**12**]ClO_4) was obtained. The spectral measurements were not performed because the yield was too low.

IV-2-2-4. [Au_4Co_2(dcpe)$_2$(D-pen)$_4$](NO$_3$)$_2$ ([13](NO$_3$)$_2$).

To a solution containing D$_2$-H_2[**12**] (50 mg, 0.04 mmol) in MeOH (2 mL) and H_2O (1 mL) was added Co(OAc)$_2$·4H_2O (12 mg, 0.05 mmol), which was stirred at room temperature for 0.5 h. A 1 M $NaNO_3$ aqueous solution (0.05 mL) was added to the resulting brown solution. After the slow evaporation at room temperature for a week, brown stick crystals of [**13**](NO$_3$)$_2$ were obtained, which were collected by filtration and washed with H_2O. Yield 34 mg (55%). Anal. Calcd for [Au_4Co_2(dcpe)$_2$(D-pen)$_4$](NO$_3$)$_2$·MeOH ·19H_2O = $C_{73}H_{174}Au_4Co_2N_6O_{34}P_4S_4$: C, 30.89; H, 6.18; N, 2.96%. Found: C, 30.94; H, 5.95; N, 2.72%. IR spectrum (cm^{-1}, KBr disk): 2925, 2851 (ν_{CH2}), 1652 (ν_{CO}), 1384 (ν_{NO}), 1447 (ν_{PC}). ^{1}H NMR spectrum in CD_3OD (δ, ppm from TMS): 3.69 (s, 2H), 1.82 (s, 6H), 1.44 (s, 6H), 2.37–1.28 (m). ^{31}P NMR spectrum in $CDCl_3$ (δ, ppm from H_3PO_4): 47.9 (s).

IV-2-2-5. [Au_2Co(dppe)(D-pen)(L-pen)]NO_3 ([14]NO_3).

To a solution containing DL-H_2[**12**] (50 mg, 0.04 mmol) in MeOH (0.75 mL) was added Co(OAc)$_2$·4H_2O (11 mg, 0.05 mmol). To the resulting purple solution was added a 1 M $NaNO_3$ aqueous solution (0.05 mL) was added. After the slow evaporation at room temperature for a week, purple small crystals of [**14**]NO_3 were obtained, which

were collected by filtration and washed with H_2O. Yield 31 mg (55%). Anal. Calcd for $[Au_2Co(dcpe)(D\text{-pen})(L\text{-pen})]NO_3\cdot 3/2MeOH\cdot 3H_2O$ = $C_{37.5}H_{78}Au_2Co_1N_3O_{11.5}P_2S_2$: C, 33.76; H, 5.89; N, 3.15%. Found: C, 33.88; H, 5.72; N, 2.96%. IR spectrum (cm^{-1}, KBr disk): 2925, 2851 (ν_{CH2}), 1651 (ν_{CO}), 1384 (ν_{NO}), 1448 (ν_{PC}). ^1H NMR spectrum in CD_3OD (δ, ppm from TMS): 3.70(s, 2H), 1.64(s, 3H), 1.62(s, 3H), 1.57 (s, 3H), 1.55 (s, 3H), 2.62–1.17 (m). ^{31}P NMR spectrum in $CDCl_3$ (δ, ppm from H_3PO_4): 48.0 (s, 1P), 47.1 (s, 0.74P).

IV-2-2-6. $[Au_2Co(dppe)(D\text{-pen})(L\text{-pen})]ClO_4$ ([14]ClO_4).

To a suspension containing DL-H_2[**12**] (50 mg, 0.04 mmol) in MeOH (1.5 mL) was added $Co(OAc)_2\cdot 4H_2O$ (12 mg, 0.05 mmol). To the resulting brown solution was added a 1 M $NaClO_4$ aqueous solution (0.075 mL). After the slow evaporation at room temperature for 4 days, purple crystals of the [**14**]ClO_4 were obtained, which were collected by filtration and washed with H_2O. Yield: 28 mg (49%). Anal. Calcd for $[Au_2Co(dcpe)(D\text{-pen})(L\text{-pen})]ClO_4\cdot 1/4NaCl\cdot 2H_2O$ = $C_{36}H_{70}Au_2CoN_2O_{10}P_2S_2Cl_{1.25}Na_{0.25}$: C, 32.76; H, 5.35; N, 2.12%. Found: C, 32.92; H, 5.64; N, 2.06%. IR spectrum (cm^{-1}, KBr disk): 2926, 2851 (ν_{CH}), 1650 (ν_{CO}), 1448 (ν_{PC}), and. 1092, 622 (ν_{ClO}). ^1H NMR spectrum in CD_3OD (δ, ppm from TMS): 3.70 (s, 2H), 1.64 (s, 3H), 1.62 (s, 3H), 1.57 (s, 3H), 1.55 (s, 3H), 2.54–1.17 (m). ^{31}P NMR spectrum in $CDCl_3$ (δ, ppm from H_3PO_4): 48.0 (s,1P), 47.2(s, 2.8P)

IV-2-2-7. $[Au_2Ni(dppe)(D\text{-pen})(L\text{-pen})]$ ([15]).

To a suspension containing DL-H_2[**12**] (50 mg, 0.04 mmol) in MeOH (10 mL) was added $Ni(OAc)_2\cdot 4H_2O$ (12 mg, 0.05 mmol), and the resulting blue solution was slowly evaporated at room temperature for 2 weeks to yield blue stick crystals of [**15**] or [**15**]′, which is the enantiomeric crystals of [**15**]. The crystals were then collected by filtration and washed with H_2O. Yield: 32 mg (60%). Anal. Calcd for $[Au_2Ni(dcpe)(D\text{-pen})(L\text{-pen})]\cdot 3H_2O$ = $C_{36}H_{72}Au_2NiN_2O_7P_2S_2$: C, 35.34; H, 5.93; N, 2.29%. Found: C, 35.17; H, 5.98; N, 2.16%. IR spectrum (cm^{-1}, KBr disk): 2925, 2850 (ν_{CH2}), 1604 (ν_{CO}), 1447 (ν_{PC}). By measuring the single crystal X-ray diffraction measurements for more than ten crystals picked from the mixture of the crystals of [**15**] or [**15**]′, the single crystal of [**15**]′ were picked and the single crystal X-ray diffraction measurement was done for not only [**15**] but also [**15**]′.

IV-2-3. Physical Measurements.

The elemental analyses (C, H, N) were performed at Osaka University by a

YANACO CHN coder MT-5 or MT-6. The IR spectra were recorded on a JASCO FT/IR-4100 infrared spectrometer using a KBr disk at room temperature. The ^{1}H NMR spectra were recorded with a JEOL ECA500 (500 MHz) spectrometer at room temperature, using tetramethylsilane (TMS) as the internal standard. The ^{31}P NMR spectra were recorded with a JEOL ECA500 (500 MHz) spectrometer at room temperature, using triphenyl phosphate as the external standard. The electronic absorption spectra were recorded on a JASCO V-570 or V-660 spectrophotometer at room temperature. The diffuse reflection spectra in solid state were recorded on a JASCO V-570 spectrophotometer. The CD spectra were recorded on a JASCO J-820 spectropolarimeter. The X-ray fluorescence spectrometries were performed on SHIMADZU EDX-720 spectrometer. The ESI-mass spectra were recorded with a Bruker micrOTOF II mass spectrometer in MeOH solvent, and the concentration was 0.1 mM.

IV-2-4. X-ray Structural Determination.

The single-crystal X-ray diffraction measurements for D_2/L_2-H_3[**12**]ClO_4, [**13**]$(NO_3)_2$ [**15**], and [**15**]′ were performed at 200 K with a Rigaku FR-E Superbright rotating-anode X-ray source with a Mo-target (λ = 0.71075 Å); a Rigaku RAXIS VII imaging plate was used as the detector. The intensity data were collected by using the ω-scan technique and were empirically corrected for absorption. The collected diffraction data were processed with the Rapid Auto software program.

The single-crystal X-ray diffraction measurement for [**14**]ClO_4) was performed at 100 K with a Rigaku Mercury 2 CCD detector with synchrotron radiation (λ = 0.7000 Å) at the BL02B1 beamline in SPring-8. The collected diffraction data were processed with the Rapid Auto software program.

The single-crystal X-ray diffraction measurements for [**11**] and [**14**]NO_3 were performed at 100 K with an ADSC Q210 CCD area detector with synchrotron radiation (λ = 0.7000 Å) at the 2D beamline at the Pohang Accelerator Laboratory (PAL). The intensity data were processed using the HKL3000 program.

The structures of the all complexes were solved via direct methods using the SHELXS2014 program. The structure refinements were carried out using full-matrix least-squares (SHELXL2014). All calculations were performed using the Yadokari-XG software package.

For [**11**], a half of [$Au^{I}_2Cl_2$(dcpe)] unit was crystallographically independent. All non-hydrogen atoms were refined anisotropically. Hydrogen atoms were included in calculated positions.

For D_2/L_2-H_3[**12**]ClO_4, a D_2/L_2-$[Au^I_2(dcpe)_2(Hpen)(H_2pen)]^+$ unit, water, and one ClO_4^- molecules were crystallographically independent. All non-hydrogen atoms except the O atoms of water molecules were refined anisotropically. Hydrogen atoms were included in calculated positions except those of a protonated carboxyl group and water molecules. DFIX restrains were used to model one penicillaminate unit, the anion molecules, and water molecules.

For [**13**]$(NO_3)_2$, a $[Au^I_4Co^{III}_2(dcpe)_2(D\text{-pen})_4]^{2+}$ unit, water, and two NO_3^- molecules were crystallographically independent. All non-hydrogen atoms except the O atoms of water molecules were refined anisotropically. Hydrogen atoms were included in calculated positions except those of water molecules. DFIX restrains were used to model nitrate anions, and water molecules.

For [**14**]NO_3, one $[Au^I_2Co^{III}(dcpe)(D\text{-pen})(L\text{-pen})]^+$ unit, water molecules, and one NO_3^- molecule were crystallographically independent. All non-hydrogen atoms except one N atom of nitrate anion and O atoms of water and nitrate molecules were refined anisotropically. Hydrogen atoms were included in calculated positions except those of water molecules. DFIX and SIMU restrains were used to model nitrate anion and pen moieties.

For [**14**]ClO_4, one $[Au^I_2Co^{III}(dcpe)(D\text{-pen})(L\text{-pen})]^+$ unit, water molecules, a sodium cation, a chloride anion, and three disordered ClO_4^- molecules were crystallographically independent. All non-hydrogen atoms except some O atoms of water molecules were refined anisotropically. Hydrogen atoms were included in calculated positions except those of water molecules. DFIX restrains were used to model perchlorate anions.

For [**15**], one $[Au^I_2Ni^{II}(dcpe)(D\text{-pen})(L\text{-pen})]$ unit and five methanol molecules were crystallographically independent. All non-hydrogen atoms were refined anisotropically. Hydrogen atoms were included in calculated positions except those of hydroxyl groups of methanol molecules. DFIX restrains were used to model methanol molecules.

For [**15**]′, one $[Au^I_2Ni^{II}(dcpe)(D\text{-pen})(L\text{-pen})]$ unit and five methanol molecules were crystallographically independent. All non-hydrogen atoms were refined anisotropically. Hydrogen atoms were included in calculated positions except those of hydroxyl groups of methanol molecules. DFIX restrains were used to model methanol molecules.

IV-3. Results and Discussion.

IV-3-1. Synthesis and Characterization of [Au_2Cl_2(dcpe)] ([11])

The reaction of Au^I with dcpe in a 3:1 ratio under the presence of Cl^- anion, in a mixed solvents of chloroform/methanol/water gave a white crystalline powder of [**11**] (Scheme 4-2). The equivalent of the Au^I ion is much more than the stoichiometric equivalent (2 equiv.). The ethylene carbon linkers between the phosphorus atoms in dcpe can take bent configuration and thus, dcpe ligand tend to coordinate in chelate mode with one or two dcpe ligands coordinating to each metal ions. For preventing the formation of such an undesired complex with lesser ligand to metal ratio (0.5 equiv. or 1 equiv.), 3 equivalents of Au^I ions were used. X-ray fluorescence spectroscopy indicated that [**11**] contained Au atom and its elemental analytical data was in agreement with the formula for a 1:2 adduct of $[Au_2(dcpe)]^{2+}$ and Cl^-. In the IR spectrum, a P-Cy stretching band at 1447 cm^{-1}, and CH_2 bands in the range of 2926–2849 cm^{-1} were observed (Figure 4-1a). The ^1H NMR spectrum in $CDCl_3$ showed many signals δ 2.02–1.25 assigned to cyclohexyl and ethylene groups of dcpe (Figure 4-2). The ^{31}P NMR spectrum in $CDCl_3$ showed one set of signal at δ 48.8 ppm (Figure 4-3). These NMR spectrum features are in agree with the expected C_2 symmetrical structure. The ESI-mass spectrum suggested the existence of [**12**]Cl^- species in a dilute MeOH solution (Figure 4-4). The structure of [**11**] in the crystal was fully characterized by single crystal X-ray diffraction analysis (*vide infra*).

IV-3-2. Synthesis and Characterization of [Au_2(dcpe)(D-Hpen)$_2$] and [Au_2(dcpe)(DL-Hpen)$_2$] (D$_2$-H$_2$[12], DL-H$_2$[12]).

Reaction of [Au_2Cl_2(dcpe)] with D-H_2pen in a 1:2 ratio in EtOH/water with base at room temperature gave a colorless solution, from which white powder (D$_2$-H$_2$[**12**]) was isolated by evaporation to dryness (Scheme 4-2). X-ray fluorescence spectroscopy indicated that D$_2$-H$_2$[**12**] contained Au atom and its elemental analytical data was in agreement with the formula for a 1:2 adduct of $[Au_2(dcpe)]^{2+}$ and D-Hpen$^-$. In the IR spectrum, a C=O stretching band for deprotonated carboxylate groups of D-pen at 1628 cm^{-1}, a P-Cy stretching band at 1448 cm^{-1}, and CH_2 bands for 2925–2850 cm^{-1} were observed (Figure 4-1b). The ^1H NMR spectrum in CD_3OD showed one set of proton signals at δ 1.36 and 1.77 ppm assigned to the methyl groups of D-pen, δ 3.47 ppm assigned to the methine group of D-pen, and many signals at δ 2.46–1.28 assigned to cyclohexyl and ethylene groups of dcpe (Figure 4-5a). The ^{31}P NMR spectrum in CD_3OD showed a singlet signal at δ 47.2 ppm (Figure 4-6a). The ESI-mass spectrum suggested the existence of D$_2$-H[**12**]$^-$ species in a dilute MeOH solution (Figure 4-7a). The absorption spectrum of D$_2$-H$_2$[**12**] in MeOH showed an absorption band around 261

nm in the region of 700-200 nm (Figure 4-8). Its circular dichroism (CD) spectrum showed a positive band at 310 nm and negative bands at 270 and 236 nm (Figure 4-8).

Reaction of $[Au_2Cl_2(dcpe)]$ with DL-H_2pen in a 1:2 ratio in EtOH at room temperature gave a white suspension, from which white powder of DL-H_2[**12**] was isolated (Scheme 4-2). X-ray fluorescence spectroscopy indicated that DL-H_2[**12**] contained Au atom and its elemental analytical data was in agreement with the formula for $[Au_2(dcpe)(Hpen)_2]\cdot 3H_2O$. In the IR spectrum, a C=O stretching band for deprotonated carboxylate groups of pen at 1626 cm^{-1}, a P–Cy stretching band at 1447 cm^{-1}, and CH_2 bands at 2925-2849 cm^{-1} were observed (Figure 4-1c). The ^{1}H NMR spectrum in CD_3OD showed two sets of proton signals at δ 1.37 and 1.35 ppm assigned to the methyl groups of pen, δ 3.47, 3.38 ppm assigned to the methine group of pen, one set of proton signals at δ 1.76 at the methyl groups of pen, 2.35–1.16 ppm assigned to cyclohexyl and ethylene groups of dcpe (Figure 4-5b). This complicated result suggested that the solution contained two species that had almost same chemical shift values, and the existence of both *meso* and *raceme*-isomers of the metalloligands are implied. The ^{31}P NMR measurement in CD_3OD showed a singlet signal at δ 47.3 ppm (Figure 4-6b). The mass spectrum suggested the existence of DL-H[**12**]$^-$ species in dilute MeOH solution (Figure 4-7b). The absorption spectrum of D-H_2[**12**] in MeOH shows an absorption band around 260 nm in the region of 700-200 nm (Figure 4-9). Its CD spectrum was silent, as expected for heterochiral nature of the meso compound (Figure 4-9). From these results, the isolation of heterochiral metalloligand was confirmed, but as expected from the result in previous studies, the chiral scrambling occurred in its solution to be the mixture of D-H_2[**12**], DL-H_2[**12**], and L-H_2[**12**].

The recrystallization of DL-H_2[**12**] from methanol solution in the presence of small amount of perchloric acid led to the formation of racemic crystals of the perchlorate salt of protonated ligand (D/L-H_3[**12**]ClO_4) instead of meso metalloligand as in the case of the crystallization of analogous heterochiral metalloligand in dppe or *trans*-dppee system (*vide infra*). The yield of this crystal was too small and no other analyses were performed.

IV-3-3. Synthesis and Characterization of $[Au_4Co_2(dcpe)_2(D\text{-}pen)_4](NO_3)_2$ ([**13**]$(NO_3)_2$).

Reaction of metalloligand D-H_2[**12**] with $Co(OAc)_2\cdot 4H_2O$ in a 1:1 ratio in MeOH at room temperature gave a brown solution by air-oxidation of cobalt center, to which was added a $NaNO_3$ aqueous solution. Purple stick crystals ([**13**]$(NO_3)_2$) were isolated from the brown reaction solution (Scheme 4-3). X-ray fluorescence spectroscopy indicated the presence of Au and Co atoms in [**13**]$(NO_3)_2$, and its elemental analytical data was in

agreement with a formula consisting of $[Au_2(dcpe)(D\text{-pen})_2]^{2-}$ (D_2-[**12**]$^{2-}$) , Co^{3+}, and NO_3^- in a 1:1:1 ratio. In the IR spectrum, a C=O stretching band for deprotonated carboxylate groups of D-pen at 1652 cm^{-1}, an N–O stretching band for nitrate anion at 1384 cm^{-1}, and a P–Cy stretching band at 1447 cm^{-1} were observed (Figure 4-1d). The ^1H NMR spectrum in CD_3OD showed one set of proton signals at δ 1.44 and 1.82 ppm assigned to the methyl groups of D-pen, δ 3.69 ppm assigned to the methine group of D-pen, and many signals δ 2.37–1.28 assigned to cyclohexyl and ethylene groups of dcpe (Figure 4-10a). The ^{31}P NMR spectrum in CD_3OD showed a singlet signal at δ 47.9 ppm (Figure 4-11a). The NMR spectra showing the signals in the normal region without paramagnetic shifts suggested that [**13**]$^{2+}$ is not a paramagnetic Co^{II} species, but a diamagnetic Co^{III} species. The absorption spectrum of [**13**]$(NO_3)_2$ in MeOH showed absorption bands at around 525 and 590 nm assigned to the d-d transition of Co^{III} center, and a shoulder at ca. 360 nm. Its CD spectrum showed positive bands at 608 and 398 nm and negative bands at 511 and 346 nm in the region of 700 to 300 nm (Figure 4-12). The absorption and CD spectra of [**13**]$^{2+}$ and $[Au_4Co_2(dppe)_2(D\text{-pen})_4]^{2+}$ in d-d transition region were essentially similar (Figure 4-13), suggesting that the [**13**]$^{2+}$ have Co^{III} centers with *trans*(O)*cis*(N)*cis*(S) coordination geometry like $[Au_4Co_2(dppe)_2(D\text{-pen})_4]^{2+}$. The diffuse reflection spectrum in the solid state showed a band at 520 nm and the CD spectrum in the solid state showed a negative band at 501 nm and a positive band at 639 nm in the region of 700-400 nm (Figure 4-14). These diffuse reflection and CD spectra in the solid state were essentially the same as the absorption and CD spectra in MeOH solution, indicating that the structure of [**13**]$(NO_3)_2$ in the solid state was retained in solution. Single-crystal X-ray analysis revealed that [**13**]$^{2+}$ was a hexanuclear divalent cationic complex, $[Au^I_4Co^{III}_2(dcpe)_2(D\text{-pen})_4]^{2+}$, in which two $[Au^I_2(dcpe)(D\text{-pen})_2]^{2-}$ moieties were bridged by two Co^{III} centers (*vide infra*).

IV-3-4. Synthesis and Characterization of $[Au_2Co(dppe)(D\text{-pen})(L\text{-pen})]NO_3$ ([14]NO_3) and $[Au_2Co(dppe)(D\text{-pen})(L\text{-pen})]ClO_4$ ([14]ClO_4).

The reaction of a methanol solution of DL-H_2[**12**] with $Co(OAc)_2{\cdot}4H_2O$ in a 1:1 ratio gave a brown solution. Purple crystals of [**14**]NO_3 were isolated by adding 1 equivalent amount of $NaNO_3$ (Scheme 4-4). X-ray fluorescence spectroscopy suggested that [**5**]NO_3 contained Co and Au atoms and its elemental analysis data was in agreement with a 1:1:1 adduct of DL-$[Au_2(dcpe)(pen)_2]^{2-}$, Co^{3+} ion, and NO_3^-. In the IR spectrum, a C=O stretching band for deprotonated carboxylate groups of D-pen at 1651 cm^{-1}, a N–O stretching band for nitrate anion at 1384 cm^{-1}, and a P–Cy stretching band at 1448 cm^{-1} were observed (Figure 4-1e). The ^1H NMR spectrum in CD_3OD showed two set of

proton signals at δ 1.64, 1.62, 1.57 and 1.55 ppm assigned to the methyl groups of D-pen, δ 3.70 and 3.69 ppm assigned to the methine group of D-pen, and many signals at δ 2.62–1.17 assigned to cyclohexyl and ethylene groups of dcpe (Figure 4-10b). All the four signals assigned as the methyl groups possessed different chemical shifts from the two signals assigned as the methyl groups in the spectrum of [**13**]$^{2+}$, and this fact suggested the formation of the complex with lower symmetry. The ^{31}P NMR spectrum in CD_3OD showed two set of signals at δ 48.0 and 47.1 ppm (Figure 4-11b). The absorption spectrum of [**14**]NO_3 in MeOH showed an absorption band at around 564 nm assigned to the d-d transition of Co^{III} center, and a shoulder at ca. 400 nm. The whole spectral pattern was different from that of [**13**]$(NO_3)_2$ in the d-d transition region, which indicate the difference in the coordination environment around Co^{III} center (Figure 4-15). The diffuse reflection spectrum in the solid state showed a band at 569 nm in the region of 700-400 nm, and it was essentially the same as the absorption spectra in MeOH solution, indicating that the structure of [**14**]NO_3 in the solid state was retained in solution (Figure 4-16). The CD spectra in solution and in the solid state were both silent (Figures 4-15, 4-16), indicating its heterochirality in solution and solid state. Single-crystal X-ray analysis revealed that [**14**]$^+$ was a trinuclear complex monocation with C1 symmetry, $[Au^I_2Co^{III}$(dcpe)(D-pen)(L-pen)$]^+$, in which $[Au^I_2$(dcpe)(D-pen)(L-pen)$]^{2-}$ moiety coordinated to one Co^{III} center in a *cis*(O)*cis*(N)*cis*(S) chelating mode (*vide infra*).

The addition of $NaClO_4$ instead of $NaNO_3$ into the reaction solution containing DL-H_2[**12**] and $Co(OAc)_2{\cdot}4H_2O$ in a 1:1 ratio led to the isolation of the crystals of $[Au_2Co$(dppe)(D-pen)(L-pen)$]ClO_4$ ([**14**]ClO_4) (Scheme 4-4). IR spectrum showed strong bands at 1650 cm^{-1} and 1092 cm^{-1}, indicative the presence of carboxyl groups and perchlorate ions, respectively (Figure 4-1f). The ^{1}H and ^{31}P NMR spectra in CD_3OD were similar to these of [**14**]NO_3 (Figure 4-10c, 4-11c). X-ray fluorescence spectroscopy suggested that [**14**]ClO_4 contained Co and Au atoms and its elemental analysis data was in agreement with a 4:4:4:1 adduct of $[Au_2$(dcpe)(D-pen)(L-pen)$]^{2-}$, Co^{3+} ion, ClO_4^-, and NaCl. The absorption spectrum of [**14**]ClO_4 in MeOH and its diffuse reflection spectrum in the solid state were almost the same as these of [**14**]NO_3, which indicate the same coordination mode to the cobalt center in solution and solid state (Figure 4-17, 4-18). Single-crystal X-ray analysis revealed that [**14**]ClO_4 was a perchlorate salt of the trinuclear complex monocation, $[Au^I_2Co^{III}$(dcpe)(D-pen)(L-pen)$]^+$, crystallized with accommodated NaCl salt (*vide infra*).

IV-3-5. Synthesis and Characterization of [Au_2Ni(dppe)(D-pen)(L-pen)] ([15]).

The reaction of a methanol solution of DL-H_2[**12**] with $Ni(OAc)_2{\cdot}4H_2O$ in a 1:1 ratio

gave a pale green solution, from which blue crystals of [**15**] were isolated (Scheme 4-4). X-ray fluorescence spectroscopy suggested that [**15**] contained Ni and Au atoms and its elemental analysis data was in agreement with a 1:1 adduct of $[Au_2(dcpe)(D\text{-pen})(L\text{-pen})]^{2-}$ and Ni^{2+} ions. In the IR spectrum, a C=O stretching band for deprotonated carboxylate groups of D-pen at 1604 cm^{-1} and a P–Cy stretching band at 1447 cm^{-1} were observed (Figure 4-1g). The absorption spectra in the region of 1200-400 nm showed two bands assignable to $^3T_{2g}\leftarrow{}^3A_{2g}$ and $^3T_{1g}\leftarrow{}^3A_{2g}$ transitions for the octahedral Ni^{II} center at 1039 and 591 nm, and its CD spectrum was silent in the region of 1000 to 400 nm (Figure 4-19). The diffuse reflection spectrum in the solid state showed two bands at 1074 and 606 nm in the region of 1200-400 nm (Figure 4-20). Single-crystal X-ray analysis revealed that [**15**] was a trinuclear neutral complex molecule, $[Au^I_2Ni^{II}(dcpe)(D\text{-pen})(L\text{-pen})]$, in which $[Au^I_2(dcpe)(D\text{-pen})(L\text{-pen})]^{2-}$ moiety coordinated to one Ni^{II} center in a *cis*(O)*cis*(N)*cis*(S) chelating mode. Notably, the space group of the crystal was a non-centrosymmetric one, which meant the spontaneous resolution behavior was observed. The crystal [**15**]′ with the opposite chirality to that of [**15**] crystallized simultaneously and the CD spectra of the single crystal in the solid state in the region of 900 to 300 nm was almost mirror image of that of [**15**] ([**15**] showed two positive bands at 561 and 423 nm and one negative band at 368 nm, while [**15**]′ showed one positive band at 373 nm, two negative bands at 548 and 413 nm were observed. Figure 4-21) (*vide infra*).

Despite many attempt for the reaction of D_2-[**12**]$^{2-}$ and Ni^{II}, no crystals of homochiral complex with Ni^{II} have been obtained yet.

IV-3-6. Crystal Structures of the dcpe Complexes.

Single-crystal X-ray diffraction analysis revealed that [**11**] crystallized in an orthorhombic space group of *Pbca*. Molecular and packing structures are shown in Figures 4-22 and 4-23. The crystallographic data are summarized in Table 4-1, and the selected bond distances and angles are listed in Table 4-2. The asymmetric unit contained a half of $[Au_2Cl_2(dcpe)]$ molecule and no solvent molecules were found. The complex molecule was comprised of two chlorido ligands and one $[Au_2(dcpe)]^{2+}$ moiety (Figure 4-22). Like a dppe analogous compound $[Au_2Cl_2(dppe)]$,[31] two chlorido ligands were bridged by a $[Au_2(dcpe)]^{2+}$ moiety, giving a linear structure in $[Au_2Cl_2(dcpe)]$. Each Au atom was in a PCl linear coordination geometry bound by one chlorido and one dcpe (Au–Cl = 2.30 Å, Au–P = 2.24 Å, and P–Au–Cl = 177.0°). There is neither intramolecular nor intermolecular aurophilic interactions (minimum Au···Au = 6.77 Å). Furthermore, it seemed that there were no strong interactions between the complex

molecules in the crystal, and the molecules were aggregated by only Van-Der-Waals interactions to a dense packing structure (Figure 4-23). In the crystal structure of dppe analogs, the [Au_2Cl_2(dppe)] molecules had intermolecular CH···π interactions between each other, however the change of phenyl rings to cyclohexyl rings led to the loss of such interaction in dcpe system. The linker carbon unit had a *trans* configuration, which was the same feature as the previously reported crystal structure of the dppe analogous complex, [Au_2Cl_2(dppe)]. This structure is one of the rare example of the dcpe complex that was found to have dcpe moiety in bridging coordination mode, because only nine crystal structures have been reported to have dcpe bridged structure in CCDC database.[25d,26b,32]

Single-crystal X-ray diffraction analysis revealed that D$_2$/L$_2$-H$_3$[**12**]ClO_4 crystallized in a monoclinic *C*2/*c* which was a centro symmetric space group. Molecular and packing structures are shown in Figures 4-24, 4-25, and 4-26. The crystallographic data are summarized in Table 4-3, and the selected bond distances and angles are listed in Table 4-4. The asymmetric unit contained a pair of homochiral molecules of [Au_2(dcpe)(D-Hpen)(D-H_2pen)] / [Au_2(dcpe)(L-Hpen)/L-H_2pen)], one independent perchlorate, and 7/2 solvated water molecules (Figure 2-24). The number of protonation was estimated to be three base on the charge compensation from the composition of the crystal which was found to contain perchlorate anion and metalloligand in 1:1 ratio by single crystal X-ray analysis, which led to the assumption that not only the amine groups of all pen units, but also one of the two carboxyl groups of pen units must be protonated to be Hpen ($^-SC(CH_3)_2CH(NH_3^+)COO^-$) and H_2pen ($^-SC(CH_3)_2CH(NH_3^+)COOH$), although the data was not good enough to distinguish whether carboxyl group was protonated. The cationic complex was comprised of one D/L-Hpen, one D/L-H_2pen, and one $[Au_2(dcpe)]^{2+}$ moieties. Like a dppe analogous compound [Au_2(dppe)(D-Hpen)$_2$],[6,7] two penicillaminate ligands were bridged by a $[Au_2(dcpe)]^{2+}$ moiety through S atoms, giving a linear structure in [Au_2(dcpe)(Hpen-*S*)(H_2pen-*S*)]. Each Au atom was in a PS linear coordination geometry bound by one penicillaminate and one dcpe (Av. Au–S = 2.31 Å, Au–P = 2.26 Å, and P–Au–S = 178.4°). In D$_2$/L$_2$-H$_3$[**12**]ClO_4, the cationic complexes were connected to each other through NH_3···OCO hydrogen bonding interaction (Av. N···O = 3.00 Å) to form an 1D infinite arrangement which contained both enantiomers (Figure 4-25). The 1D infinite arrangements were heterochiral and the metalloligands in the infinite structure were arranged in [···D$_2$-H$_3$[**12**]$^+$···D$_2$-H$_3$[**12**]$^+$···L$_2$-H$_3$[**12**]$^+$···L$_2$-H$_3$[**12**]$^+$···]$_\infty$ order that the pairs of metalloligands with same chirality (D$_2$-H$_3$[**12**]$^+$···D$_2$-H$_3$[**12**]$^+$) were alternatively settled with the pairs with opposite chirality (L$_2$-H$_3$[**12**]$^+$···L$_2$-H$_3$[**12**]$^+$). The perchlorate

anions were accommodated between these 1D infinite arrangements, and aggregated into dimer (Figure 4-26). There were no direct interactions between the infinite arrangements of the metalloligands.

Single-crystal X-ray diffraction analysis revealed that [**13**]$(NO_3)_2$ crystallized in an orthorhombic space group of $P2_12_12_1$ which was a non-centro symmetric space group. Molecular and packing structures are shown in Figures 4-27, 4-28 4-29, and 4-30. The crystallographic data are summarized in Table 4-5, and the selected bond distances and angles are listed in Table 4-6. The asymmetric unit contained a whole cationic complex of $[Au_4Co_2(dcpe)_2(D\text{-pen})_4]^{2+}$, two independent nitrate, and 29 solvated water molecules. In the $[Au_4Co_2(dcpe)_2(D\text{-pen})_4]^{2+}$ complex, the two D_2-[**12**]$^{2-}$ metalloligands each bound to two Co^{III} atoms in a bis(tridentate-*N,O,S*) mode such that each Co^{III} atoms was in a *cis*(*N*)*trans*(*O*)*cis*(*S*)-$N_2O_2S_2$ octahedral environment (Av. Co–S = 2.27 Å, Co–O = 1.92 Å, Co–N = 1.96 Å, S–Co–S = 94.5°, O–Co–O= 174.9°, N–Co–N = 95.5°) to form a cyclic 18-membered ring composed of $Au_4Co_2S_4P_4C_4$ (Figure 4-28, 4-29a) with the *R* configurational asymmetric bridging S atoms. The geometric configurations having trans(*O*) in the $[Co(D\text{-pen-}N,O,S)_2]^-$ octahedral units and the bond lengths around the cobalt centers were essentially the same as those in the reported $[Au_4Co_2(dppe)_2(D\text{-pen})_4]^{2+}$ (Figure 4-29b) and supporting the similarity of their ABCD spectra in the visible region in the solution.[6,7] On the other hand, the shape of cyclic 18-membered ring in [**13**]$^{2+}$ was bent on the diphosphinoethane parts with the relatively close Au···Au distances (3.380(2) and 3.349(2) Å), indicative of the presence of a weak aurophilic interaction.[18] This bent structural feature was distinct from straight one in a $[Au_4Co_2(dppe)_2(D\text{-pen})_4]^{2+}$ cation. The nitrate anions were located between the cationic complexes alternatively, and no aggregation of the cationic complexes and inorganic anions like that in the crystal of $[Au_4Co_2(dppe)_2(D\text{-pen})_4](NO_3)_2$ was found (Figure 4-30), probably due to the loss of CH···π interaction that formed the cationic aggregation in dppe analogs.

By single-crystal X-ray diffraction analysis, [**14**]NO_3 was found to crystallize in an achiral triclinic space group of *P*-1. Its molecular and packing structures are shown in Figures 4-31, 4-32, 4-33, and 4-34. The crystallographic data are summarized in Table 4-7, and the selected bond distances and angles are listed in Table 4-8. The asymmetric unit contained a cationic complex of $[Au_2Co(dcpe)(D\text{-pen})(L\text{-pen})]^+$, one nitrate anions, and one water molecule (Figure 4-31). Methanol molecules were not found by single-crystal X-ray analysis possibly because of low data quality. Both D/L-penicillamine moieties of $[Au_2(dcpe)(D\text{-pen})(L\text{-pen})]^{2-}$ coordinate an octahedral Co^{III} center in a bis(tridentate-*N,O,S*) mode such that each Co^{III} atoms was in a

cis(*N*)*cis*(*O*)*cis*(*S*)-$N_2O_2S_2$ octahedral environment (Av. Co–S = 2.24 Å, Co–O = 2.06 Å, Co–N = 1.85 Å, S–Co–S = 98.0 °, O–Co–O= 88.8°, N–Co–N = 113.7°) to form a cyclic 9-membered ring composed of $Au_2Co_1S_2P_2C_2$ in trinuclear complex, in which the metalloligand acts as a chelating ligand (Figure 4-32). Its geometric configuration in the octahedral Co unit was optically active all *cis* type (Discriminated by the N,S-chelate ring, *Δ* and *Λ* configurations are determined. For detailed scheme of nomenclature, see Figure 4-33), which was different from that of the $[Au_4Co_2(dppe)_2(D\text{-pen})_4]^{2+}$ with trans(*O*). Because of centrosymmetric space group, *P*-1, a unit cell contained a pair of enantiomers, *Δ* and *Λ*. Indeed, solid state CD spectra showed silent. It should be noted that the strong intramolecular aurophilic interaction with the close Au···Au distance (Au···Au = 2.9334(9) Å) works to support the formation of the Au_2Co trinuclear complex. In the packing structure the cations and anions were arranged in an alternative way (Figure 4-34). There were no hydrogen bonding interaction between pen moieties and anion, and the cationic complexes formed dimeric structure via weak NH_2···COO hydrogen bonds (Av. N···O = 3.24 Å).

Single-crystal X-ray diffraction analysis revealed that [**14**]ClO_4 crystallized in a tetragonal space group of *P*4/*n* which was also centrosymmetric space group as [**14**]NO_3. Molecular and packing structures are shown in Figures 4-35 and 4-36. The crystallographic data are summarized in Table 4-9, and the selected bond distances and angles are listed in Table 4-10. The asymmetric unit contained a cationic complex of $[Au_2Co(dcpe)(D\text{-pen})(L\text{-pen})]^+$, three perchlorate anions which were disordered into three parts, Cl^-, Na^+, and 8 solvated water molecules (Figure 4-35). The molecular structure of the cationic complex was similar to that of [**14**]NO_3, but the supramolecular structure was completely different. Interestingly, in the crystal structure of [**14**]ClO_4, four *Δ*-[**14**]$^+$ complexes or four *Λ*-[**14**]$^+$ complexes aggregate to form tetrameric assembly around chloride anion via hydrogen bonds (N···Cl^-: 3.294 Å, N···O: 2.797(9) Å and N···O: 2.852(9) Å), which was indicative of the anion templating effect (Figure 4-36a). The tetrameric assembly composed of *Δ*-[**14**]$^+$ arranged on the *ab* plane to form a sheet structure (Figure 4-36b). Further, the sheet structures stack along *c* axis to form an alternate *Δ* and *Λ* stacking structure (Figure 4-36c).

Single-crystal X-ray diffraction analysis revealed that [**15**] crystallized in an orthorhombic space group of $P2_12_12_1$ which was a non-centrosymmetric space group. Molecular and packing structures are shown in Figures 4-37, 4-38, 4-39, and 4-40. The crystallographic data are summarized in Table 4-11, and the selected bond distances and angles are listed in Table 4-12. The asymmetric unit contained a whole molecule of $[Au_2Ni(dcpe)(D\text{-pen})(L\text{-pen})]$, and five solvated methanol molecules (Figure 4-37). Both

D/L-penicillamine moieties of $[Au_2(dcpe)(D\text{-pen})(L\text{-pen})]^{2-}$ coordinate an octahedral Ni^{2+} center in a bis(tridentate-*N,O,S*) mode to form a cyclic 9-membered ring composed of $Au_2Ni_1S_2P_2C_2$ (Figure 4-38a). Its geometric configuration in the octahedral Ni^{2+} unit was optically active all *cis* type with the *Δ* form (Figure 4-39a). Indeed, the absorption and solid CD spectra showed a different feature from the reported $[Au_4Ni_2(dppe)_2(D\text{-pen})_4]^{2+}$ with trans(*O*) (Figure 4-19).[6,9] In a similar way to [**14**]$^+$, the intramolecular aurophilic interaction with the close Au···Au distance (2.9693(6) Å) worked strongly for the formation of the Au_2Ni trinuclear complex. The crystallographic data for [**15**]′, enantiomeric crystal of [**15**] were summarized in Table 4-11, and the selected bond distances and angles were listed in Table 4-13. The absolute configurations of [**15**] and [**15**]′ were confirmed by flack parameters in X-ray crystallography (Table 4-11). In the [**15**] crystal, the homochiral trinuclear complexes formed an aggregation of 1D right-handed helical chain along *a* axis via NH_2···OCO hydrogen bonds (Figure 4-40a, N···O = 2.97, 3.04 Å). The enantiomeric crystal [**15**]′ had trinuclear complexes with opposite chirality around Ni center (Figure 4-38b, 4-39b), and the trinuclear complexes aggregated into hydrogen bonded left-handed helical chains, which was enantiomeric to that in [**15**] (Figure 4-40b).

IV-3-7. Aggregation Behavior of the Trinuclear Complexes.

It is worth to pay attention to the fact that the similar molecules, DL-Au_2Co and DL-Au_2Ni, formed totally different types of the packings. While DL-Au_2Co complexes [**14**]$^+$ crystallized in centrosymmetric space groups (*P*-1 for nitrate salt and *P*4/*n* for perchlorate salt) and a crystal of [**14**]NO_3 or [**14**]ClO_4 contained both *Δ*- and *Λ*-DL-Au_2Co complexes, DL-Au_2Ni complexes crystallized in non-centrosymmetric $P2_12_12_1$ space group and a crystal of [**15**] contained only one kind of *Δ*-DL-Au_2Ni complexes. As a result, in [**15**], only *Δ* forms crystallized in a crystal though [**15**] had an enantiomer. Therefore, a spontaneous resolution was expected and other crystals which contained the optically active complex having the opposite geometric configuration, *Λ*, should be found. As we expected, we succeeded in picking up another crystal [**15**]′ which contained optically active *Λ* complexes, which was confirmed by single crystal X-ray diffraction analysis and flack parameter. Each single crystal of [**15**] (*Δ*) and [**15**]′ (*Λ*) showed CD spectra enantiomeric to each other as already explained.

In general, a meso isomer crystallizes in not a non-centrosymmetric but a centrosymmetric space group. However, in this study, we generated the chirality on the achiral meso isomers by coordination to metal centers (metalloligand approach), which led to the chiral crystal packing. To the best of our knowledge, this was the first

example of spontaneous resolution composed of an achiral meso isomeric metalloligand. Considering both results of [**15**] and [**14**]X ($X^- = NO_3^-$, ClO_4^-), we assumed that the presence of coulombic interaction affected the distinct difference in whether spontaneous resolution takes place in [**15**] or not in [**14**]X ($X^- = NO_3^-$, ClO_4^-). Because $[\mathbf{14}]^+$ was a cationic species, coulombic interaction between $[\mathbf{14}]^+$ and achiral anion worked for an assist of aggregation, resulting in an achiral packing, also, there must be coulombic repulsions between the Co centers in each cation, which may lead to the formation of weaker hydrogen bonding interactions than these in neutral Ni species, contributing to the construction of the chiral helical chain-like aggregate found in the crystal structure of [**15**]. On the other hand, in [**15**] owing to all neutral species, no coulombic interaction worked during crystallization. As a result, in [**15**], only *Δ* forms crystallized in a crystal and the same was the case with *Λ* forms in [**15**]′. In the end, we showed a serendipity of spontaneous resolution controlled by coulombic interaction.

IV-3-8. Comparison with dppe Complexes.

In the molecular structure of homochiral $[\mathbf{13}]^{2+}$ determined by single crystal X-ray diffraction analysis, the cyclic 18-membered metalloring was distorted on the bridging diphosphinoethane part to form a bent structure while that of $[Au_4Co_2(dppe)_2(D\text{-pen})_4]^{2+}$ which crystallized in Cubic *F*23 formed a straight shape. It was implied that the bent structure was affected by the less flexibility of the restricted bridging diphosphinoethane part in dcpe due to the steric hindrance of cyclohexyl group compared with phenyl group. In addition, the molecular structure of $[Au_4Co_2(dppe)_2(D\text{-pen})_4]^{2+}$ was carefully checked with focusing on the intramolecular interactions. In $[Au_4Co_2(dppe)_2(D\text{-pen})_4]^{2+}$, it was found that intramolecular CH···π interactions in two parts played an important role to form a straight molecular shape (Figure 4-41). Considering the bulkiness of cyclohexyl group which cannot form CH···π interaction, it is easy to imagine that the replacement of phenyl group with cyclohexyl group is impossible. As a result, $[\mathbf{13}]^{2+}$ preferred a bent structure to a straight one to avoid the steric repulsion. It was concluded, in this discussion part, that the steric hindrance of cyclohexyl group in dcpe had an influence on the flexibility on the bridging diphosphinoethane part as well as intramolecular interactions, which led a bent form of $[\mathbf{13}]^{2+}$.

In dppe coordination system, the crystals of not only homochiral hexanuclear structure ($[Au_4Co_2(dppe)_2(D\text{-pen})_4]^{2+}$) but also the homochiral trinuclear structure ($[Au_2Co(dcpe)(D\text{-pen})_2]^+$) were found in the different crystallization conditions. On the other hand, the dcpe homochiral system could produce only the hexanuclear structure $[Au_4Co_2(dcpe)_2(D\text{-pen})_4]^{2+}$ ($[\mathbf{13}]^{2+}$). Based on the molecular modeling examinations of

homochiral trinuclear and homochiral hexanuclear structure, it was found that the homochiral trinuclear structure had a distorted tetrahedral geometry around bridging S atoms rather than the case for homochiral hexanuclear structure (Figure 4-42). Therefore, the homochiral trinuclear structure is less homochiral hexanuclear structure. In spite of the less stability, the crystals containing $[Au_2Co(dcpe)(D\text{-pen})_2]^+$ cations could be isolated probably due to the increment of crystallinity by CH···π and π···π interactions of phenyl groups in dppe ligands, which are not present in dcpe systems. The less supramolecular interaction ability of dcpe systems probably induced the different result from dppe systems.

In our previous work, we found that, in dppe system, chiral-scrambling reaction produced the mixture of homochiral D_4- and L_4-Au_4Co_2 hexanuclear complexes and a heterochiral D_2L_2-Au_4Co_2 hexanuclear complex, whereas heterochiral DL-trinuclear complex was also obtained in some conditions. To clarify the factor in controlling the formation of hexanuclear or trinuclear complexes, the careful comparison of the crystal structures of these complexes were attempted. It was found that in $[Au_2Co(dppe)(D\text{-pen})(L\text{-pen})]^+$, the bridging diphosphinoethane part was closed to form 9-membered ring. On the other hand, in $[Au_4Co_2(dppe)_2(D\text{-pen})_4]^{2+}$, the bridging diphosphinoethane part was expanded to form the 18-membered ring and sterically more constrained than in a trinuclear complex. Against the constraint, the intramolecular interactions such as CH-π interactions from phenyl group assisted in forming a hexanuclear complex more preferentially than a trinuclear complex in dppe system. This structural feature implied that the motion of the bridging phosphinoethane part and the interactivity of ligands directly affected the selectivity of the formation of hexanuclear or trinuclear complexes.

As described in the above discussion, it is clear that the steric hindrance of cyclohexyl group in dcpe strongly restricts the motion of the bridging diphosphinoethane part. Therefore, it was expected that in dcpe system the formation of a trinuclear complex was preferred to that of a hexanuclear one. As we expected, in this thesis, the reaction of heterochiral metalloligand, $[Au_2(dcpe)(D\text{-Hpen})(L\text{-Hpen})]$, with Co^{III} and Ni^{II} formed only heterochiral trinuclear complexes, [**14**]$^+$ and [**15**] respectively. Therefore, we succeeded in the selective formation of trinuclear complexes from heterochiral metalloligand. Also, in the previous discussion, we demonstrated that a hexanuclear complex, $[Au_4Co_2(dcpe)_2(D\text{-pen})_4]^{2+}$ was obtained from the reaction of homochiral metalloligand, $[Au_2(dcpe)(D\text{-Hpen})_2]$. From these results, we revealed that the chirality control of penicillaminate govern the selectivity of the formation of hexanuclear and trinuclear complexes.

Considering the result of chiral scrambling in our previous work,[6,8] the synthetic conditions in which using racemic mixture of [Au_2(dcpe)(D-Hpen)(L-Hpen)] for [**14**]$^+$ and [**15**] might produce three possible isomers of trinuclear DD-/LL-/DL-Au_2Co and Au_2Ni, respectively. However, only heterochiral DL-form was obtained in both systems. The formation of the heterochiral trinuclear complex, [**14**]$^+$, containing the [Co(D-pen)(L-pen)]$^-$ unit, in addition to the expected homochiral trinuclear complex containing the [Co(D-pen)$_2$]$^-$ unit, was presumably caused by the thermodynamic stability, that is, the Co^{III} center in an all-*cis*-$N_2O_2S_2$ octahedral environment might be more stable than that in a *trans*(*O*)-$N_2O_2S_2$ environment. In previous works, the DFT calculation revealed the stability of the all-*cis* isomer of heterochiral species compared with the *trans*(*O*) isomer of homochiral species by 1.13 kcal/mol (Table 4-14 and Figure 4-43)[6c], which supported the selective formation of the heterochiral trinuclear complex.

IV-4. Summary.

In this chapter, a new heteroleptic digold(I) metalloligand with mixed diphosphine and penicillaminate, $[Au_2(dcpe)(pen)_2]^{2-}$, was developed and its coordination behavior was explored to identify the factors in controlling the formation of trinuclear vs. hexanuclear structure by focusing on the homo- and hetero-chirality of penicillaminate. It was found that the homochiral metalloligand formed the Au_4M_2 hexanuclear complexes, while the heterochiral metalloligand formed the Au_2M trinuclear complexes (M = Co^{III}, Ni^{II}). It is likely that the homochiral metalloligand prefers a bent form of the hexanuclear structure rather than a straight one, as found in the dppe hexanuclear complex, due to the steric hindrance and the less interactivity of cyclohexyl groups. The difference in the molecular shapes and interactivities probably prevents the hexanuclear complex cations ($[Au^{I}_4Co^{III}_2(dcpe)_2(D\text{-}pen)_4]^{2+}$) from constructing the unusual separate supramolecular structure of inorganic anions and complex cations, which was found in the dppe analogous complex, $[Au^{I}_4Co^{III}_2(dppe)_2(D\text{-}pen)_4]^{2+}$.

Furthermore, the steric hindrance of the cyclohexyl groups restricted the motion of the bridging diphosphinoethane part, which led to the formation of the trinuclear structure rather than the hexanuclear one in the heterochiral system. In trinuclear complexes, the neutral $Au^{I}_2Ni^{II}$ complex showed a spontaneous resolution, whereas the cationic $Au^{I}_2Co^{III}$ complex did not. We assume that the coulombic interaction between the cationic $Au^{I}_2Co^{III}$ complex and the achiral anions induces a templating effect to be aggregated into the achiral structure, and thus does not show spontaneous resolution behavior. The spontaneous resolution behavior in [**15**] was the first example found in discrete heterochiral molecules composed of an enantiomeric pair of chiral subunits.

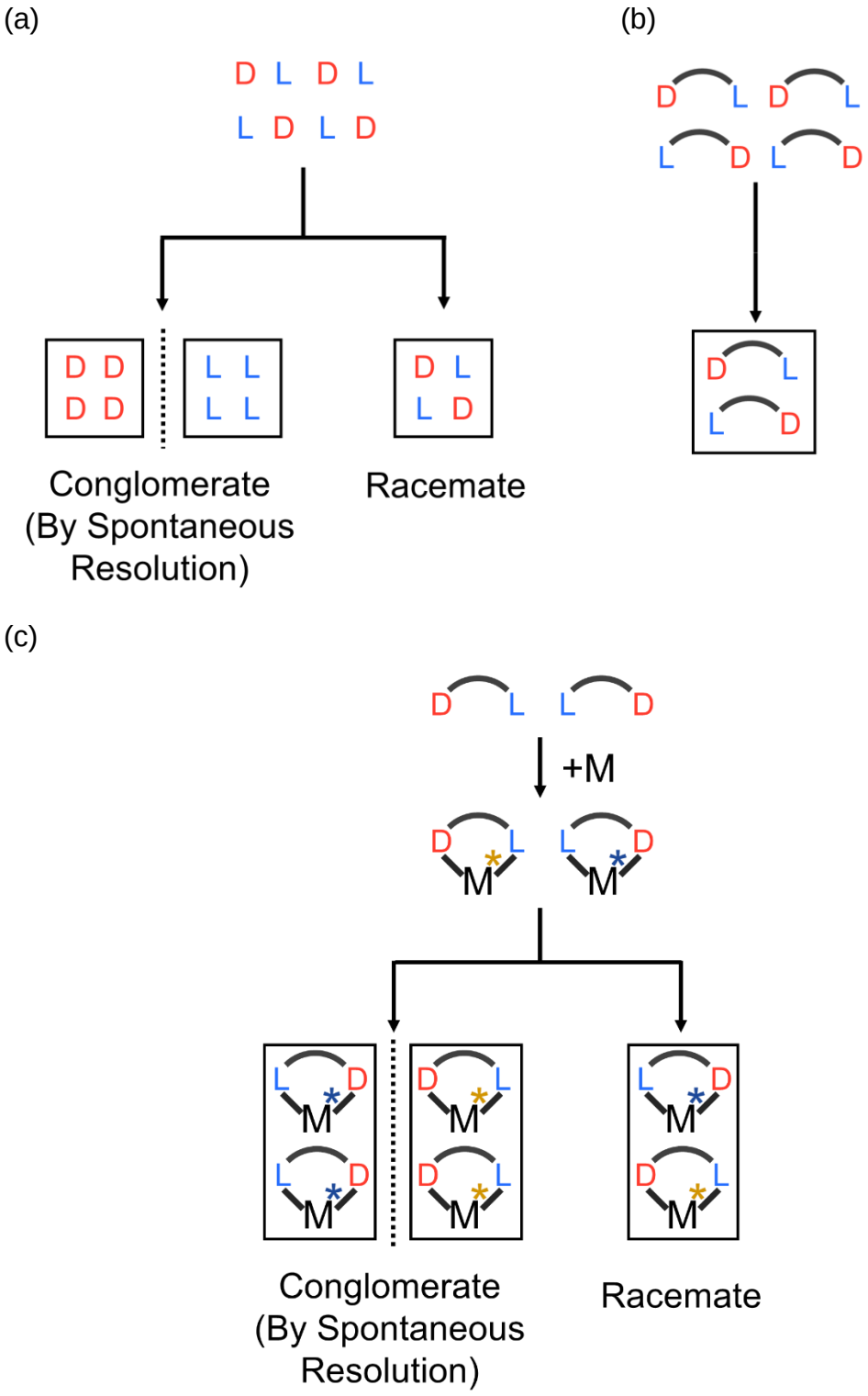

Scheme 4-1. Crystallization behavior of (a) racemic mixture, or racemic conglomerate, (b) racemic mixture of meso isomeric metalloligands, (c) racemic mixture of metal complexes with meso isomeric metalloligands and racemic conglomerate of metal complexes with meso isomeric metalloligands.

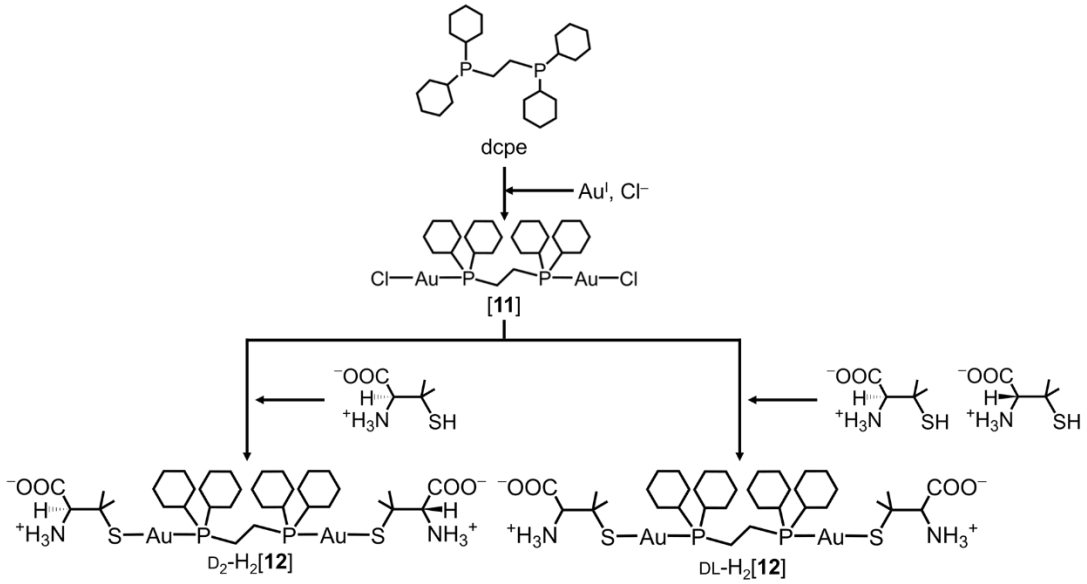

Scheme 4-2. Synthesis of the Au^{I}_2 complex [**11**], homochiral Au^{I}_2 metalloligand with dcpe linker unit, D$_2$-H$_2$[**12**], and heterochiral Au^{I}_2 metalloligand with dcpe linker unit, DL-H$_2$[**12**].

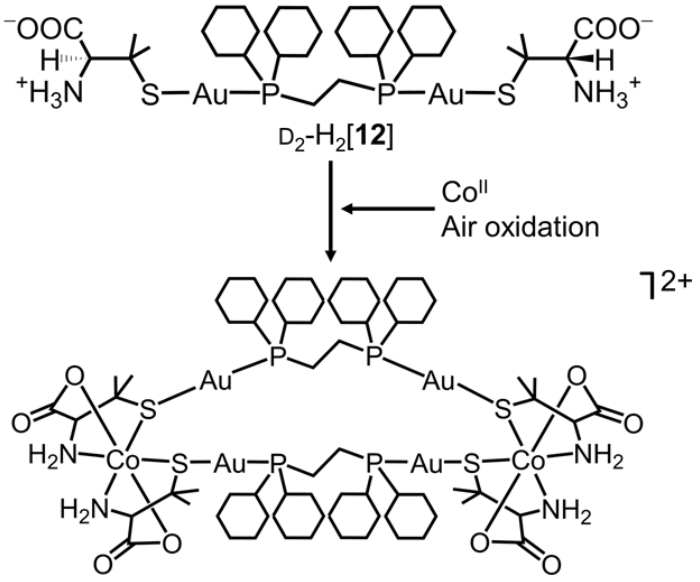

Scheme 4-3. Synthesis of the homochiral $Au^{I}_4Co^{III}_2$ complex cation, [**13**]$^{2+}$.

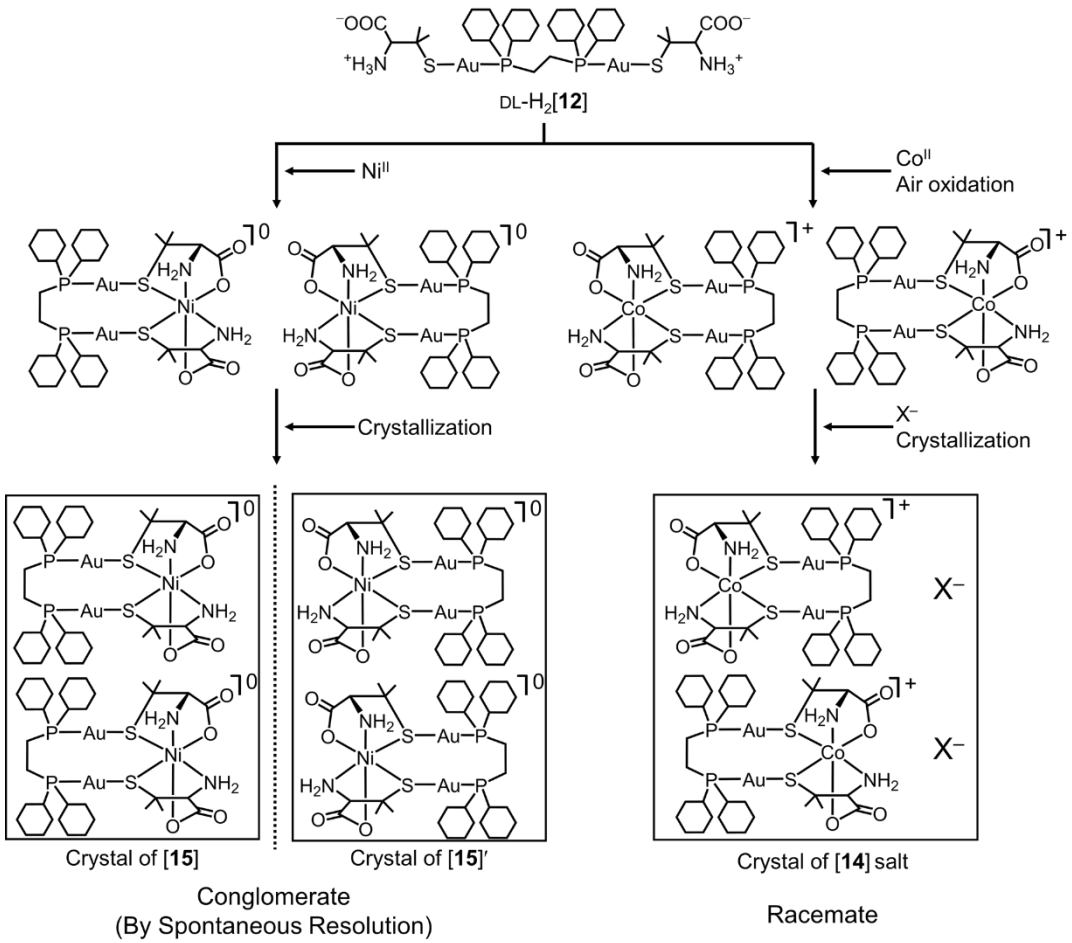

Scheme 4-4. Synthesis of the heterochiral $Au^{I}_{2}Ni^{II}$ neutral complex and $Au^{I}_{2}Co^{III}$ complex cation, and the chiral crystallization behavior of these complexes. The $Au^{I}_{2}Ni^{II}$ neutral complex crystallized as conglomerate of the enantiopure crystals ([**15**] and [**15**]′) by spontaneous resolution, but $Au^{I}_{2}Co^{III}$ complex cation, [**14**]X crystallized as racemate crystals that contained both enantiomeric pairs of the trinuclear complex cations.

Table 4-1. Crystallographic data for [**11**].

	[**11**]
Formula	$C_{26}H_{48}Au_2P_2Cl_2$
Formula weight	887.41
Crystal color	colorless
Crystal size, mm^3	0.067 x 0.061 x 0.097
Crystal system	orthorhombic
Space group	*Pbca*
a, Å	11.38480(10)
b, Å	15.54040(10)
c, Å	16.37190(10)
V, $Å^3$	2896.59(4)
Z	4
ρ(calc), g/cm^3	2.035
$R1$ ($I>2\sigma(I)$) [a)]	0.0215
w$R2$ ($I>2\sigma(I)$) [b)]	0.0744
$R1$ (all data) [a)]	0.0230
w$R2$ (all data) [b)]	0.0762

a) $R1 = \Sigma|(|F_o|-|F_c|)|/\Sigma(|F_o|)$

b) $wR2 = [\Sigma_w(|F_o|^2-|F_c|^2)^2/\Sigma_w(|F_o|^2)^2]^{1/2}$

Table 4-2. Selected bond distances (Å) and angles (°) for [**11**]

		distances	
Au(1)-P(1)	2.2392(4)	Au(1)-Cl(1)	2.2965(4)
C(1)-C(1)′	1.540(3)		
		angles	
P(1)-Au(1)-Cl(1)	177.022(15)	C(1)′-C(1)-P(1)	114.23(14)

Symmetry code: (') 2–x, –y, 1‑z.

Table 4-3. Crystallographic data for D_2/L_2-H_3[**12**]ClO_4.

	D_2/L_2-H_3[**12**]ClO_4·3.5H_2O
Formula	$C_{36}H_{77}Au_2N_2O_{11.5}P_2S_2Cl$
Formula weight	1277.43
Crystal color	colorless
Crystal size, mm^3	0.50 x 0.20 x 0.03
Crystal system	monoclinic
Space group	*C*2/*c*
a, Å	9.6195(2)
b, Å	46.3440(11)
c, Å	23.6728(6)
β, °	99.505(7)
V, $Å^3$	10408.6(5)
Z	8
ρ(calc), g/cm^3	1.630
*R*1 ($I>2\sigma(I)$) [a)]	0.0861
w*R*2 ($I>2\sigma(I)$) [b)]	0.2192
*R*1 (all data) [a)]	0.1454
w*R*2 (all data) [b)]	0.2431

a) $R1 = \Sigma||F_o|-|F_c||/\Sigma|F_o|$

b) $wR2 = [\Sigma_w(|F_o|^2-|F_c|^2)^2/\Sigma_w(|F_o|^2)^2]^{1/2}$

Table 4-4. Selected bond distances (Å) and angles (°) for D_2/L_2-H_3[**12**]ClO_4

		distances	
Au(1)-P(1)	2.252(3)	Au(1)-S(1)	2.312(4)
Au(2)-P(2)	2.261(3)	Au(2)-S(2)	2.299(4)
Au(1)···Au(2)	3.1083(7)	C(11)-C(12)	1.575(17)
		angles	
P(1)-Au(1)-S(1)	178.94(12)	P(2)-Au(2)-S(2)	177.90(13)
C(12)-C(11)-P(1)	114.8(9)	C(11)-C(12)-P(2)	116.1(9)

Table 4-5. Crystallographic data for [**13**]$(NO_3)_2$.

	[**13**]$(NO_3)_2 \cdot 29H_2O$
Formula	$C_{72}H_{132}Au_4Co_2N_6O_{42}P_4S_4$
Formula weight	2911.67
Crystal color	brown
Crystal size, mm^3	0.15 x 0.10 x 0.10
Crystal system	orthorhombic
Space group	$P2_12_12_1$
a, Å	13.769(12)
b, Å	22.278(19)
c, Å	38.81(4)
V, $Å^3$	11904(18)
Z	4
ρ(calc), g/cm^3	1.625
*R*1 ($I>2\sigma(I)$) [a)]	0.0737
w*R*2 ($I>2\sigma(I)$) [b)]	0.1363
*R*1 (all data) [a)]	0.1393
w*R*2 (all data) [b)]	0.1573

a) $R1 = \Sigma(||F_o|-|F_c||)/\Sigma(|F_o|)$

b) $wR2 = [\Sigma_w(|F_o|^2-|F_c|^2)^2/\Sigma_w(|F_o|^2)^2]^{1/2}$

Table 4-6. Selected bond distances (Å) and angles (°) for [**13**]$(NO_3)_2$.

		distances	
Au(1)-P(4)	2.276(5)	Au(1)-S(1)	2.348(5)
Au(2)-P(1)	2.277(6)	Au(2)-S(2)	2.346(5)
Au(3)-P(2)	2.271(5)	Au(3)-S(3)	2.341(5)
Au(4)-P(3)	2.270(6)	Au(4)-S(4)	2.324(5)
Co(1)-O(1)	1.913(13)	Co(1)-O(3)	1.936(11)
Co(1)-N(1)	1.980(15)	Co(1)-N(2)	1.980(14)
Co(1)-S(2)	2.260(5)	Co(1)-S(1)	2.289(6)
Co(2)-O(7)	1.904(14)	Co(2)-N(4)	1.917(16)
Co(2)-O(5)	1.923(13)	Co(2)-N(3)	1.943(15)
Co(2)-S(4)	2.240(6)	Co(2)-S(3)	2.285(6)
C(21)-C(22)	1.58(3)	C(23)-C(24)	1.57(3)
		angles	
P(4)-Au(1)-S(1)	179.57(18)	P(1)-Au(2)-S(2)	177.59(18)
P(2)-Au(3)-S(3)	178.43(18)	P(3)-Au(4)-S(4)	173.38(19)
O(1)-Co(1)-O(3)	174.5(6)	O(1)-Co(1)-N(1)	82.1(7)
O(3)-Co(1)-N(1)	94.4(6)	O(1)-Co(1)-N(2)	94.3(6)
O(3)-Co(1)-N(2)	81.9(6)	N(1)-Co(1)-N(2)	95.8(6)
O(1)-Co(1)-S(2)	91.8(4)	O(3)-Co(1)-S(2)	91.8(4)
N(1)-Co(1)-S(2)	173.7(5)	N(2)-Co(1)-S(2)	86.0(4)
O(1)-Co(1)-S(1)	91.1(4)	O(3)-Co(1)-S(1)	92.7(4)
N(1)-Co(1)-S(1)	84.1(5)	N(2)-Co(1)-S(1)	174.6(5)
S(2)-Co(1)-S(1)	94.62(19)	O(7)-Co(2)-N(4)	83.4(8)
O(7)-Co(2)-O(5)	175.2(7)	N(4)-Co(2)-O(5)	93.9(8)
O(7)-Co(2)-N(3)	94.5(7)	N(4)-Co(2)-N(3)	95.1(8)
O(5)-Co(2)-N(3)	81.8(7)	O(7)-Co(2)-S(4)	91.7(5)
N(4)-Co(2)-S(4)	84.2(5)	O(5)-Co(2)-S(4)	92.0(5)
N(3)-Co(2)-S(4)	173.6(6)	O(7)-Co(2)-S(3)	91.5(5)
N(4)-Co(2)-S(3)	174.6(6)	O(5)-Co(2)-S(3)	91.3(5)
N(3)-Co(2)-S(3)	86.9(6)	S(4)-Co(2)-S(3)	94.4(2)
C(22)-C(21)-P(1)	114.3(14)	C(21)-C(22)-P(2)	112.9(13)
C(24)-C(23)-P(3)	117.1(14)	C(23)-C(24)-P(4)	114.9(14)

Table 4-7. Crystallographic data for [**14**]NO_3.

	[**14**]$NO_3 \cdot H_2O$
Formula	$C_{36}H_{66}Au_2CoN_3O_8P_2S_2$
Formula weight	1247.84
Crystal color	purple
Crystal size, mm^3	0.104 x 0.041 x 0.028
Crystal system	triclinic
Space group	*P*-1
a, Å	9.3019(5)
b, Å	12.9421(7)
c, Å	20.2034(11)
α, °	88.753(3)
β, °	88.106(5)
γ, °	82.750(3)
V, $Å^3$	2411.1(2)
Z	2
ρ(calc), g/cm^3	1.719
*R*1 ($I>2\sigma(I)$) [a)]	0.0959
w*R*2 ($I>2\sigma(I)$) [b)]	0. 2658
*R*1 (all data) [a)]	0.1580
w*R*2 (all data) [b)]	0.2851

a) $R1 = \Sigma|(|F_o|-|F_c|)|/\Sigma(|F_o|)$

b) $wR2 = [\Sigma_w(|F_o|^2-|F_c|^2)^2/\Sigma_w(|F_o|^2)^2]^{1/2}$

Table 4-8. Selected bond distances (Å) and angles (°) for [**14**]NO_3.

		distances	
Au(1)-P(1)	2.258(4)	Au(1)-S(1)	2.318(4)
Au(2)-P(2)	2.254(5)	Au(2)-S(2)	2.290(8)
Co(1)-N(1)	1.65(3)	Co(1)-O(1)	1.98(2)
Co(1)-N(2)	2.04(4)	Co(1)-O(3)	2.14(3)
Co(1)-S(1)	2.192(7)	Co(1)-S(2)	2.292(12)
C(11)-C(12)	1.53(3)	Au(1)···Au(2)	2.9334(9)
		angles	
P(1)-Au(1)-S(1)	177.11(18)	P(1)-Au(1)-Au(2)	94.53(11)
S(1)-Au(1)-Au(2)	87.81(14)	P(2)-Au(2)-S(2)	179.1(3)
P(2)-Au(2)-Au(1)	95.63(13)	S(2)-Au(2)-Au(1)	85.3(2)
N(1)-Co(1)-O(1)	84.7(14)	N(1)-Co(1)-N(2)	113.7(15)
O(1)-Co(1)-N(2)	82.1(12)	N(1)-Co(1)-O(3)	173.1(14)
O(1)-Co(1)-O(3)	88.8(13)	N(2)-Co(1)-O(3)	67.6(16)
N(1)-Co(1)-S(1)	86.6(8)	O(1)-Co(1)-S(1)	85.2(9)
N(2)-Co(1)-S(1)	154.8(14)	O(3)-Co(1)-S(1)	90.5(10)
N(1)-Co(1)-S(2)	95.4(12)	O(1)-Co(1)-S(2)	176.8(10)
N(2)-Co(1)-S(2)	94.9(10)	O(3)-Co(1)-S(2)	91.2(8)
S(1)-Co(1)-S(2)	98.0(3)	C(12)-C(11)-P(1)	115.7(14)
C(11)-C(12)-P(2)	112.1(14)		

Table 4-9. Crystallographic data for [**14**]ClO_4.

	[**14**]$ClO_4 \cdot 0.25NaCl \cdot 5.25H_2O$
Formula	$C_{36}H_{66}Au_2CoN_2O_{13.25}P_2S_2Cl_{1.25}Na_{0.25}$
Formula weight	1367.89
Crystal color	purple
Crystal size, mm^3	0.39 x 0.39 x 0.03
Crystal system	tetragonal
Space group	*P*4/*n*
a, Å	22.119(2)
c, Å	21.9664(12)
V, $Å^3$	10747(2)
Z	8
ρ(calc), g/cm^3	1.691
*R*1 ($I>2\sigma(I)$) [a)]	0.0582
w*R*2 ($I>2\sigma(I)$) [b)]	0.1389
*R*1 (all data) [a)]	0.0947
w*R*2 (all data) [b)]	0.1564

a) $R1 = \Sigma|(|F_o|-|F_c|)|/\Sigma(|F_o|)$

b) $wR2 = [\Sigma_w(|F_o|^2-|F_c|^2)^2/\Sigma_w(|F_o|^2)^2]^{1/2}$

Table 4-10. Selected bond distances (Å) and angles (°) for [**14**]ClO_4.

		distances	
Au(1)-P(1)	2.271(2)	Au(1)-S(1)	2.324(2)
Au(2)-P(2)	2.258(2)	Au(2)-S(2)	2.324(2)
S(1)-Co(1)	2.276(2)	S(2)-Co(1)	2.242(2)
O(1)-Co(1)	1.951(6)	O(3)-Co(1)	1.928(5)
N(2)-Co(1)	1.948(7)	N(1)-Co(1)	1.941(7)
C(11)-C(12)	1.536(13)	Au(1)···Au(2)	2.9651(4)
		angles	
P(1)-Au(1)-S(1)	175.91(7)	P(2)-Au(2)-S(2)	178.61(8)
O(3)-Co(1)-N(1)	176.0(3)	O(3)-Co(1)-N(2)	80.9(3)
N(1)-Co(1)-N(2)	97.4(3)	O(3)-Co(1)-O(1)	94.1(2)
N(1)-Co(1)-O(1)	82.2(3)	N(2)-Co(1)-O(1)	88.9(3)
O(3)-Co(1)-S(2)	89.92(18)	N(1)-Co(1)-S(2)	93.6(2)
N(2)-Co(1)-S(2)	88.4(2)	O(1)-Co(1)-S(2)	174.67(18)
O(3)-Co(1)-S(1)	94.49(18)	N(1)-Co(1)-S(1)	86.9(2)
N(2)-Co(1)-S(1)	172.3(2)	O(1)-Co(1)-S(1)	85.33(18)
S(2)-Co(1)-S(1)	97.80(8)	C(12)-C(11)-P(1)	113.8(7)
C(11)-C(12)-P(2)	116.5(7)		

Table 4-11. Crystallographic data for [**15**] and [**15**]′.

	[**15**]·5MeOH	[**15**]′·5MeOH
Formula	$C_{41}H_{86}Au_2NiN_2O_9P_2S_2$	$C_{41}H_{86}Au_2NiN_2O_9P_2S_2$
Formula weight	1329.82	1329.82
Crystal color	blue	blue
Crystal size, mm^3	0.30 x 0.27 x 0.27	0.30 x 0.10 x 0.08
Crystal system	orthorhombic	orthorhombic
Space group	$P2_12_12_1$	$P2_12_12_1$
a, Å	10.249(3)	10.1952(2)
b, Å	20.838(6)	20.8062(4)
c, Å	24.500(6)	24.5344(5)
V, $Å^3$	5232(2)	5204.32(18)
Z	4	4
ρ(calc), g/cm^3	1.688	1.697
*R*1 ($I>2\sigma(I)$) [a)]	0.0368	0.0353
w*R*2 ($I>2\sigma(I)$) [b)]	0.0754	0.0754
*R*1 (all data) [a)]	0.0509	0.0411
w*R*2 (all data) [b)]	0.0812	0.0776

a) $R1 = \Sigma|(|F_o|-|F_c|)|/\Sigma(|F_o|)$

b) $wR2 = [\Sigma_w(|F_o|^2-|F_c|^2)^2/\Sigma_w(|F_o|^2)^2]^{1/2}$

Table 4-12. Selected bond distances (Å) and angles (°) for [**15**].

		distances	
Au(1)-P(1)	2.2607(19)	Au(1)-S(1)	2.3079(18)
Au(2)-P(2)	2.2520(18)	Au(2)-S(2)	2.3095(19)
Ni(1)-O(3)	2.057(5)	Ni(1)-N(1)	2.065(6)
Ni(1)-O(1)	2.084(6)	Ni(1)-N(2)	2.087(6)
Ni(1)-S(1)	2.443(2)	Ni(1)-S(2)	2.445(2)
Au(1)···Au(2)	2.9660(7)	C(11)-C(12)	1.539(10)
		angles	
P(1)-Au(1)-S(1)	176.61(7)	P(2)-Au(2)-S(2)	177.47(7)
O(3)-Ni(1)-N(1)	170.2(3)	O(3)-Ni(1)-O(1)	91.9(2)
N(1)-Ni(1)-O(1)	78.3(3)	O(3)-Ni(1)-N(2)	78.8(2)
N(1)-Ni(1)-N(2)	100.2(3)	O(1)-Ni(1)-N(2)	90.8(3)
O(3)-Ni(1)-S(1)	97.17(16)	N(1)-Ni(1)-S(1)	83.21(18)
O(1)-Ni(1)-S(1)	86.39(17)	N(2)-Ni(1)-S(1)	175.0(2)
O(3)-Ni(1)-S(2)	89.65(18)	N(1)-Ni(1)-S(2)	99.9(2)
O(1)-Ni(1)-S(2)	172.61(17)	N(2)-Ni(1)-S(2)	82.4(2)
S(1)-Ni(1)-S(2)	100.57(7)	C(12)-C(11)-P(1)	116.8(5)
C(11)-C(12)-P(2)	118.1(5)		

Table 4-13. Selected bond distances (Å) and angles (°) for [**15**]′.

		distances	
Au(1)-P(1)	2.263(2)	Au(1)-S(1)	2.316(2)
Au(2)-P(2)	2.258(2)	Au(2)-S(2)	2.316(2)
Ni(1)-O(3)	2.058(6)	Ni(1)-N(1)	2.072(7)
Ni(1)-N(2)	2.090(7)	Ni(1)-O(1)	2.101(6)
Ni(1)-S(2)	2.441(3)	Ni(1)-S(1)	2.449(3)
Au(1)···Au(2)	2.9692(5)	C(11)-C(12)	1.531(12)
		angles	
P(1)-Au(1)-S(1)	177.05(8)	P(1)-Au(1)-Au(2)	93.64(6)
S(1)-Au(1)-Au(2)	89.19(5)	P(2)-Au(2)-S(2)	177.64(9)
P(2)-Au(2)-Au(1)	92.00(6)	S(2)-Au(2)-Au(1)	89.56(6)
O(3)-Ni(1)-N(1)	170.0(3)	O(3)-Ni(1)-N(2)	78.7(3)
N(1)-Ni(1)-N(2)	100.4(3)	O(3)-Ni(1)-O(1)	92.0(3)
N(1)-Ni(1)-O(1)	78.0(3)	N(2)-Ni(1)-O(1)	91.0(3)
O(3)-Ni(1)-S(2)	89.7(2)	N(1)-Ni(1)-S(2)	100.1(2)
N(2)-Ni(1)-S(2)	82.5(2)	O(1)-Ni(1)-S(2)	172.9(2)
O(3)-Ni(1)-S(1)	96.52(18)	N(1)-Ni(1)-S(1)	83.7(2)
N(2)-Ni(1)-S(1)	174.0(2)	O(1)-Ni(1)-S(1)	85.5(2)
S(2)-Ni(1)-S(1)	101.17(8)	C(12)-C(11)-P(1)	117.3(6)
C(11)-C(12)-P(2)	118.2(6)		

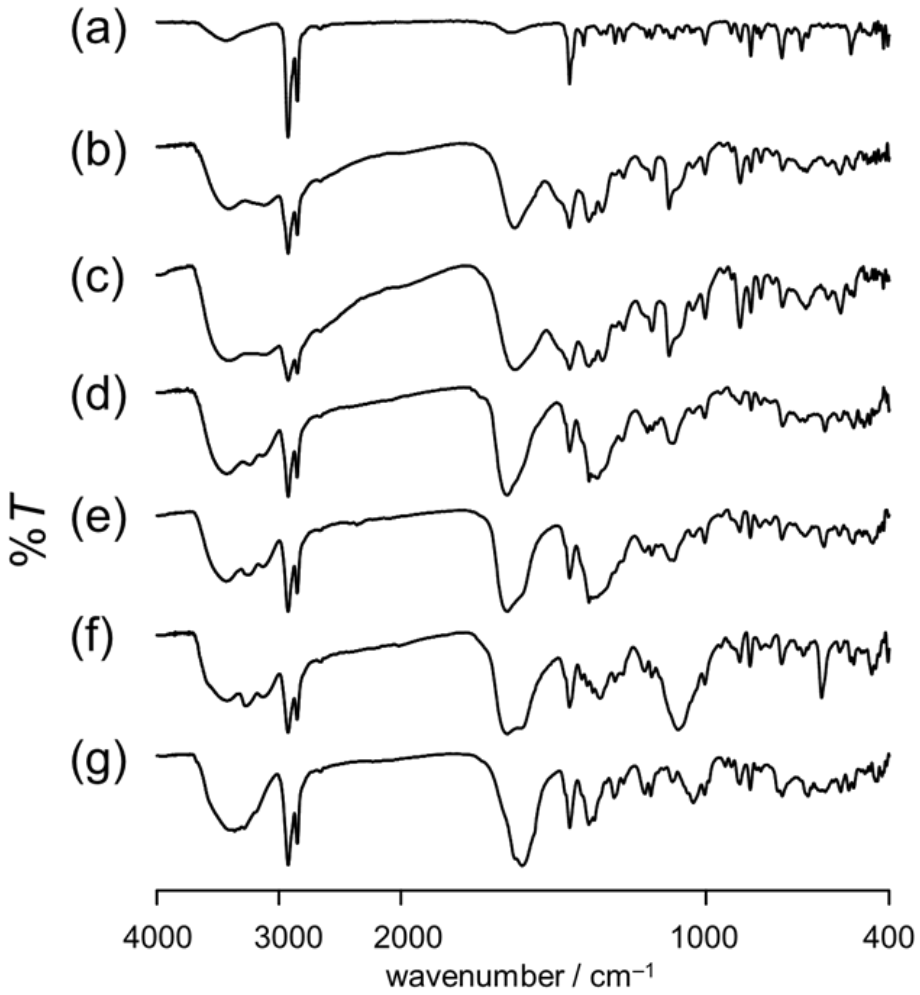

Figure 4-1. IR spectra of (a) [**11**], (b) D$_2$-H$_2$[**12**], (c) DL-H$_2$[**12**], (d) [**13**](NO$_3$)$_2$, (e) [**14**]NO$_3$, (f) [**14**]ClO$_4$, and (g) [**15**] (KBr disk).

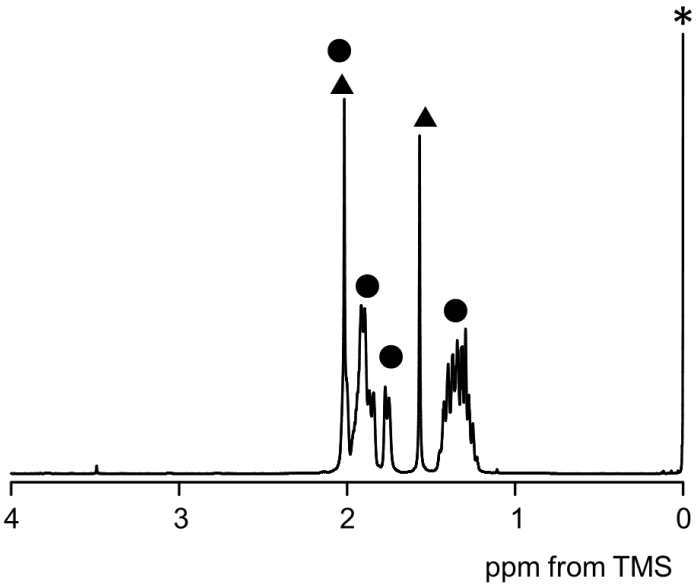

Figure 4-2. ^{1}H NMR spectrum of [**11**] in $CDCl_3$. Filled circles (●) represent the methylene and the methine signals of Cy moieties and filled triangles (▲) represent the methylene signals of linker C2 chain moieties. The * marks represent the signals of solvents and TMS signals.

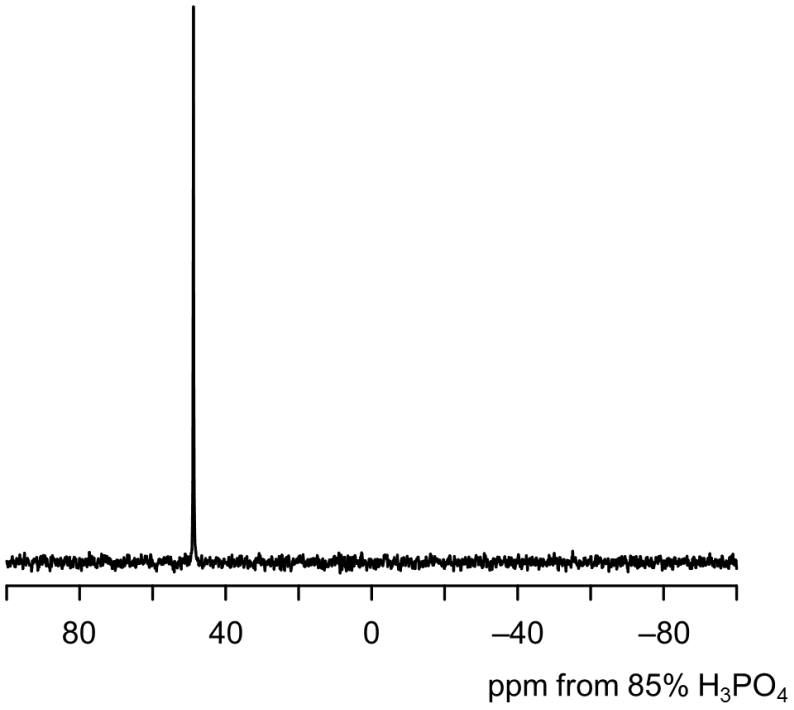

Figure 4-3. ^{31}P NMR spectrum of [**11**] in $CDCl_3$.

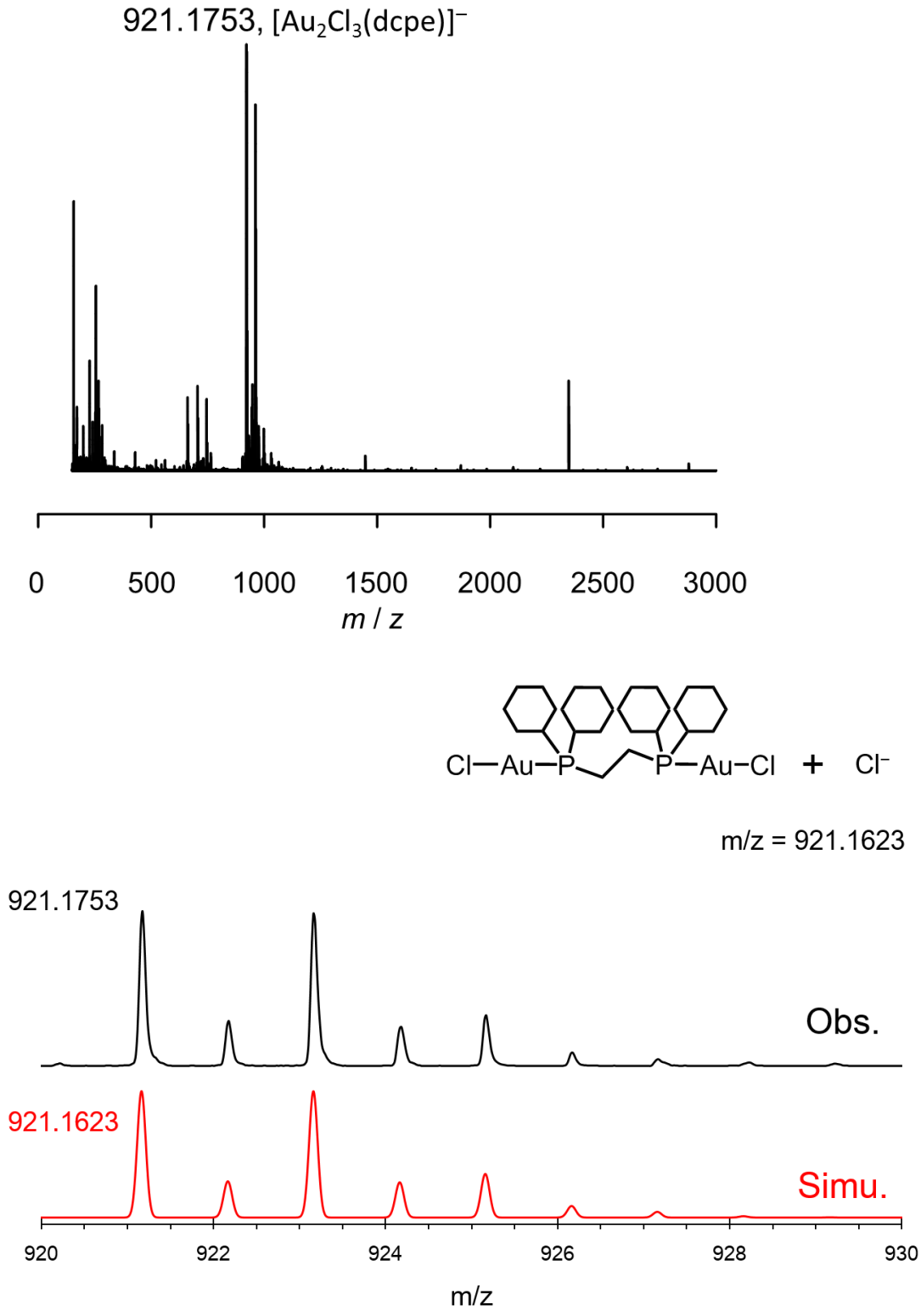

Figure 4-4. ESI-MS spectrum of [**11**]. Signals from $[Au_2Cl_3(dcpe)]^-$ were magnified.

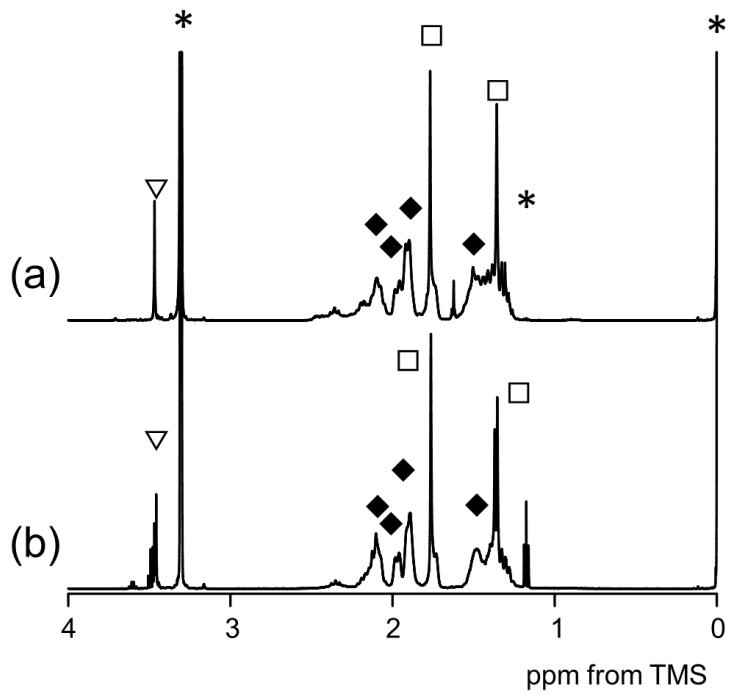

Figure 4-5. ^{1}H NMR spectra of (a) D$_2$-H$_2$[**12**] and (b) DL-H$_2$[**12**] in CD$_3$OD. Filled diamonds (◆) represent the signals of dcpe moieties, open squares (□) represent the methyl signals of pen moieties and open reversed triangles (▽) represent the methine signals of pen moieties. The * marks represent the signals of solvents and TMS signals.

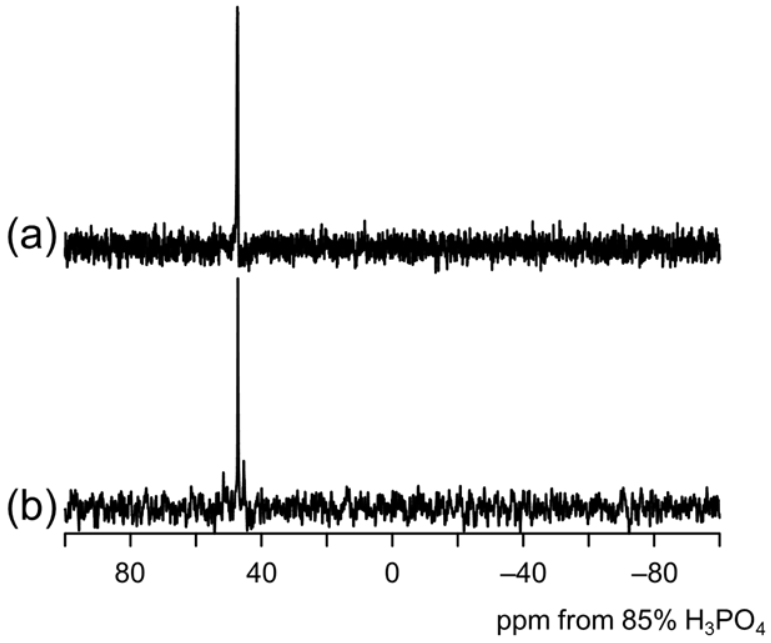

Figure 4-6. ^{31}P NMR spectra of (a) D$_2$-H$_2$[**12**] and (b) DL-H$_2$[**12**] in CD$_3$OD.

(a)

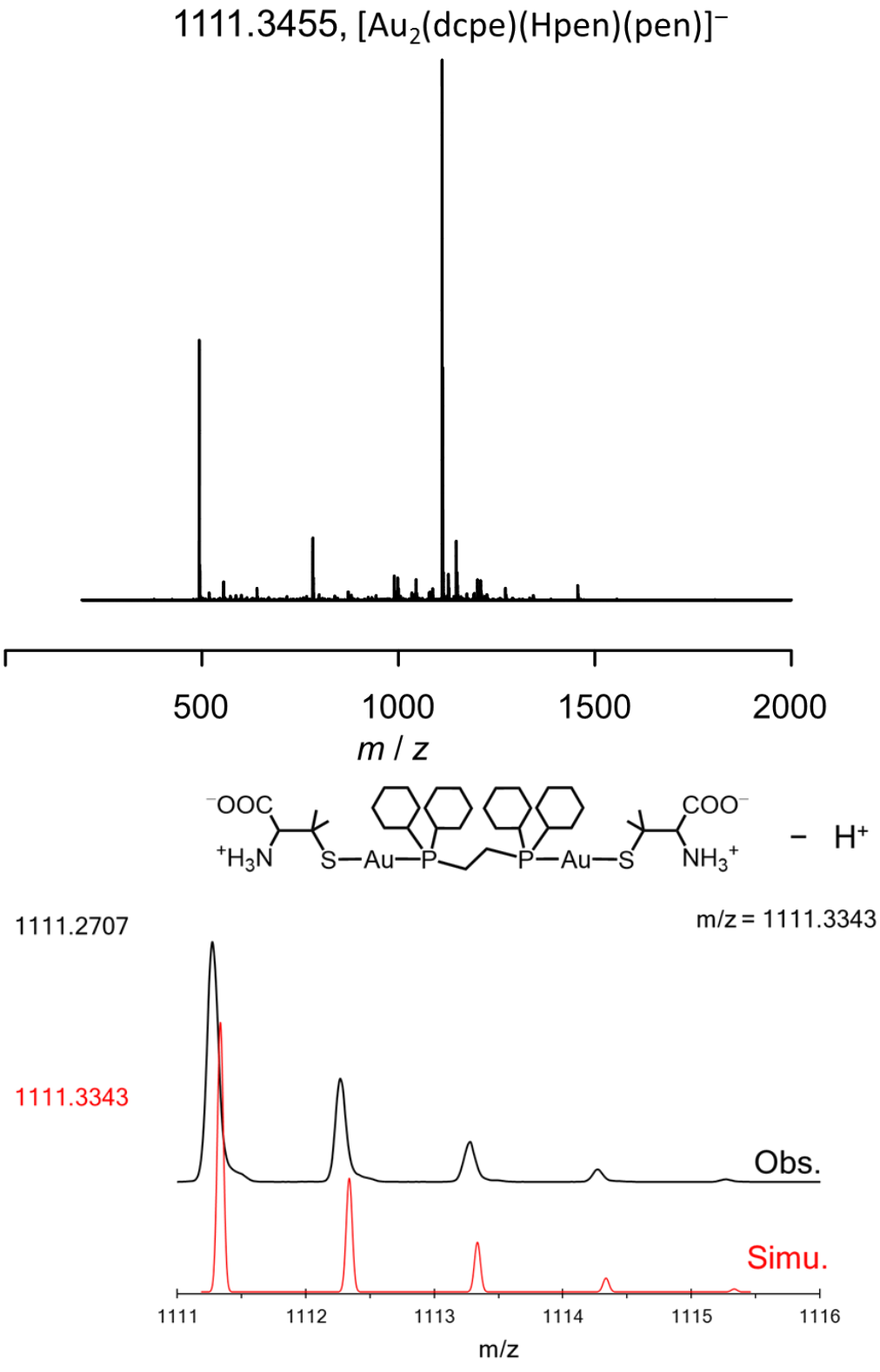
1111.3455, [Au2(dcpe)(Hpen)(pen)]−
500
1000
1500
2000
m / z
−OOC
+H3N
S—Au—P
P—Au—S
COO−
NH3+
− H+
1111.2707
1111.3343
m/z = 1111.3343
Obs.
Simu.
1111
1112
1113
1114
1115
1116
m/z

(b)

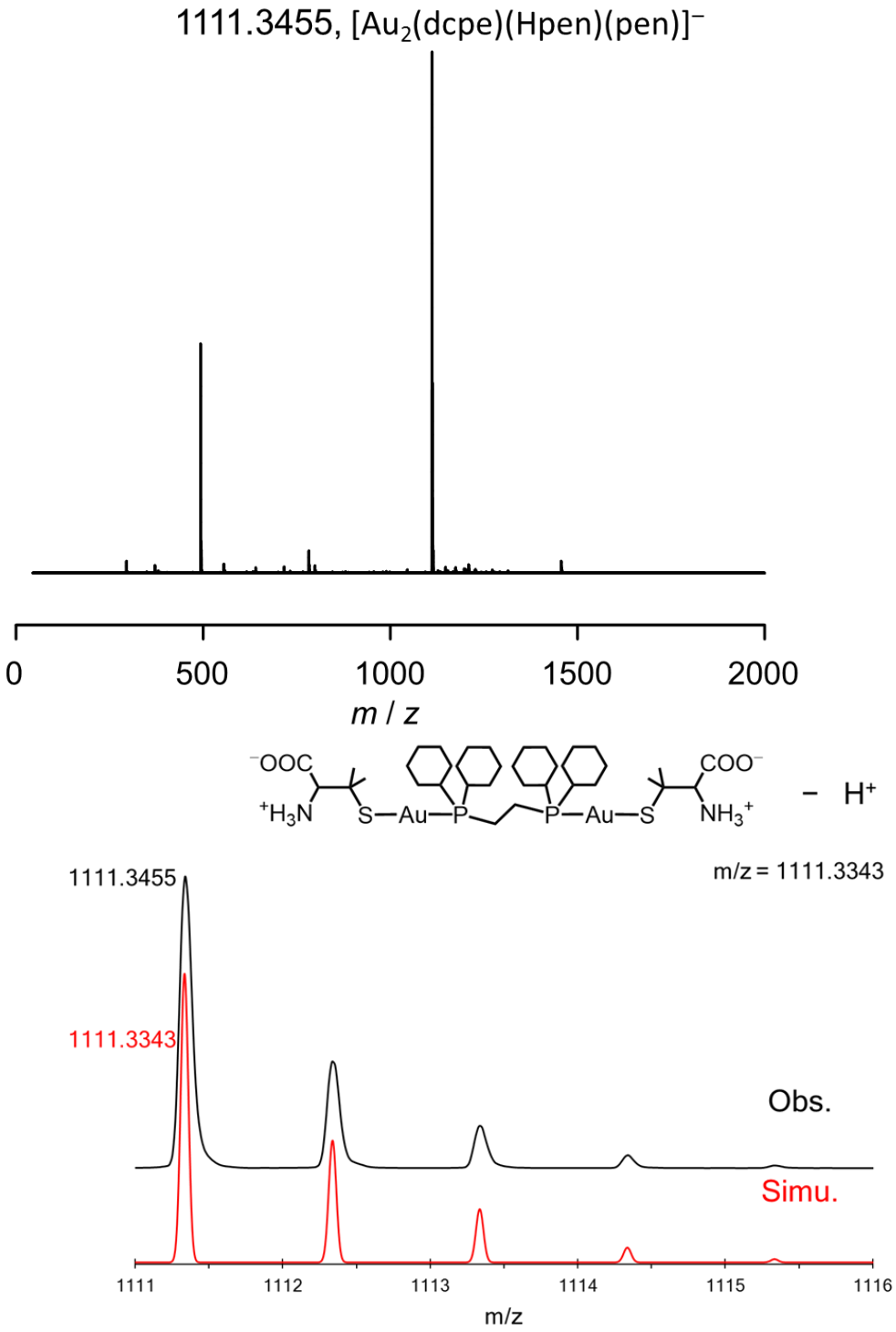

Figure 4-7. ESI-MS spectra of (a) D_2-H_2[**12**] and (b) DL-H_2[**12**] with simulated spectra. The signals from $[Au_2(dcpe)(Hpen)(pen)]^-$ were magnified for each spectrum.

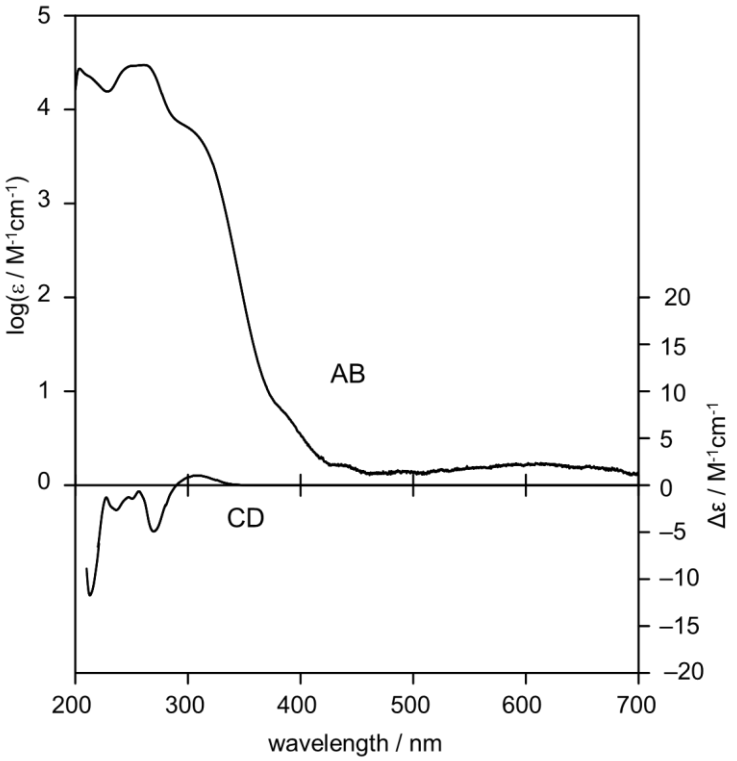

Figure 4-8. Absorption (AB) and CD spectra of D2-H2[**12**] in MeOH.

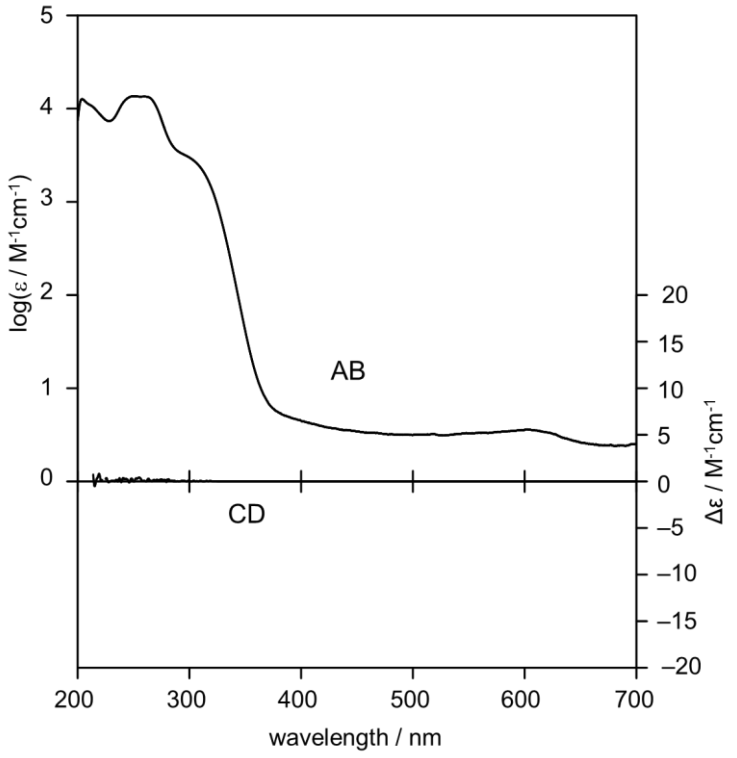

Figure 4-9. Absorption (AB) and CD spectra of DL-H2[**12**] in MeOH.

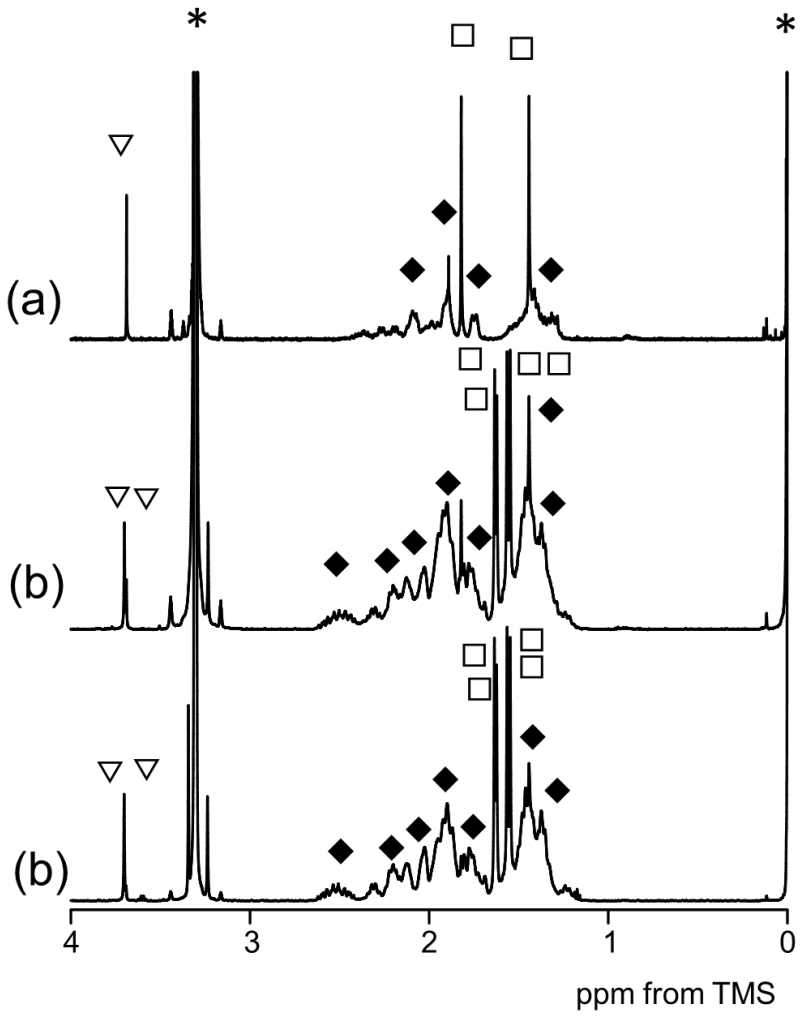

Figure 4-10. ^{1}H NMR spectra of (a) [**13**]$(NO_3)_2$, (b) [**14**]NO_3, and (c) [**14**]ClO_4 in CD_3OD. Filled diamonds (◆) represent the signals of dcpe moieties, open squares (□) represent the methyl signals of pen moieties and open reversed triangles (▽) represent the methine signals of pen moieties. The * marks represent the signals of solvents and TMS signals.

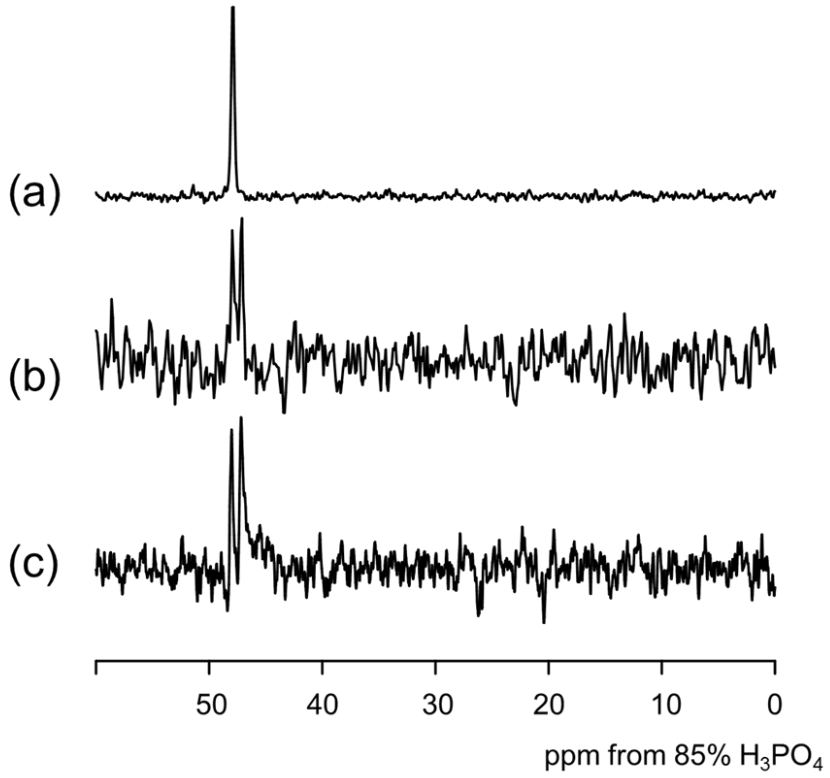

Figure 4-11. ^{31}P NMR spectra of (a) [**13**]$(NO_3)_2$, (b) [**14**]NO_3, and (c) [**14**]ClO_4 in CD_3OD.

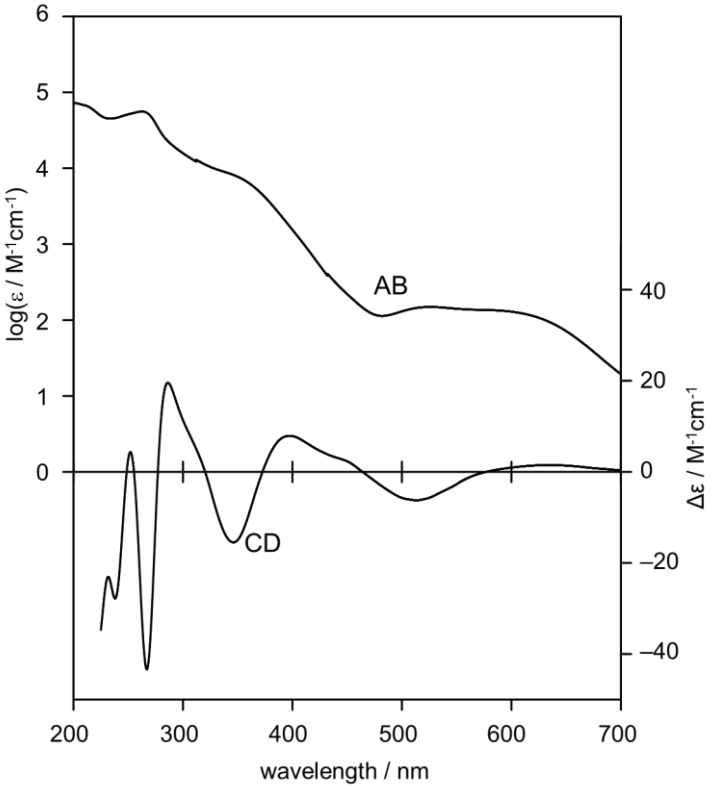

Figure 4-12. Absorption (AB) and CD spectra of [**13**]$(NO_3)_2$ in MeOH.

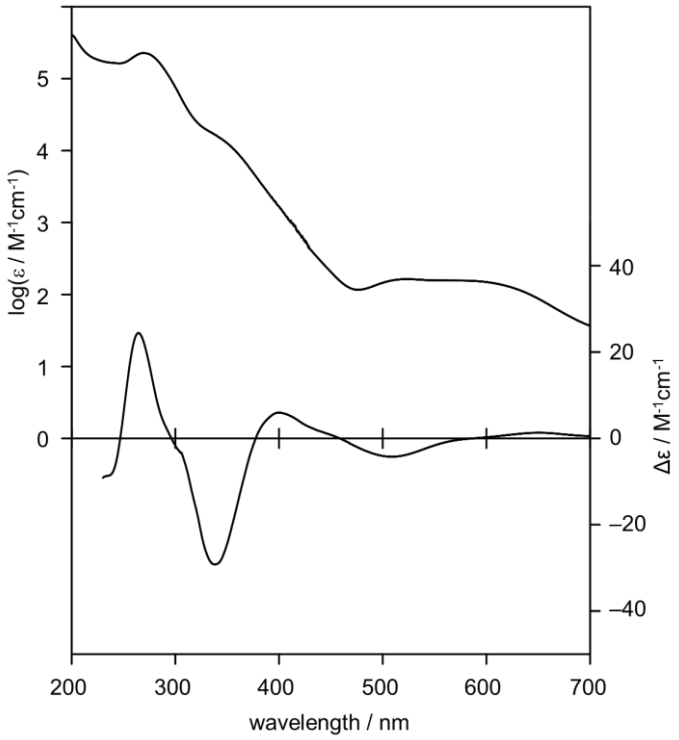

Figure 4-13. Absorption (AB) and CD spectra of $[Au_4Co_2(dppe)_2(D\text{-pen})_4]Cl_2$ in MeOH.[7]

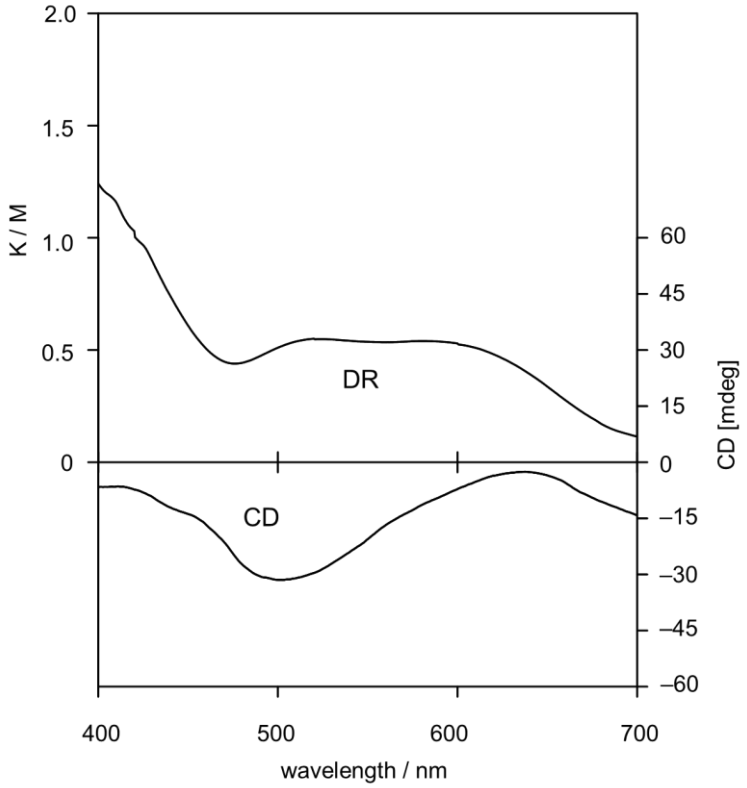

Figure 4-14. Diffuse reflection (DR) and CD spectra of [**13**]$(NO_3)_2$ in the solid state.

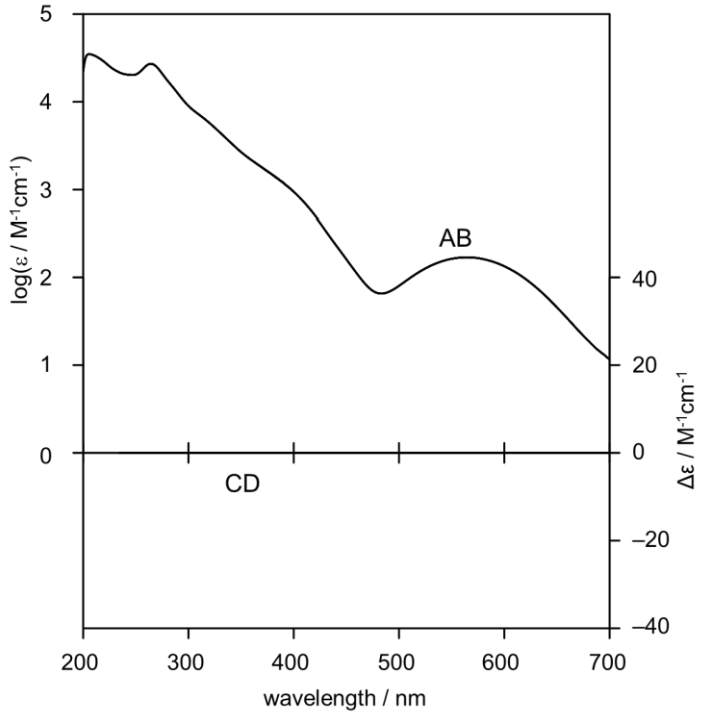

Figure 4-15. Absorption (AB) and CD spectra of [**14**]NO_3 in MeOH.

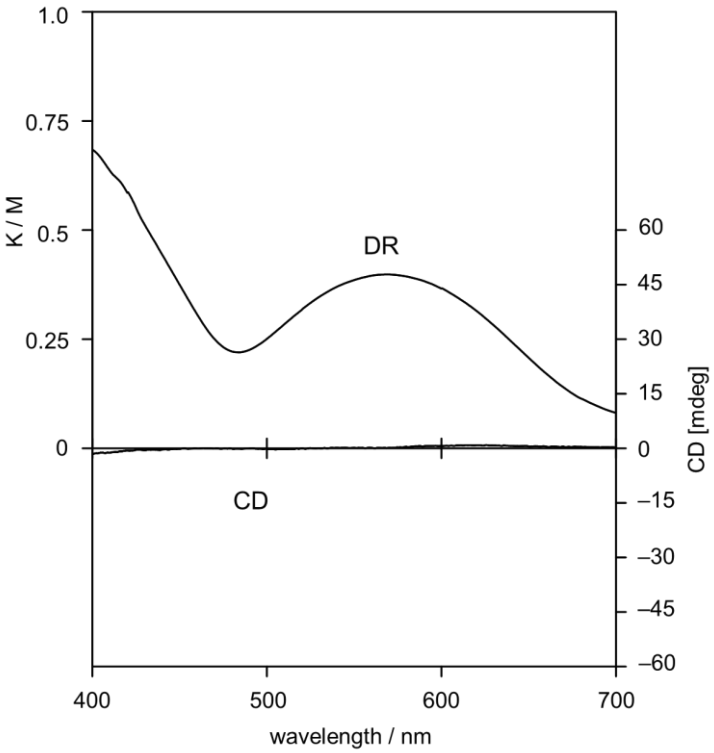

Figure 4-16. Diffuse reflection (DR) and CD spectra of [**14**]NO_3 in the solid state.

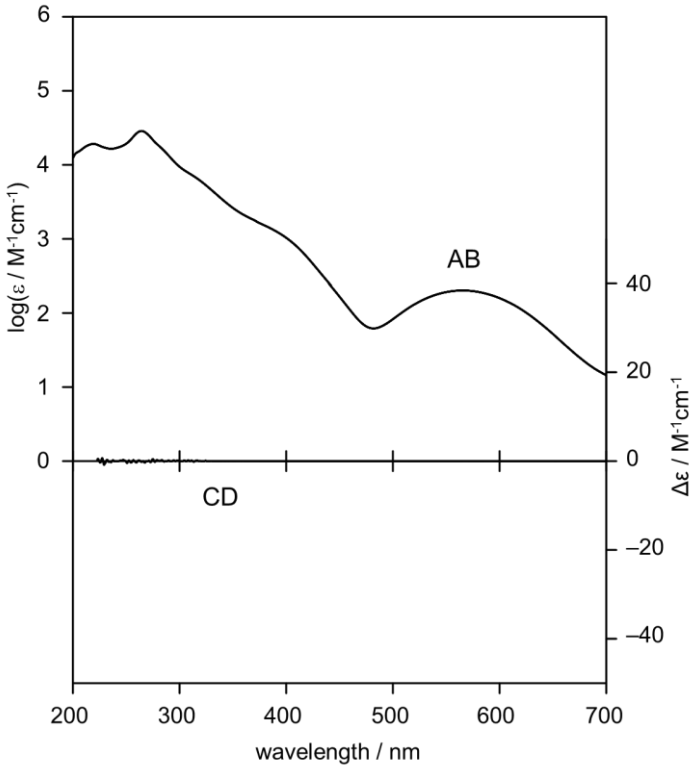

Figure 4-17. Absorption (AB) and CD spectra of [**14**]ClO_4 in MeOH.

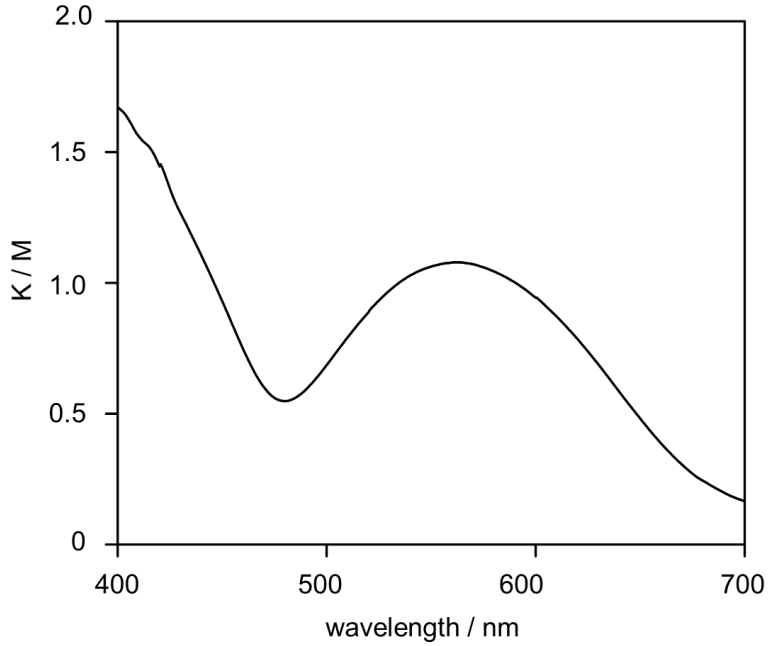

Figure 4-18. Diffuse reflection (DR) spectrum of [**14**]ClO_4 in the solid state.

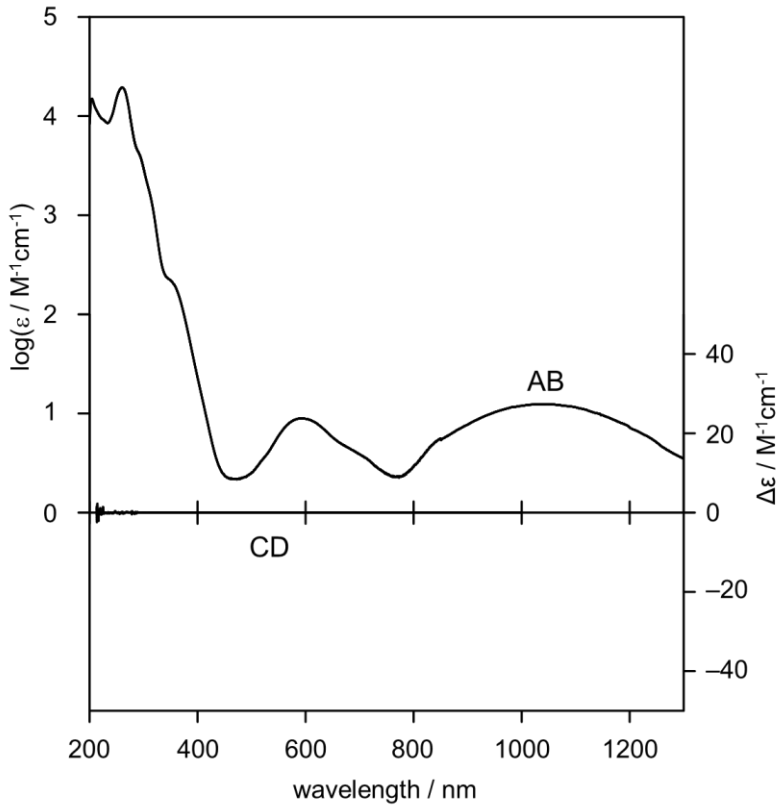

Figure 4-19. Absorption (AB) and CD spectra of [**15**] in MeOH.

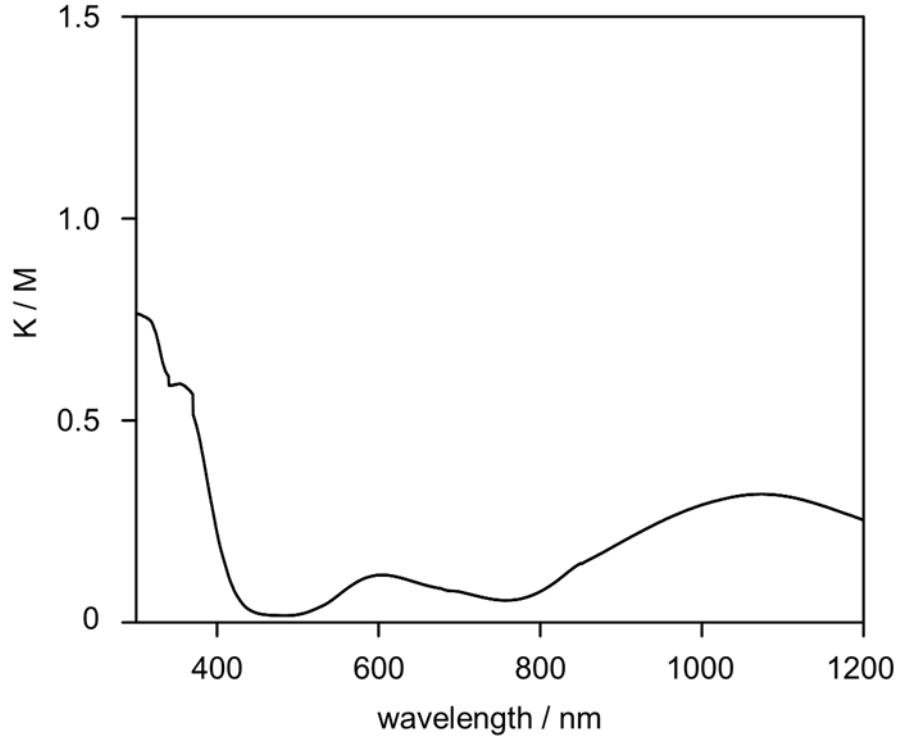

Figure 4-20. Diffuse reflection (DR) spectrum of [**15**] in the solid state.

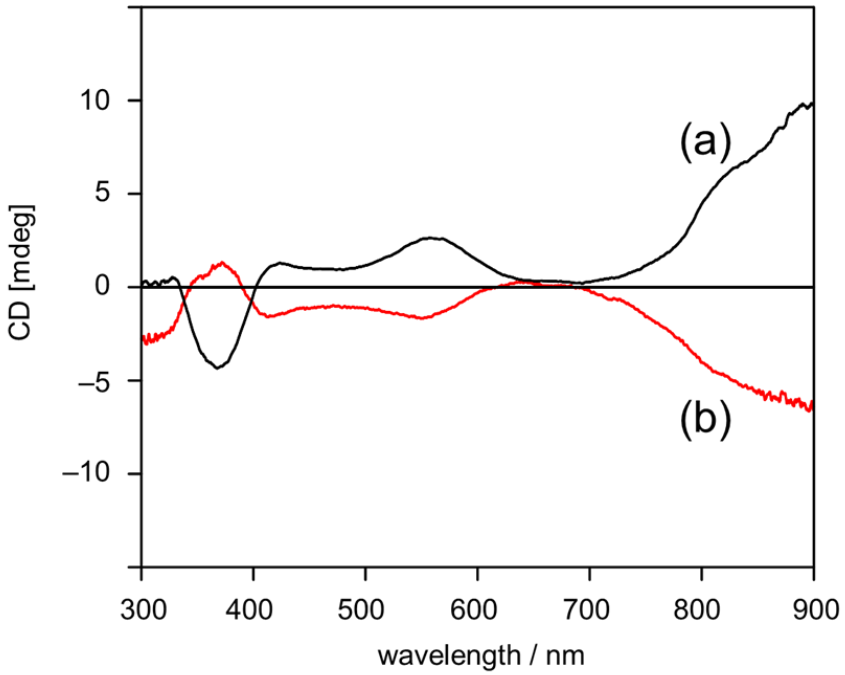

Figure 4-21. CD spectra of a single crystal of (a) [**15**] and (b) [**15**]′ in the solid state.

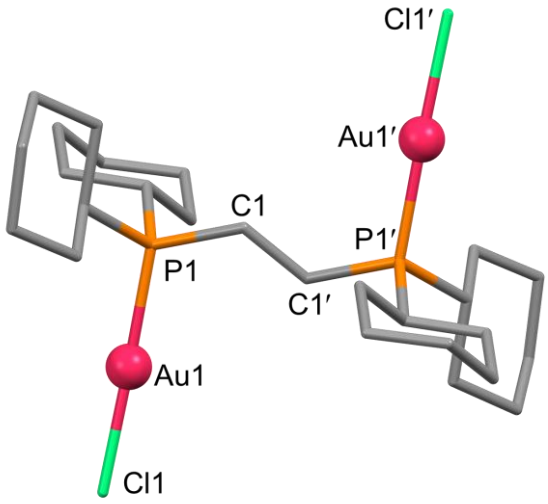

Figure 4-22. A drawing of complex molecule in [**11**] with some of the atomic labeling scheme. Hydrogen atoms are omitted for clarity. One part of the disordered atoms is omitted. Symmetry code: (') x, 1–y, 1–z.

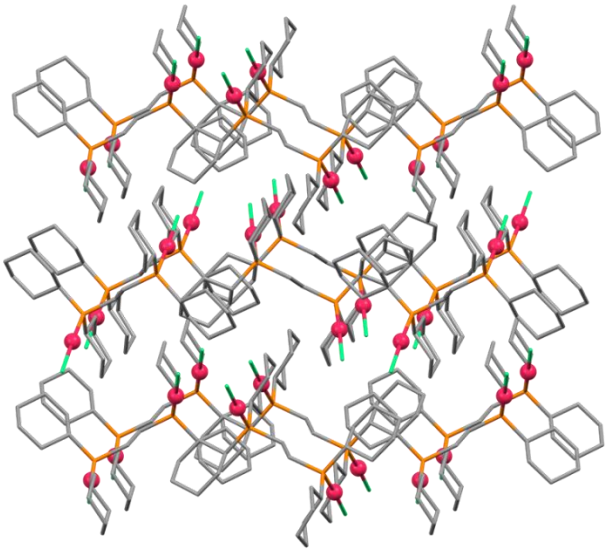

Figure 4-23. A closely packed structure of complex molecules in the crystal [**11**].

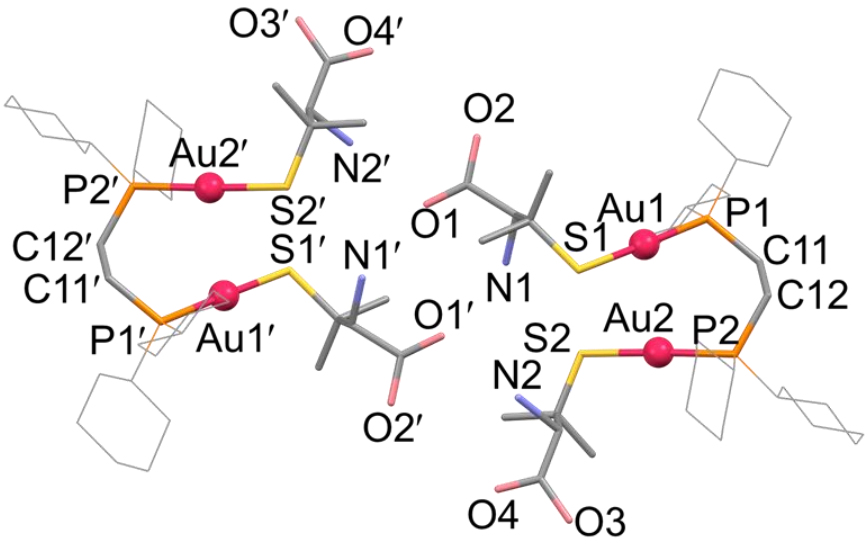

Figure 4-24. A drawing of two complex molecules in D_2/L_2-H_3[**12**]ClO_4 with the atomic labeling scheme. The complex molecule in the asymmetrical unit is D_2-H_3[**12**]$^+$ but the enantiomeric L_2-H_3[**12**]$^+$ molecule also appeared by symmetrical expansion. Hydrogen atoms are omitted for clarity. Symmetry code: (') 2–x, –y, 2–z.

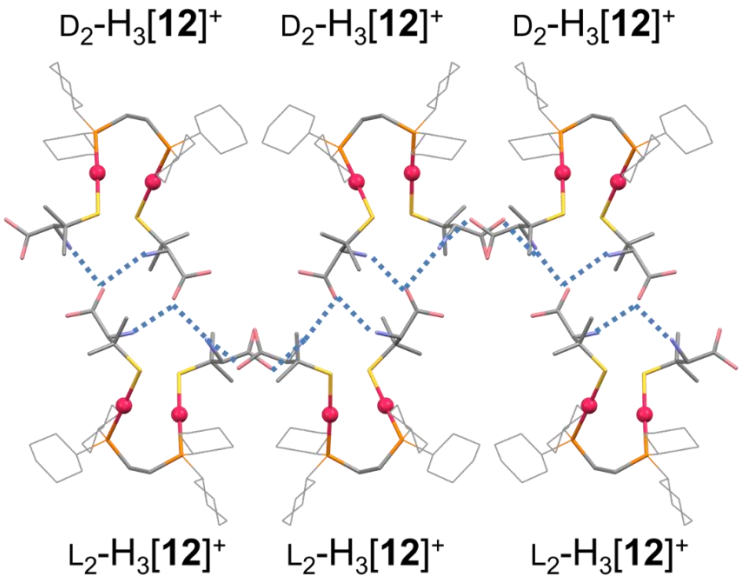

Figure 4-25. A hydrogen bonded chain-like aggregate of the complex cation in D_2/L_2-H_3[**12**]ClO_4. Dashed lines indicate hydrogen bonds.

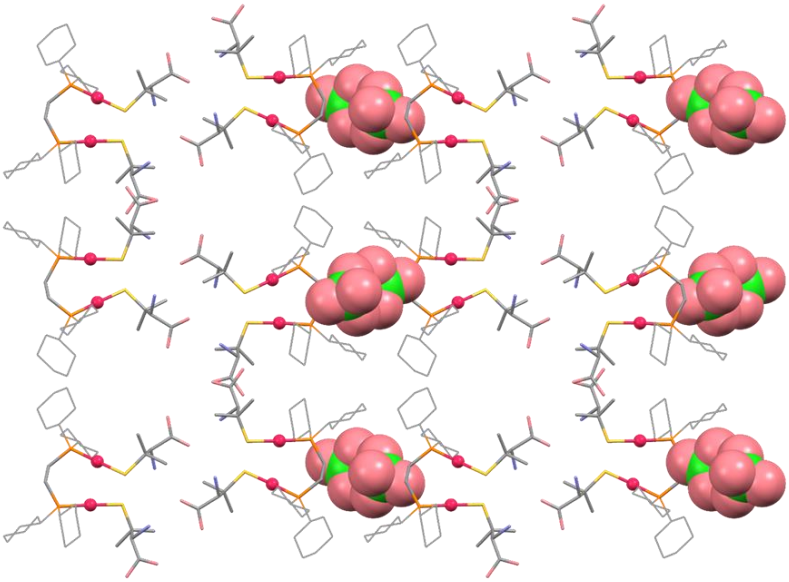

Figure 4-26. A packing structure of complex cations and perchlorate anions in the crystal of D_2/L_2-H_3[**12**]ClO_4.

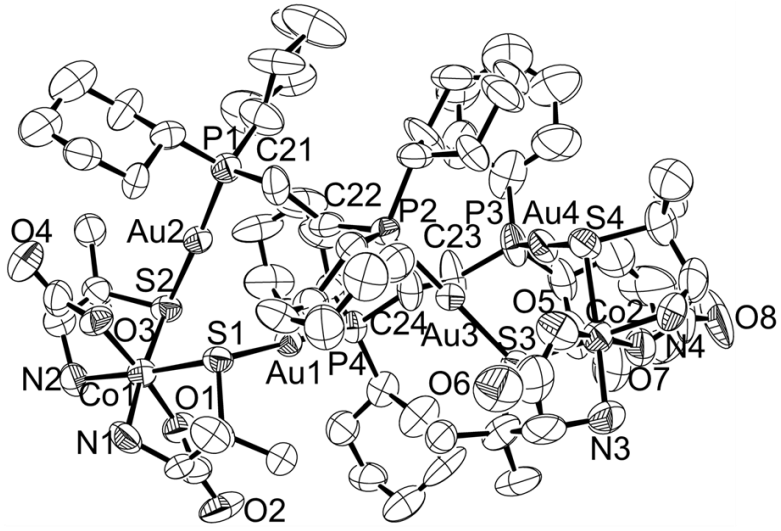

Figure 4-27. An ortep drawing of complex cation in [**13**]$(NO_3)_2$ with the atomic labeling scheme. Hydrogen atoms are omitted for clarity. Thermal ellipsoids were drawn in a 50 % level.

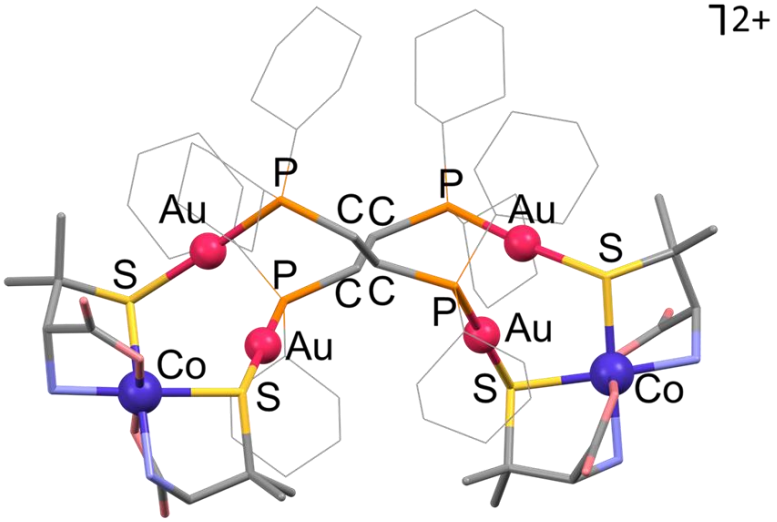

Figure 4-28. A bent 18-membered metalloring structure in [**13**]$(NO_3)_2$.

(a)

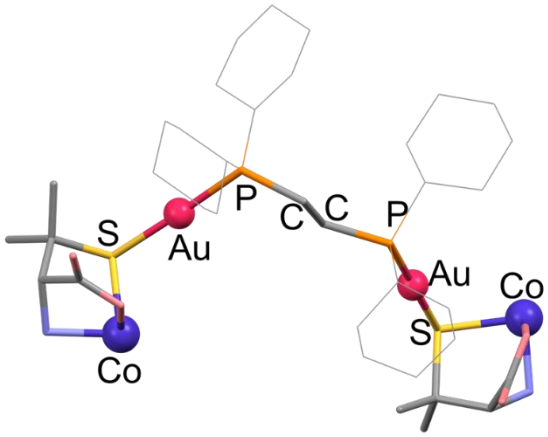

(b)

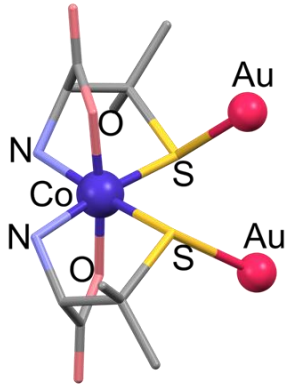

Figure 4-29. (a) Bis(tridentate-*N*,*O*,*S*) coordination mode of the metalloligand, and (b) *trans*-O coordination geometry of Co^{III} atom in [**13**]$(NO_3)_2$.

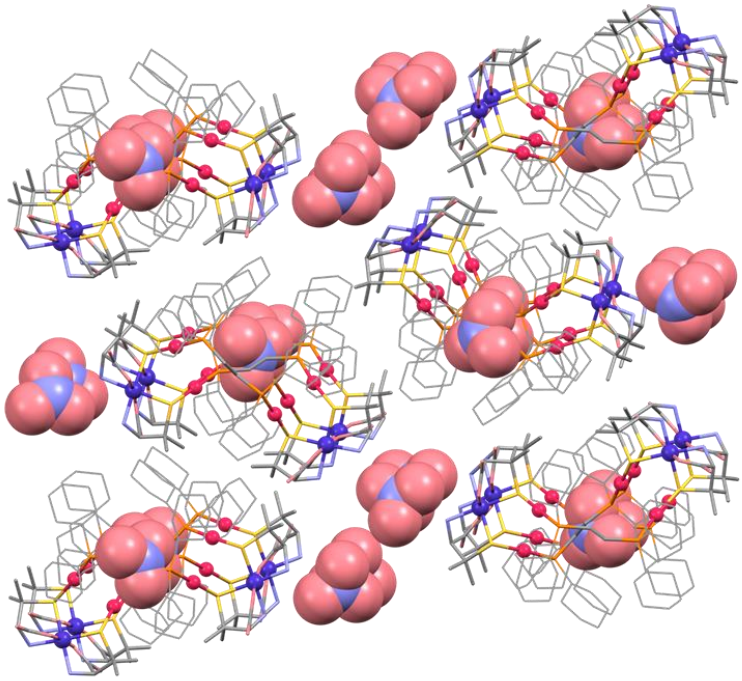

Figure 4-30. A packing structure of complex cations and nitrate anions in the crystal of [**13**]$(NO_3)_2$.

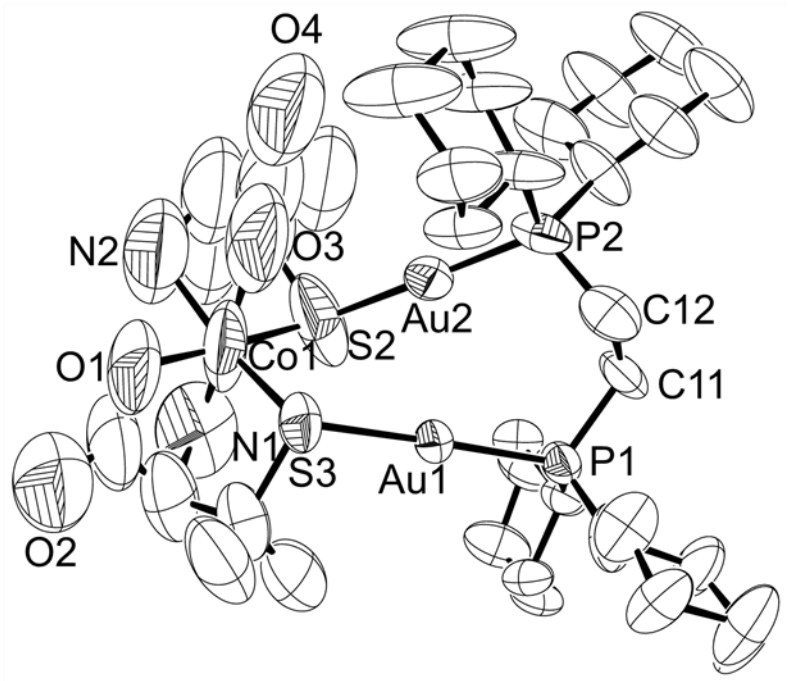

Figure 4-31. An ortep drawing of complex cation in [**14**]ClO_4 with the atomic labeling scheme. Hydrogen atoms are omitted for clarity. Thermal ellipsoids were drawn in a 50 % level.

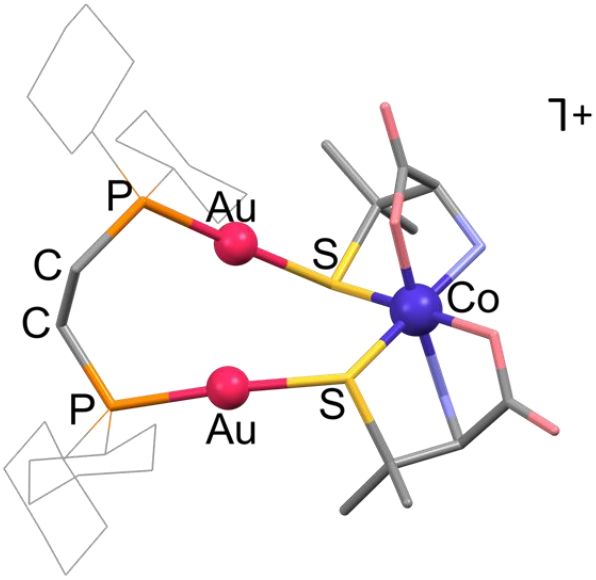

Figure 4-32. A 9-membered metalloring structure of [**14**]$^{+}$.

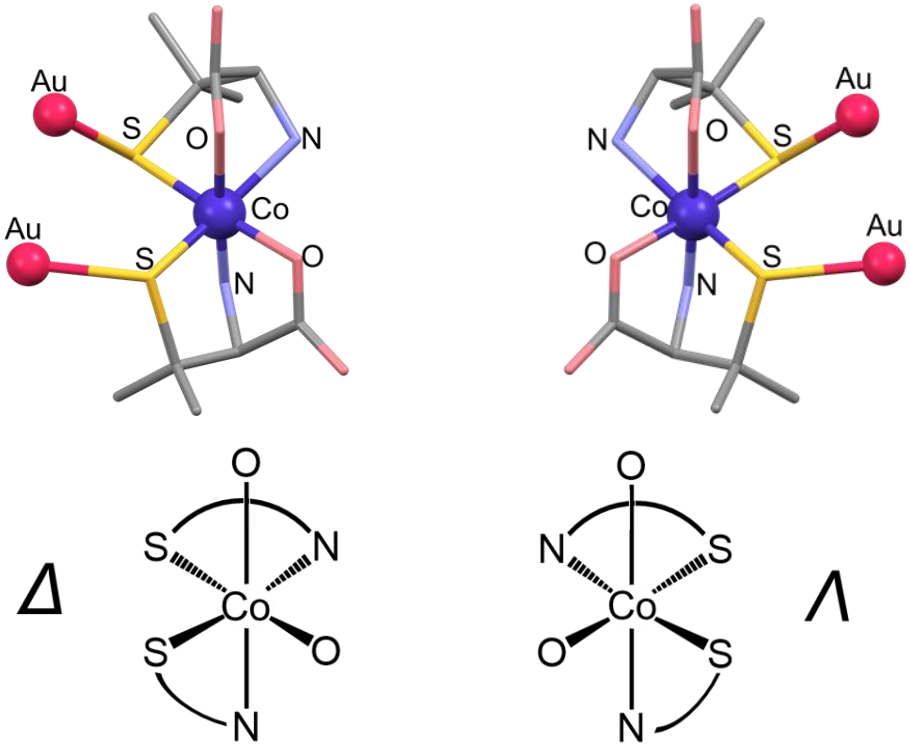

Figure 4-33. Schematic drawings of *cis*-O coordination geometry of Co^{III} atom in enantiomeric pair of the trinuclear complexes in [**14**]$^{+}$ with the definition of the configuration around Co by SN chelation.

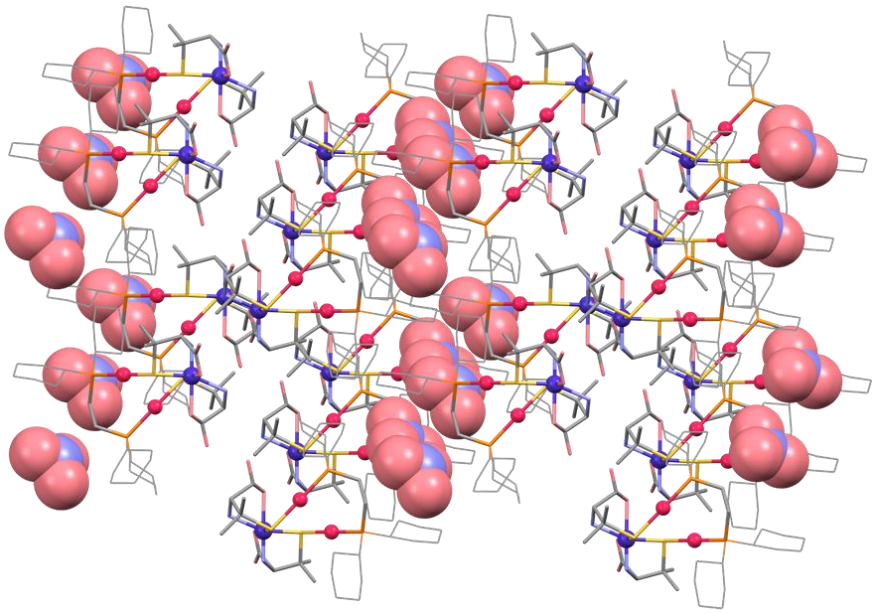

Figure 4-34. A packing structure of complex cations and nitrate anions in the crystal of [**14**]NO_3.

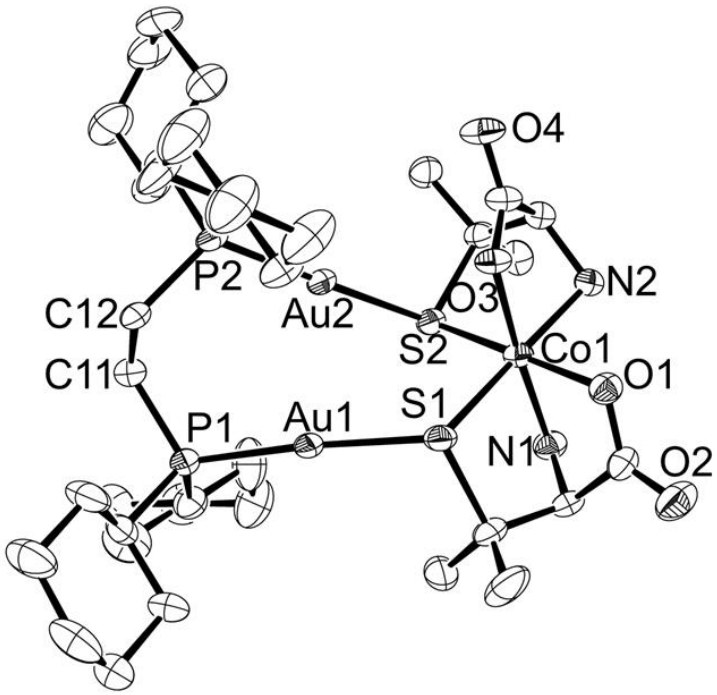

Figure 4-35. An ortep drawing of complex cation in [**14**]ClO_4 with the atomic labeling scheme. Hydrogen atoms are omitted for clarity. Thermal ellipsoids were drawn in a 50 % level.

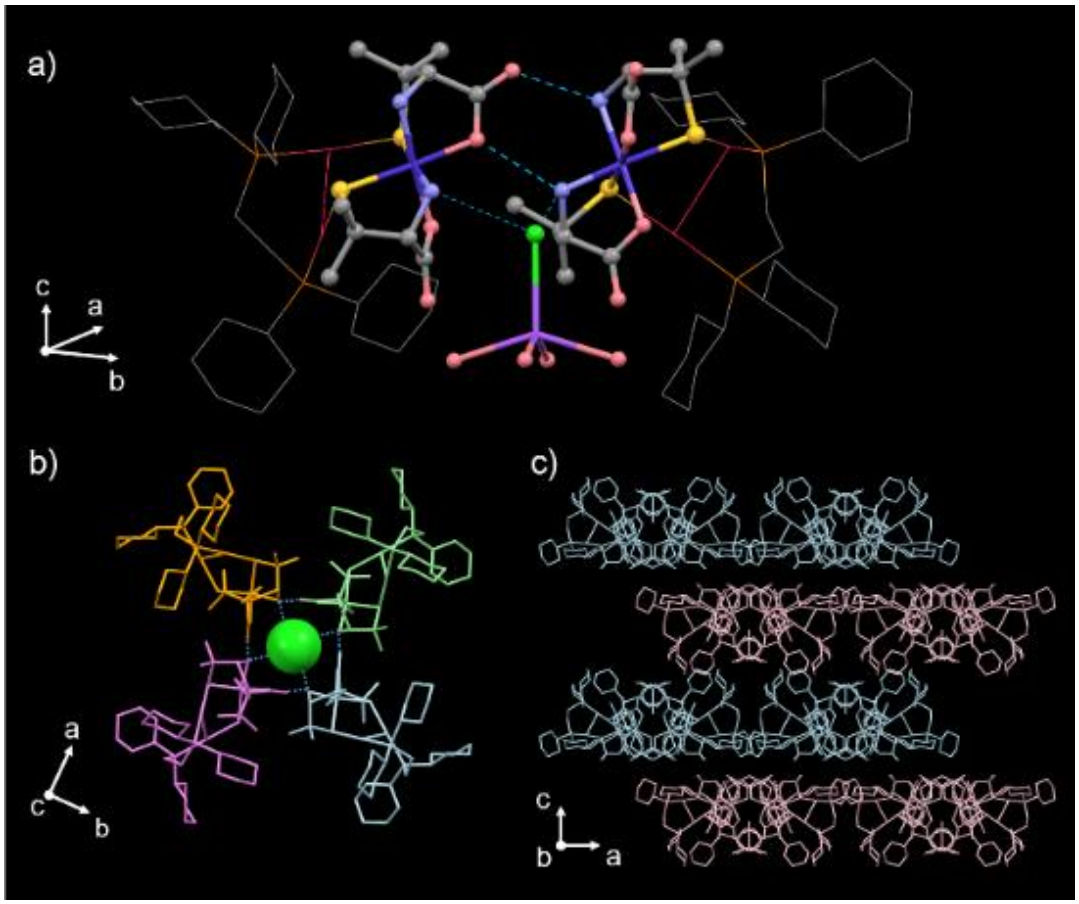

Figure 4-36. Crystal structure of [**14**]ClO_4. (a) Hydrogen bond interaction between trinuclear complexes. (b) Tetrameric assembly (Δ_4 or Λ_4) around Cl^- via hydrogen bond. The atom represented by space-filling model is the chloride anion. (c) Alternative stacking layers of two kinds of diastereomers (Δ layer (pink) and Λ layer (light blue)). The dashed lines indicate the hydrogen bonds.

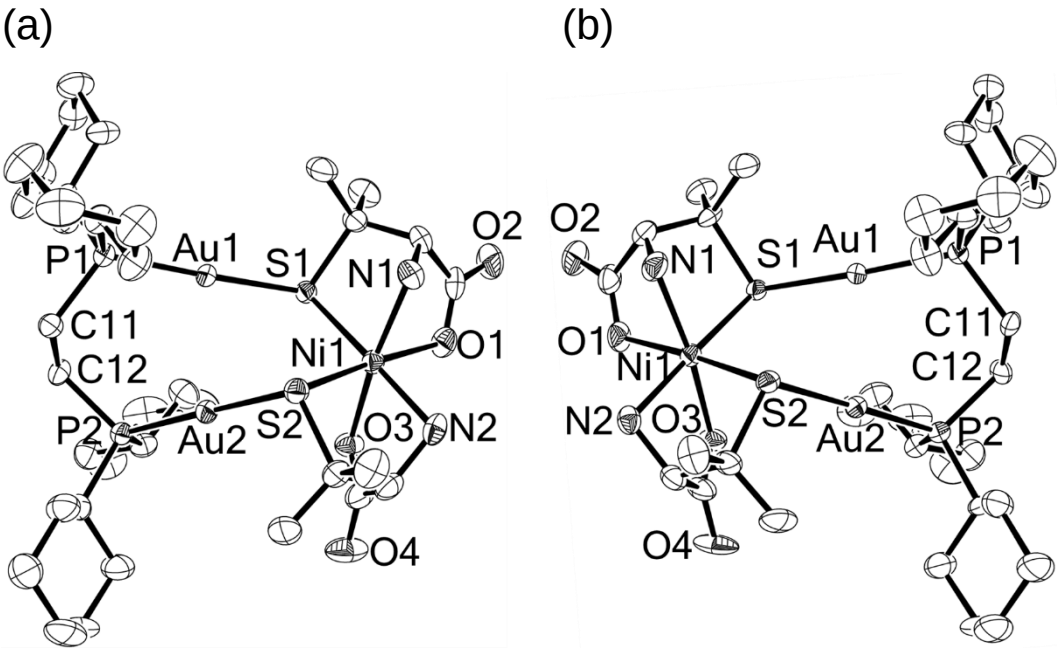

Figure 4-37. Ortep drawings of complex cation in (a) [**15**] and (b) [**15**]′ with the atomic labeling scheme. Hydrogen atoms are omitted for clarity. Thermal ellipsoids were drawn in a 50 % level.

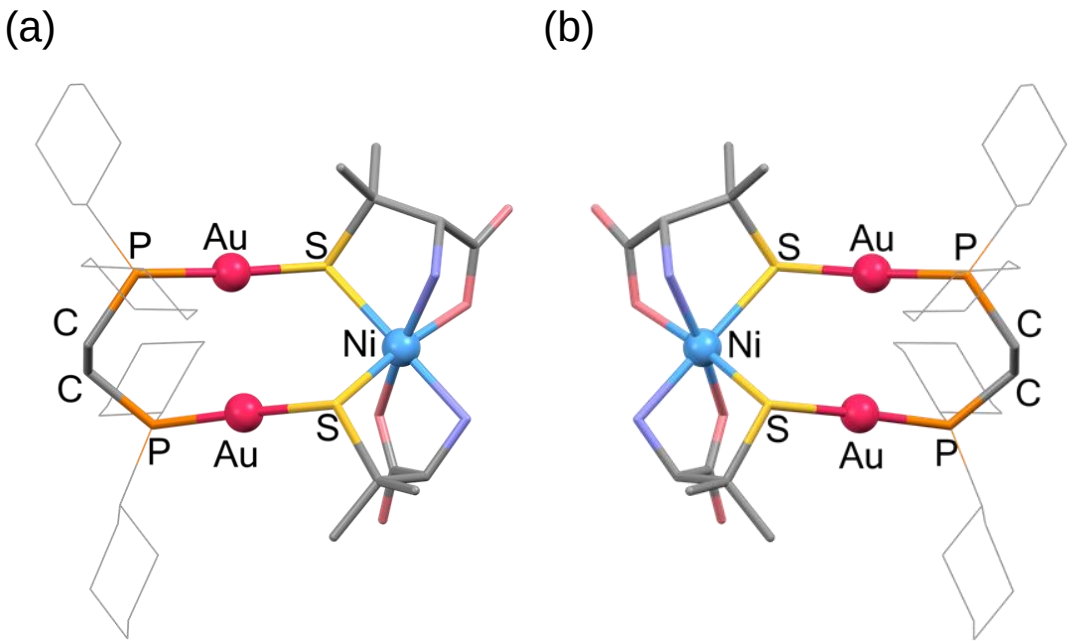

Figure 4-38. 9-membered metalloring structures in (a) [**15**] and (b) [**15**]′.

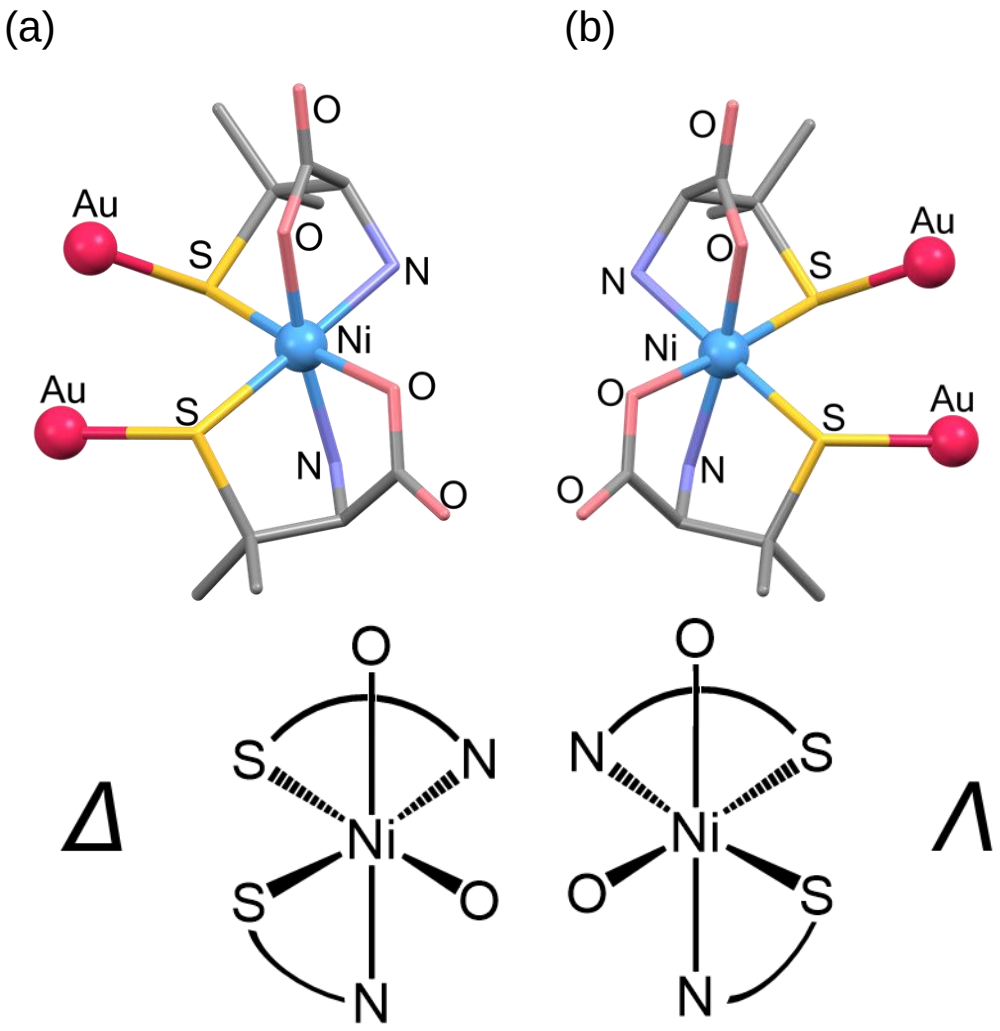

Figure 4-39. Schematic drawings of *cis*-O coordination geometry of Ni^{II} atom in (a) [**15**] and (b) [**15**]′ with the definition of the configuration around Ni by SN chelation.

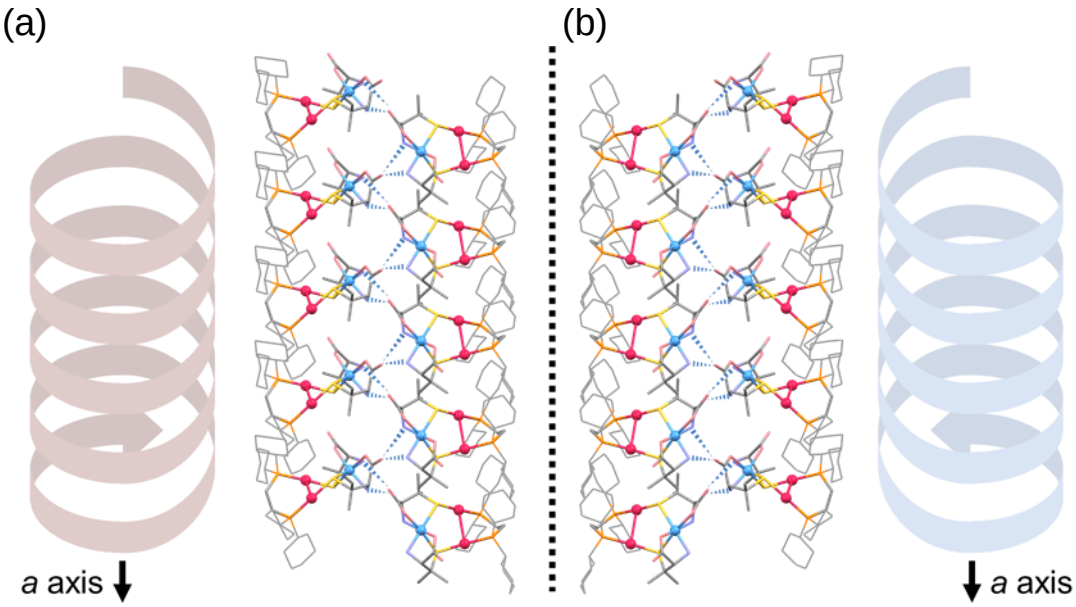

Figure 4-40. The 1D chain structure composed of hydrogen bond along *a* axis in (a) [**15**] and (b) [**15**]′.

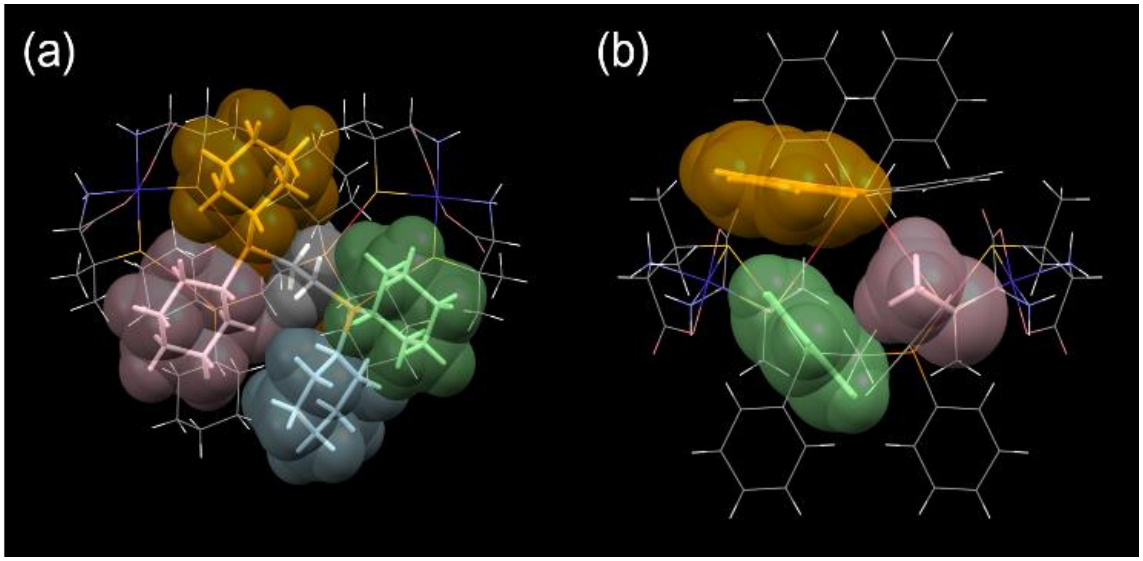

Figure 4-41. Perspective views of (a) $[\mathbf{4}]^{2+}$ with emphasizing diphosphine ligand by colored transparent space filling model and (b) $[Au_4Co_2(dppe)_2(D\text{-}pen)_4]^{2+}$ with emphasizing two parts of CH-π interactions by colored transparent space filling model.

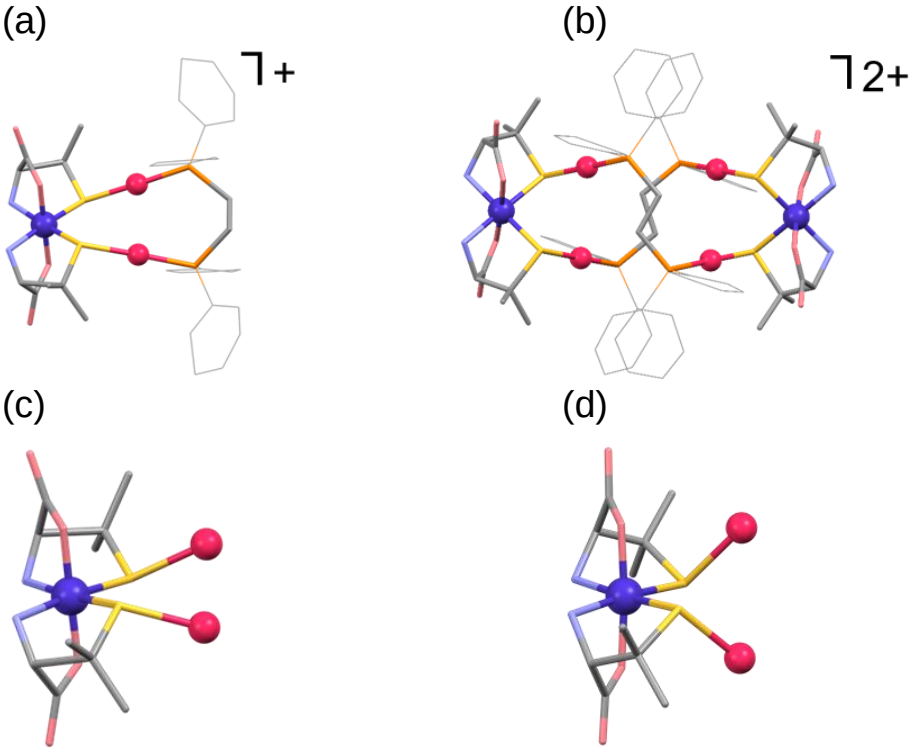

Figure 4-42. Perspective views of the structures of (a) $[Au_2Co(dppe)(D\text{-pen})_2]^+$ and (b) $[Au_4Co_2(dppe)_2(D\text{-pen})_4]^{2+}$, with the conformation of D-pen moieties around a Co center in (c) trinuclear, and (d) hexanuclear complex cations.[7c]

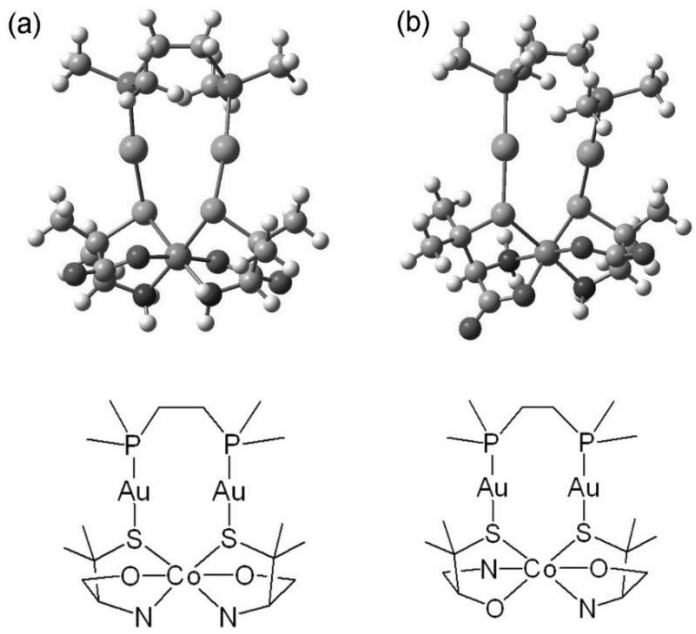

Figure 4-43. Perspective views of the optimized structures of (a) $[Au_2Co(dpmp)(D\text{-pen})_2]^+$ and (b) $[Au_2Co(dpmp)(D\text{-pen})(L\text{-pen})]^+$ (dpmp = 1,2-bis(dimethylphosphino)ethane).[7c]

Chapter V. Conclusion.

In this thesis, the crystal structures of the complexes composed of the digold(I) metalloligands were thoroughly investigated with the aim of discussing about the effect of the conformationally constrained bridging ligand on the resulting supramolecular structures. For this purpose, two kinds of diphosphines were used as a bridging ligand for the comparison with dppe; one was *trans*-dppee with a rigid C=C double bond between the two P atoms and another was dcpe with bulky cyclohexyl substituents on the P atoms (dppe = 1,2-bis(diphenylphosphino)ethane), *trans*-dppee = *trans*-1,2-bis(diphenylphosphino)ethylene, and dcpe = 1,2-bis(dicyclohexylphosphino)ethane). As a result, large differences were found not only in the molecular and supramolecular structures but also in the physical properties. In the reaction of the *trans*-dppee bridged metalloligand with cobalt(II), the rearrangement of inorganic anions in the anionic cluster was found, and furthermore the metastable Co^{II} species were successfully isolated. The reaction of the *trans*-dppee bridged metalloligand with nickel(II) led to the construction of two kinds of structures; one was the 1D infinite polymer structure that has never been found in the dppe system, and another was the discrete molecular structure that is crystallized with inorganic acids, in which the reverse absorption/desorption behavior toward ammonia in single-crystal-to-single-crystal manner was observed for the acid-incorporated crystals. By the reaction using metalloligands bridged by dcpe, the unique chiral behavior depending on the charge of the complexes was observed, together with the spontaneous resolution from the achiral *meso* isomer.

In the Chapter II, it was found that the reaction of the homochiral metalloligand, D_2- or L_2-[Au^I_2(*trans*-dppee)(Hpen)$_2$] (D_2-[**2**] or L_2-[**2**]), with Co^{II} led to the formation of the $Au^I_4Co^{III}_2$ hexanuclear complex [$Au^I_4Co^{III}_2$(*trans*-dppee)$_2$(D-pen)$_4$]$^{2+}$ ([**3**]$^{2+}$) or [$Au^I_4Co^{III}_2$(*trans*-dppee)$_2$(L-pen)$_4$]$^{2+}$ ([**4**]$^{2+}$), by air oxidization. In the crystal structure, the six cations were aggregated to form hexamers that are closely packed in a face-centered cubic (fcc) arrangement. These aggregation structures were formed through multiple CH$\cdots\pi$ and hydrogen bonding interactions. In the hydrophilic interstice in the fcc structure, there were ten monovalent anions with an adamantane-like aggregation structure or six divalent anions with an octahedral aggregation structure. Such a multistep aggregation of the complex cation accompanied by the aggregation of inorganic anions was also found in the dppe system,[5] but the aggregation structures of the inorganic anions were slightly different in terms of the molecular orientation. The use of the rigid diphosphine linker (*trans*-dppee), instead of the flexible linker (dppe), resulted in the formation of the complex cation with the

longer Co···Co distance, which led to the formation of the larger hexameric cation cluster. As a result, smaller hydrophilic tetrahedral interstices were formed in the *trans*-dppee complexes, and inorganic anions in the tetrahedral interstice were arranged more closely. Thus, the subtle control of the anion aggregation structures by the change of diphosphine linkers was achieved. In the latter half of Chapter II, the effect of the chirality on the aggregation behavior and the physical properties was investigated, by the reactions of a racemic mixture of the chiral metalloligands, D_2- or L_2-[Au^I_2(*trans*-dppee)(Hpen)$_2$] (D_2-[**2**] or L_2-[**2**]), with Co^{II} or Co^{III}. The reaction with Co^{II} with PbO_2 gave the heterochiral $Au^I_4Co^{III}_2$ complex, D_2L_2-[$Au^I_4Co^{III}_2$(*trans*-dppee)$_2$(pen)$_4$]$(NO_3)_2$ ([**6**]$(NO_3)_2$), which showed no specific supramolecular aggregation behavior. In this reaction, the homochiral $Au^I_4Co^{III}_2$ complexes, D_4- or L_4-[$Au^I_4Co^{III}_2$(*trans*-dppee)$_2$(pen)$_4$]$(NO_3)_2$ ([**3**]$(NO_3)_2$ and [**4**]$(NO_3)_2$), were also formed, in addition to [**6**]$(NO_3)_2$. The reaction of a racemic mixture of the metalloligands with Co^{II} in air gave the $Au^I_4Co^{II}_2$ heterochiral complex, D_2L_2-[$Au^I_4Co^{II}_2$(*trans*-dppee)$_2$(pen)$_4$] ([**5**]). This reaction was different from that of the homochiral case; the reaction of the homochiral metalloligand with Co^{II} in air gave only the $Au^I_4Co^{III}_2$ homochiral complex through the air oxidation. Thus, it was found that the chirality affects not only their structures (the unique separate aggregation behavior was found only in the homochiral complex), but also their physical properties (the stabilization of the Co^{II} oxidation state in the heterochiral complex).

In Chapter III, the $Au^I_4Ni^{II}_2$ hexanuclear complexes, [$Au^I_4Ni^{II}_2$(*trans*-dppee)$_2$(D-pen)$_4$]·HX ([**7**]·HX; HX = $2HClO_4$, $4/3HNO_3$), and the $Au^I_2Ni^{II}$ chain complex, [$Au^I_2Ni^{II}$(*trans*-dppee)(D-pen)$_2$]$_\infty$ ([**9**]), were synthesized by the reactions of the chiral metalloligand, [Au^I_2(*trans*-dppee)(D-Hpen)$_2$] (D_2-H_2[**2**]), with Ni^{II} in the presence of different inorganic anions. In these complexes, the metalloligand coordinated to two Ni^{II} ions to form the twisted metalloring structure in [**7**]·HX and the chain structure in [**9**]. The 1D neutral chain structure observed in [**9**] has never been found for the dppe system. Interestingly, the crystal of [**7**]·HX was isostructural to that of [$Au^I_4Co^{III}_2$(*trans*-dppee)$_2$(D-pen)$_4$]$^{2+}$ ([**3**]$^{2+}$), and six inorganic anions formed an anionic cluster as found in [**3**]X_2 in spite of the neutral charge of [**7**], indicating that the inorganic acids were incorporated into the neutral crystal lattice composed of [**7**]. This result stimulated us to investigate the reactivity of [**7**] to the basic molecules via acid-base reactions. The crystals accommodating an inorganic acid showed the incorporation of NH_3 molecules from the exposed atmosphere with the retention of the crystallinity. Importantly, [**7**]·$2HClO_4$ absorbed NH_3 molecules not only from gaseous ammonia, but also from an aqueous ammonia, transforming to [**7**]·$2NH_4ClO_4$, which

was reversibly changed to [**7**]·2$HClO_4$ in a single-crystal-to-single-crystal conversion manner. The analogous compound having dppe ligands, $[Au^{I}_4Ni^{II}_2(dppe)_2(D\text{-pen})_4]$ ·2$HClO_4$ ([**8**]·2$HClO_4$), was also prepared by a similar method, but its reactivity toward ammonia was quite different from that of [**7**]·2$HClO_4$. This result was explained via the rigid nature of the bridging moiety in the *trans*-dppee system, which made the overall packing structure stable.

In Chapter IV, diphosphine dcpe was applied as a bridging ligand instead of dppe, and the effect of functional groups on the phosphorus atom to the structure was examined. The reaction of the homochiral metalloligand with Co^{II} produced the $Au_4Co^{III}_2$ hexanuclear complex, $[Au^{I}_4Co^{III}_2(dcpe)_2(D\text{-pen})_4]^{2+}$, while the heterochiral metalloligand gave the Au_2M trinuclear complexes, $[Au_2M(dcpe)(D\text{-pen})(L\text{-pen})]^{n+}$ (M = Co^{III} or Ni^{II}). The homochiral metalloligand is assumed to prefer a bent form of the hexanuclear structure to a straight form as observed in the dppe system, due to the steric hindrance and the less interactivity of the cyclohexyl group in the dcpe ligand. The differences in the molecular shape and the interactivity probably prevent the hexanuclear complex cation from constructing the unusual separate aggregation structure of inorganic anions and complex cations. Furthermore, the steric hindrance of the cyclohexyl groups restricted the motion of the bridging diphosphinoethane part, which led to the formation of the trinuclear complex rather than the hexanuclear complex in the heterochiral system. The heterochiral Au_2Ni complex showed spontaneous resolution behavior, and this is a rare example of the discrete heterochiral molecule that undergoes spontaneous resolution.

Finally, in this study, the crystal structures and physical properties of the multinuclear complexes composed of the digold(I) metalloligands ($[Au^{I}_2(dppx)(Hpen)_2]$, dppx = *trans*-dppee or dcpe) and metal ions (Co^{II}, Co^{III}, Ni^{II}) were thoroughly investigated, and it was found that the molecular and supramolecular structures were indeed affected by the diphosphine linkers (*trans*-dppee, dcpe vs. dppe), the metal ions (Co^{II}, Co^{III}, Ni^{II}), and the chirality (homochiral vs. heterochiral). Small changes in these building parts gave a large influence on the resulting crystal structures and their properties, which were rationally explained from the view of the molecular structures of the building units. The author believes that these results contribute to the development of the supramolecular chemistry from the point of view of the control of supramolecular aggregation structures. Based on the present synthetic and structural chemistry, in the near future, the unique physical properties and the reactivity originating from the separate aggregation of cations and anions should be explored.

References

1. a) J. -M. Lehn, *Angew. Chem. Int. Ed*. **1988**, *27*, 89–112. b) J. -M. Lehn, *Angew. Chem. Int. Ed*. **1990**, *29*, 1304–1319. c) F. Vögtle, *Supramolecular Chemie*, Teuber, Stuttgart, **1991**. d) C. Seel, F. Vögtle, *Angew. Chem. Int. Ed.* **1992**, *31*, 528–549. e) J. -M. Lehn, *Pure. Appl. Chem.* **1994**, *66*, 1961–1966. f) J. -M. Lehn, *Supramolecular chemistry-concepts and perspective*, VHC, Weinheim, **1995**. g) D. Philp, J. F. Stoddart, *Angew. Chem. Int. Ed.* **1996**, *35*, 1154–1196. h) F. M. Raymo, J. F. Stoddart, *Current Opinion in Colloid & Interface Science*, **1996**, *1*, 116–126. i) M. C. T. Fyfe, J. F. Stoddart, *Acc. Chem. Res*. **1997**, *30*, 393–401. j) F. Zeng, S. C. Zimmerman, *Chem. Rev*. **1997**, *97*, 1681–1712. k) R. G. Chapman, J. C. Sherman, *Tetrahedron*, **1997**, *53*, 15911–15945. l) A. P. Davis, R. S. Wareham, *Angew. Chem. Int. Ed*. **1999**, *38*, 2978–2996. m) M. Ruben, J. Rojo, F. J. Romero-Salguero, L. H. Uppadine, J. -M. Lehn, *Angew. Chem. Int. Ed*. **2004**, *43*, 3644–3662. n) D. Braga, F. Grepioni, *Angew. Chem. Int. Ed*, **2004**, *43*, 4002–4011. o) A. Corma, H. Garcia, *Eur. J. Inorg. Chem.* **2004**, 1143–1164. p) O. Lukin, F. Vögtle, *Angew. Chem. Int. Ed.* **2005**, *44*, 1456–1477.

2. a) G. Wenz, *Angew. Chem. Int. Ed*. **1994**, *33*, 803–822. b) D. B. Amabilino, J. F. Stoddart, D. J. Williams, *Chem. Mater*. **1994**, *6*, 1159–1167. c) V. Böhmer, *Angew. Chem. Int. Ed.* **1995**, *34*, 713–745. d) D. B. Amabilino, P. R. Ashton, C. L. Brown, E. Córdova, L. A. Godínez, T. T. Goodnow, A. E. Kaifer, S. P. Newton, M. Pietraszkiewicz, D. Philp, F. M. Raymo, A. S. Reder, M. T. Rutland, A. M. Z. Slawin, Neil Spencer, J. F. Stoddart, D. J. Williams, *J. Am. Chem. Soc.* **1995**, *117*, 1271–1293. e) C. G. Claessens, J. F. Stoddart, *J. Phys. Org. Chem.* **1997**, *10*, 254–272. f) I. Higler, P. Timmerman, W. Verboom, D. N. Reinhoudt, *Eur. J. Org. Chem*. **1998**, 2689–2702. g) A. Jasat, J. C. Sherman, *Chem. Rev*. **1999**, *99*, 931–967. h) P. A. Gale, *Coord. Chem. Rev*. **2000**, *199*, 181–233. i) C. Schmuck, W. Wienand, *Angew. Chem. Int. Ed*. **2001**, *40*, 4363–4369. j) D. M. Rudkevich, *Bull. Chem. Soc. Jpn*. **2002**, *75*, 393–413. k) P. D. W. Boyd, C. A. Reed, *Acc. Chem. Res.* **2005**, *38*, 235–242. l) Z. Niu, H. W. Gibson, *Chem. Rev*. **2009**, *109*, 6024–6046. m) M. Xue, Y, Yang, X. Chi, Z. Zhang, F. Huang, *Acc. Chem. Res.* **2012**, *45*, 1294–1304.

3. a) J. L. Atwood. *Inclusion Phenomena and Molecular Recognition*, Plenum, **1990**. b) H.-J. Schneider, H. Dürr, *Frontiers in Supramolecular Organic Chemistry and Photochemistry*, VCH, **1991**. c) J. L. Atwood, J. E. D. Davies, D. D. Manicol, F.Vogtle, *Comprehensive Supramolecular Chemistry*, Pergamon, **1996**. d) C. Wieser, C. B. Dieleman, D. Matt, *Coord. Chem. Rev*. **1997**, *165*, 93–161. e) S. R. Batten, R. Robson, *Angew. Chem. Int. Ed*. **1998**, *37*, 1460–1494. f) G. F. Swiegers, T. J. Malefetse, *Chem. Rev.* **2000**, *100*, 3483–3537. g) N. Gimeno, R. Vilar, *Coord. Chem. Rev*. **2006**, *250*,

3161–3189. h) J. A. Thomas, *Chem. Soc. Rev*. **2007**, *36*, 856–868. i) R. W. Saalfrank, H. Maid, A. Scheurer, *Angew. Chem. Int. Ed*. **2008**, *47*, 8794–8824. j) I. Beletskaya, V. S. Tyurin, A. Y. Tsivadze, R. Guilard, C. Stern, *Chem. Rev*. **2009**, *109*, 1659–1713. k) Y. E. Alexeev, B. I. Kharisov, T. C. H. García, A. D. Garnovskii, *Coord. Chem. Rev.* **2010**, *254*, 794–831. l) R. Chakrabarty, P.S. Mukherjee, P. J. Stang, *Chem. Rev*. **2011**, *111*, 6810–6918. m) T. R. Cook, Y. -R. Zheng, P. J. Stang, *Chem. Rev.* **2013**, *113*, 734–777.

4. a) C. O. Dietrich-Buchecker, J. -F. Nierengarten, J. -P. Sauvage, N. Armaroli, V. Balzani, L. D. Cola, *J. Am. Chem. Soc*. **1993**, *115*, 11237–11244. b) V. R. Vangala, B. R. Bhogala, A. Dey, G. R. Desiraju, C. K. Broder, P. S. Smith, R. Mondal, J. A. K. Howard, C. C. Wilson, *J. Am. Chem. Soc*. **2003**, *125*, 14495–14509. c) J. A. Mata, A. R. Chianese, J. R. Miecznikowski, M. Poyatos, E. Peris, J. W. Faller, R. H. Crabtree, *Organometallics*, **2004**, *23*, 1253–1263. d) J. Yang, G. -D. Li, J. -J. Cao, Q. Yue, G. -H. Li, J. -S. Chen, *Chem. Eur. J.* **2007**, *13*, 3248–3261. e) M. -X. Zhu, W. Lu, N. Zhu, C. -M. Che, *Chem. Eur. J.* **2008**, *14*, 9736–9746. f) M. L. Singleton, R. M. Jenkins, C. L. Klemashevich, M. Y. Darensbourg, *C. R. Chimie*, **2008**, *11*, 861–874. g) D. C. Caskey, T. Yamamoto, C. Addicott, R. K. Shoemaker, J. Vacek, A. M. Hawkridge, D. C. Muddiman, G. S. Kottas, J. Michi, P. J. Stang, *J. Am. Chem. Soc.* **2008**, *130*, 7620–7628. h) A. I. Buvailo, E. Gumienna-Kontecka, S. V. Pavlana, I. O. Fritsky, M. Haukka, *Dalton Trans.* **2010**, *39*, 6266–6275. i) J. -R. Li, A. A. Yakovenko, W. Lu, D. J. Timmons, W. Zhuang, D. Yuan, H. -C. Zhou, *J. Am. Chem. Soc*. **2010**, *132*, 17599–17610. j) T. Mandai, H. Masu, H. Seki, K. Nishikawa, *Bull. Chem. Soc. Jpn*. **2012**, *85*, 599–605. k) F. A. A. Paz, J. Klinowski, S. M. F. Vilela, J. P. C. Tomé, J. A.S. Cavaleiro, J. Rocha, *Chem. Soc. Rev*. **2012**, *41*, 1088–1110. l) Y. D. Lampeka, L. V. Tsymbal, A. V. Barna, Y. L. Shuĺga, S. Shova, V. B. Arion, *Dalton Trans*. **2012**, *41*, 4118–4125. m) J Zhang, X. Wang, X. Zhang, W. Wu, G. Zhang, S. Xu, M. Shi, ACS Catal. **2013**, *3*, 2311–2317. n) S. Khullar, S. J. Mandal, *Cryst. Growth Des.* **2013**, *13*, 3116–3125. o) A. Mambanda, D. Jaganyi, *Dalton Trans*. **2013**, *41*, 908–920. p) X. Wang, J. Luan, H. Lin, Q. Lu, C. Xu, G. Liu, *Dalton Trans.* **2013**, *42*, 8375–8386. q) L. Liu, K. Konstas, M. R. Hill, S. G. Telfer, *J. Am. Chem. Soc.* **2013**, *135*, 17731–17734. r) C. R. M. O. Matos, F. S. Miranda, J. W. de M. Carneiro, C. B. Pinheiro, C. M. Ronconi, *Phys. Chem. Chem. Phys.* **2013**, *15*, 13013–13023.

5. a) Y. Huang, R. J. Drake, D. W. Stephan, *Inorg. Chem.* **1993**, *32*, 3022–3028. b) B. Wenzel, P. Lönnecke, E. Hey-Hawkins, *Organometallics* **2002**, *21*, 2070–2075. c) F. Paul, S. Goeb, F. Justaud, G. Argouarch, L. Toupet, R. F. Ziessel, C. Lapinte, *Inorg. Chem.* **2007**, *46*, 9036–9038. d) N. Gómez-Blanco, J. J. Fernández, A. Fernández, D. Vázquez-García, M. López-Torres, J. M. Vila, *Eur. J. Inorg. Chem.* **2009**, 3071–3083.

e) M. Ferrer, A. Gutiérrez, M. Mounir, L. Rodríguez, O. Rossell, M. Font-Bardia, P. Gómez-Sal, A. Martín, X. Solans, *Organometallics* **2011**, *30*, 3419–3429. f) V. Cámara, N. Barquero, D. Bautista, J. Gil-Rubio, J. Vicente, *Chem. Eur. J.* **2015**, *21*, 1992–2002.

6. N. Yoshinari, T. Konno, *Chem. Rec.* **2016**, *16*, 1647–1663.

7. a) R. Lee, A. Igashira-Kamiyama, H. Motoyoshi, T. Konno, *CrystEngComm*. **2012**, *14*, 1936–1938. b) R. Lee, A. Igashira-Kamiyama, M. Okumura, T. Konno, *Bull. Chem. Soc. Jpn.* **2013**, *86*, 908–920. c) R. Lee, The Doctor's Thesis, Osaka University, **2011**.

8. N. Yoshinari, C. Li, N. Kuwamura, A. Igashira-Kamiyama, T. Konno, *Inorg. Chem.* **2015**, *54*, 8881–8883.

9. A. Igashira-Kamiyama, N. Matsushita, R. Lee, K. Tsuge, T. Konno, *Bull. Chem. Soc. Jpn.* **2012**, *85*, 706–708.

10. N. Yoshinari, A. Kakuya, R. Lee, T. Konno, *Bull. Chem. Soc. Jpn.* **2015**, *88*, 59–68.

11. a) Y. Hashimoto, N. Yoshinari, N. Matsushita, T. Konno, *Eur. J. Inorg. Chem.* **2014**, 3474–3478. b) Y. Hashimoto, N. Yoshinari, N. Kuwamura, T. Konno, *Bull. Chem. Soc. Jpn.* **2015**, *88*, 1144–1146. c) Y. Hashimoto, The Doctor's Thesis, Osaka University, **2014**.

12. a) N. I. Veletsky, I. A. Dementiev, A. Y. Ershov, A. B. Nikol'skii, *J. Photochem. Photobiol. A-Chem.* **1995**, *89*, 99-103, b) S. Onaka, Y. Katsukawa, M. Shiotsuka, O. Kanegawa, M. Yamashita, *Inorg. Chim. Acta* **2001**, *312*, 100–110. c) M.-C. Brandys, R. J. Puddephatt, *J. Am. Chem. Soc.* **2001**, *123*, 4839–4840. d) J.-L. Chen, L.-Y. Zhang, Z.-N. Chen, L.-B. Gao, M. Abe, Y. Sasaki, *Inorg. Chem.* **2004**, *43*, 1481–1490. e) S. Onaka, M. Yaguchi, R. Yamauchi, T. Ozeki, M. Ito, T. Sunahara, Y. Sugiura, M. Shiotsuka, K. Nunokawa, M. Horibe, K. Okazaki, A. Iida, H. Chiba, K. Inoue, K. Sato, *J. Organomet. Chem.* **2005**, *690*, 57–68. f) W. J. Hunks, M. C. Jennings, R. J. Puddephatt, *Inorg. Chim.* Acta **2006**, *359*, 3605–3616. g) J. B. Foley, S. E. Gay, M. J. Vela, B. M. Foxman, A. E. Bruce, M. R. M. Bruce, *Eur. J. Inorg. Chem.* **2007**, 4946–4951.

13. a) B. –C. Tzeng, A. Schier, H. Schmidbaur, *Inorg. Chem.* **1999**, *38*, 3978–3984. b) W. J. Hunks, M. C. Jennings, R. J. Puddephatt, *Inorg. Chem.* **2002**, *41*, 4590–4598.

14. a) J. J. Fernández, N. Gómez-Blanco, Alberto Fernández, D. Vázquez-García, M. López-Torres, J. M. Vila, *Polyhedron*, **2009**, *28*, 2679–2683, b) M. Ferrer, A. Gutiérrez, L. Rodríguez, O. Rossell, E. Ruiz, M. Engeser, Y. Lorenz, R. Schilling, P. Gómez-Sal, A. Martín, *Organometallics*, **2012**, *31*, 1533–1545

15. a) D. S. Eggleston, J. V. McArdle, G. E. Zuber, *J. Chem. Soc. Dalton. Trans.* **1987**, 677–679. b) C. K. Mirabelli, D. T. Hill, L. F. Faucette, F. L. McCabe, G. R.

Girard, D. B. Bryan, B. M. Sutton, J. O. Bartus, S. T. Crooke, R. K. Johnson, *J. Med. Chem.* **1987**, *30*, 2181**–**2190. c) H. Schmidbaur, G. Reber, A. Schier, F. E. Wagner, G. Müller, *Inorg. Chim. Acta* **1988**, *147*, 143–150.

16. a) G. M. Sheldrick, *Acta Cryst.* **2008**, *A64*, 112–122. b) C. Kabuto, S. Akine, T. Nemoto, E. Kwon, *Nihon Kessho Gakkaishi* **2009**, *51*, 218–224. c) A. L. Spek, *Acta Cryst.* **2009**, *D65*, 148–155. d) G. M. Sheldrick, *Acta Cryst.* **2015**, *C71*, 3–8.

17. K. Nakamoto, *Infrared and Raman Spectra of Inorganic and Coordination Compounds*, Wiley, New York, **1997**.

18. a) N. Runeberg, M. Schütz, H. -J. Werner, *J. Chem. Phys.* **1999**, *110*, 7210–7215. b) S.-G. Wang, W. H. Eugen Schwarz, *J. Am. Chem. Soc.* **2004**, *126*, 1266–1276. c) H. Schmidbaur, A. Schier, *Chem. Soc. Rev.* **2008**, *37*, 1931–1951. d) H. Schmidbaur, A. Schier, *Chem. Soc. Rev.* **2012**, *41*, 370–412.

19. T. Steiner, *Angew*. *Chem*. *Int*. *Ed*. **2002**, *41*, 48–76.

20. a) L. E. Cheruzel, M. S. Mashuta, R. M. Buchanan, *Chem. Commun.* **2005**, 2223–2225. b) J. Berger, M. Oberhuber, *Chem. Biodivers.* **2010**, *7*, 2581–2615. c) X. Feng, K. Chen, Y.-Q. Zhang, S.-F. Xue, Q.-J. Zhu, Z. Tao, A. I. Day, *CrystEngComm*, **2011**, *13*, 5049–5051.

21. a) M. A. Harmer, Q. Sun, *Appl. Catal. A* **2001**, *221*, 45–62. b) J. Wu, X. Li, W. Du, C. Dong, L. Li, *J. Mater. Chem*. **2007**, *17*, 2233–2240. c) A. Satsuma, K. Shimizu, T. Hattori, H. Nishiyama, *Sens. Actuators B-Chem.* **2007**, *123*, 757–762. d) B. Chang, J. Fu, Y. Tian, X. Dong, *J. Phys. Chem. C* **2013**, *117*, 6252–6258. e) A.-Q. Wang, X.-L. Wu, J.-X. Wang, H. Pan, X.-Y. Tian, Y.-L. Xing, *RSC Adv*. **2015**, *5*, 19652–19658. f) J. P. Soetardji, J. C. Claudia, Y.-H. Ju, J. A. Hriljac, T.-Y. Chen, F. E. Soetaredjo, S. P. Santoso, A. Kurniawan, S. Ismadji, *RSC Adv.* **2015**, *5*, 83689–83699. g) P. Kumar, K.-H. Kim, E. E. Kwon, J. E. Szulejko, *J. Mater. Chem. A* **2016**, *4*, 345–361.

22. a) A. Bondi, *J. Phys. Chem.* **1964**, *68*, 441–451. b) M. Kawata, S. Ten-no, S. Kato, *J. Am. Chem. Soc.* **1995**, *117*, 1638–1640. c) C. Taboada-Pan, I. Brandariz, J. L. Barriada, T. Vilariño, M. E. Sastre de Vincente, *Fluid Phase Equilib.* **2001**, *180*, 313–325.

23. a) M. Uğurlu, M. H. Karaoğlu, *Microporous Mesoporous Mater.* **2011**, *139*, 173-178. b) L. Lin, Z. Lei, L. Wang, X. Liu, Y. Zhang, C. Wan, D. -J. Lee, J. H. Tay, *Sep. Purif. Technol.* **2013**, *103*, 15–20. c) I. V. Zadinelo, H. J. Alves, A. Moesch, L. M. S. Colpini, L. C. R. da Silva, L, D, dos Santos, *J. Mater. Sci.* **2015**, *50*, 1865–1875

24. a) D. Britt, D. Tranchemontagne, O. M. Yaghi, *P. P. Natl. Acad. Sci. U.S.A.* **2008**, *105*, 11623–11627. b) E. Borfecchia, S. Maurelli, D. Gianolio, E. Groppo, M. Chiesa, F. Bonino, C. Lamberti, *J. Phys. Chem. C* **2012**, *116*, 19839–19850. c) I. Spanopoulos, P.

Xydias, C. D. Malliakas, P. N. Trikalitis, *Inorg. Chem.* **2013**, *52*, 855–862. d) O. T. Wilcox, A. Fateeva, A. P. Katsoulidis, M. W. Smith, C. A. Stone, M. J. Rosseinsky, *Chem. Commun.* **2015**, *51*, 14989–14991. e) M. J. Katz, A. J. Howarth, P. Z. Moghadam, J. B. DeCoste, R. Q. Snurr, J. T. Hupp, O. K. Farha, *Dalton Trans.* **2016**, *45*, 4150–4153.

25. a) J. T. Mague, M. J. Fink, C. A. Recatto, *Acta Cryst.* **1993**, *C49*, 1176–1178. b) P. Barthazy, M. Wörle, H. Rüegger, A. Mezzetti, *Inorg. Chem.* **2000**, *39*, 4903–4912. c) Q. Wang, A. C. Marr, A. J. Blake, C. Wilson, M. Schröder, *Chem. Commun.* **2003**, 2776–2777. d) I. O. Koshevoy, Y.-C. Chang, Y.-A. Chen, A. J. Karttunen, E. V. Grachova, S. P. Tunik, J. Jänis, T. A. Pakkanen, P.-T. Chou, *Organometallics*, **2014**, *33*, 2363–2371. e) C. Mitzenheim, T. Braun, R. Laubenstein, B. Braun, R. Herrmann, *Dalton Trans.* **2016**, *45*, 6394–6404.

26. a) F. R. Bennett, F. M. Elms, M. G. Gardiner, G. A. Koutsantonis, C. L. Raston, N. K. Roberts, *Organometallics*, **1992**, *11*, 1457–1459. b) Y. Pan, J. T. Mague, M. J. Fink, *J. Am. Chem. Soc.* **1993**, *115*, 3842–3843. c) R. Kampe, A. Spannenberg, H.-J. Drexler, D. Heller, *Z. Kristallogr. New Cryst. Struct.* **2001**, *216*, 165–168. d) A. J. Edwards, M. Retbøll, E. Wenger, *Acta Cryst.* **2002**, *E58*, m497–m499. e) M. A. Bennett, L. Kwan, A. D. Rae, E. Wenger, A. C. Willis, *J. Chem. Soc. Dalton Trans.* **2002**, 226–233. f) A. Dybov, O. Blacque, H. Berke, *Eur. J. Inorg. Chem.* **2011**, 652–659.

28. a) A. E. Cherian, G. J. Domski, J. M. Rose, E. B. Lobkovsky, G. W. Coates, *Org. Lett.* **2005**, **7**, 5135–5137. b) H. Sun, J. S. Ritch, P. G. Hayes, *Dalton Trans.* **2012**, **41**, 3701–3713.

29. a) S. Sato, Y. Saito, *Acta Cryst.* **1978**, *B34*, 420–425. b) L. Cattalini, G. Micheion, G. Marangoni, G. Pelizzi, *J. Chem. Soc. Dalton Trans.* **1979**, 96–101. c) A. Varadarajan, S. E. Johnson, F. A. Gomez, S. Chakrabarti, C. B. Knobler, M. F. Hawthorne, *J. Am. Chem. Soc.* **1992**, *114*, 9003–9011.

30. a) S. Khatua, H. Stoeckli-Evans, T. Harada, R. Kuroda, M. Bhattacharjee, *Inorg. Chem.* **2006**, *45*, 9619–9621. b) H.-B. Wu, Q.-M. Wang, *Angew. Chem. Int. Ed.* **2009**, *48*, 7343–7345. c) J. He, G. Zhang, D. Xiao, H. Chen, S. Yan, X. Wang, J. Yang, R. Yuan, E. Wang, *J. Mol. Struct*. **2012**, *1018*, 131–136. d) X.-Z. Li, P.-P. Hao, D. Wang, L.-N. Zhu, *CrystEngComm,* **2013**, *15*, 2800–2803. e) K. Wu, K. Li, Y.-J. Hou, M. Pan, L.-Y. Zhang, L. Chen, C.-Y. Su, *Nat. Commun.* **2016**, *7*, 10847.

31. a) P. A. Bates, J. M. Waters, *Inorg. Chim. Acta*, **1985**, *98*, 125–129. b) D. S. Eggleston, D. F. Chodosh, *Inorg. Chim. Acta*, **1985**, *108*, 221–226.

32. a) H. Deng, S. G. Shore, *Organometallics* **1991**, *10*, 3486–3498. b) W. P. Schaefer, T. M. McCleskey, H. B. Gray, *Acta Cryst.* **1992**, *C48*, 1397–1399.

Acknowledgement

I wish to express my deepest gratitude to Prof. Takumi Konno for his expert guidance during all course of my work.

The deepest gratitude must be also given for Prof. Kohei Funahashi, and Prof. Naoto Ishikawa for their expert guidance.

I would like to thank Professor Masaki Kawano and Dr. Hiroyoshi Ohtsu at Tokyo Institute of Technology and Dr. Yumi Yakiyama at Osaka University for assisting with the single-crystal X-ray diffraction measurements at the Pohang Accelerator Laboratory.

I am also grateful to Dr. Asako Igashira-Kamiyama, Dr. Nobuto Yoshinari, Dr. Naoto Kuwamura, Dr. Tatsuhiro Kojima and Dr. Mihoko Yamada for their valuable advices.

Many special thanks go to the cheerful and helpful members of laboratory, Dr. Raeeun Lee, Dr. Chan Li, Dr. Yuji Hashimoto, Dr. Peishan Lee, Dr. Yusuke Takino, Mr. Takehiro Choshi and Dr. Suringwong Sireenart for their useful views and warm assistance. My thanks also go to Mr. Kousuke Igawa, Ms. Kiyoka Nakamura-Kurozumi, Ms. Anzu Yokoi, Mr. Atsushi Kakuya, Ms. Yuka Takino-Arai, Ms. Misaki Ueda, Mr. Shuntarou Kodera and all the others who are/were members of our laboratory for their friendship and support.

March. 2017